NASA Contractor Report 2996

Flight Effects on Noise Generated by the JT8D Engine With Inverted Primary/Fan Flow as Measured in the NASA-Ames 40- by 80-Foot Wind Tunnel

Frank G. Strout

CONTRACT NAS2-9302
JUNE 1978

NASA

NASA Contractor Report 2996

Flight Effects on Noise Generated by the JT8D Engine With Inverted Primary/Fan Flow as Measured in the NASA-Ames 40- by 80-Foot Wind Tunnel

Frank G. Strout
Boeing Commercial Airplane Company
Seattle, Washington

Prepared for
Ames Research Center
under Contract NAS2-9302

NASA
National Aeronautics
and Space Administration

**Scientific and Technical
Information Office**

1978

CONTENTS

CONTENTS (Concluded)

FIGURES

FIGURES (Continued)

FIGURES (Concluded)

FLIGHT EFFECTS ON NOISE GENERATED BY THE JT8D ENGINE WITH INVERTED PRIMARY/FAN FLOW AS MEASURED IN THE NASA-AMES 40- BY 80-FOOT WIND TUNNEL

Frank G. Strout
Boeing Commercial Airplane Company

1.0 SUMMARY

Tests were conducted at the Boeing-Boardman site and the NASA-Ames Research Center (ARC) 40- by 80-Foot Wind Tunnel to study the static and flight noise characteristics of the JT8D engine with inverted primary and fan flow. The objectives of the program were to:

- Design and fabricate a primary/fan inverter duct for the JT8D engine
- Determine static noise characteristics of the engine with uninverted and inverted flow
- Determine flight effects on noise generated by the inverted profile and compare with previously obtained results for uninverted and mixed flows
- Evaluate static and flight noise suppression potential of the inverted profile with several exhaust nozzle modifications

The test at the Boardman, Oregon site was conducted to establish proper engine match, measure thrust performance, and define static far field noise characteristics and near to far field correlations. Configurations included the baseline (uninverted flow with conical nozzle), the inverter with a conical nozzle and a plug nozzle, and the inverter combined with a 20 lobe external mixing nozzle. The 20 lobe configuration was tested with and without an acoustically lined shield. Noise data were measured on three sidelines covering a range of far field angles from 50^{o} to 155^{o} and near field angles from 30^{o} to 165^{o}. At takeoff power and a 649 m sideline the basic inverter (conical nozzle) achieved static peak to peak PNL and EPNL suppression values of 5.5 PNdB and 5.0 EPNdB relative to the baseline. Suppression values ranged up to 10 EPNdB for the inverter configuration with 20 lobe nozzle and acoustic shield.

The wind tunnel test results showed that significant noise changes occur in going from static to flight operation. Relatively large reductions were observed in the peak to peak PNL suppression values. The PNL suppression of the basic inverter was reduced from the static value of 5.5 PNdB to 2.5 PNdB under flight conditions. The EPNL suppression was not as severely influenced by forward velocity, changing from a static value of 5.0 EPNdB to an in-flight value of 4.0 EPNdB.

The inverter with 20 lobe nozzle and acoustic shield provided the highest in-flight EPNL suppression of 7.5 EPNdB.

The inverted flow profile produces lower noise than the mixed profile under both static and flight conditions at takeoff power. The inverter noise is lower by 3 EPNdB during static operation and by 1 EPNdB during flight operation.

The inverter configurations experience thrust loss relative to the baseline. The thrust loss at takeoff power ranged from 1.5% for the basic inverter to 5% for the inverter with 20 lobe nozzle.

2.0 INTRODUCTION

Static model tests conducted by Boeing and others in industry have shown that inverting the primary and fan streams of a turbofan engine offers significant potential for reducing jet noise. The suppression concept is of particular interest to Advanced Supersonic Transport (AST) engine cycle studies where high jet velocities create a serious noise problem during takeoff operation. NASA is sponsoring programs to determine the effect of forward velocity on the suppression characteristics of model jets with inverted flow. The influence of scaling and engine operating characteristics on the effectiveness of the inverted flow concept will remain as a major concern.

The purpose of this program is to establish the static and flight noise characteristics of a JT8D engine with inverted primary and fan flow. The JT8D engine matches important AST cycle flow parameters reasonably well and allows a large scale evaluation of the inverted flow concept to be made. The static data were acquired at the Boeing test facility at Boardman, Oregon while the simulated flight data were measured in the NASA-Ames Research Center 40- by 80-Foot Wind Tunnel (40 by 80). The feasibility of using the 40 by 80 wind tunnel to determine flight effects on engine noise was established by NASA-Ames Contract NAS2-8213 (references 1 to 3). The program included model tests with near and far field measurements and full scale JT8D engine tests using near field measurements. The model test showed that flight effects measured in the near field are the same as those measured in the far field. The JT8D engine test showed that the flight noise determined in the wind tunnel matched measured flight noise of the 727/JT8D for a baseline and quiet nacelle installation.

The inverted flow program consists of the following major elements:

- Design and fabricate a primary/fan inverter duct for the JT8D engine
- Conduct a static, free field test to define far field noise characteristics and establish near to far field correlations
- Conduct a flight effects test in the 40 by 80

Wind tunnel derived flight effects for the JT8D with inverted flow and a conical nozzle are compared with corresponding results previously obtained for the JT8D configured as a baseline and internal mixer. Static and wind tunnel tests were also conducted with Boeing supplied nozzle variations to further explore the noise suppression potential of the inverted flow concept. The add-on configurations were designed to increase the mixing perimeter and mixing rate of the high velocity primary flow. This was done by replacing the conical nozzle with a plug nozzle and a 20 lobe nozzle. The effect of an acoustic shield on noise was also evaluated.

3.0 ABBREVIATIONS AND SYMBOLS

amb	ambient
ARC	Ames Research Center
AST	Advanced Supersonic Transport
B&K	Bruel & Kjaer
C_∞	ambient speed of sound, m/s
C_V	engine thrust coefficient
C/L	centerline
CONFIG	configuration
dB	decibel
D	diameter, m
EPNL	effective perceived noise level, EPNdB
EPNdB	unit of effective perceived noise level
EPR	engine pressure ratio – P_{T7}/P_{T2}
EXTR	extrapolated
FREQ	one-third octave band center frequency, Hz
GRD	ground
kn	knot
L	length, m
m	velocity exponent corrected for source convection
MIC	microphone
M_∞	freestream Mach number
n	velocity index

NPR	nozzle pressure ratio – P_{T7}/P_{amb}
OASPL	overall sound pressure level, dB
OB	octave band
P&WA	Pratt & Whitney Aircraft
PNdB	unit of perceived noise
PNL	perceived noise level, PNdB
P_{amb}	ambient pressure, N/m^2
P_T	total pressure, N/m^2
P_{T2}	engine inlet total pressure, N/m^2
P_{T7}	exhaust nozzle primary total pressure, N/m^2
P_{TF7}	exhaust nozzle fan total pressure, N/m^2
P_{TM7}	exhaust nozzle mixed total pressure, N/m^2
R	radial distance from sound source to observer, m
RC	round convergent
RE	referenced to
RH	relative humidity, percent
S/N	Strouhal number
SL	sideline
SPL	sound pressure level, dB
T	temperature, ^oC
T_{amb}	ambient temperature, ^oC
T_{T7}	primary total temperature, ^oC
T_{TF7}	fan total temperature, ^oC
V	velocity, m/s

V_{fan}	engine fan jet velocity, m/s
V_{mix}	jet velocity of mixed fan and primary flows, m/s
V_{pri}	engine primary jet velocity, m/s
V_R	relative jet velocity = $V_{pri} - V_\infty$, m/s
V_∞	aircraft or tunnel velocity, m/s
X_s	axial distance from nozzle exit to noise source, m
40 by 80	NASA-Ames 40- by 80-Foot Wind Tunnel
Δ	delta
λ	wave length, m
θ	angle, deg
θ_F	far field angle, deg
θ_s	noise emission angle, deg
∞	ambient

4.0 TEST DESCRIPTION

4.1 STATIC TEST

The static test phase of the inverter program was conducted at the Boeing facility located at Boardman, Oregon during the period January 4 to 31, 1977.

4.1.1 FACILITY DESCRIPTION

The facility includes a steel test stand that is attached to a concrete footing. A concrete acoustic arena is adjacent to the concrete footing and covers an area of approximately 5575 sq.m. (60,000 sq. ft.). The test stand and part of the acoustic arena are shown in figure 1. The test engine is mounted as a 727 center engine at a centerline height of 4 m (13 ft). The surface between the engine centerline and the near field microphone array was covered with a 7.6 cm (3 in.) thick pad of polyurethane foam (figure 1).

4.1.2 ENGINE DESCRIPTION

The test engine was a JT8D-17R turbofan with bypass ratio 1.1 and a nominal air flow rate of 148 kg/sec (326 lb/sec). The engine develops a thrust of 77.9 kn (16,400 lb) at a pressure ratio of 2.2. The engine has a two-stage fan, and eleven-stage high pressure compressor, a single-stage high pressure turbine, and a three-stage low pressure turbine.

4.1.3 TEST HARDWARE DESCRIPTION

Each configuration was tested with a Pratt & Whitney (P&WA) reference bellmouth inlet (engine match and thrust) and a quiet nacelle two-ring inlet (acoustics). All acoustic runs included both upper and lower cowling. A schematic drawing of test configurations is provided in figure 2.

4.1.3.1 Inverter Duct

The inverter duct is a series of constant area, nested duct elements that invert the fan and primary flow streams of the JT8D engine (figure 3). The welded assembly includes eight primary and eight fan gas flow passages and has a length of 0.914 m (3 ft). The flow at the inverter exit consists of an outer annulus of high temperature primary gas and an inner annulus of fan air. The inverter attaches at the engine "M" flange on the upstream end and mates with a modified production tailpipe on the downstream end. Some mixing occurs between the two streams prior to exhausting through a conical nozzle.

4.1.3.2 Baseline

The baseline configuration operated with conventional or uninverted flow with the high velocity primary on the inside and the low velocity fan flow on the outside. The two streams merge downstream of the fan splitter case and exhaust through a 0.76 m (2.5 ft) diameter production conical nozzle.

4.1.3.3 Inverter

The primary/fan inverter configuration was operated with the inverter duct installed downstream of the splitter case. The inverter duct is followed by a modified production tailpipe and a conical exhaust nozzle. The high velocity primary is located in an outer, annular flow region with the fan air located on the inside. The nozzle diameter is about the same as the baseline although slightly larger to compensate for the inverter duct pressure loss. At takeoff power the primary to fan area ratio is 1.4 and the velocity ratio is 1.6.

4.1.3.4 Inverter/Plug

This configuration included the inverter duct but replaced the conical nozzle with a conical plug nozzle. The plug has a maximum diameter of 0.54 m (1.76 ft) providing a total to flow area ratio of 1.5.

4.1.3.5 Inverter/Mixer

This configuration replaces the conical nozzle of the inverter/plug with a 20 lobe external mixing nozzle. The lobes are designed to penetrate the outer primary flow (about 12.7 cm) and rapidly mix this flow with ambient air. Each lobe has a length of 25.4 cm (10 in.).

4.1.3.6 Inverter/Mixer/Shield

An acoustic shield is added to the inverter/mixer to provide a reflecting/absorbing barrier between the jet and observer. The shield has a length and diameter of 1.27 m (4.2 ft) covering a 180^{o} segment. The inner shield surface includes bulk absorber acoustic lining covered by a perforated plate. The shield was tested in a hardwall and lined configuration. The shield was designed to reflect and absorb the high frequency pre-merged mixing noise generated by the 20 lobe nozzle.

4.1.4 INSTRUMENTATION

4.1.4.1 Engine Instrumentation

In addition to thrust, rotor speed, and fuel flow, normal engine gas flow pressures and temperatures were measured. Engine air flow was measured during performance runs by means of a calibrated bellmouth inlet. A survey of the inverter exhaust flow was made with a rake having 40 total pressure and 40 total temperature probes. A 180^{o} segment was covered by the survey.

4.1.4.2 Acoustic Instrumentation

The acoustic instrumentation (table 1) included three microphone arrays located on sidelines of 3.05 m (10 ft), 15.2 m (50 ft), and 30.5 m (100 ft). The near array employed 16 centerline microphones covering a range of angles from 30^{o} to 165^{o} referenced to the nozzle exit plane and inlet axis. The intermediate array used 15 ground microphones covering angles from 30^{o} to 160^{o}. The far array were also ground microphones and included 12 microphones from 50^{o} to 155^{o}. The near array used 0.64 cm (0.25 in.) Bruel &

Kjaer (B&K) 4136 microphones that were oriented for grazing incidence (figure 1). The other two arrays used 1.27 cm (0.5 in.) B&K 4134 microphones that were oriented downward, 1.27 cm (0.5 in.) above individual steel plates.

Noise data were recorded on a fourteen track Sangamo model 3500 tape recorder. On-line data were processed by a General Radio 1925 filter, 1926 detector, and a Hewlett Packard 7001A plotter.

4.1.5 ACOUSTIC DATA REDUCTION

Data reduction provided one-third octave band (OB) spectra in the form of a digital magnetic tape.

4.1.6 TEST PROCEDURE

Each configuration included an engine match run, a thrust performance run, and an acoustic run. The match run was made to assure that the engine was operating within limits prescribed by P&WA for a flight-worthy engine. The inverter duct included tabs to adjust the relative fan and primary flow areas. The nozzle exit area was also adjusted to assure proper engine operation with the inverter test hardware. The engine match and thrust performance runs were conducted with the bellmouth inlet. Following engine start and a nominal five minute warm-up, the test conditions were set starting with the lowest pressure ratio. After a three minute stabilization time at each pressure ratio, engine performance data were recorded. During acoustic runs, noise data recording began as soon as the target condition was established. Engine performance was calculated on-site immediately after each test condition to assure that the desired condition was set.

4.1.7 TEST CONDITIONS

Engine test conditions for the acoustic runs are listed in table 1. Match and thrust performance runs generally covered a range of pressure ratios from 1.4 to 2.2.

4.2 WIND TUNNEL TEST

The wind tunnel test phase of the inverter program was conducted at the NASA-Ames Research Center 40- by 80-Foot Wind Tunnel (40 by 80) during the period June 13 to 24, 1977.

4.2.1 FACILITY DESCRIPTION

The 40 by 80 is a closed circuit wind tunnel powered by six 12.2 m diameter fans and six 4480 kw electric motors. The test section is 24.4 m long in the tunnel airflow direction and has a cross section consisting of a 12.2 m square and two semicircles of 12.2 m diameter on each side of the square section (figure 4). The tunnel operates with a stagnation pressure equal to the atmospheric pressure. The tunnel stagnation temperature is time variant because of the wind tunnel drive power and engine exhaust. Typically the temperature would range between 15°C to 55°C (60°F to 130°F). About 400 sq. m of 7.6 cm-thick

polyurethane foam was installed on the floor and part way up the sidewalls. The lining extended approximately 3 m upstream of the engine exit plane and 15 m downstream. The test installation is shown in figures 4 and 5.

4.2.2 TEST CONFIGURATIONS

The following configurations were tested in the 40 by 80:

- Inverter (figure 4)
- Inverter/plug (figure 5)
- Inverter/mixer (figure 6)
- Inverter/mixer/lined shield (figure 7)

Each configuration included the quiet nacelle two-ring inlet and full engine cowling. Additional configuration description is provided in section 4.1.3. The JT8D-17 engine configured as a baseline and with an internal mixer were tested in the 40 by 80 during Contract NAS2-8213 (*references* 1 and 2).

4.2.3 INSTRUMENTATION

4.2.3.1 Engine Instrumentation

Engine operating parameters were measured including rotor speeds, fan and primary static, and total pressures and temperatures.

4.2.3.2 Acoustic Instrumentation

Acoustic data for flight effects analysis were recorded by a pair of traversing microphones in sweep mode (figures 4 and 5). The microphones were 0.64 cm (0.25 in.) B&K type 4136 with B&K UA 0385 aerodynamic nose cones. They were mounted at engine centerline height (4 m) on a 3.05 m sideline relative to the center of the jet. The traverse moved at a steady rate of 0.15 m/sec (0.5 ft/sec) and covered a range of angles from 30^{o} to 168^{o} relative to the nozzle exit plane and inlet axis. In addition to the traverse microphones, two fixed microphones were installed on the side opposite the traverse. One fixed microphone was mounted at centerline height on a 3.05 m sideline at 160^{o} for on-line monitoring. The second fixed microphone was positioned on the same sideline but at a height of 1.8 m and an angle of 8^{o}. These data were recorded and used as an indication of the reverberant field noise level. The noise data were recorded on a fourteen track Sangamo model 3500 type recorder for later reduction at Boeing.

4.2.3.3 Facility Instrumentation

Tunnel parameters were recorded on the Boeing data system including static and total pressure, total temperature, and relative humidity. It is noted that engine thrust was not measured.

4.2.4 ACOUSTIC DATA REDUCTION

The sweep data were analyzed to define one-third octave band spectra each 5^{o} from 30^{o} through 110^{o} and every 2.5^{o} from 112.5^{o} through 167.5^{o}. A one second integration time was used, 0.5 second before and after the desired angle.

4.2.5 TEST PROCEDURE

Engine test conditions were set by monitoring nozzle pressure ratio (P_{T7}/P_{amb}) and on-line calculated primary jet velocity. At the start of each run, the desired primary jet velocity was set and maintained as closely as possible until all data were recorded. The traverse microphones were positioned in the region of peak noise where gains were set and on-line data were recorded. The traverse was then moved to a position just downstream of 30^{o}. A sweep was then made to an angle of 168^{o} with each microphone output recorded on two channels at different gain settings. One channel recorded the microphone position voltage output and another the voice input. Two propulsion data points were recorded during each traverse, one near the beginning and the other near the end.

Selection of engine power setting and tunnel velocity was made on the basis of tunnel heating. Periods with the engine at idle power and test section ventilation doors open were used on occasion to reduce tunnel temperature prior to another run.

4.2.6 TEST CONDITIONS

Engine and wind tunnel test conditions are listed in table 2 for each configuration.

5.0 DATA ANALYSIS

5.1 ANALYSIS TECHNIQUE

5.1.1 NOISE SOURCE LOCATIONS

The technique for determining flight effects in a closed wind tunnel requires that noise source locations and directivities be known for the frequencies of interest. The multiple sideline noise measurement procedure described in references 1 to 3 is used to define the required source location correlations. Sound pressure level (SPL) directivities were plotted as a function of $1/\tan(180^{o} - \theta)$ for the three sideline microphone arrays and each one-third octave band from 50 to 10,000 Hz. Typical plots for the inverter configuration are shown in figure 8 for takeoff power and a range of frequencies. The difference in peak noise levels is used as a basis for relating a given signal that propagates from the source through the three sidelines. This peak to peak difference includes the effect of spherical divergence, atmospheric absorption, and noise measurement in the near field. For high frequencies the peak to peak increment is adjusted to account for longer or shorter propagation paths relative to the peak noise. The adjustment is determined by multiplying the difference in propagation length by the atmospheric absorption coefficient. The procedure is illustrated in figure 8a for frequencies of 200 and 250 Hz. The peak to peak SPL increments for 200 Hz are about 14 dB between the 30.5 and 3.05 m sidelines and 6 dB between the 30.5 and 15.2 m sidelines. Since atmospheric attenuation is very small for this frequency range, the 14 dB and 6 dB increments are used to track a given signal from each 30.5 m microphone station to a corresponding station on the other sidelines. For each measured SPL on the 30.5 m sideline, increments of 6 dB and 14 dB are added and define intercepts on the 15.2 m and 3.05 m sidelines respectively. The intercepts on each sideline are joined by the dashed lines of figure 8a that establish propagation paths for each signal.

The intercept of the dashed lines with each sideline defines an axial station equal to the sideline distance times $(1/\tan(180^{o} - \theta)$. These results are plotted as shown in figure 9. A line drawn from the 30.5 m measurement position through the corresponding points from the other two sidelines defines the apparent source location and directivity for a given signal. The source locations of figure 9 show that noise propagating to low angles appears to emanate from a point near the nozzle exit. The source location moves downstream as the propagation angle increases.

The source location and directivity from figure 9 is replotted as shown in figure 10. The source location, in terms of nozzle diameters, is defined as a function of noise emission angle for takeoff power and the available range of Strouhal numbers. Source location results for nozzle pressure ratios of 1.4 to 2.2 were used to define the correlation curves of figure 11. These relationships covered a wide range of Strouhal numbers and served as inputs to a computer program that extrapolated data from the three sidelines to a 122 m (400 ft) sideline. The 122 m data were treated as far field, thus permitting point source extrapolations to other sidelines.

The near field level effect described in reference 3 is also observed for the full scale data. The correlation shown in figure 12 was used as an input to the data extrapolation program to compensate for this effect. For the 3.05 m data (SL/D = 4) the near field effect is up to 2 dB. The 15.2 m and 30.5 m data require no level adjustment for near field effects.

The source location and near field level correlations of figures 11 and 12 were used to extrapolate the Boardman static data and the 40 by 80 wind tunnel data for the inverter configuration. Similar correlations were defined for each of the other configurations that are evaluated in this report.

5.1.2 WIND TUNNEL REVERBERANT FIELD

Although part of the test section hard surface was covered by polyurethane foam, a prominent reverberant field problem remains. The reverberant field is found to be a function of frequency, engine power condition, nozzle configuration, and tunnel velocity. The reverberant level at a given frequency appears to be strongly related to the peak level that is generated. Thus the reverberant field becomes a problem at off-peak angles (low and high) and is more pronounced when there is a large fall-off in SPL at off-peak angles, Since the reverberant field is related to the peak SPL values, it will vary with the engine power condition and tunnel velocity. The nozzle configuration will influence the peak noise generated at each frequency and the directivity characteristics.

Reverberant field spectra were defined for each engine configuration, engine power condition, and wind tunnel operating velocity. The spectra for the inverter configuration are shown in figure 13 and represent nominal reverberant field noise levels within the test section for the specified test condition. The 40 by 80 noise data were corrected by logarithmically subtracting the reverberant field spectra from the measured engine noise spectra at each angle.

Different techniques were used to determine the reverberant field noise level for tunnel-off and -on operation. The tunnel-off reverberant field was determined by logarithmically subtracting free field SPL's from the 40 by 80 SPL values at equal primary jet velocity. This procedure is illustrated in figure 14 for takeoff power and several frequencies. The reverberant field noise level at a given frequency appears to be relatively constant through the test section. A nominal reverberant field level is estimated for each frequency and tunnel-off power condition to form the spectra shown in figure 13a.

A different procedure is required to estimate the reverberant field for tunnel-on operation. As indicated in figure 13a, the tunnel-off reverberant field level is quite sensitive to engine power condition. It is reasonable that as the engine power is reduced the reverberant field level will be lower due primarily to reduced noise source strengths at each frequency. Tunnel velocity should have an effect similar to engine power reduction since source strengths are reduced as tunnel velocity increases. Two methods were combined to estimate the reverberant field level during tunnel-on conditions. One method employed a correlation between peak SPL and reverberant field level while the other method relied on 8^{o} microphone spectra measured in the 40 by 80 test section.

The peak SPL correlation is shown in figure 15 and is based on the tunnel-off reverberant field data. Each data point represents the difference between the peak SPL measured on the 3.05 m sideline and the resulting reverberant field level for a given engine power condition and frequency. Data are included for NPR's of 1.1 to 2.1 and show that the reverberant field level is closely related to the peak SPL that is generated. The directivity of the peak SPL undoubtedly influences the resulting reverberant field level. That is, spherical

divergence noise reduction beyond the 3.05 m sideline will be less at 90° than in an upstream or downstream direction. The solid symbols of figure 15 reflect a spherical divergence level adjustment due to changes in peak noise directivity. The adjustment is made relative to directivity characteristics of the NPR = 2.1 condition. The data for NPR 2.1 and the adjusted data for lower power conditions collapse reasonably well. The purpose of this correlation is to show that the change in reverberant field level will follow the change in measured peak SPL. Although the difference in peak SPL between NPR 2.1 and NPR 1.1 is quite large for all frequencies (about 20 dB), the resulting reverberant levels are predictable within approximately 1 dB based on figure 15. This finding is used to determine the tunnel-on reverberant field level by incrementing from the tunnel-off level. The increment is determined for each frequency by the change in peak SPL between tunnel-off and tunnel-on operation at a given power condition. Adjustment for changes in peak noise directivity is made, if required.

The second method for estimating the tunnel-on reverberant field level used spectra measured by a microphone located in the forward part of the test section. The microphone was positioned opposite the traverse on a 3.05 m sideline at an angle of 8° referenced to the nozzle exit station and the inlet axis. It was surmised that the measured signal might be representative of the test section reverberant field level due to the low engine noise radiated to this position. Typical 8° microphone spectra are provided in figure 16 for takeoff power and both tunnel-off and tunnel-on operation. It is noted that the tunnel-on spectra have been corrected for tunnel background noise. Tunnel-off reverberant field levels determined by the method of figure 14 are plotted for comparison with the tunnel-off 8° microphone spectra. The agreement is good as it was for lower power conditions and the other configurations.

This analysis shows that the 8° microphone spectra provides a good estimate of reverberant field level for tunnel-off conditions. When corrected for background noise, the 8° microphone spectra should also provide a reasonable estimate for tunnel-on operation. The tunnel-on 8° microphone spectra of figure 16 is lower than the tunnel-off spectra which is expected. A check on the level is made by applying the change-in-peak-SPL method that was previously described. The incremental reductions in peak SPL between tunnel-off and tunnel-on are equated to corresponding reductions in reverberant field level. The increments are subtracted from the tunnel-off reverberant field level and define an estimated tunnel-on reverberant field level as shown in figure 16. The resulting spectra compare favorably with the measured 8° microphone spectra for tunnel-on operation. Thus both methods appear to provide about the same estimate for the tunnel-on spectra of figure 13. The spectra are based primarily on the measured 8° microphone spectra. Level checks and adjustments were made by the peak SPL increment method. For cases where tunnel background noise obscured the 8° microphone data, the SPL increment technique was used exclusively.

5.1.3 BACKGROUND NOISE

Wind tunnel background noise levels were subtracted from the tunnel-on data. Background noise was measured during the inverter test and the inverter/mixer test with and without shield. No significant difference was noted due to configuration; thus the background noise taken during the inverter test was used for all configurations. A background noise spectra was defined for each angle of interest between 30° and 165° as typified by figure 17.

5.2 BASELINE ANALYSIS

Data for the JT8D-17R engine configured as a baseline (uninverted flow) was acquired during the Boardman test phase. Wind tunnel data were measured during contract NAS2-8213 (references 1 and 2) using a JT8D-17 engine. The -17 and -17R engines generate near identical static jet noise; consequently, the flight effects measured for the -17 are assumed to be applicable to the -17R.

5.2.1 STATIC DATA ANALYSIS

The measured 30.5 m (100 ft) sideline data were extrapolated to the far field using source location correlations described in reference 1. The resulting spectra, OASPL and PNL directivities, and EPNL characteristics are compared with corresponding data for the suppressor configurations in following sections. In general, spectra comparisons are made on a 122 m (400 ft) sideline that is considered to be far field. Directivity and EPNL comparisons emphasize a 649 m (2128 ft) sideline (AST noise certification sideline). Some comparisons are also provided for an intermediate sideline of 457 m (1500 ft) to establish trends as a function of sideline distance.

5.2.2 WIND TUNNEL DATA ANALYSIS

The wind tunnel data from the previous test were re-processed using the technique described in section 5.0. The resulting tunnel-off and tunnel-on OASPL and PNL directivities are compared in figure 18 for NPR 2.1 and 1.8. The results of figure 18 are converted to velocity coefficients (n) in figure 19 where:

$$n = \frac{OASPL_{static} - OASPL_{flight}}{10 \log \frac{V_{pri}}{V_R}}$$

Effective perceived noise level (EPNL) is used to evaluate the noise reduction effectiveness of the various suppressor configurations in this report. EPNL is the logarithmic summation of PNL each 0.5 second between the 10 PNdB down points from the peak PNL. The calculation for both static and flight EPNL assumes a single engine moving past an observer at a velocity of 91.5 m/s (300 ft/sec) and at a distance of 649 m (2128 ft). Installation on an aircraft, angle of attack, flight trajectory, ground reflections, and extra ground attenuation are factors that are not included in the calculation.

A static and flight EPNL comparison is provided in figure 20 for the baseline configuration. The static or solid line is plotted as a function of primary velocity and defines a throttle line for comparison with flight EPNL. The EPNL values are calculated using far field static PNL data assuming no change in level due to forward velocity. The diamond symbols represent flight EPNL's and are plotted versus primary relative velocity.

The flight levels are calculated by applying PNL velocity exponents (figure 19) to the static PNL values where:

$$PNL_{flight} = PNL_{static} - 10n \log \frac{V_{pri}}{V_R}$$

The comparison of figure 20 shows that the EPNL reduction due to flight is less than predicted by relative velocity. That is, the diamond symbols would fall on the solid throttle line if the relative velocity prediction were correct. The departure from the throttle line is less at high power than at low power.

5.3 INVERTER ANALYSIS

The analysis of the inverter configuration data is given major emphasis in this report. Analysis of the other configurations was done in a similar manner but is not reported in as much depth.

5.3.1 STATIC DATA ANALYSIS

5.3.1.1 Comparison of Near and Far Field Data

Comparisons are made between static noise data measured on the three sidelines and extrapolated to the same far field sideline using source location correlations. Spectra are compared in figure 21 for the 3.05 and 30.5 m data at a NPR of 2.1. The spectra compare reasonably well in terms of shape and absolute level. OASPL and PNL directivities are compared in figure 22 for the noted pressure ratios. Agreement between the three sidelines is generally good in terms of level and directivity shape.

Another method of comparing near and far field data is illustrated by figures 23 and 24 that plot OASPL and PNL as a function of ideal primary velocity. The slope and level of OASPL and PNL compare well between the extrapolated 3.05 and 30.5 m data. These comparisons along with the spectra and directivity plots indicate that the noise source location correlations of figure 11 are satisfactory. Near and far field comparisons were also made at lower power conditions with similar favorable results.

Good agreement between near and far field results is quite important to the analysis of the wind tunnel data. These measurements are restricted to the 3.05 m sideline and must be extrapolated to define far field flight effects. Verification of the source location correlations provides confidence that the resulting flight effects for the inverter will be relatively accurate.

5.3.1.2 Comparison of Inverter and Baseline Data

Static data for the inverter configuration are compared with data for the baseline configuration in this section. In all cases the data were measured on the 30.5 m sideline and extrapolated to the far field using source location correlations. Spectra comparisons are provided in figures 25 to 29 for NPR's of 2.2, 2.1, 1.8, 1.6, and 1.4. Emphasis is placed on the NPR

2.1 condition since this represents the highest power tested for flight effects in the 40 by 80. At low angles (figure 26) the inverter is not effective in reducing noise, relative to the baseline, regardless of frequency. As the angle increases toward the jet axis the inverter shows increasing reduction in the low and middle frequency range. At angles of 130^{o} to 155^{o} (figures 26e and 26f) the amount of reduction is quite substantial in particular for frequencies in the region of 200 to 400 Hz (6 to 10 dB). At high frequencies (above 1600 Hz) the baseline and inverter have comparable noise levels. Similar results are observed for the other power conditions.

Baseline and inverter static OASPL and PNL directivities are compared in figure 30 for NPR's of 2.2 to 1.4. In general, the inverter is an effective suppressor at angles of 120^{o} and higher. At takeoff power (NPR 2.2) peak to peak suppression for OASPL is 6.0 dB and for PNL is 5.5 PNdB. The low angle (50^{o} to 110^{o}) suppression of OASPL and PNL is relatively small.

Static EPNL characteristics are compared in figure 31, where flight PNL's are assumed to equal static values. At takeoff power (600 m/s) the inverter provides an EPNL suppression of 5.0 EPNdB. The amount of EPNL suppression is reduced slightly as the engine power is reduced.

5.3.2 WIND TUNNEL DATA ANALYSIS

5.3.2.1 Comparison of Free Field and Tunnel-Off Data

Boardman free field data are compared with 40 by 80 tunnel-off data in this section. The data are measured on a 3.05 m (10 ft) sideline and extrapolated to a 122 m (400 ft) sideline using source location correlations. Low angle and high angle spectra are compared in figure 32 for a NPR of 2.1. The two sets of data compare reasonably well indicating the validity of the reverberant field corrections. It is noted that spikes were observed in the 40 by 80 spectra at frequencies up to 200 Hz and low angles after correcting for the reverberant field. These spikes were smoothed to fair in with the adjacent frequencies to minimize errors in calculated OASPL and PNL.

OASPL and PNL directivities are compared in figure 33 for the NPR 2.1 condition. The agreement is basically acceptable for both OASPL and PNL. An exact agreement is not expected due to the entrained velocity that results during tunnel-off operation. The comparison is made by interpolating the free field data at the wind tunnel primary relative velocity. A comparison at equal primary velocity would result in a better match at low angles where the effect of forward velocity is generally small. Comparisons of spectra and directivities at lower power conditions also show good agreement between free field and wind tunnel.

5.3.2.2 Flight Effects for NPR 2.1

Flight effects on engine noise for the inverter configuration at NPR 2.1 are evaulated in this section. The analysis includes spectra, OASPL and PNL directivity, and SPL directivity. Velocity exponents are defined for OASPL, PNL, and SPL.

5.3.2.2.1 Spectra

Tunnel-off and tunnel-on spectra are compared in figure 34 for NPR 2.1 and angles of 50^{o} to 155^{o}. The sideline is at 122 m (400 ft) and the angles are representative of far field. The results show that tunnel velocity produces negligible noise reduction at low angles (50^{o} to 100^{o}, figures 34a to 34c). The low frequencies (50 to 315 Hz) indicate a slight reduction (about 1 dB). The intermediate to high frequencies show either no reduction or a slight increase in noise level with forward velocity. As the angle increases from 110^{o} to 150^{o} the amount of SPL reduction with forward velocity increases at all frequencies. At 140^{o} to 155^{o} the reduction of the peak noise (125 Hz) is greater than higher or lower frequencies.

5.3.2.2.2 OASPL and PNL Directivity

Tunnel-off and tunnel-on OASPL and PNL directivities are compared in figures 35 and 36 for NPR 2.1. The sideline varies from 122 to 649 m for tunnel velocities of 150 and 185 kn. Tunnel velocity results in relatively small reductions in OASPL and PNL at angles of 50^{o} to 100^{o}. As the angle increases, the amount of reduction increases. For the 185 kn tunnel condition and a 649 m sideline (figure 36c) a reduction of 5 dB or 5 PNdB results at an angle of 140^{o}. The corresponding reductions on the 122 m sideline are slightly less (4.6 dB and 4.0 PNdB). This difference is the result of atmospheric attenuation that changes the spectra shape and weighting of frequencies.

5.3.2.2.3 SPL Directivity

Tunnel-off and tunnel-on SPL directivities are compared in figure 37 for NPR 2.1 and one-third octave band frequencies from 50 Hz to 10,000 Hz. The data reflect a sideline of 122 m and tunnel velocities of 150 and 185 kn. In general, tunnel velocity causes a small reduction in SPL at low angles (50^{o} to 100^{o}). Large reductions (6 to 7 dB) are experienced at higher angles for frequencies of 100 Hz to 250 (figures 37b to 37d). The reduction of high frequency SPL with tunnel velocity is more modest at high angles ranging from 1 dB to 3 dB depending upon frequency.

5.3.2.2.4 Velocity Exponents

The results of figures 35 to 37 are converted to velocity exponents for OASPL, PNL, and SPL in figures 38 to 40. Velocity exponents (n) are provided for OASPL and PNL at sidelines of 122, 457, and 649 m in figure 38. An alternate velocity exponent (m) is shown in figure 39 for a 649 m sideline where the source convection correction is made as follows:

$$m = \frac{PNL_{static} - PNL_{flight}}{10 \log \frac{V_{pri}}{V_R}} - \frac{\log(1 - M_\infty \cos\theta)}{\log \frac{V_{pri}}{V_R}}$$

The velocity exponent curves for OASPL and PNL are consistent with small flight noise reductions at low angles and large reductions at angles near the jet axis. The effect of sideline is most prominent for PNL at high angles where higher n values result at the further sidelines.

The velocity exponent curves for discrete frequencies (figure 40) were arrived at by plotting the n values as a function of frequency (figure 41). This was done to minimize the effects of data scatter and assumes that reasonably smooth variations in n will occur with frequency at a given angle. The n curves of figure 40 are defined by the faired data from plots similar to figure 41.

5.3.2.3 Flight Effects for NPR 1.8

Tunnel-off and tunnel-on data are compared for an NPR of 1.8 in figures 42 to 45. Spectra comparisons are provided in figure 42 for a 122 m sideline and angles of 50^{o} to 155^{o}. The effects of tunnel velocity on the tunnel-off spectra are comparable with the NPR 2.1 condition described in section 5.3.2.2.1.

OASPL and PNL directivity plots are shown for 100 and 150 kn tunnel speeds in figure 43. Tunnel velocity causes a small reduction in OASPL and PNL at low angles (50^{o} to 100^{o}) with increasing reduction at higher angles. Velocity exponents are provided in figures 44 and 45 for a 649 m sideline and are similar to the NPR 2.1 curves in terms of trend with angle.

5.3.2.4 Flight Effects for NPR 1.6 and NPR 1.4

Tunnel-off and tunnel-on spectra are provided in figure 46 for an NPR of 1.6 and a 122 m sideline. OASPL and PNL directivities are compared in figure 47 and are used to define the velocity exponent curves of figures 48 and 49. The peak velocity exponent values at this power condition are significantly less than those at the higher power conditions (figures 38c and 44).

Tunnel-off and tunnel-on OASPL and PNL directivities are compared in figure 50 for an NPR of 1.4 and a 649 m sideline. Only the directivity plot is shown for this power condition due to the small difference in test relative velocity between the tunnel-off and -on cases. The noise reduction trend with angle is comparable to the higher power conditions. Velocity exponents are not calculated because of the small difference in relative velocity and the sensitivity of n values to this parameter.

5.3.2.5 Summary and Comparison of Flight Effects

Flight effects for the inverter configuration are summarized in this section by evaluating trends with relative velocity and by comparison of static and flight OASPL, PNL, and EPNL suppression relative to the baseline. Tunnel-off and tunnel-on OASPL and PNL are plotted as a function of primary relative jet velocity in figure 51. The results are for a 649 m sideline and cover a range of angles from 50^{o} to 155^{o}. Static data from the Boardman test are included and are used to define the throttle lines shown on each plot. The departure of the tunnel-on data from the static throttle line is quite pronounced at low angles (50^{o} to 100^{o}, figures 51a to 51f). The use of relative velocity to predict flight noise would result in large errors for this range of angles (low predicted noise level). At 110^{o} and 120^{o} (figures 51g and 51h) the tunnel-on data approaches the throttle line. At angles of 130^{o} and higher the tunnel-on data fall on the throttle line or show the same slope with relative velocity.

Based on these characteristics one approach to estimating the flight noise of inverted profiles for other engines or cycle conditions is as follows: Flight OASPL or PNL can be defined by assuming a relative velocity relationship at angles of 120° and higher. That is, interpolate static data or calculate noise levels at a primary velocity equal to flight relative velocity (V_{pri} - $V_{airplane}$). The reduction of OASPL and PNL at lower angles will best be estimated by using the velocity exponents provided in this report. The reduction of low angle noise is small regardless of power setting for the JT8D and appears to be a characteristic of the inverted flow profile. Any error in true flight PNL reductions at low angle will generally have a small effect on the flight EPNL estimate.

Static and flight EPNL's are plotted as a function of primary relative velocity in figure 52. The static EPNL values are based on Boardman static PNL's assuming no reduction in level due to flight. The flight EPNL values are calculated by applying the velocity exponent curves of figures 38c, 44, and 48 to the static PNL's. The flight EPNL's are higher than predicted by relative velocity. The departure from the throttle line increases as the engine power is decreased.

Static and flight OASPL and PNL comparisons are provided in figures 53 and 54 for the baseline and inverter configurations at takeoff power. The static curves are based on Boardman 30.5 m data that are extrapolated to the 649 m sideline using source location correlations. The flight noise levels are obtained by applying the velocity exponent curves (figures 19a and 38c) to the static OASPL and PNL values. The peak OASPL suppression is reduced slightly in going from static to flight operation (from 6 dB to 5.5 dB). The in-flight OASPL suppression is less at low angles and greater at angles of 140° and higher. The peak PNL suppression is reduced significantly by flight going from 5.5 PNdB to 2.5 PNdB. This is due to the inverter having a peak static PNL at 120° in contrast to 135° for the baseline (figure 54). The reduction of PNL with forward velocity is much smaller for the inverter at 120° than the baseline at 135° and results in a substantial loss of peak PNL suppression. Generally suppressor nozzles have peak PNL values in the 110° to 120° region that are dominated by relatively high frequencies. The high frequencies originate close to the nozzle exit and experience small level reductions with forward velocity. In contrast, the peak PNL of the baseline is dominated by low frequencies having source locations further downstream. The low frequencies are substantially reduced by forward velocity providing a corresponding large reduction in PNL for the baseline. The in-flight PNL suppression is essentially zero at low angles but is greater than the static value at angles of 140° and higher. Basically the inverter is an effective suppressor of OASPL at angles of 120° and higher and PNL at 125° and higher.

The in-flight EPNL characteristics of the inverter and baseline are compared in figure 55. At takeoff power (600 m/s) the suppression is 4.0 EPNdB. This compares with a static data estimate of 5.0 EPNdB (figure 31) indicating a suppression loss of 1.0 EPNdB due to flight. The loss of EPNL suppression is due to the poor in-flight PNL suppression characteristics at low angles (figure 54).

5.4 INTERNAL MIXER ANALYSIS

Static and wind tunnel data for the 12 lobe internal mixer were measured using a JT8D-17 engine as reported in references 1 and 2.

5.4.1 STATIC DATA ANALYSIS

Static data were measured on a 30.5 m (100 ft) sideline and extrapolated to the far field using source location correlations reported in reference 1. Comparisons of OASPL, PNL, and EPNL are made with the baseline and inverter in the following section.

5.4.2 WIND TUNNEL DATA ANALYSIS

The wind tunnel data from the previous test were reprocessed using the technique described in section 5.1. Tunnel-off and tunnel-on OASPL and PNL directivities are shown in figure 56 for NPR 2.1 and 1.8. From these results the velocity exponent curves of figure 57 are determined.

Static and flight EPNL's are plotted versus primary relative velocity in figure 58. The procedure for calculation of the EPNL values was previously described in section 5.2.2. The in-flight EPNL values fall slightly above the throttle line similar to the baseline (figure 20). It is noted that the slope of the throttle line for the internal mixer is steeper than that of the baseline. Thus equal departure from the throttle line in terms of EPNL would show up as a gain in flight suppression for the internal mixer.

Static and flight OASPL and PNL directivities for the baseline, inverter, and internal mixer are compared in figures 59 and 60. The curves were defined in the manner described in section 5.3.2.5. The three configurations represent extremes in jet flow profile. The profile ranges from: the low velocity outer fan and high velocity inner primary flows (baseline); relatively well mixed fan and primary flows (internal mixer); to the high velocity outer primary and low velocity inner fan flows (inverter). The comparison of static OASPL shows that the inverter and internal mixer produce equal suppression at low angles (50^{o} to 110^{o}) but the inverter is significantly better at higher angles. The peak OASPL suppression for the inverter is about 6.0 dB while the internal mixer shows about 2 dB. In flight the internal mixer provides about 1 dB lower noise at low angles while the inverter noise is significantly lower at high angles. The in-flight peak OASPL suppression of the internal mixer improves relative to static operation, going from about 2 dB to 3 dB. The inverter experiences a slight loss of peak OASPL suppression due to flight, going from 6.0 dB to 5.5 dB.

The effect of flight on PNL suppression characteristics is more pronounced than observed for OASPL. Under static conditions (figure 60) the inverter and internal mixer show equal suppression at low angles but the inverter suppression at high angles is clearly superior. The peak PNL suppression of the internal mixer is about 2 PNdB as opposed to 5.5 PNdB for the inverter.

Under flight conditions the peak PNL suppression of the two configurations is approximately the same (2.5 PNdB). The internal mixer shows a slight gain in peak PNL suppression with forward velocity while the inverter undergoes a significant loss. The primary cause of peak PNL suppression loss for the inverter is the low static peak noise angle (120^{o}) and relatively small flight PNL reduction at this angle (see section 5.3.2.5). The internal mixer provides more PNL suppression at low angles; however, the inverter is the better suppressor of PNL at high angles.

Static and flight EPNL characteristics for the three configurations are compared in figures 61 and 62. At takeoff power (600 m/s) and with static PNL values, the EPNL suppressions are 2 EPNdB for the internal mixer and 5 EPNdB for the inverter. At lower power conditions the difference in suppression becomes smaller. It is noted that the internal mixer has less thrust loss than the inverter, as configured for this test. A slight improvement in low power suppression would result for the internal mixer relative to the inverter for equal in-flight thrust.

At takeoff power the in-flight EPNL suppression values are 3 EPNdB for the internal mixer and 4 EPNdB for the inverter. Relative to static operation this represents a gain in suppression of 1 EPNdB for the internal mixer and a loss of 1 EPNdB for the inverter. At a jet velocity of 500 m/s the in-flight suppression of the two configurations is equal (about 3 EPNdB).

On the basis of these comparisons the inverted flow profile will produce about 1 EPNdB lower noise in flight than the internal mixer at takeoff power. At lower power settings the two concepts are basically equivalent. There is a trend indicated that increasing the primary jet velocity above 600 m/s will favor the suppression potential of the inverted flow profile. Higher jet velocities will tend to shift the static peak noise of the inverter to a higher angle where a more favorable flight effect will result. This will help in reducing the in-flight EPNL in relation to the baseline and internal mixer. This is of importance to AST engines where primary jet velocities of about 760 m/s will be required during takeoff operations.

5.5 INVERTER/PLUG ANALYSIS

5.5.1 STATIC DATA ANALYSIS

Static data for the inverter/plug configuration are compared with the baseline and inverter configurations in figures 63 to 65. The spectra plots of figure 63 show that only a slight reduction of SPL occurs relative to the baseline at low angles. The reduction at higher angles (figure 64) is more substantial at all frequencies. When compared with the inverter spectra the inverter/plug produces lower high frequency noise (figure 65). The low frequency noise at angles near the jet axis (140^{o}) is slightly higher, however.

OASPL and PNL directivities are compared in figure 65 for a NPR of 2.2. The inverter/plug produces lower noise in the low angle region primarily because of the reduced high frequency noise. The inverter/plug peak PNL suppression is slightly greater than the inverter (6.0 versus 5.5 PNdB). The peak OASPL suppression of the inverter/plug is slightly less (5 versus 6 dB). At angles near the jet axis the inverter produces lower OASPL and PNL than the inverter/plug. This is the result of reduced low frequency noise in this region that is generated by the inverter.

5.5.2 WIND TUNNEL DATA ANALYSIS

Wind tunnel test results for the inverter/plug are provided in figures 66 to 70. Tunnel-off and tunnel-on spectra are compared in figure 66 for an NPR of 2.1 and a range of angles from 60^{o} to 150^{o}. In general, the effect of tunnel velocity on the inverter/plug spectra is comparable with the inverter (figure 34); that is, relatively small reduction of SPL at low angles with increasing reduction at higher angles.

Tunnel-off and tunnel-on OASPL and PNL directivities are shown in figure 67 for NPR's of 2.1 and 1.8. Tunnel velocity causes a small reduction of OASPL and PNL at low angles (50^{o} to 100^{o}). The amount of reduction increases at higher angles with maximum reduction occurring in the 140^{o} to 145^{o} range. Velocity index values are calculated from the results of figure 67 and are plotted in figure 68. At an NPR of 2.1 and 649 m sideline the velocity exponent values for the inverter/plug at low angles are slightly greater than the values for the inverter (figure 38c). At high angles the inverter n values are larger indicating greater reduction of noise with forward velocity in this region relative to the inverter/plug.

OASPL and PNL are plotted as a function of primary relative velocity in figure 69 for several angles. The reduction of OASPL and PNL with tunnel velocity follows relative velocity at high angles (figure 69c) but not at low angles (figures 69a and 69b). This result is consistent with trends observed for the inverter configuration (figure 51).

Static and flight EPNL's are plotted versus primary relative velocity in figure 70. The relationship of the flight EPNL values with the throttle line is similar to results obtained for the inverter (figure 52). Static and flight OASPL, PNL and EPNL characteristics of the inverter/plug are compared with the baseline and other inverter configurations in section 5.7.

5.6 INVERTER/MIXER ANALYSIS

The inverter/plug configuration was tested with a 20 lobe external mixing nozzle. This configuration was tested with and without an acoustically lined shield that was designed to reflect and absorb pre-merged mixing noise (see figures 6 and 7). Results and analysis for both mixer configurations are presented and described in this section.

5.6.1 STATIC DATA ANALYSIS

Static spectra comparisons are made for the baseline and inverter/mixer configurations with and without shield in figure 71. The 20 lobe nozzle configuration produces a large reduction in low frequency noise relative to the baseline, in particular at angles near the jet axis (figure 71b). A significant component of pre-merged mixing noise is generated by the mixing between the primary jets and the entrained ambient air. This frequency component is centered at about 1250 Hz and causes a crossover of noise relative to the baseline at the lower angles (figure 71a). The lined shield markedly reduces the pre-merged mixing noise component at all angles. The greatest reduction (up to 10 dB) occurs at angles near the jet axis (140^{o}, figure 71b). The reduction is also considerable at low angles (figure 71a) with the pre-merged component lowered by about 5 to 6 dB. The shield is least effective in the region of peak noise (120^{o}, figure 71b) where only 2 to 3 dB reductions are observed. It is known from model tests that the effectiveness of a shield is very sensitive to shield size, orientation, and spacing relative to the noise source. It is likely that a shield of similar dimensions could be designed to more effectively reduce the pre-merged noise in the region of peak noise. There is also a change in low frequency noise that results when the shield is installed. The shield causes an increase in the low frequency noise at low angles (figure 71a). This may be caused by a slight directivity change in the shielded jet since the jet is turned toward the shield. The jet turning is the result of low pressure created between the jet and shield by the jet pumping process.

Static OASPL and PNL directivities are provided in figure 72 for the baseline and 20 lobe mixer configurations. The comparison reflects an NPR of 2.2 and a sideline of 649 m. The mixer is an effective suppressor of OASPL, relative to the baseline, at all angles. A peak OASPL suppression of about 9.5 dB is achieved. The shield has a small effect on OASPL providing an additional 1 dB reduction in peak OASPL. The mixer provides little suppression of PNL at low angles (50^{o} to 110^{o}) but substantially reduces PNL at the higher angles. The peak PNL suppression is 5 PNdB; however, the suppression at 140^{o} is about 9.5 PNdB. The shield is effective in reducing the PNL at all angles but shows more reduction at off-peak noise locations. The peak PNL suppression of the shielded configuration is about 7.5 PNdB while the suppression at 140^{o} is 13 PNdB.

5.6.2 WIND TUNNEL DATA ANALYSIS

Tunnel-off and tunnel-on takeoff power spectra are compared for the 20 lobe mixer in figure 73 and for the mixer with shield in figure 74. Wind tunnel velocity reduces the low frequency noise at high angles by a substantial amount (figure 73c). At low angles (figures 73a and 73b) the low frequencies are reduced by a modest amount. The pre-merged mixing noise component undergoes a slight increase (figure 73a) or slight decrease (figures 73b and 73c) with tunnel velocity, depending upon angle. The effect of tunnel velocity on the mixer with shield configuration is quite similar to the effect on the mixer without shield (figure 74).

Tunnel-off and tunnel-on OASPL and PNL directivities are provided in figures 75 and 76 for the 20 lobe mixer without and with shield. The data reflect an NPR of 2.1 and a sideline of 649 m. At low angles forward velocity has little effect on the OASPL or PNL of the 20 lobe mixer configuration (figure 75). At angles from 50^{o} to 60^{o} a slight increase in noise results while at angles from 70^{o} to 100^{o} a slight decrease in noise occurs with increasing tunnel velocity. A modest reduction of peak noise is observed with larger reductions at angles near the jet axis. The same trends with tunnel velocity are observed for the 20 lobe nozzle with shield (figure 76).

The results of figures 75 and 76 and similar data for NPR 1.8 are used to define the velocity exponent curves of figures 77 and 78. In general the velocity exponent characteristics for the 20 lobe nozzle with shield are superior to the configuration without shield. The shielded configuration produces higher velocity exponents at angles of 120^{o} and above for the takeoff power condition (figures 77a and 78a). This is the result of the lower pre-merged mixing noise in the shielded spectra (figure 71b) where both OASPL and PNL are dominated by low frequency. The low frequency noise experiences a more favorable flight effect than the higher pre-merged frequencies that are more dominant in the spectra of the mixer without shield.

Tunnel-off and tunnel-on OASPL and PNL values are plotted as a function of primary relative velocity in figures 79 and 80 for the 20 lobe mixer without and with shield. For the mixer without shield the reduction of OASPL and PNL with tunnel velocity is small at low angles compared with the throttle line (figure 79a). At 60^{o} and high power the noise is observed to increase slightly with forward velocity. At 140^{o} and 150^{o} (figures 79c and 79d) the tunnel-on data follow a slope close to that of the throttle line. That is, the in-flight OASPL and PNL can be predicted by applying the relative velocity principle. The relative velocity trends for the mixer with shield are basically the same as those observed for the mixer without shield (figure 80).

Static and flight EPNL's are plotted versus primary relative velocity in figures 81 and 82 for the two 20 lobe mixer configurations. In each case the flight EPNL shows a significant departure from the throttle line. This is the result of the small reductions in PNL at low angles through peak that occur with forward velocity.

Static and flight OASPL, PNL, and EPNL for the 20 lobe mixer with and without shield are compared with the baseline, inverter, and inverter/plug configurations in section 5.7.

5.7 COMPARISON OF STATIC AND FLIGHT NOISE OF INVERTER CONFIGURATIONS

Static and flight OASPL, PNL, and EPNL comparisons are provided in figures 83 to 86 for the family of inverter configurations evaluated in this report. The static noise levels are based on Boardman 30.5 m (100 ft) sideline data that are extrapolated to a 649 m (2128 ft) sideline using source location correlations. The flight noise levels are based on 40 by 80 wind tunnel results and are defined by applying velocity exponents to the static data. Peak suppression values for OASPL, PNL, and EPNL are defined relative to the baseline and are summarized in table 3.

5.7.1 OASPL DIRECTIVITY COMPARISON

Static and flight OASPL directivities are compared in figure 83 for the various inverter configurations. Under static conditions the peak OASPL suppression ranges from 5.0 dB for the inverter/plug to 10.5 dB for the inverter with 20 lobe mixer nozzle plus shield (table 3). The in-flight peak OASPL suppression ranges from 5.0 dB for the 20 lobe nozzle to 7.0 dB for the 20 lobe nozzle with shield. The inverter/plug peak OASPL suppression is slightly higher in flight than under static conditions (6 versus 5 dB). The biggest loss of peak OASPL suppression due to flight is experienced by the 20 lobe nozzle in going from 9.5 to 5 dB. In general, the inverter family provides significant OASPL suppression at angles of 120^{o} and higher during flight. The OASPL suppression at lower angles (50^{o} to 110^{o}) is modest.

5.7.2 PNL DIRECTIVITY COMPARISON

Static and flight PNL directivities are compared in figure 84 for the inverter configurations. During static operation the peak PNL suppression varies from 5 PNdB for the 20 lobe nozzle to 7.5 PNdB for the 20 lobe nozzle with shield. Forward velocity causes a significant loss in peak noise suppression. The in-flight suppression values range from 0.5 PNdB for the 20 lobe nozzle to 3.5 PNdB for the inverter/plug. The loss of peak PNL suppression varies from 2.5 PNdB for the inverter/plug to 4.5 PNdB for the 20 lobe nozzle with and without shield.

The relatively low in-flight peak PNL suppression values are primarily the result of where the static peak PNL's occur. The inverter configurations have peak PNL's at relatively low angles (110^{o} to 120^{o}) compared with the baseline (135^{o}). The reduction in PNL with forward velocity is considerably less at low angles than at high angles. For this reason the inverter configurations experience a significant loss of peak noise suppression due to flight.

The in-flight PNL suppression of the inverter configurations is substantial at angles of 130^{o} and higher. At low angles (50^{o} to 110^{o}) these configurations are not effective in reducing PNL relative to the baseline.

5.7.3 EPNL SUPPRESSION COMPARISON

Static and flight EPNL comparisons are made for the inverter configurations in figures 85 and 86. The static EPNL results of figure 85 assume that PNL's, measured under static conditions, are not changed with forward velocity. The resulting static EPNL suppression values range from about 5 EPNdB for the basic inverter to nearly 10 EPNdB for the inverter/20 lobe nozzle with acoustic shield at takeoff power (600 m/s).

Under flight conditions (figure 86) the inverter, inverter/plug, and inverter/20 lobe nozzle all have EPNL suppression values of about 4 EPNdB at takeoff power. The largest in-flight suppression is provided by the 20 lobe nozzle with acoustic shield (7.5 EPNdB). Although the in-flight EPNL suppression is less than static, the loss is relatively modest. The EPNL suppression is 1 EPNdB lower for the basic inverter and 3 EPNdB lower for the 20 lobe nozzle in going from static to flight conditions.

It is evident from the comparison of figure 86 that the 20 lobe nozzle with acoustic shield has considerable potential for reducing in-flight EPNL. This potential is the result of rapid mixing of the high velocity primary with ambient air and subsequent removal of the high frequency pre-merged mixing noise. The 20 lobe nozzle without shield is not effective at low power but improves significantly as the primary velocity increases. At high primary velocity the post-merged mixing noise becomes more dominant in relation to the pre-merged mixing noise. The resulting flight effects are more favorable and the in-flight suppression potential of this configuration improves. At an extrapolated primary velocity of 650 m/s the EPNL suppression of the 20 lobe nozzle is estimated to be 1 EPNdB greater than the basic inverter. This favorable trend with increasing primary velocity makes the 20 lobe nozzle (or similar external mixing nozzle) more attractive for application with high velocity engines such as those being studied for AST.

5.8 ENGINE/INVERTER DUCT PERFORMANCE

Thrust performance characteristics of the inverter configurations are compared in figure 87. The performance is presented as thrust coefficient (C_V) versus pressure ratio of the mixed flow. The thrust data were measured during the Boardman static test with a bell mouth inlet replacing the two ring acoustic inlet. At takeoff power ($PTM7/P_{amb} = 2.1$) thrust loss values are 1.5% for the basic inverter, 3.0% for the inverter/plug, and 5.0% for the inverter/20 lobe nozzle relative to the baseline (figure 87a). The 20 lobe nozzle with shield was not tested with a bell mouth inlet. Performance characteristics of the 20 lobe nozzle with and without shield are compared in figure 87b where both configurations included the two ring inlet. No significant difference in thrust coefficient is evident due to the presence of the shield. It is noted that force balance data were not measured during the 40 by 80 test; thus the effect of forward velocity on thrust performance is not known.

Representative results of the inverted flow total pressure and temperature surveys are provided in figures 88 to 90. The data are for a takeoff power (NPR 2.1) and are typical of

results obtained at other engine power conditions. Lines of constant total pressure are plotted in figure 88 for one quadrant of the nozzle exit station. The lobe formation is typical of this type of flow ducting. An assessment of total pressure loss due to the inverter duct is difficult to make from these measurements. On the basis of the thrust coefficient loss for this configuration (1.5%) it is estimated that the effective total pressure loss of both streams is 2.5 to 3.0%.

The total temperature data of figure 89 show that the high temperatures associated with the primary are confined to the outer flow region. The temperature profile in this region is far from uniform and indicates a lobe characteristic similar to the total pressure results of figure 88. The temperature lobe is caused by heat transfer between the primary and fan streams within the inverter duct and downstream of the duct prior to exhausting from the nozzle.

The total pressure and temperature data are combined to define the exhaust velocity plot provided in figure 90. The lobe characteristic is evident in the outer flow region and reflects similar results obtained for both total pressure and total temperature profiles. The influence of the non-uniform flow region on noise characteristics is difficult to assess but is probably minor.

5.9 MODEL RESULTS

Model tests were conducted by Boeing prior to the JT8D engine inverted flow program. The one-seventh scale models were tested under static conditions to determine the influence of flow profile on jet noise characteristics. Some of the model data are included in figures 91 and 92 for comparison with full scale results. Model OASPL and PNL directivities are shown in figure 91 for the baseline (uninverted), mixed, and inverted flow profiles. The results are for a takeoff power condition and a 457 m sideline. Similar OASPL and PNL directivity curves are provided for the full scale engine in figures 59 and 60, but for a 649 m sideline. The model data indicates larger OASPL and PNL suppression than the full scale data for both the inverter and internal mixer. Recent findings show that the baseline model data is high by several dB relative to the suppressors. This is based on comparisons with full scale results and recent model tests in a new facility. The model OASPL directivity characteristics of the internal mixer relative to the inverter are similar to full scale results (figures 91 and 59). The same comparison for PNL directivity indicates significant differences between model and full scale results (figures 91 and 60). The full scale data show the inverter PNL's to be lower relative to the internal mixer at angles up to about 150^{o}.

Model and full scale peak PNL values are plotted versus velocity ratio in figure 92. The model data indicate minimum PNL at a partially inverted velocity ratio. A partially inverted flow profile assumes that the interchange of primary and fan streams is not complete. Thus the average outer flow velocity is slightly less than the fully inverted primary velocity while the average inner velocity is slightly greater than the fully inverted fan velocity. The full scale results show that the peak noise of the fully inverted flow is lower than the fully mixed flow. This finding is not necessarily contrary to the model results. The model velocity profiles were relatively more uniform than the full scale profiles for a given outer or inner velocity regime. The engine internal mixer did not provide a uniform, fully mixed flow nor the inverter a uniform inverted profile. The resulting unique flow profiles for the

internal mixer and inverter could explain the different model and full scale curve shapes in figure 92. For example, the poorly mixed, high velocity regions in the internal mixer flow could raise the peak PNL relative to a uniform profile. In contrast, the non-uniformity of the inverted profile may be representative of a partially inverted flow and cause a reduction in peak PNL relative to a uniform, fully inverted profile. These two occurrences would justify the shape of the full scale curve. In effect, the full scale internal mixer and inverter data points are plotted at an invalid velocity ratio and should be shifted toward the right in figure 92. The magnitude of the shift is difficult to evaluate but would be in a direction to make the model and full scale curves more alike.

The model and full scale comparisons indicate that model profile tests can be used to indicate general trends. Full scale engines designed for a unique profile will likely include significant non-uniformities in flow profiles. This may make accurate predictions of full scale noise levels from model results difficult to achieve for both static and flight conditions.

6.0 CONCLUSIONS

The following conclusions are made as a result of the test program to determine static and wind tunnel-derived flight noise characteristics of the JT8D-17R engine with inverted primary and fan flows. The suppression results described are relative to the baseline configuration (uninverted flow) and reflect takeoff power at a 649 m sideline.

6.1 BASIC INVERTER

1. The basic inverter configuration (inverter with conical nozzle) provides an in-flight EPNL suppression of 4.0 EPNdB. The comparable static suppression (summation of static PNL's) is 5.0 EPNdB, indicating a relatively modest loss of EPNL suppression due to flight.

2. Forward velocity causes a significant loss of peak PNL suppression. The in-flight peak PNL suppression is 2.5 PNdB compared with a static value of 5.5 PNdB. The inverter is effective in suppressing PNL at angles of 130^{o} and higher but ineffective at lower angles where the inverter peak noise occurs.

3. The influence of forward velocity on OASPL suppression is relatively small. The peak OASPL suppression changes from 6.0 dB to 5.5 dB in going from static to flight conditions. Significant in-flight OASPL suppression is achieved at angles of 120^{o} and higher. Suppression of OASPL at lower angles is modest.

4. The inverted flow provides lower EPNL than the mixed flow under both static and flight conditions. Static EPNL suppression is 5.0 EPNdB for the inverter and 2.0 EPNdB for the internal mixer. The in-flight suppression values are 4.0 and 3.0 EPNdB respectively.

5. The inverter configuration experienced a thrust loss of 1.5% relative to the baseline. The lower thrust is largely due to total pressure losses in the primary/fan inverter duct.

6.2 INVERTER/PLUG

1. Replacing the conical nozzle with a plug nozzle produced minor reductions in the flight noise levels determined for the basic inverter. Improvements in peak OASPL and PNL suppression values were 0.5 dB and 1.0 PNdB respectively. The in-flight EPNL suppression was virtually the same for the two nozzle configurations.

2. The inverter/plug had a thrust loss of 3.0% compared with 1.5% for the basic inverter. The additional thrust loss may have contributed to the slightly lower noise levels generated by this configuration.

6.3 INVERTER/20 LOBE MIXER

1. The inverter with 20 lobe mixer nozzle provided improved static EPNL suppression when compared with the basic inverter (7.0 versus 5.0 EPNdB). In-flight suppression values were equal indicating a larger loss of EPNL suppression for the 20 lobe configuration with forward velocity.

2. The inverter with 20 lobe nozzle and lined acoustic shield produced the lowest EPNL for both static and flight operation. A static EPNL suppression of about 10 EPNdB was achieved while the flight suppression was 7.5 EPNdB. The improved suppression was caused by the absorption and reflection of high frequency pre-merged mixing noise.

3. The thrust loss of the 20 lobe nozzle configurations was 5%. The thrust loss, weight, and design integration factors must be considered in evaluating potential applications for this suppressor concept.

6.4 MODEL RESULTS

1. Static model data for the JT8D baseline, internal mixer, and inverter indicate trends similar to those measured for the full scale engine. This includes OASPL and PNL directivities and peak PNL as a function of flow profile velocity ratio. Some differences in model and full scale results are noted, but are generally explainable due to non-uniformity in the full scale flow profiles.

REFERENCES

1. Strout, F. G.; *Flight Effects on Noise Generated by the JT8D-17 Engine in A Quiet Nacelle and a Conventional Nacelle as Measured in the NASA-Ames 40- by 80-Foot Wind Tunnel*, NASA CR-137797, January 1976.

2. Strout, F. G., *Flight Effects on Noise Generated by the JT8D-17 Engine in a Quiet Nacelle and a Conventional Nacelle as Measured in the NASA-Ames 40- by 80-Foot Wind Tunnel – Summary Report*, NASA CR-2576, June 1976.

3. Jaeck, C. L., *Static and Wind Tunnel Near Field/Far Field Jet Noise Measurements from Model Scale Single-Flow Baseline and Suppressor Nozzles – Summary Report*, NASA CR-2841, June 1977.

Table 1.—Acoustic Test Conditions and Microphone Locations for Boardman Static Test

Configuration		Nozzle pressure ratio
Baseline		1.05; 1.1; 1.2; 1.3; 1.4; 1.5; 1.6; 1.7; 1.8; 1.9; 2.0; 2.1; 2.2
Inverter		1.05; 1.1; 1.2; 1.3; 1.4; 1.5; 1.6; 1.7; 1.8; 1.9; 2.0; 2.1; 2.2
Inverter/Plug		1.05; 1.1; 1.2; 1.3; 1.4; 1.5; 1.6; 1.7; 1.8; 1.9; 2.0; 2.1; 2.2
Inverter/Mixer		1.05; 1.1; 1.2; 1.3; 1.4; 1.5; 1.6; 1.7; 1.8; 1.9; 2.0; 2.1; 2.2
Inverter/Mixer/Hard Shield		1.1; 1.4; 1.6; 1.8; 2.1; 2.2
Inverter/Mixer/Lined Shield		1.1; 1.4; 1.6; 1.8; 2.1; 2.2
Microphone sideline	Type	Microphone angle
3.05 m (10 ft)	C/L	30^{o}, 40^{o}, 50^{o}, 60^{o}, 70^{o}, 80^{o}, 90^{o}, 100^{o}, 110^{o} 120^{o}, 130^{o}, 140^{o}, 150^{o}, 155^{o}, 160^{o}, 165^{o}
15.2 m (50 ft)	ground	30^{o}, 40^{o}, 50^{o}, 60^{o}, 70^{o}, 80^{o}, 90^{o}, 100^{o}, 110^{o}, 120^{o}, 130^{o}, 140^{o}, 150^{o}, 155^{o}, 160^{o}
30.5 m (100 ft)	ground	50^{o}, 60^{o}, 70^{o}, 80^{o}, 90^{o}, 100^{o}, 110^{o}, 120^{o}, 130^{o}, 140^{o}, 150^{o}, 155^{o}

Table 2.—Test Conditions for 40- by 80-Foot Wind Tunnel Test

Configuration	Tunnel velocity (knots)	Nozzle pressure ratio
Inverter	0	1.1; 1.3; 1.4; 1.5; 1.6; 1.8; 1.9; 2.1
	100	1.1; 1.4; 1.6; 1.8
	150	1.6; 1.8; 2.1
	185	2.1
Inverter/Plug	0	1.3; 1.4; 1.6; 1.8; 2.1
	100	1.4; 1.6; 1.8
	150	1.6; 1.8; 2.1
	185	2.1
Inverter/Mixer	0	1.3; 1.4; 1.6; 1.8; 2.1
	100	1.4; 1.6; 1.8
	150	1.8; 2.1
	185	2.1
Inverter/Mixer/Shield	0	1.4; 1.6; 1.8; 2.1
	100	1.6; 1.8
	150	1.8; 2.1
Inverter and Inverter/Mixer	100	1.0 - Noise Floor
	150	1.0
	185	1.0
Inverter/Mixer/Shield	100	1.0

Table 3.—Summary of Inverter Suppression Characteristics

Configuration	OASPL suppression—db			PNL suppression—PNdB			EPNL suppression—EPNdB		
	Static	Flight	Change	Static	Flight	Change	Static	Flight	Change
Inverter	6.0	5.5	-0.5	5.5	2.5	-3.0	5.0	4.0	-1.0
Inverter/Plug	5.0	6.0	+1.0	6.0	3.5	-2.5	5.2	4.0	-1.2
Inverter/20 Lobe	9.5	5.0	-4.5	5.0	0.5	-4.5	7.0	4.0	-3.0
Inverter/20 Lobe with Lined Shield	10.5	7.0	-3.5	7.5	3.0	-4.5	9.8	7.5	-2.3
Internal Mixer	2.0	3.0	+1.0	2.0	2.5	+0.5	2.0	3.0	+1.0

Note: Peak noise suppression relative to baseline at takeoff power and 649m (2128 ft) sideline

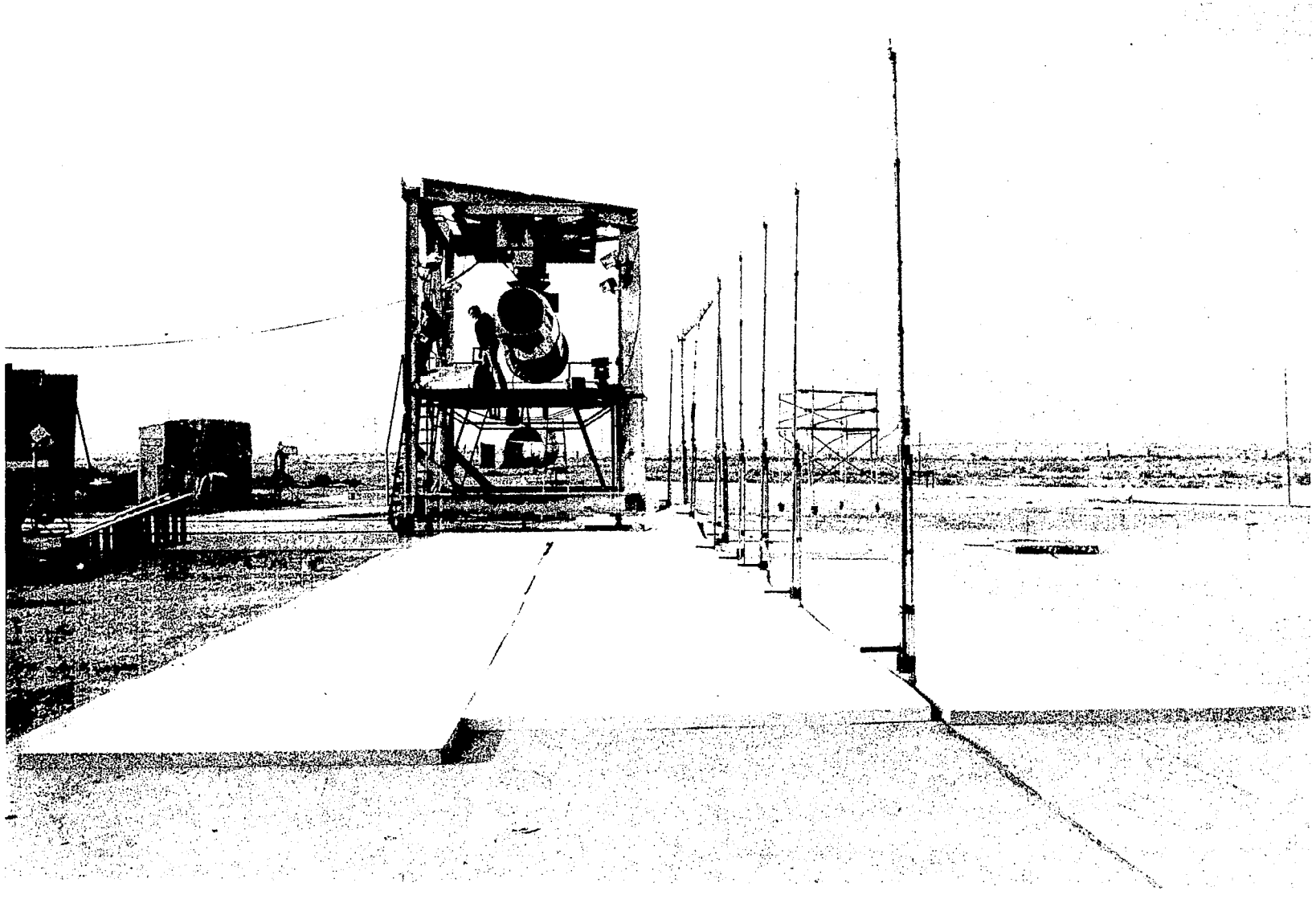

Figure 1.—Static Test Installation, Inverter Configuration

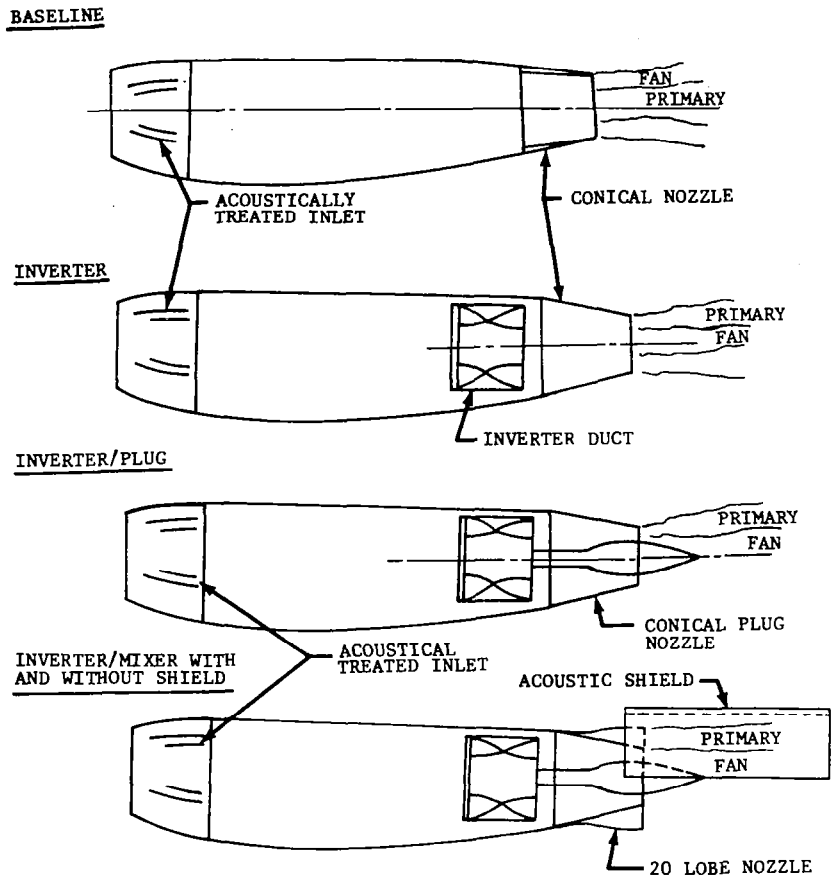

Figure 2.—Test Configuration Schematic

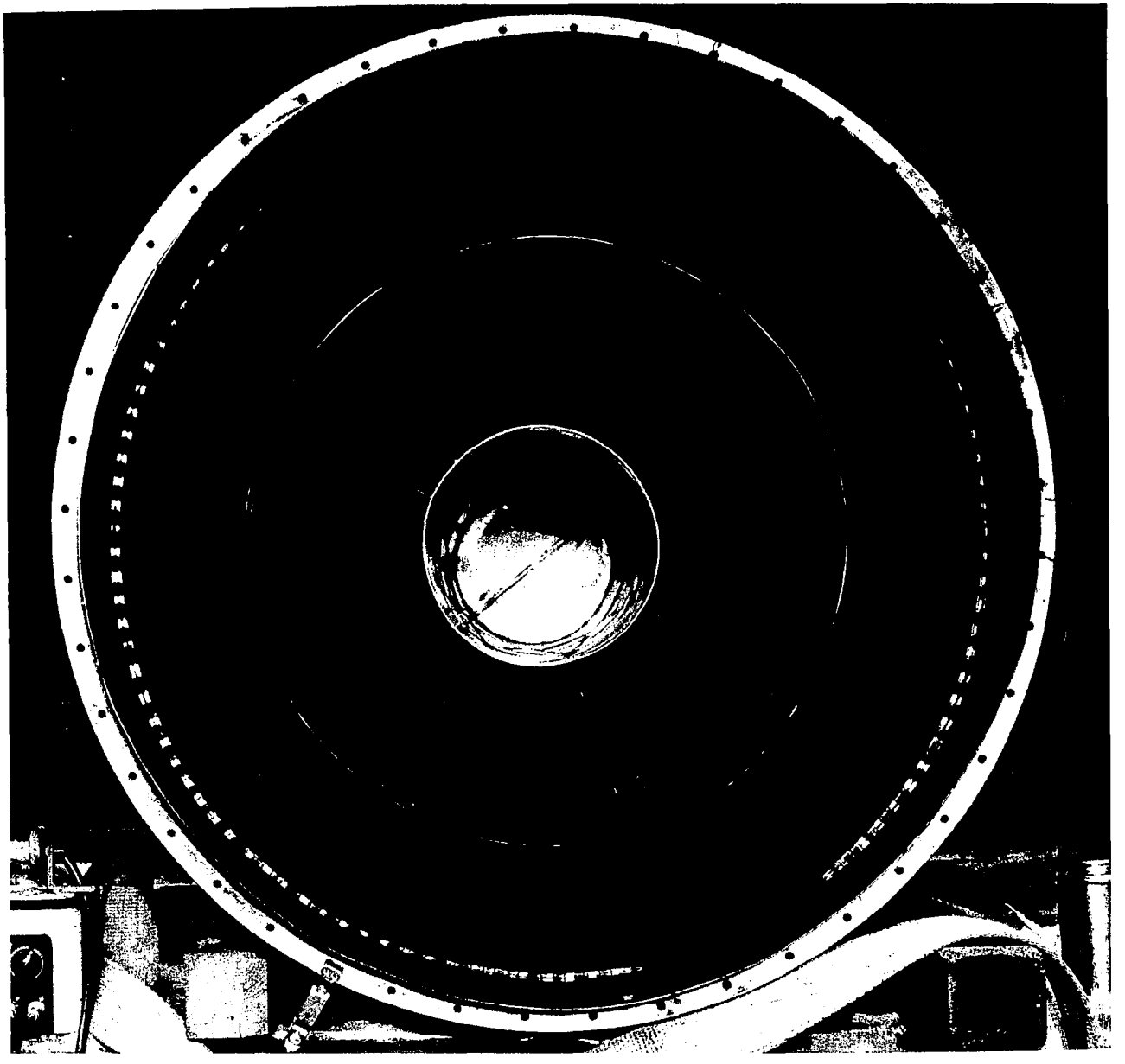

Figure 3.—Primary/Fan Flow Inverter, Exit Station

Figure 4.—Test Installation in 40 by 80 Wind Tunnel

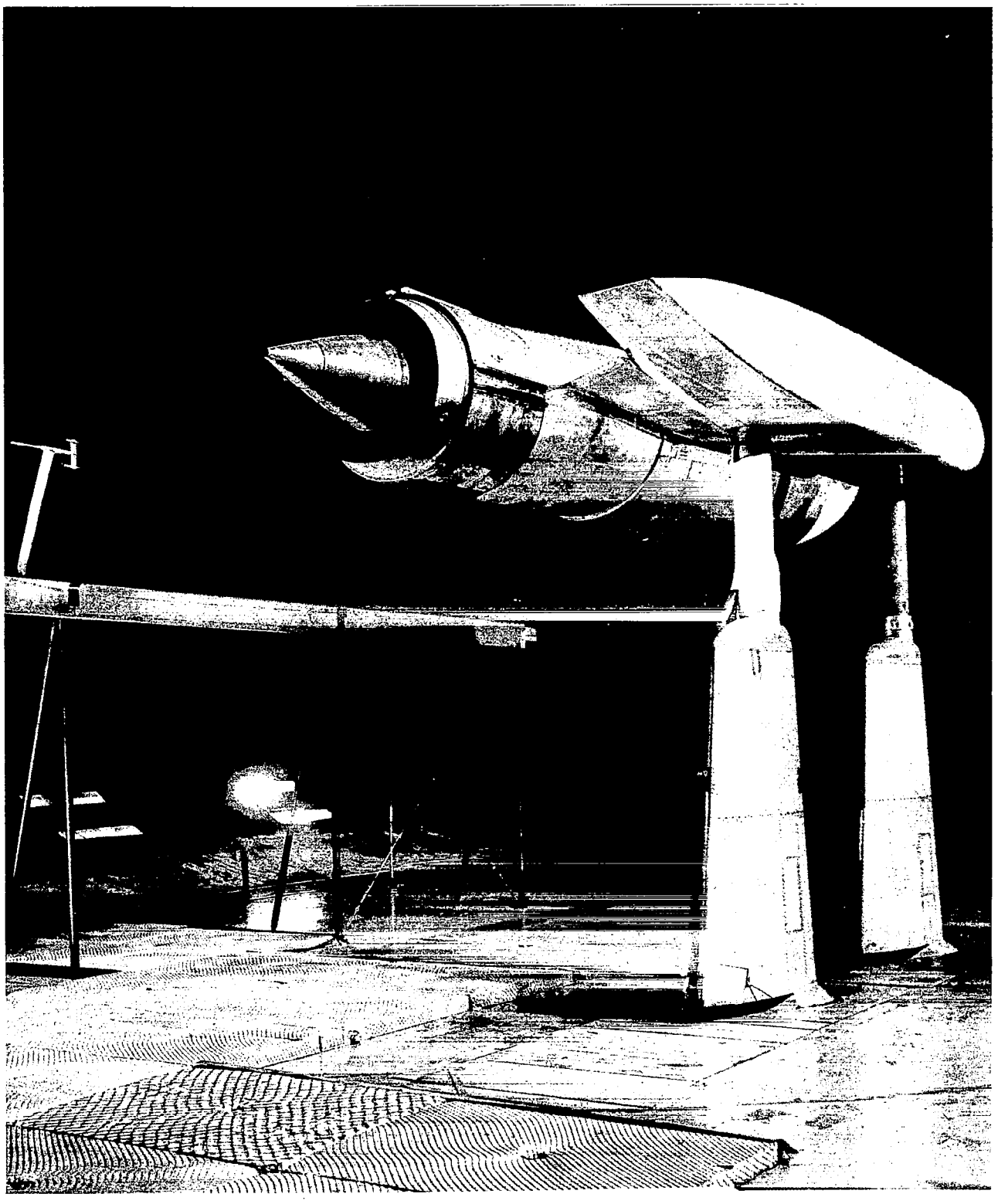

Figure 5.—Inverter/Plug Configuration

Figure 6.—Inverter/20 Lobe Mixer Configuration

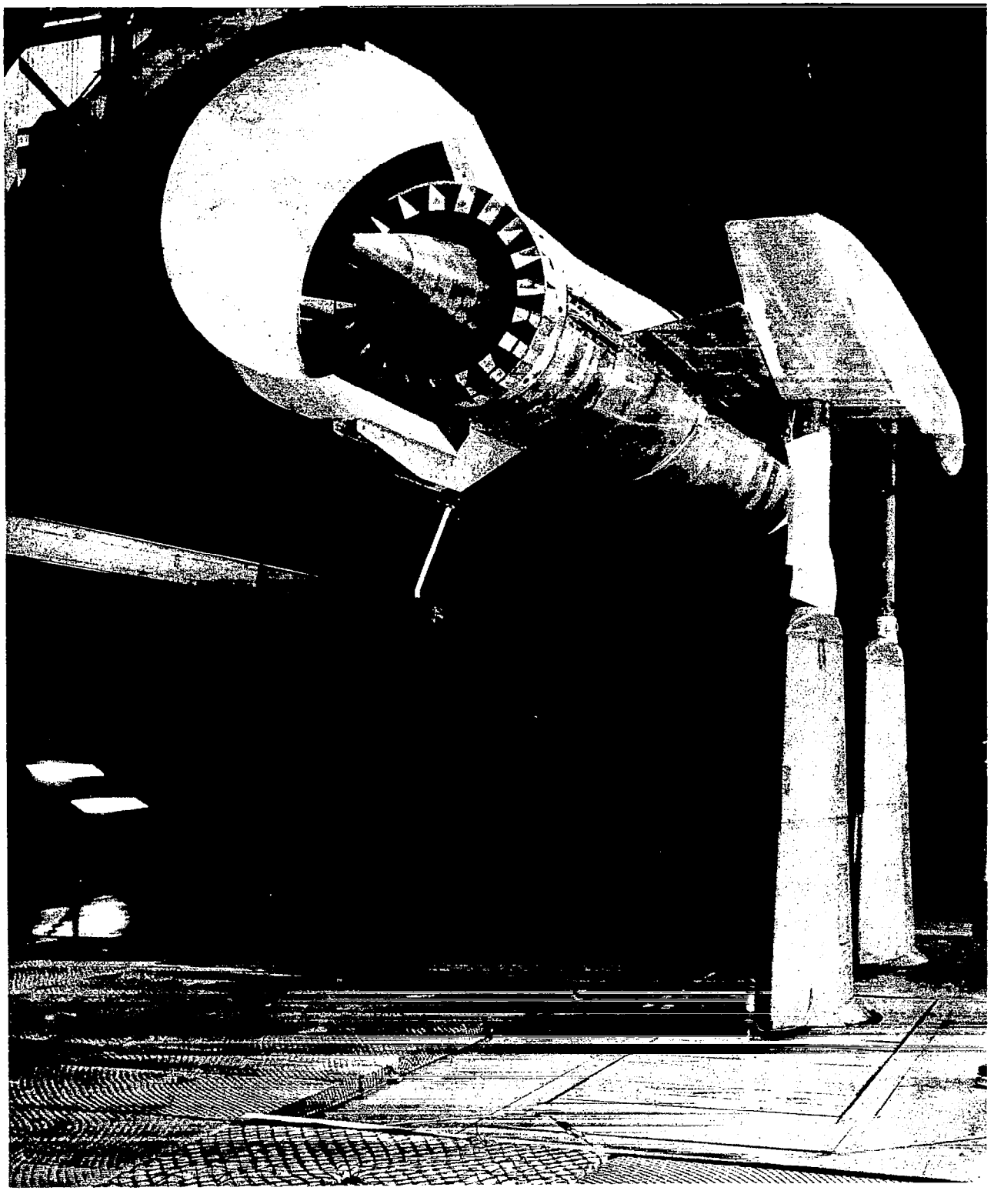

Figure 7.—Inverter/20 Lobe Mixer Configuration with Acoustic Shield

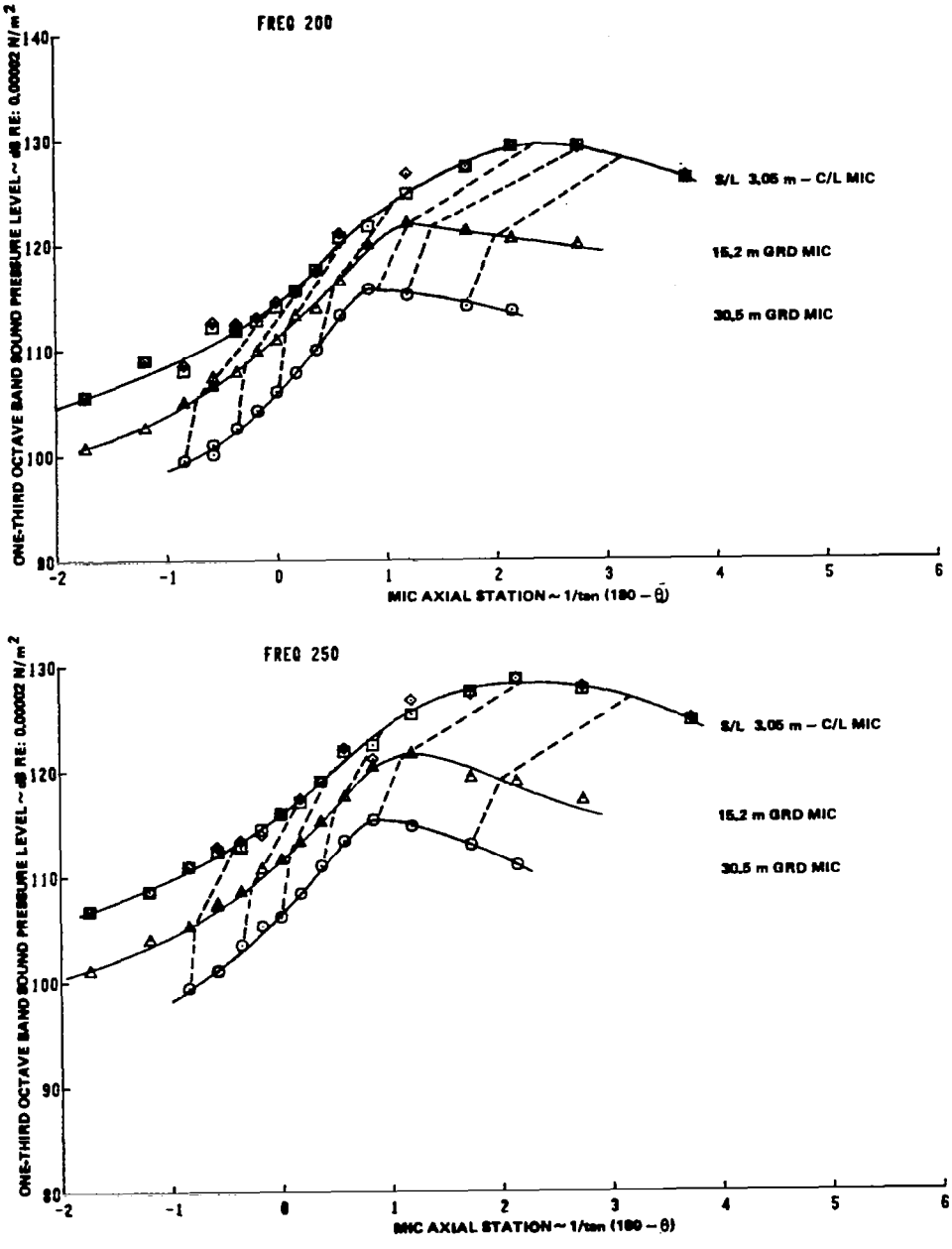

(a) Freq 200 & 250

Figure 8.—Multiple Sideline SPL Directivity JT8D-17R Engine with Inverter Configuration

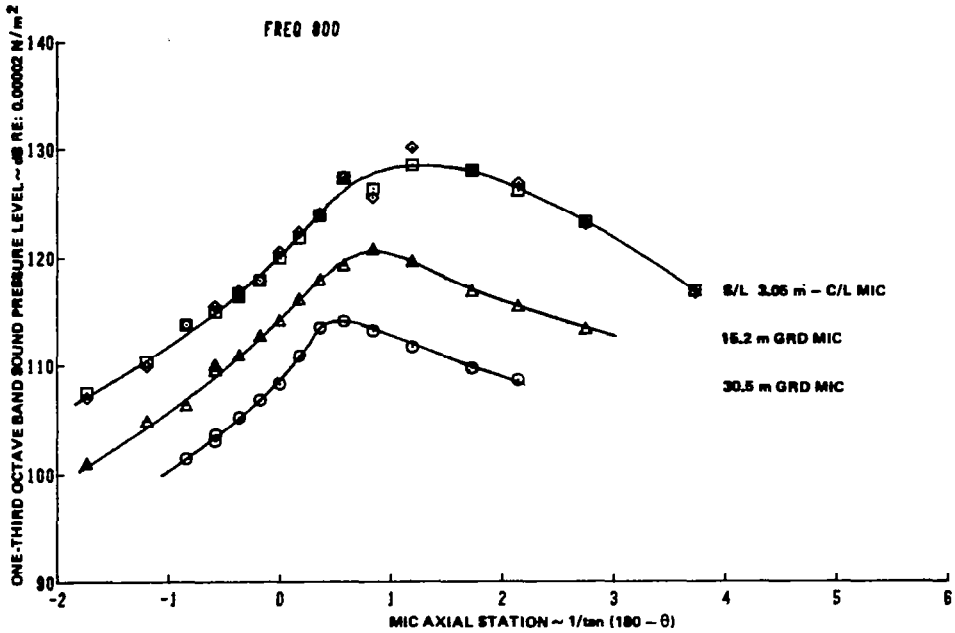

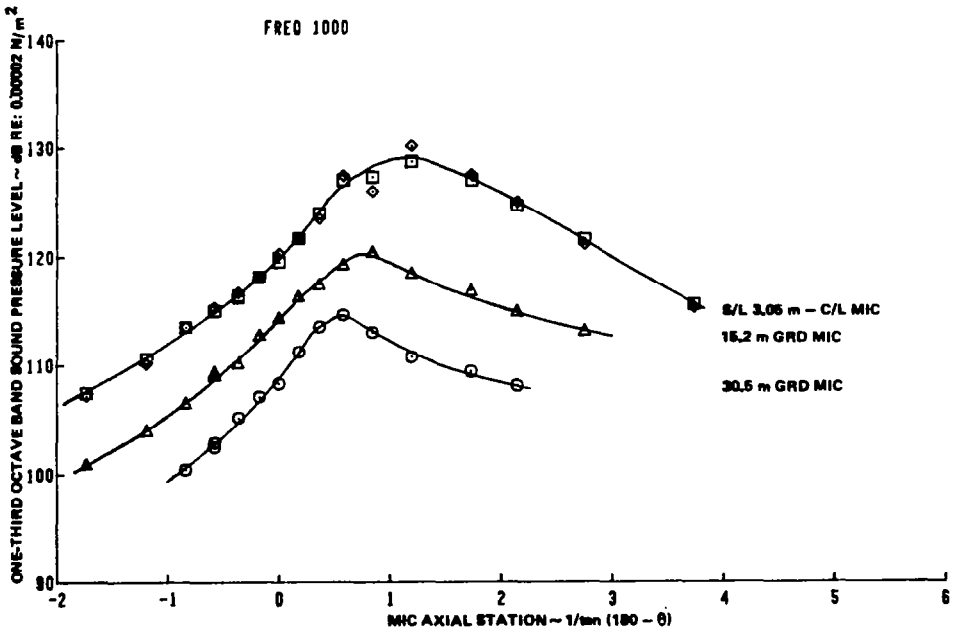

(b) Freq 800 & 1000

Figure 8.—(Continued)

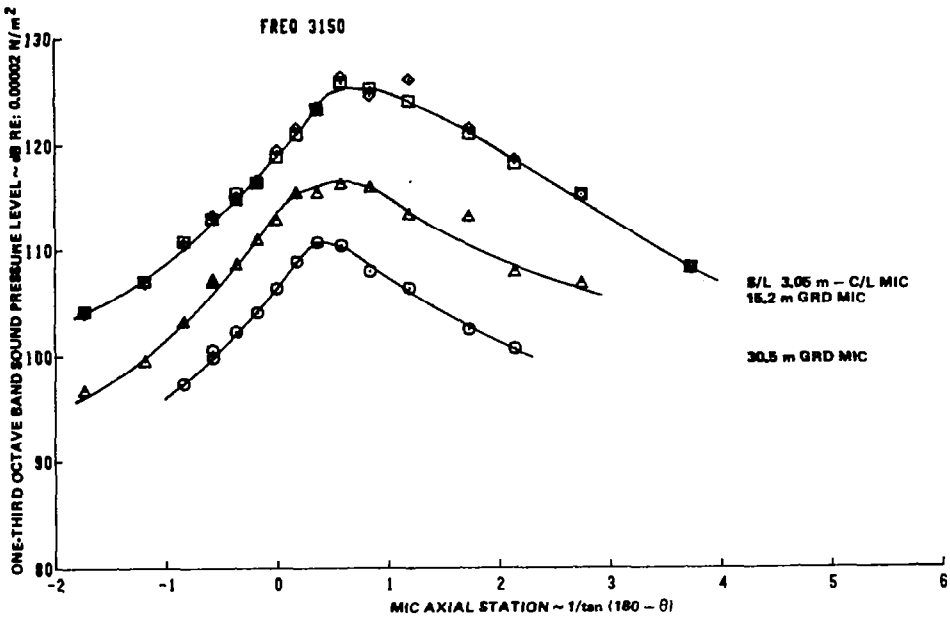

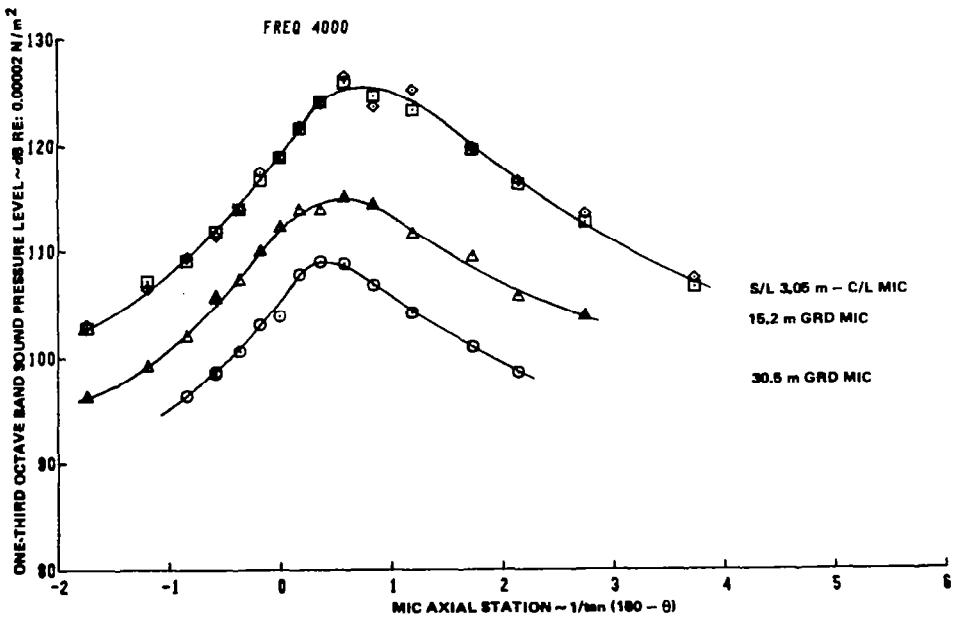

(c) Freq 3150 & 4000

Figure 8.—(Concluded)

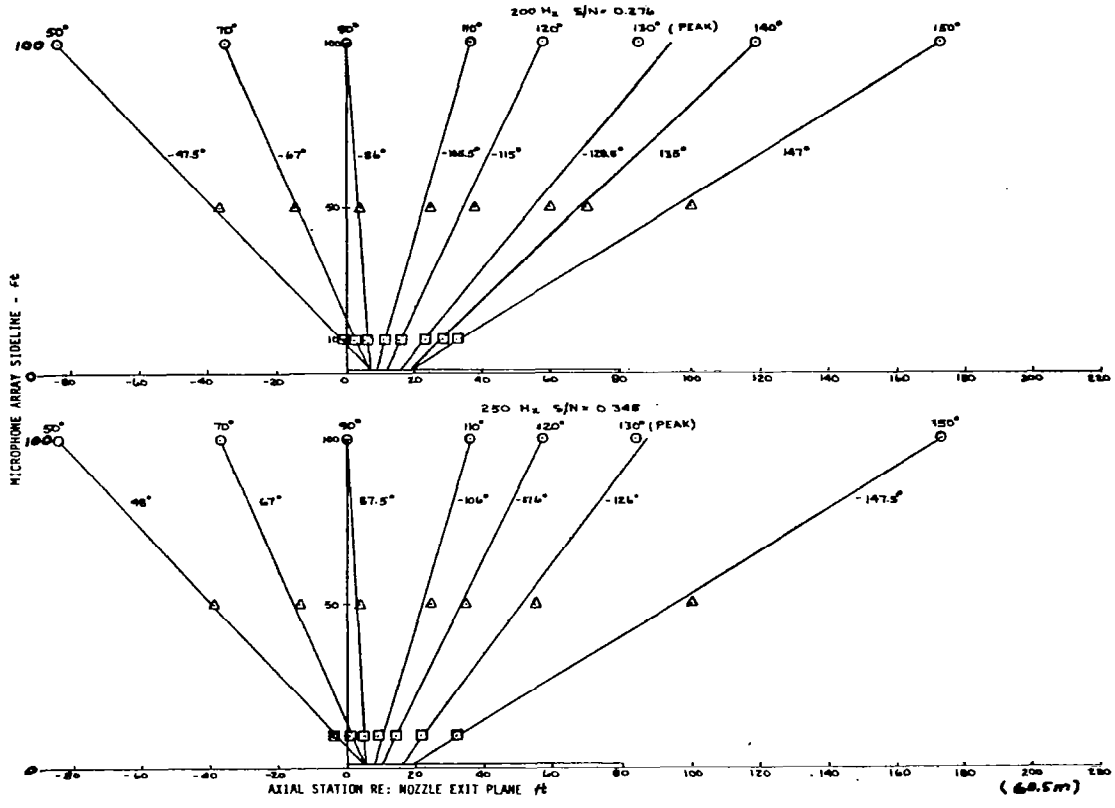

(a) Freq 200 Hz & 250 Hz

Figure 9.—Determination of Noise Source Location, Inverter Configuration

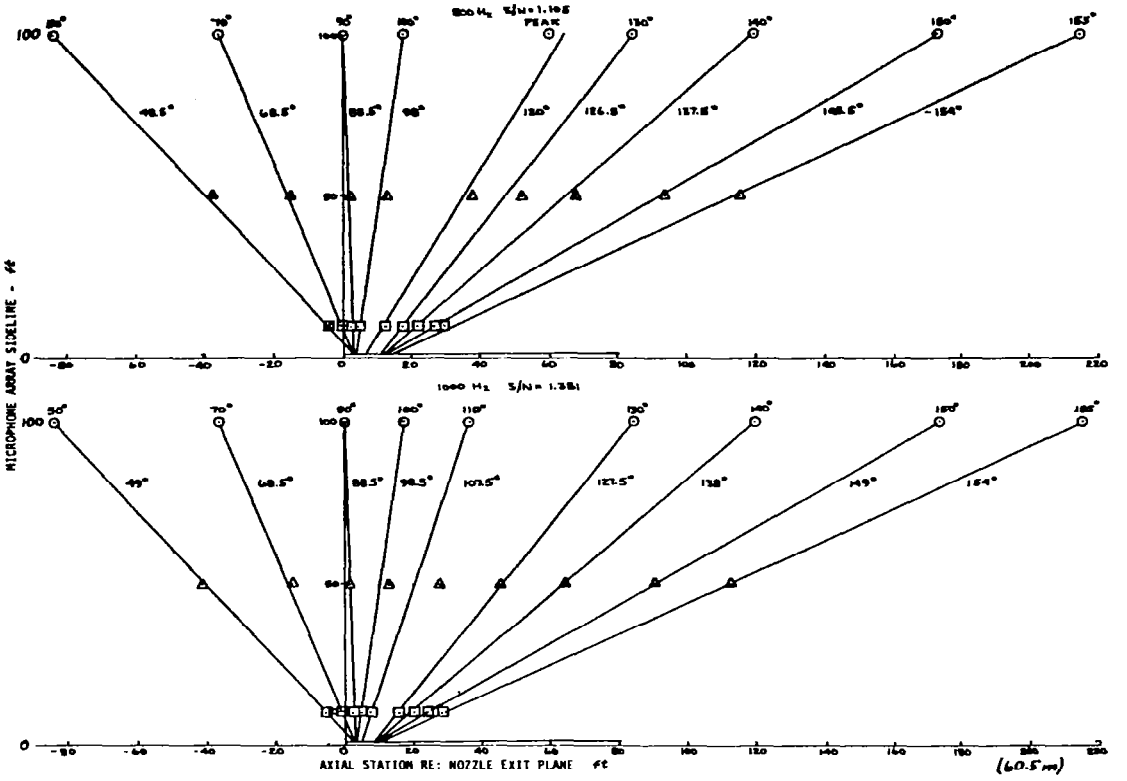

(b) Freq 800 Hz & 1K Hz

Figure 9.—(Continued)

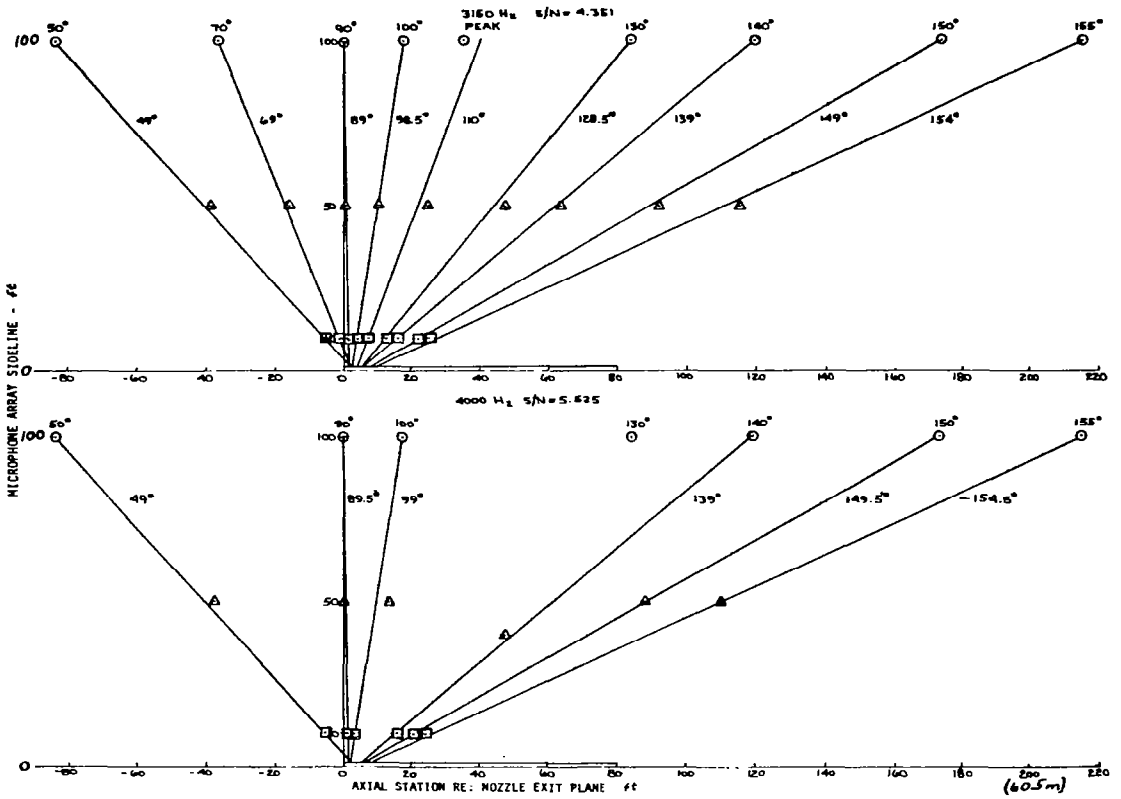

(c) 3150 Hz & 4K Hz

Figure 9.—(Concluded)

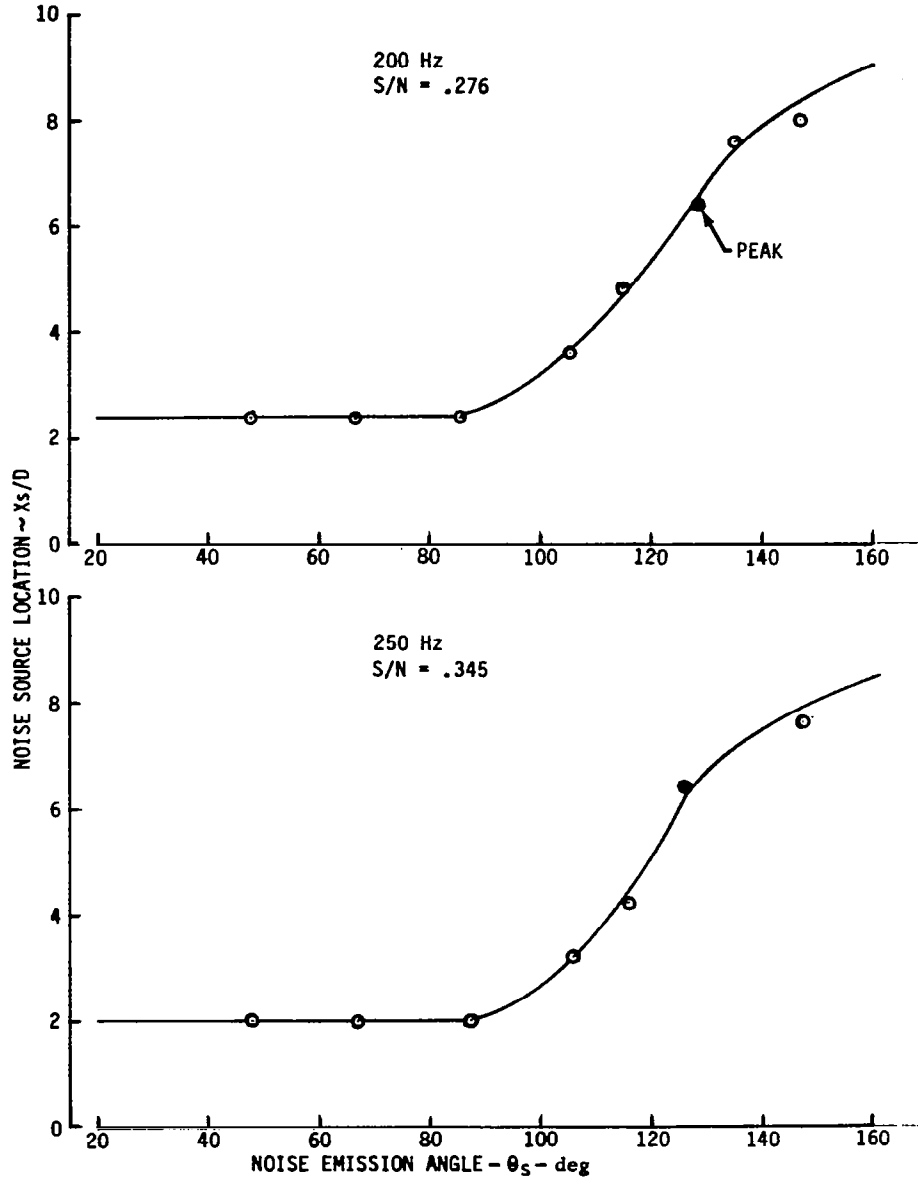

(a) 200 & 250 Hz

Figure 10.—Noise Source Location versus Emission Angle, Inverter Configuration

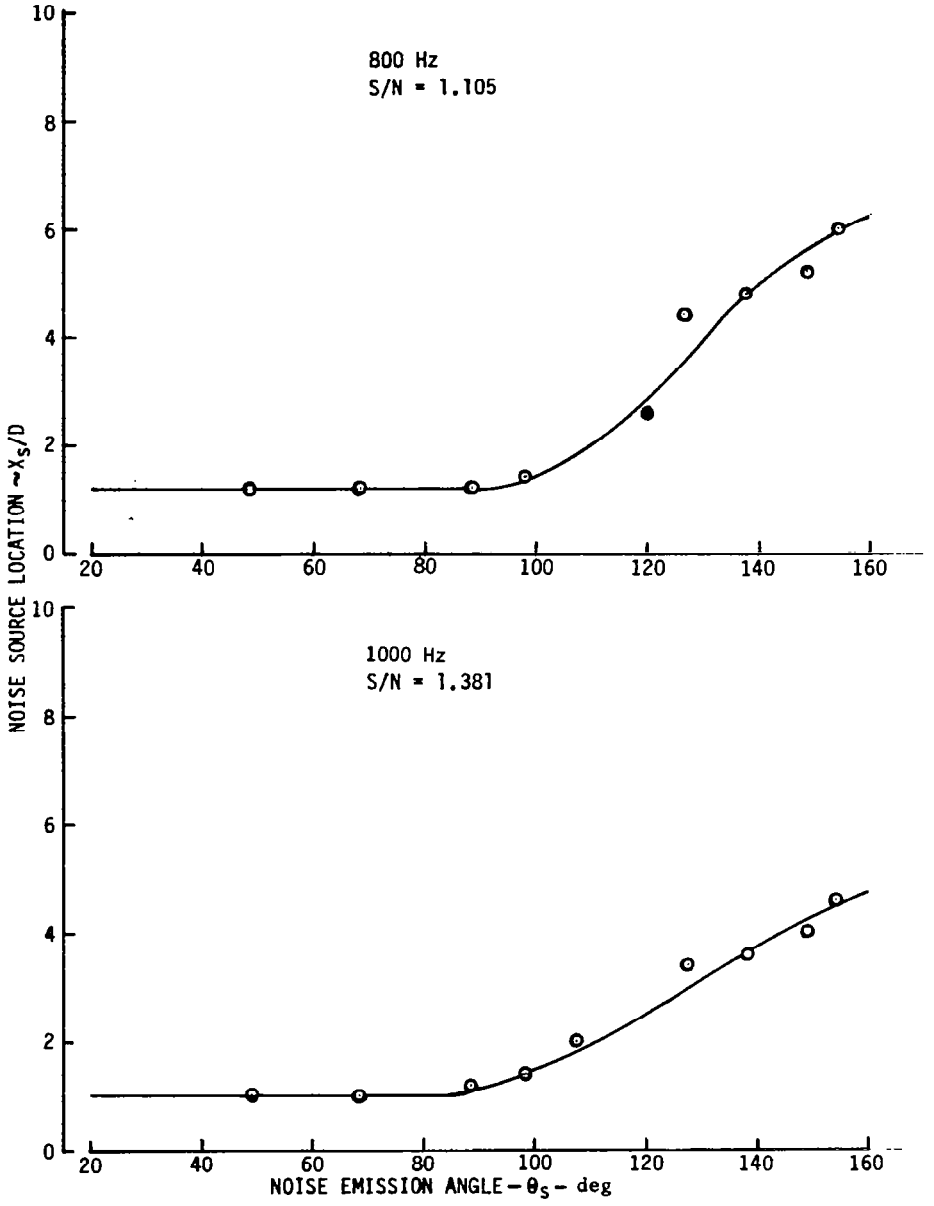

(b) 800 & 1 K Hz

Figure 10.—(Continued)

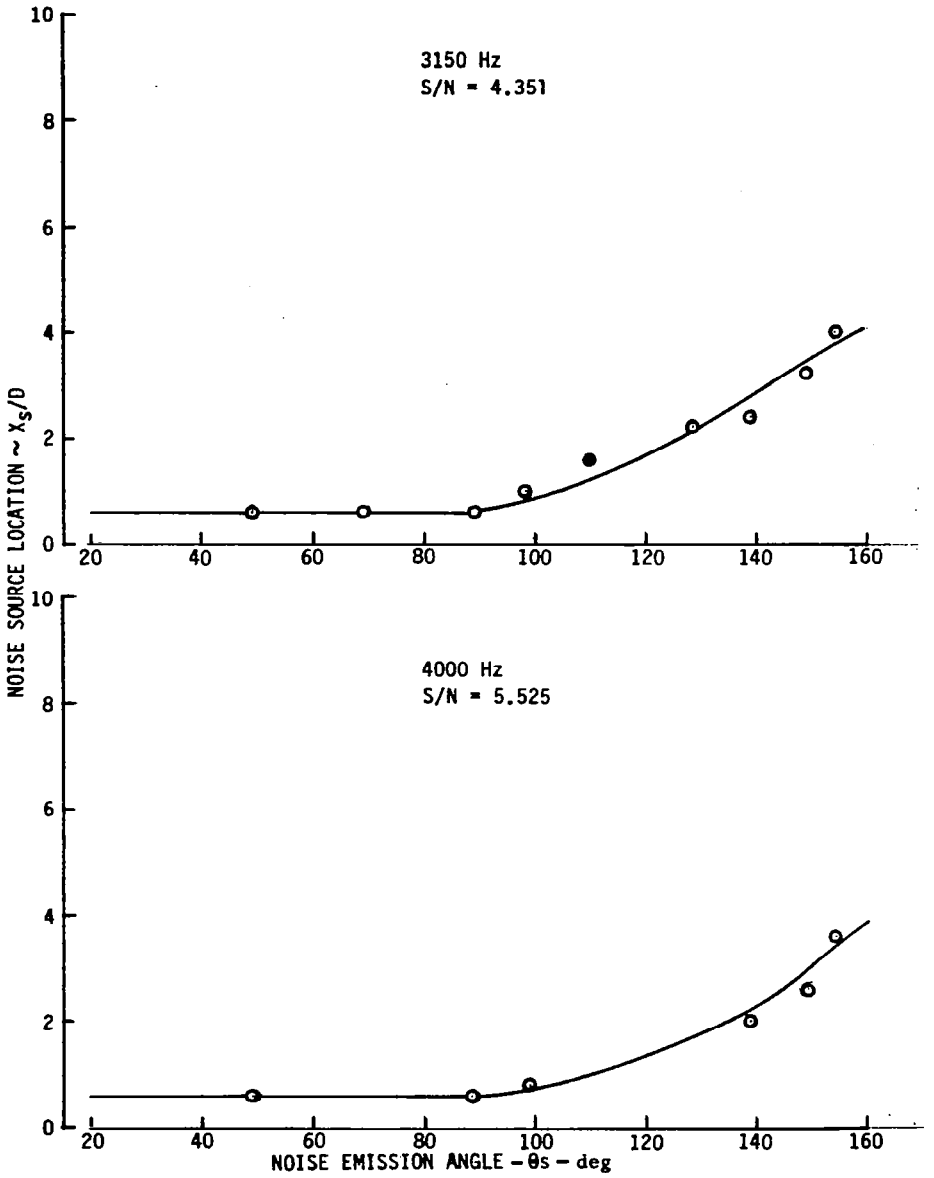

(c) 3150 & 4 K Hz

Figure 10.—(Concluded)

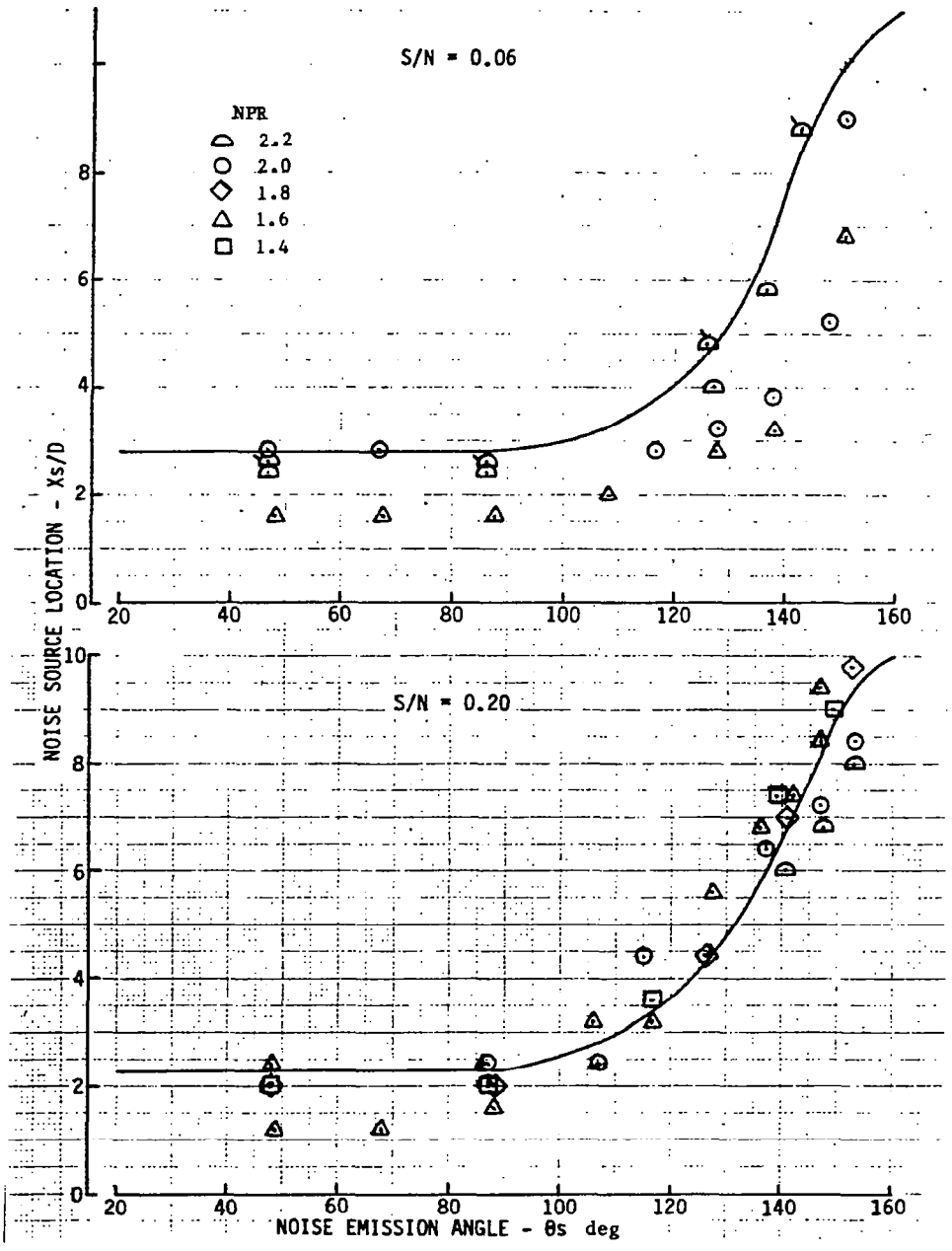

(a) S/N = 0.06 & 0.20

Figure 11.—Noise Source Location Correlation for Inverter Configuration

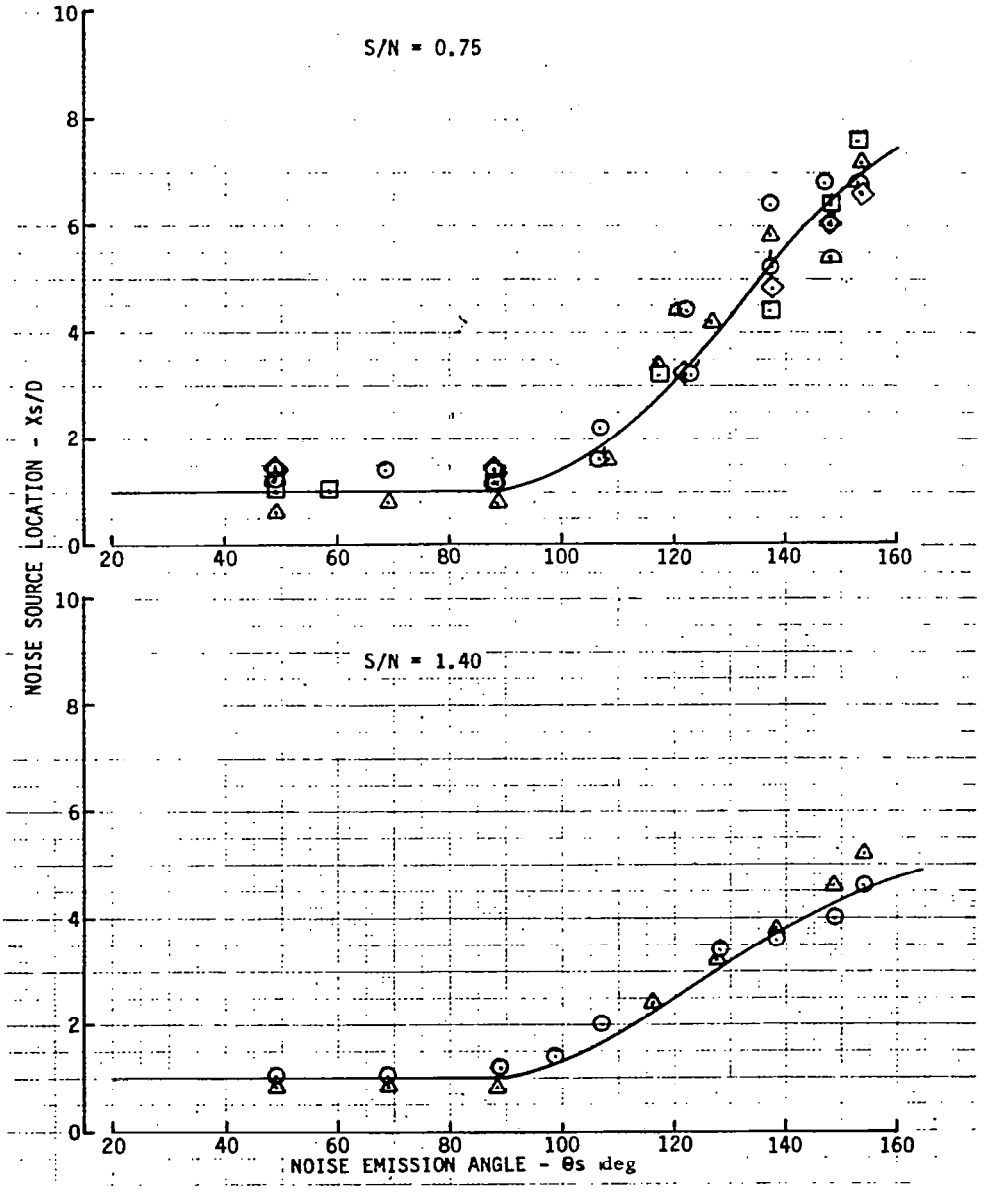

(b) S/N = 0.75 & 1.40

Figure 11.—(Continued)

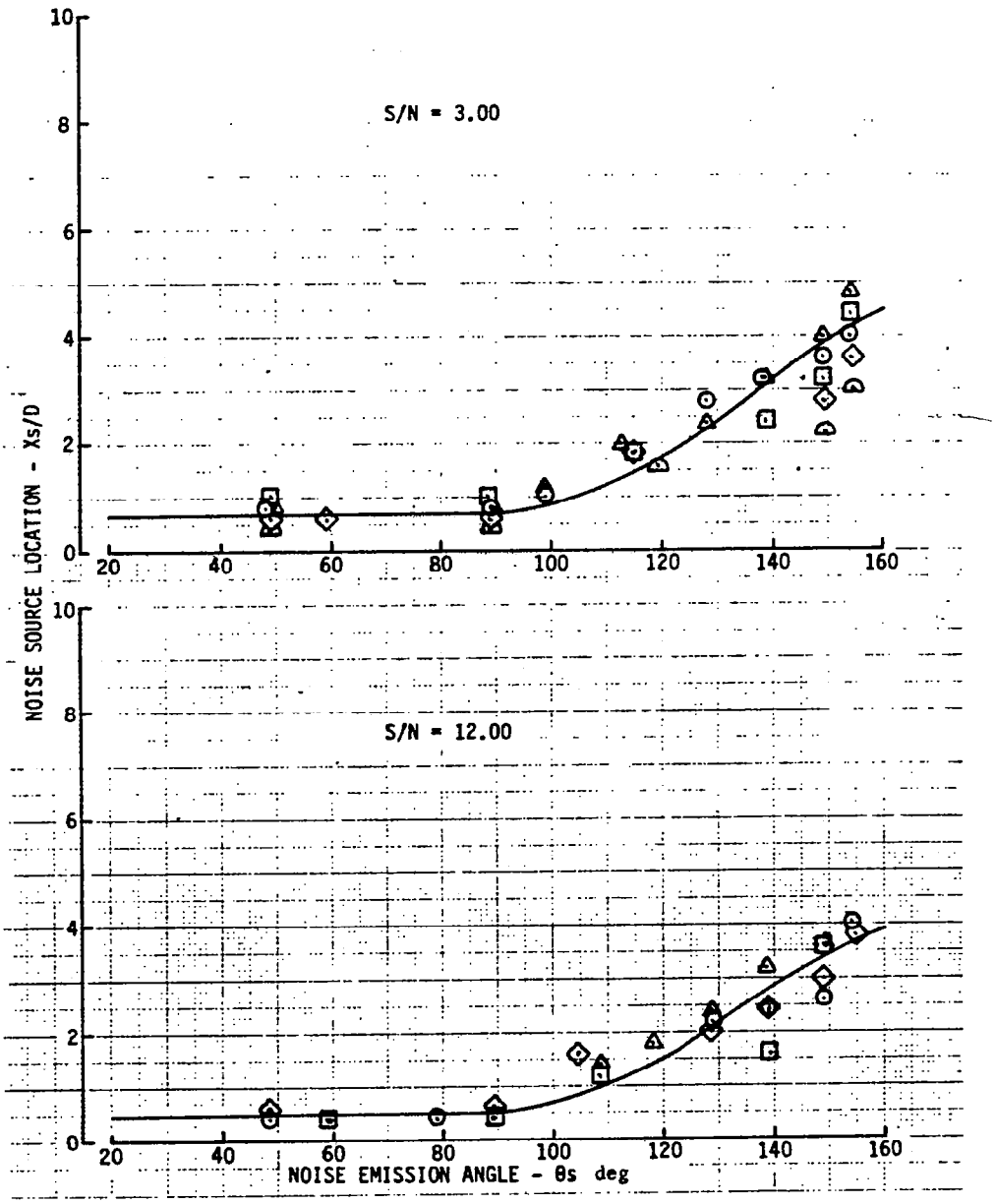

(c) S/N = 3.00 & 12.00

Figure 11.—(Continued)

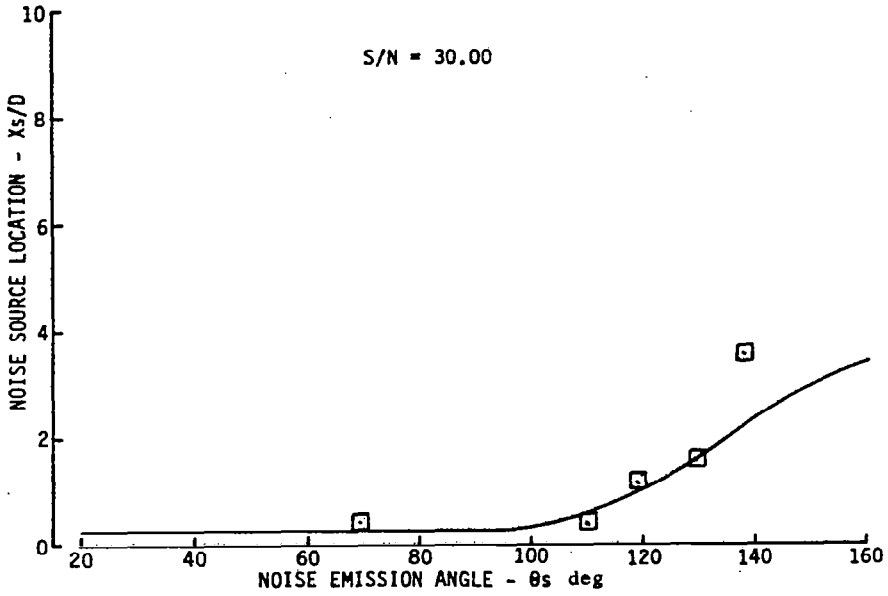

(d) S/N = 30.00

Figure 11.—(Concluded)

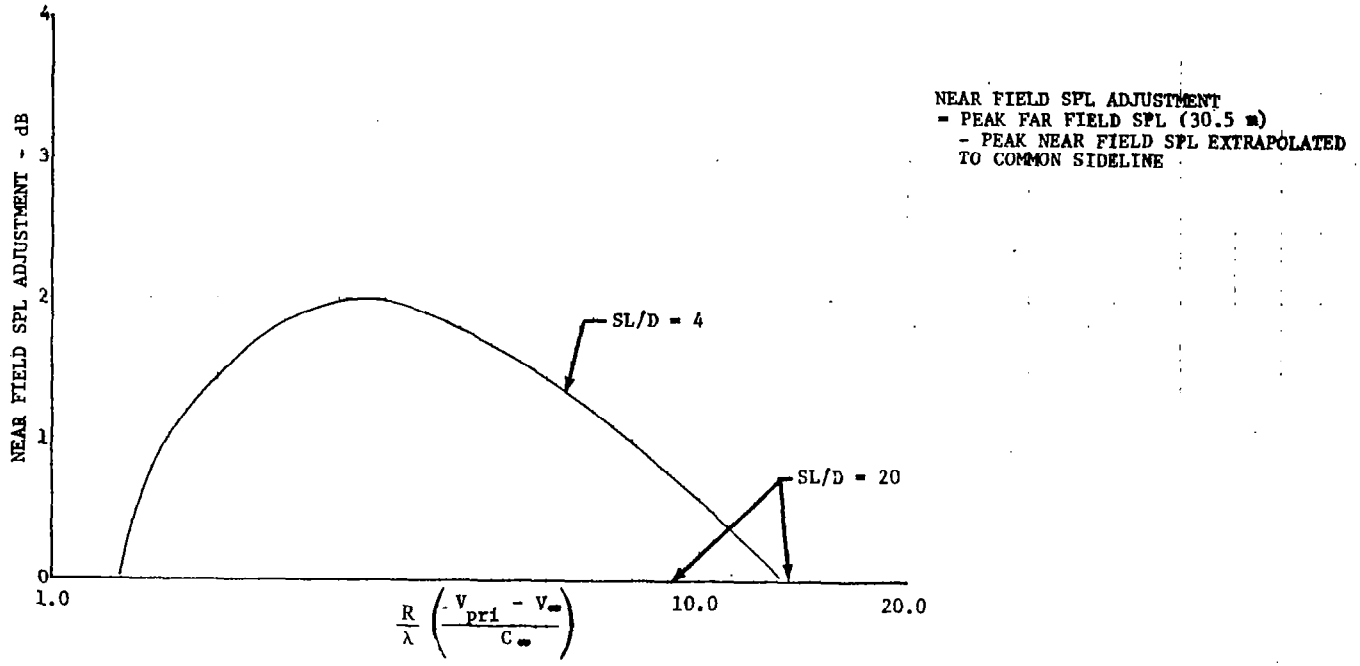

Figure 12.—Near Field SPL Adjustment

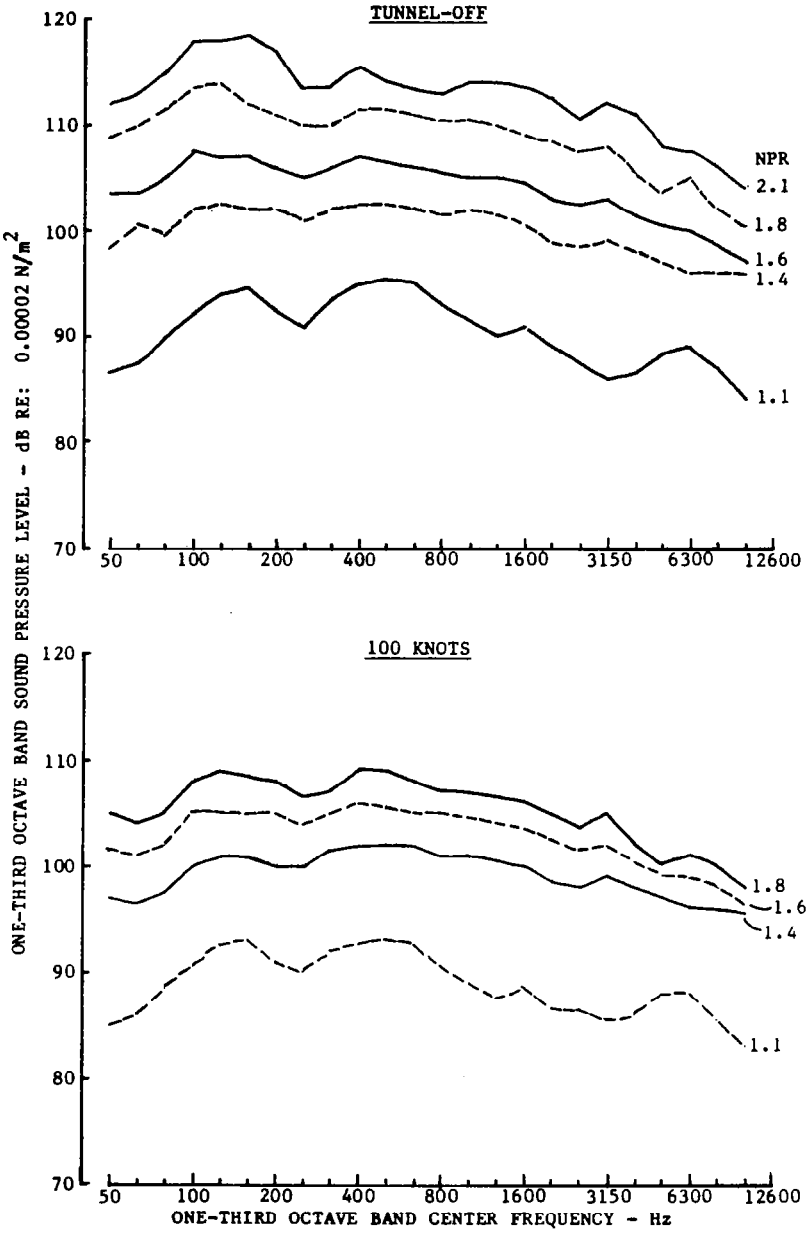

(a) Tunnel-Off & 100 Knots

Figure 13.—Reverberant Field Spectra for Inverter Configuration

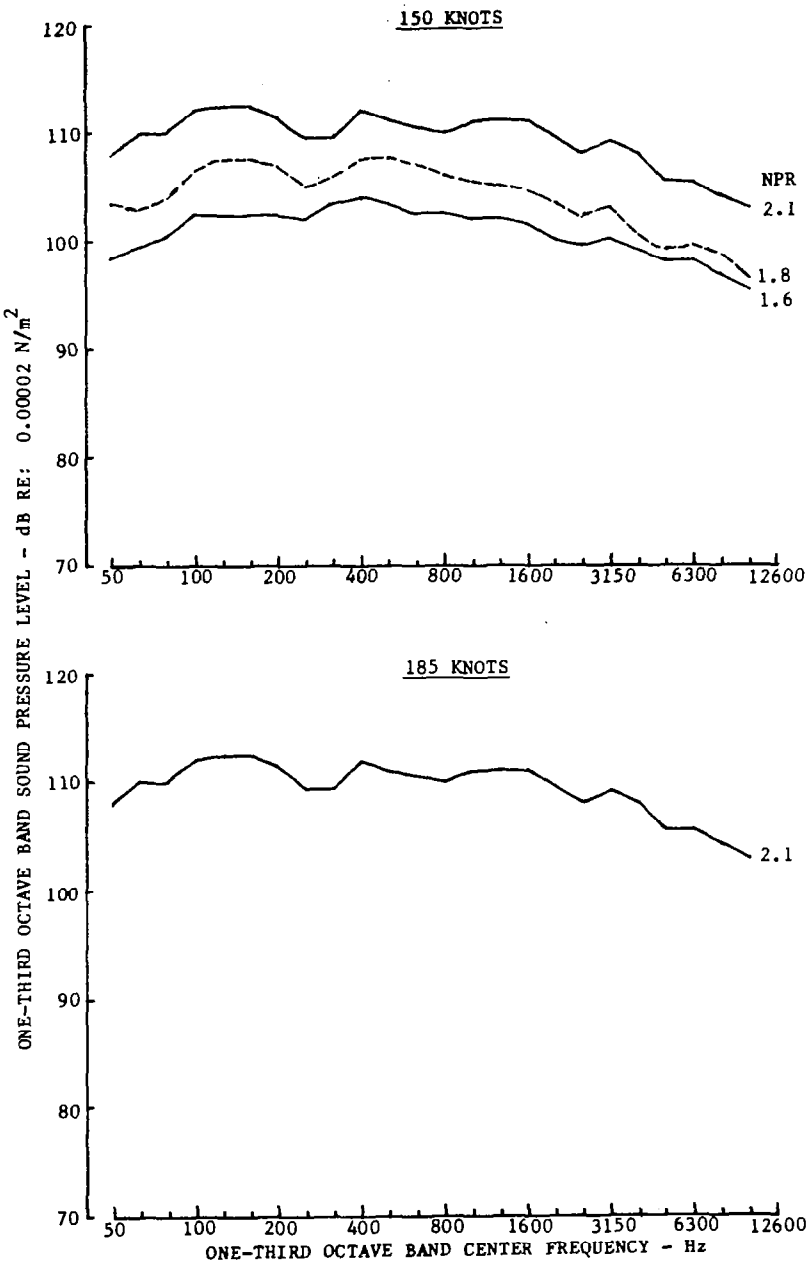

(b) 150 Knots & 185 Knots

Figure 13.—(Concluded)

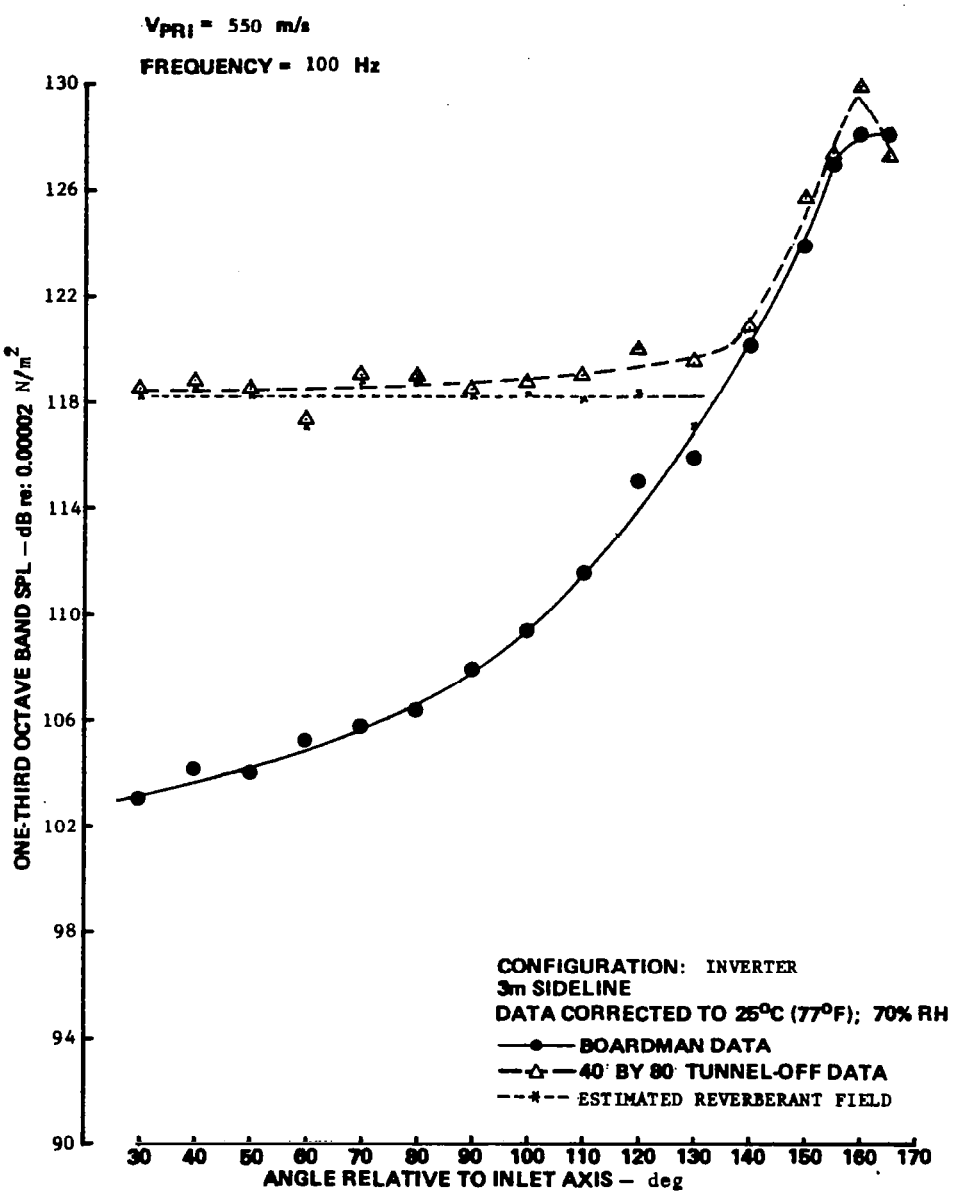

(a) Freq 100 Hz

Figure 14.—Comparison of Free Field and 40 by 80 SPL Directivity, Inverter Configuration

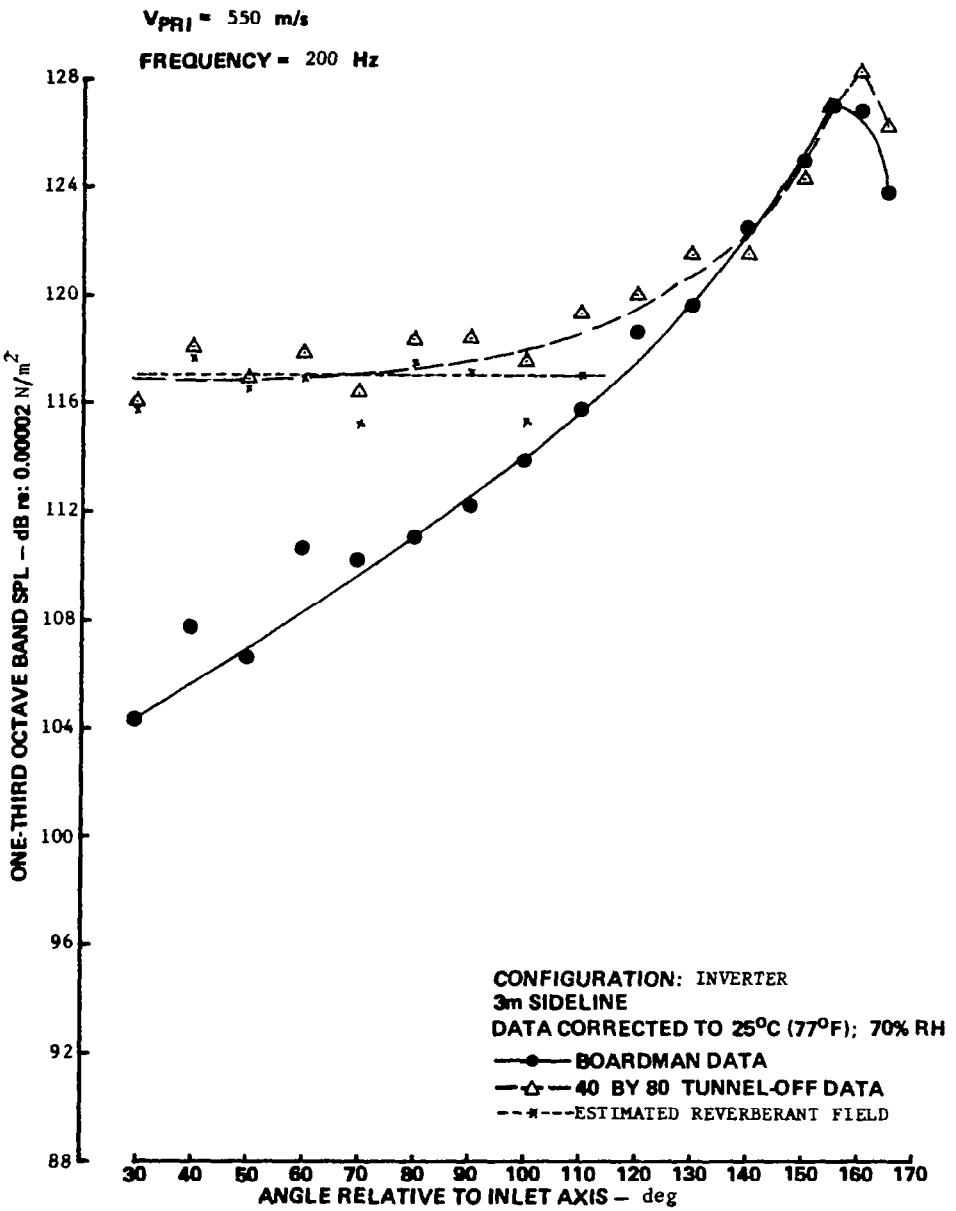

(b) Freq 200 Hz

Figure 14.—(Continued)

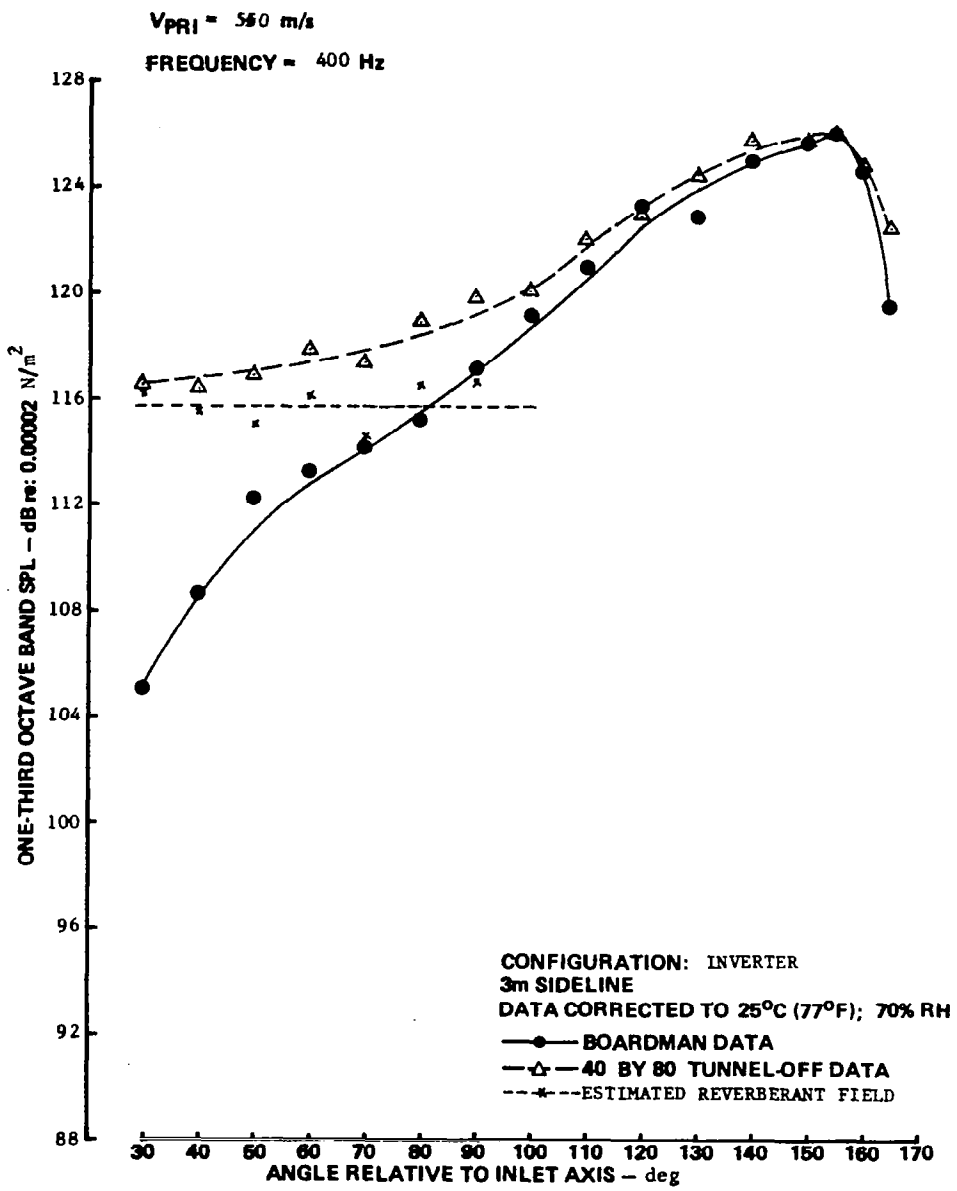

(c) Freq 400 Hz

Figure 14.—(Continued)

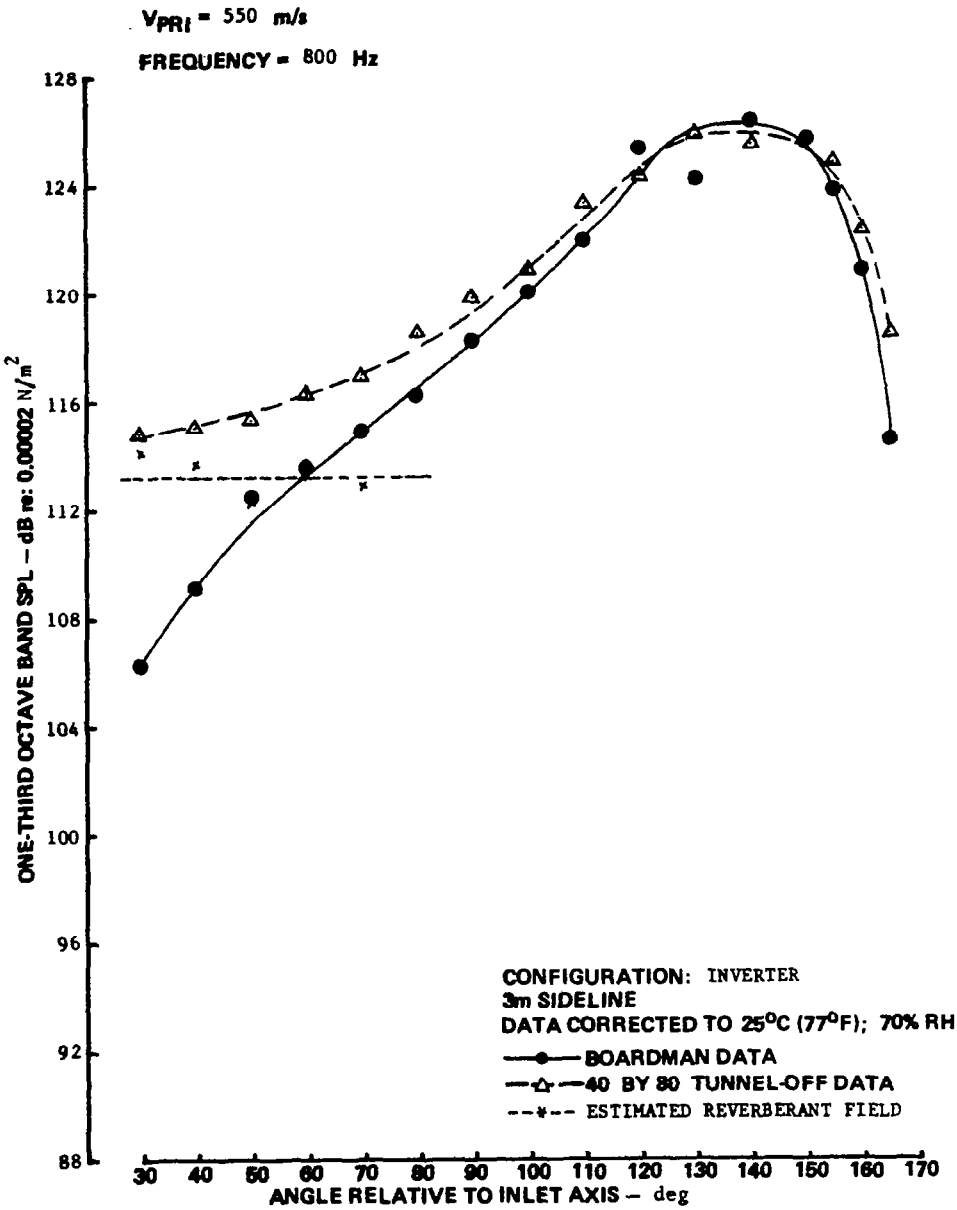

(d) Freq 800 Hz

Figure 14.–(Continued)

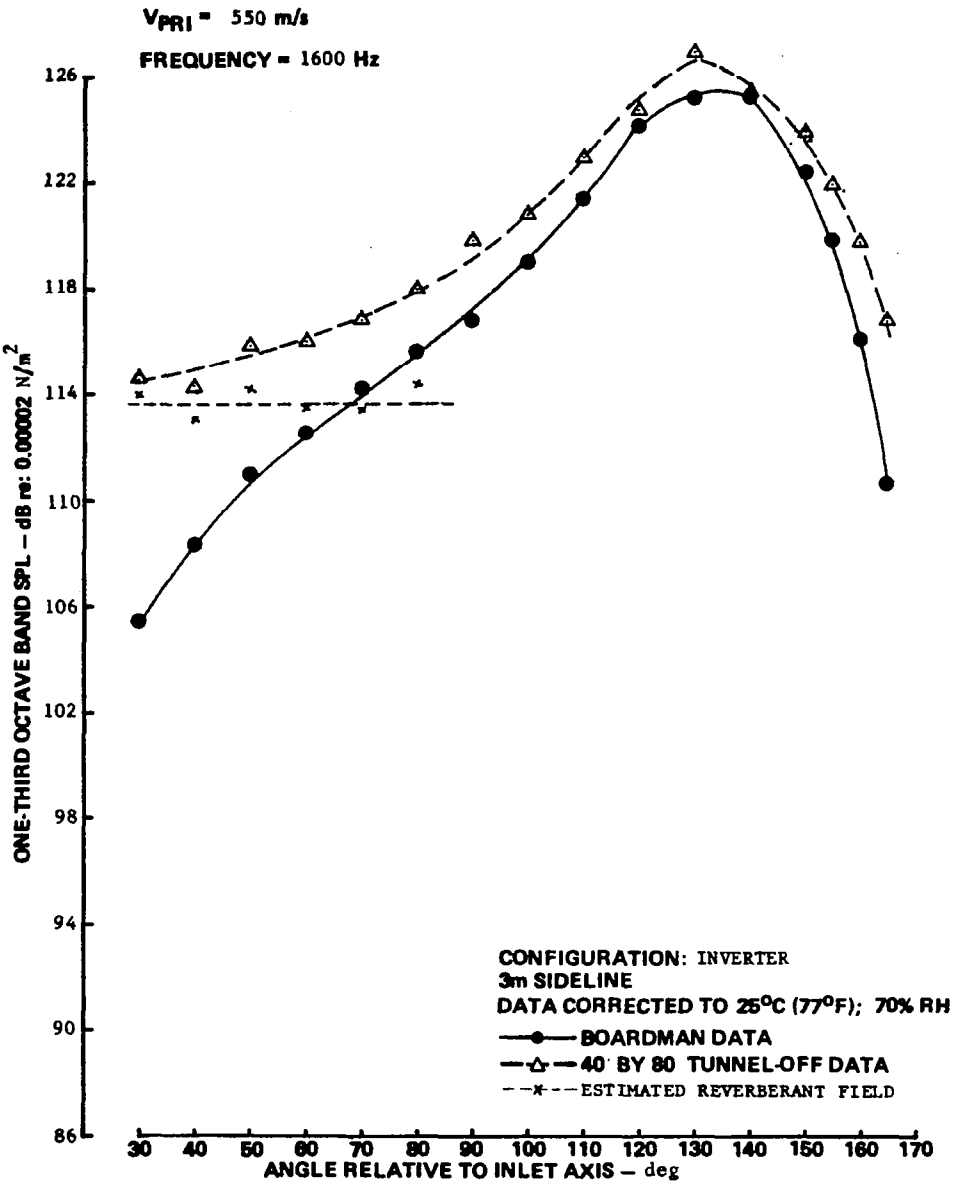

(e) Freq 1600 Hz

Figure 14.—(Continued)

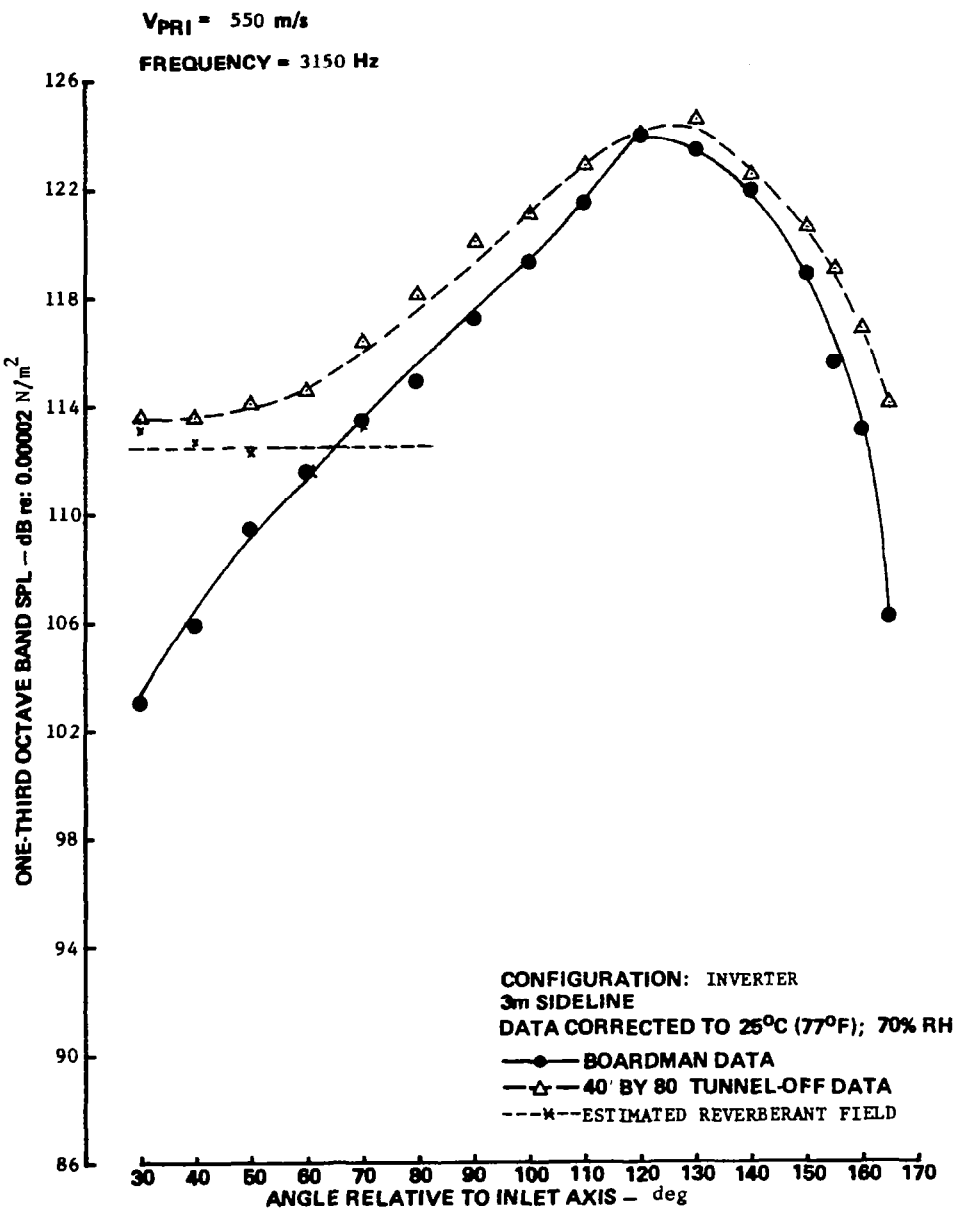

(f) Freq 3150 Hz

Figure 14.—(Concluded)

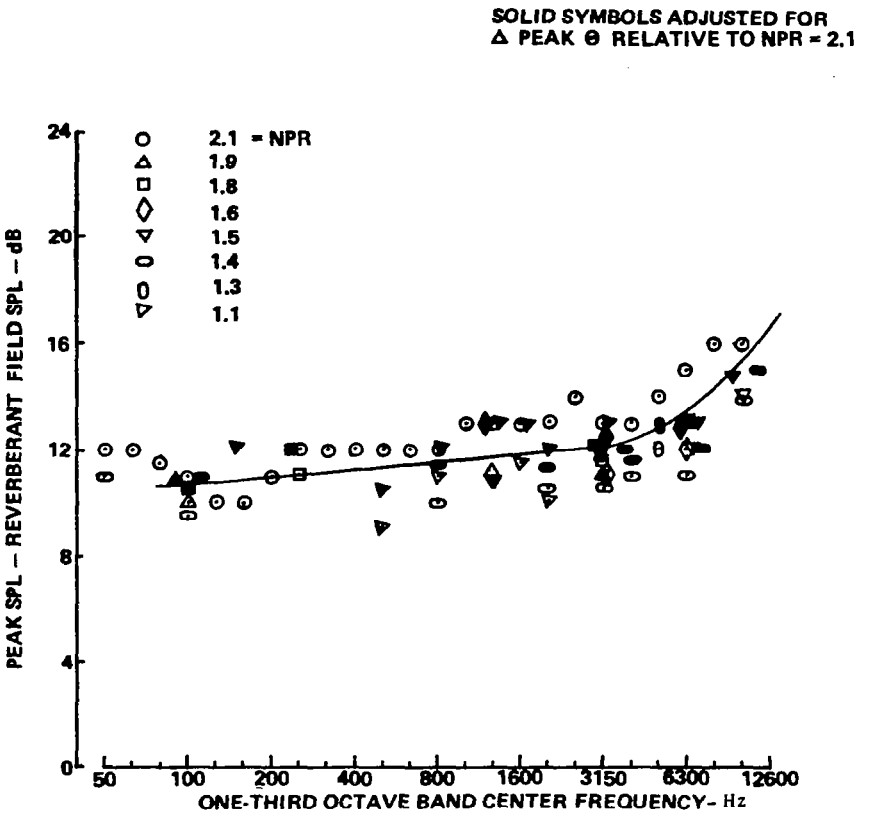

Figure 15.—Relationship of Reverberant Field SPL to Peak SPL, Inverter Configuration

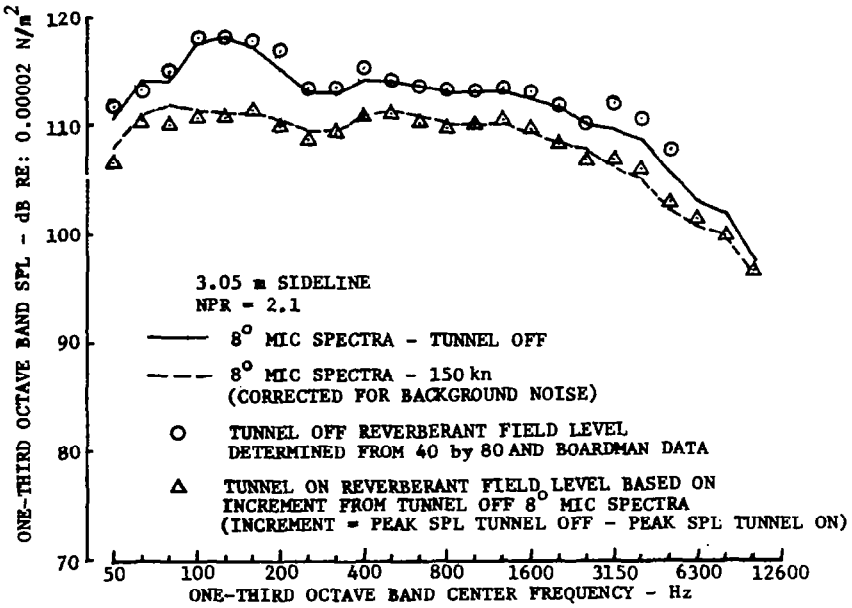

Figure 16.—Comparison of Reverberant Field Spectra, Inverter Configuration

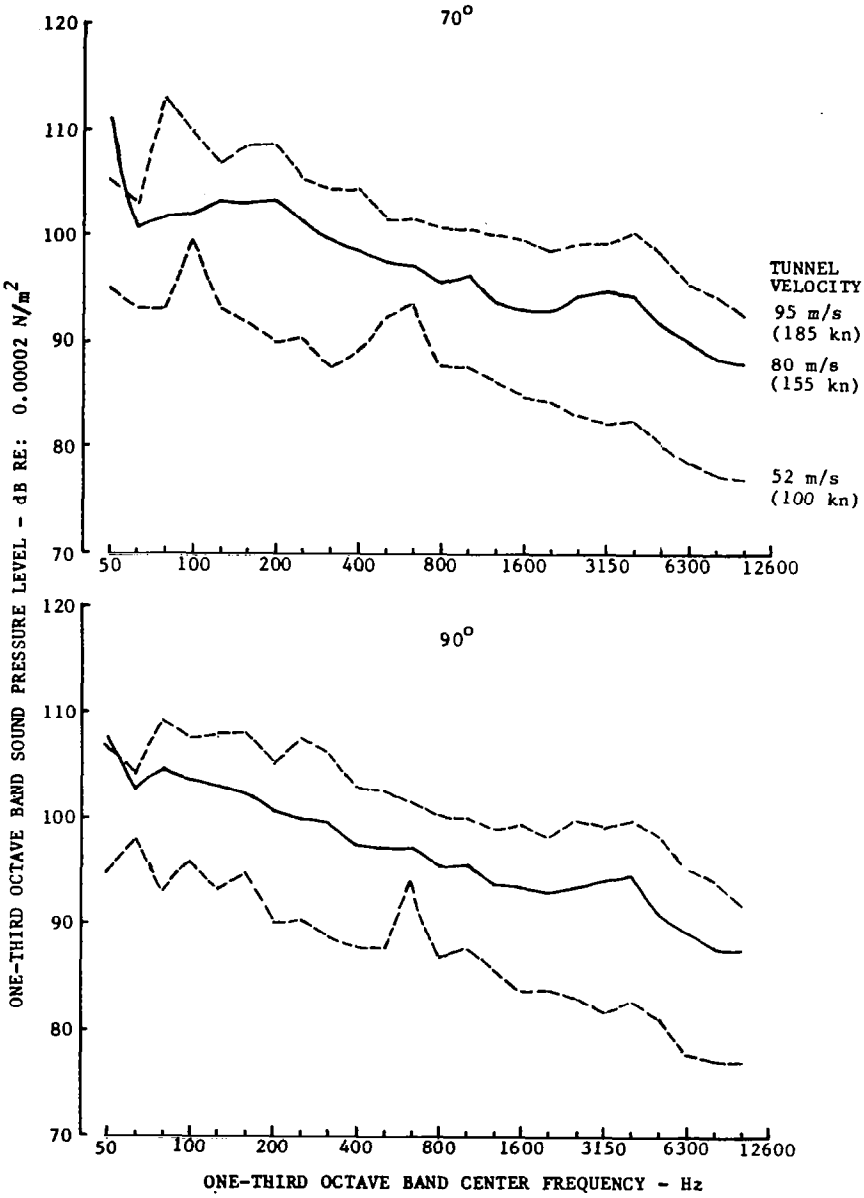

Figure 17.—Tunnel Background Noise Spectra

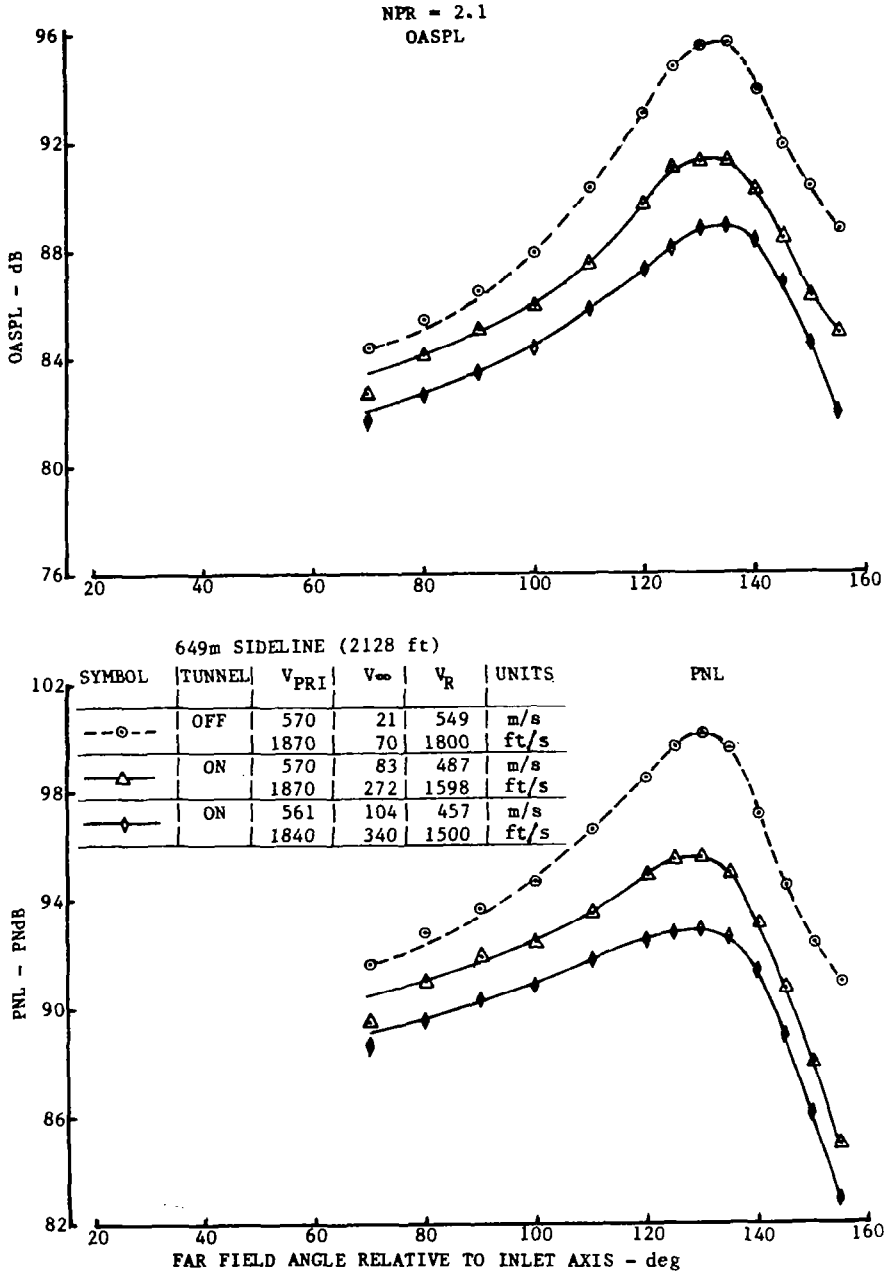

SYMBOL	TUNNEL	V_{PRI}	V_∞	V_R	UNITS
--⊙--	OFF	570	21	549	m/s
		1870	70	1800	ft/s
—△—	ON	570	83	487	m/s
		1870	272	1598	ft/s
—◇—	ON	561	104	457	m/s
		1840	340	1500	ft/s

(a) NPR = 2.1

Figure 18.—Comparison of Tunnel-Off and -On OASPL and PNL Directivities, Baseline Configuration

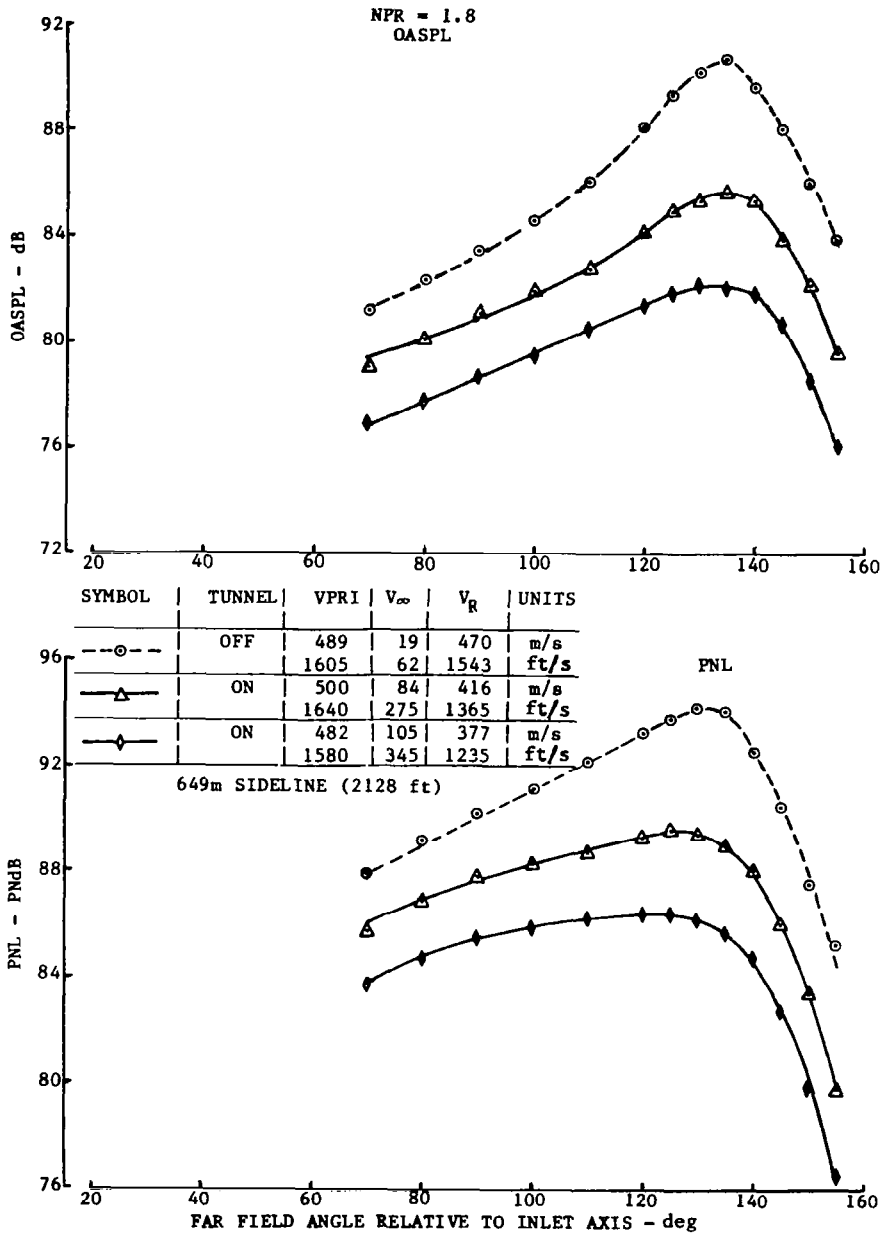

(b) NPR = 1.8

Figure 18.—(Concluded)

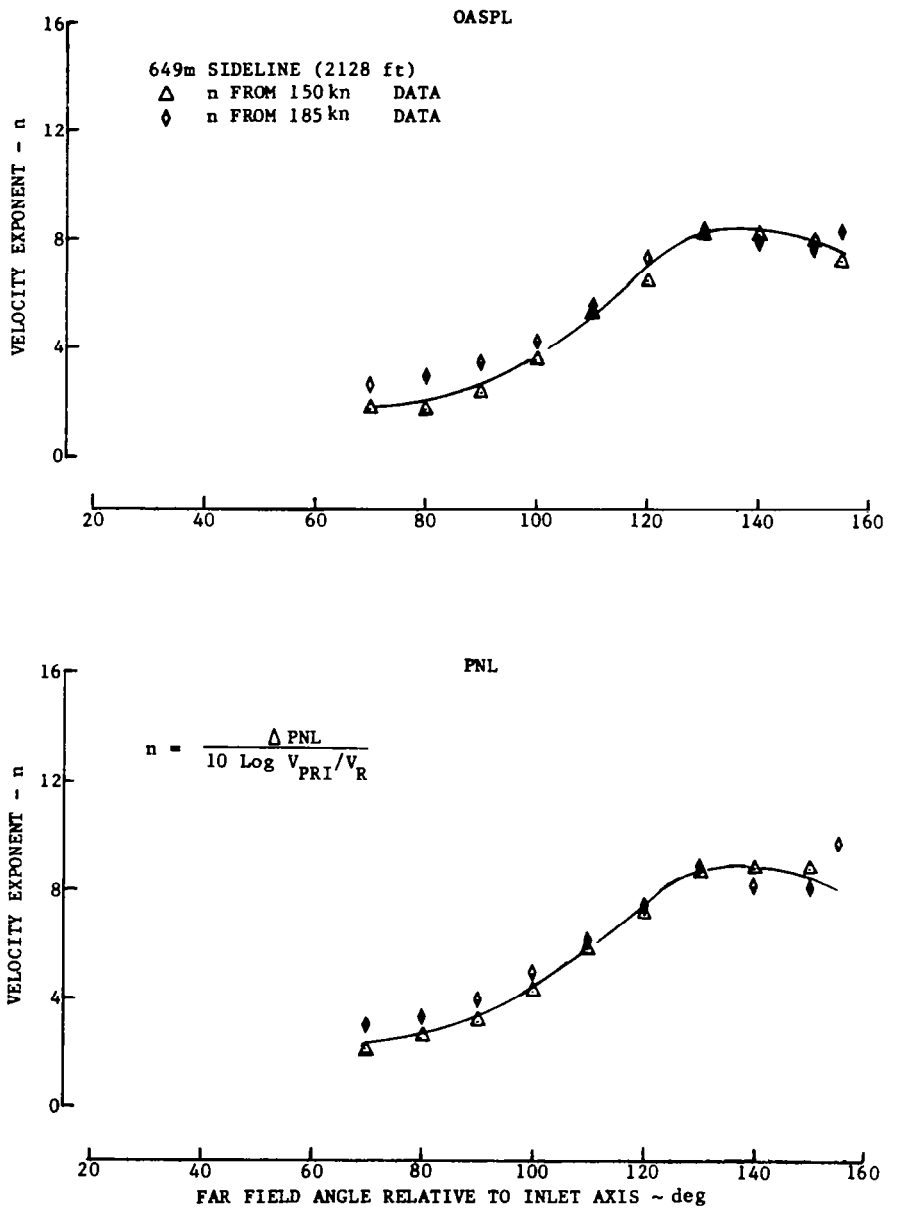

(a) NPR = 2.1

Figure 19.—Velocity Exponents for OASPL and PNL, Baseline Configuration

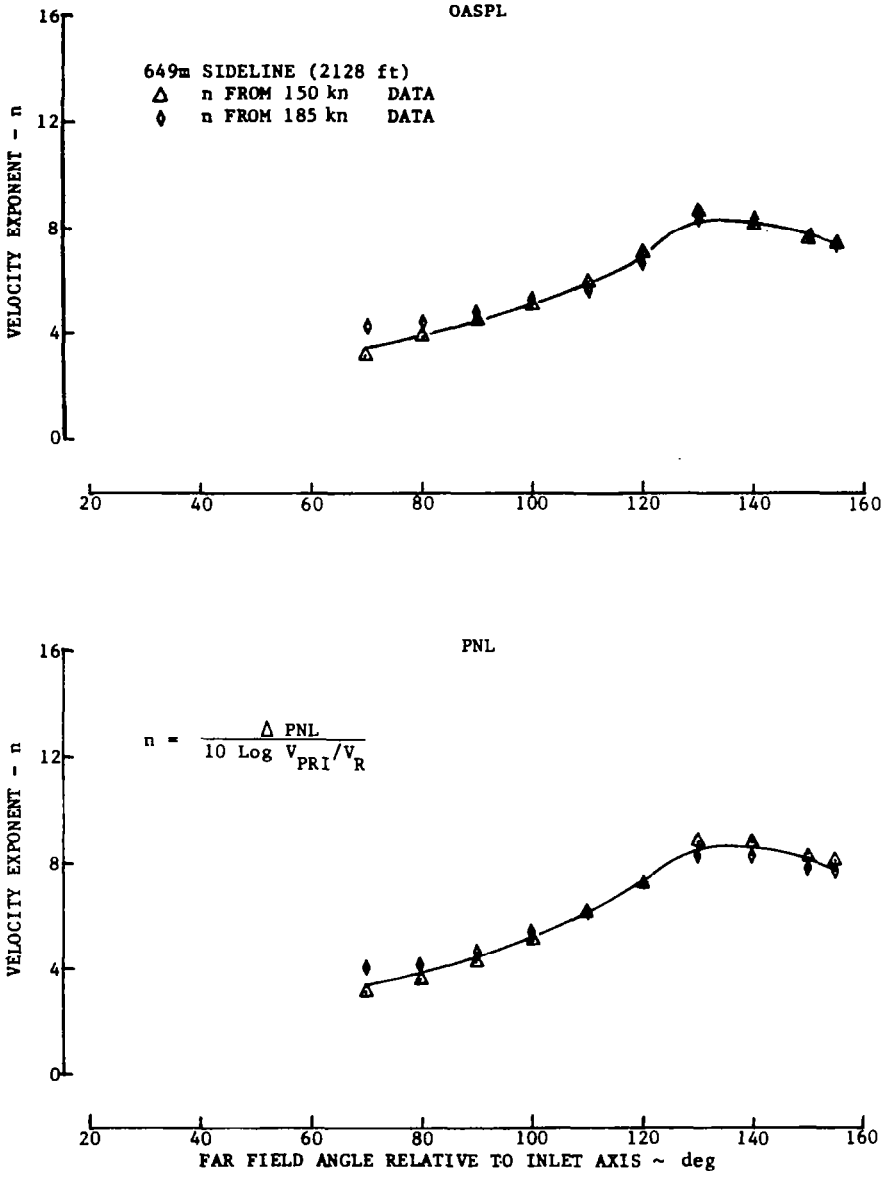

(b) NPR = 1.8

Figure 19.—(Concluded)

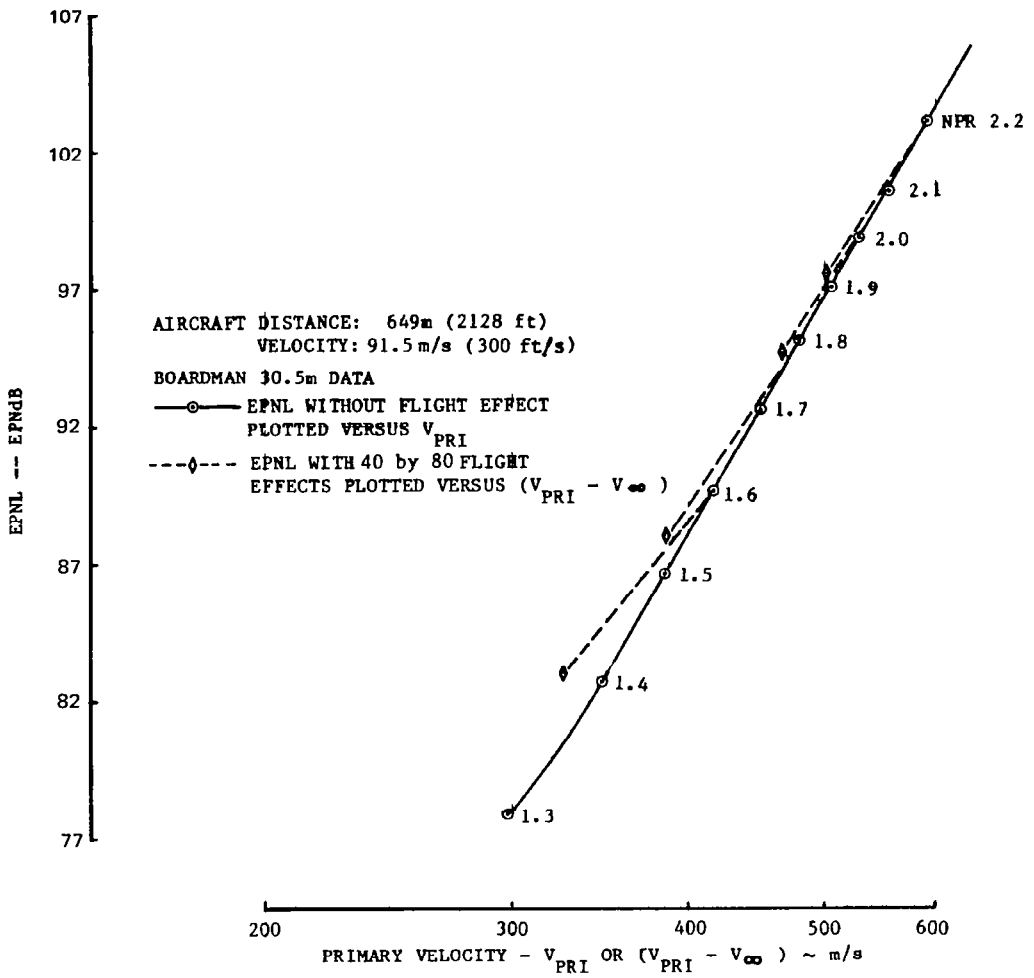

Figure 20.—Static and Estimated Flight EPNL Characteristics, Baseline Configuration

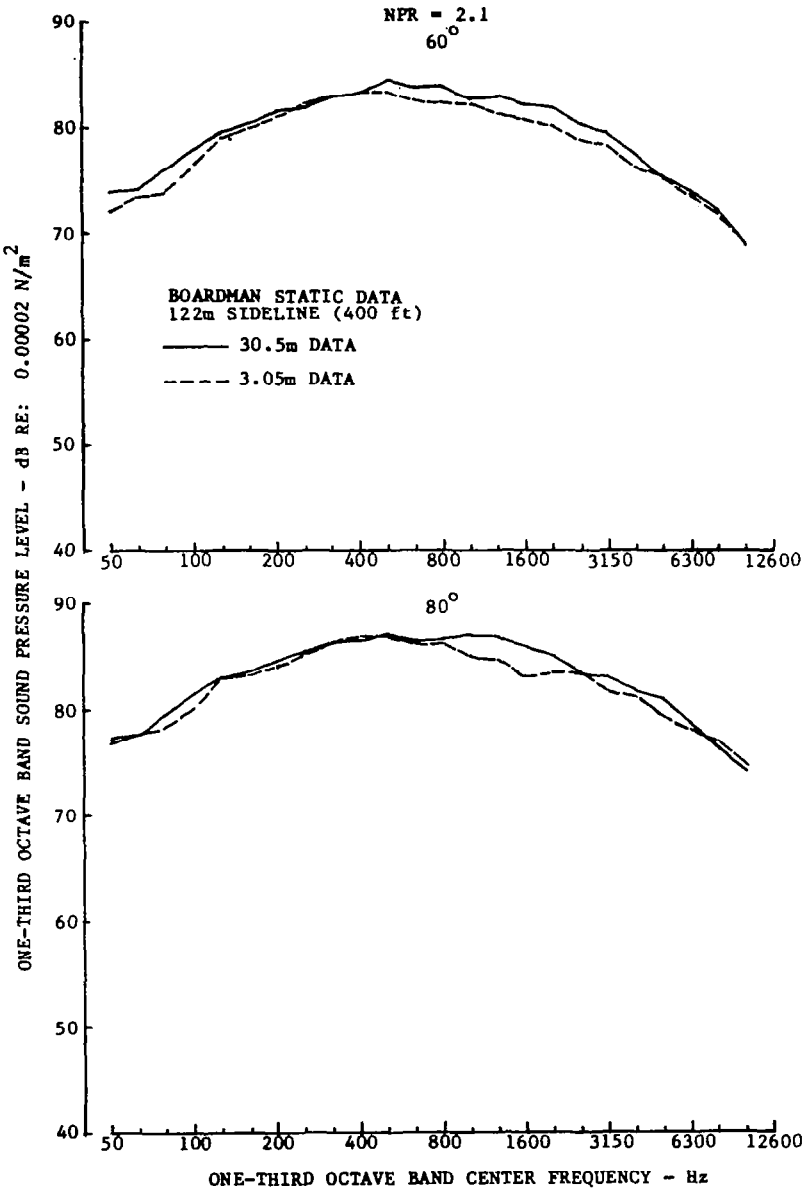

(a) 60° & 80°

Figure 21.—Comparison of Near and Far Field Spectra, Inverter Configuration

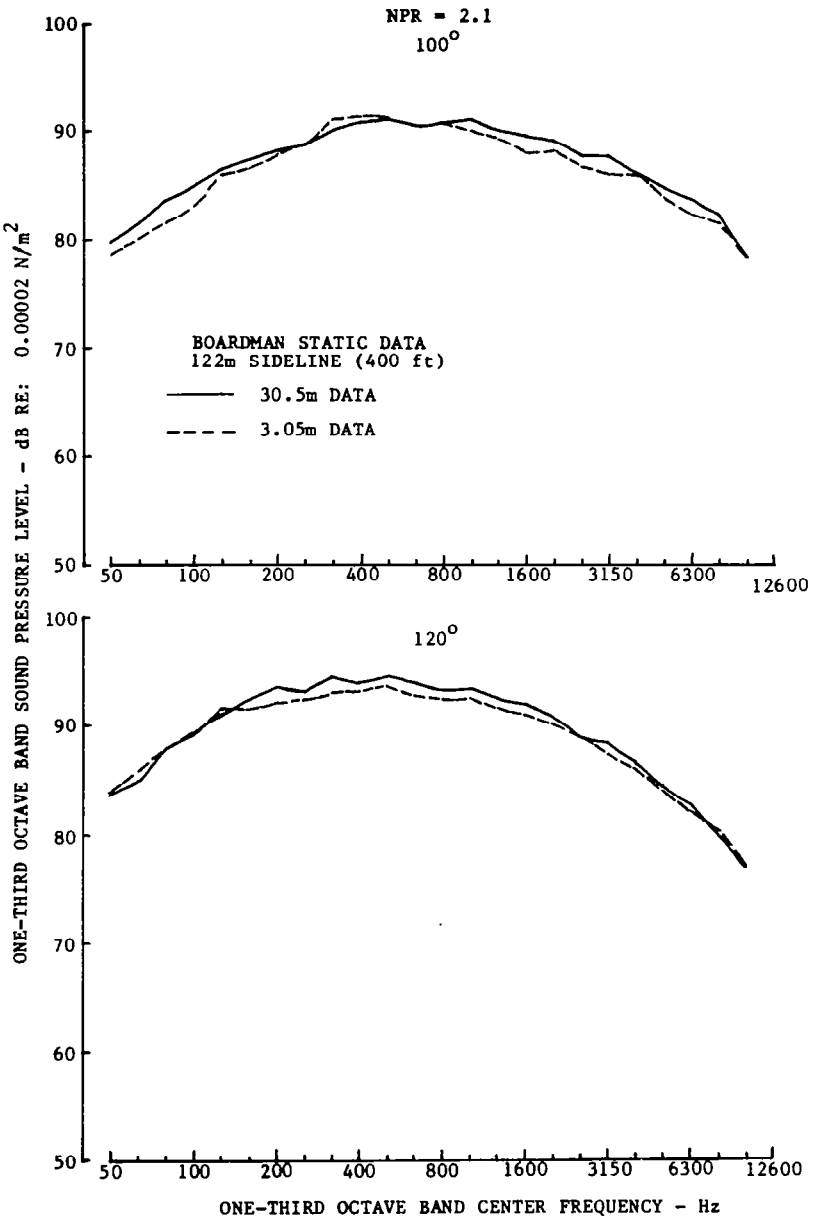

(b) 100° & 120°

Figure 21.—(Continued)

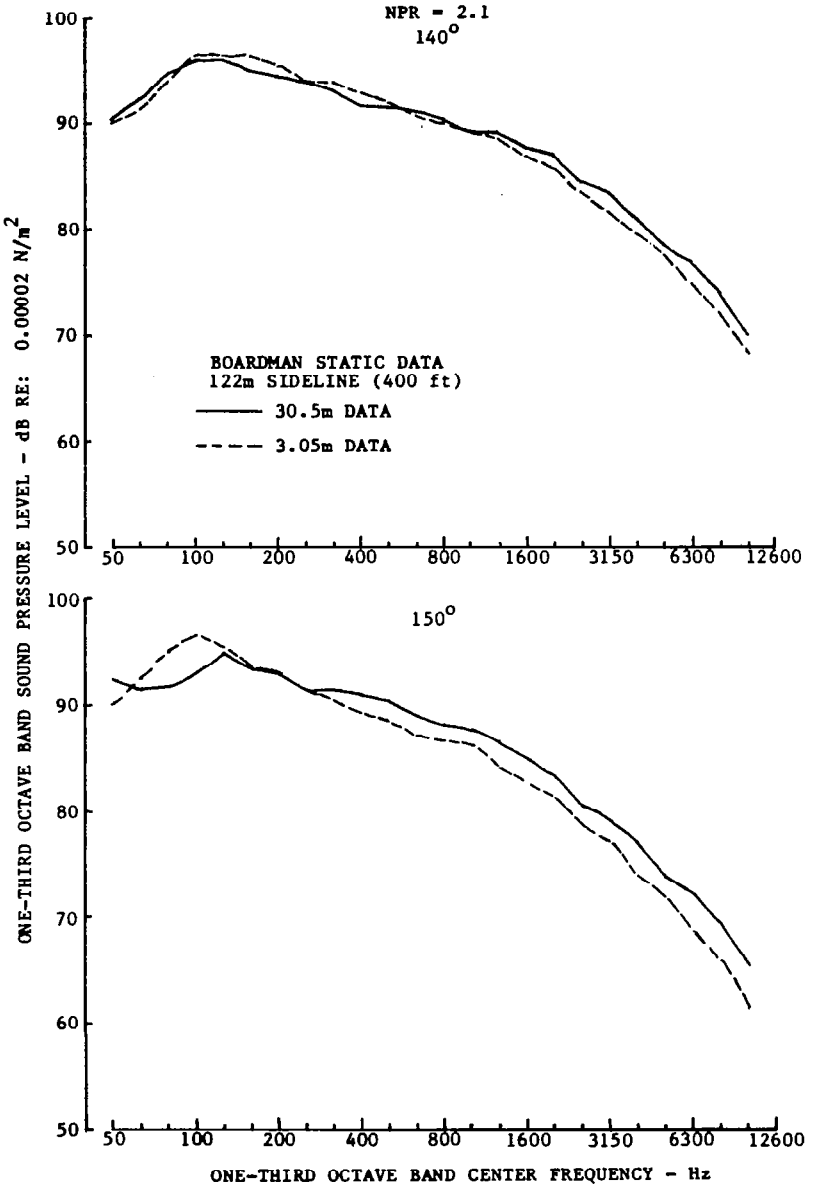

(c) 140° & 150°

Figure 21.—(Concluded)

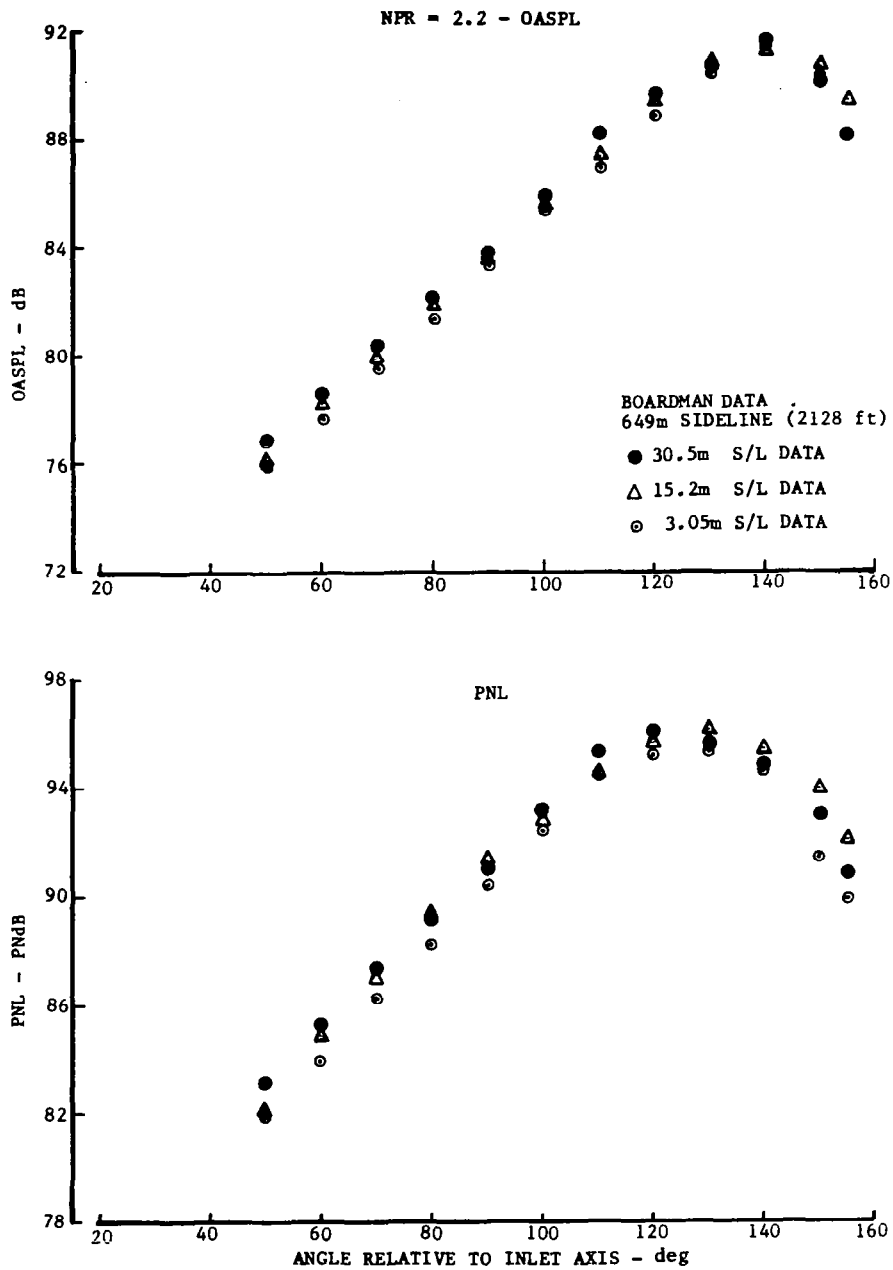

(a) NPR = 2.2

Figure 22.—Comparison of Near and Far Field OASPL and PNL Directivity, Inverter Configuration

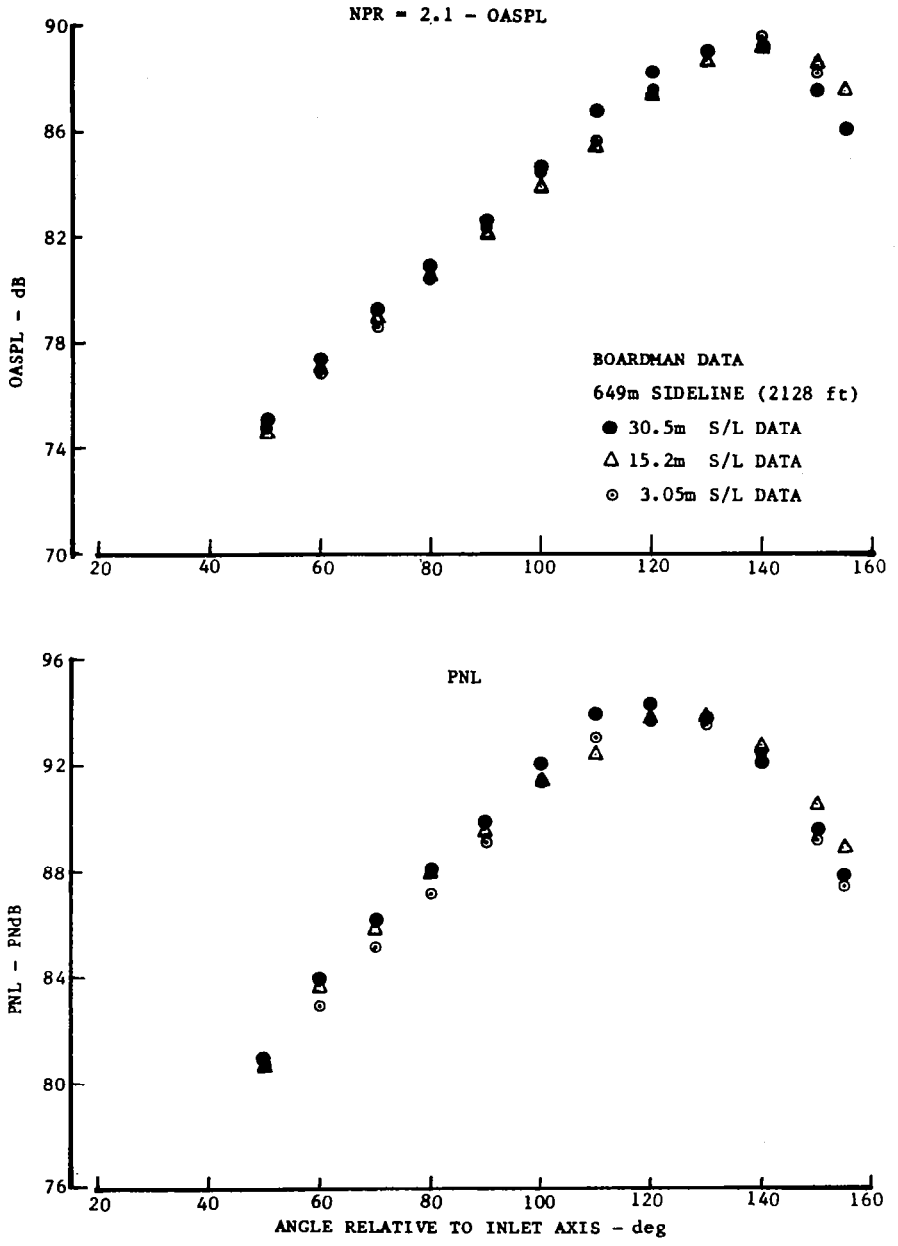

(b) NPR = 2.1

Figure 22.—(Continued)

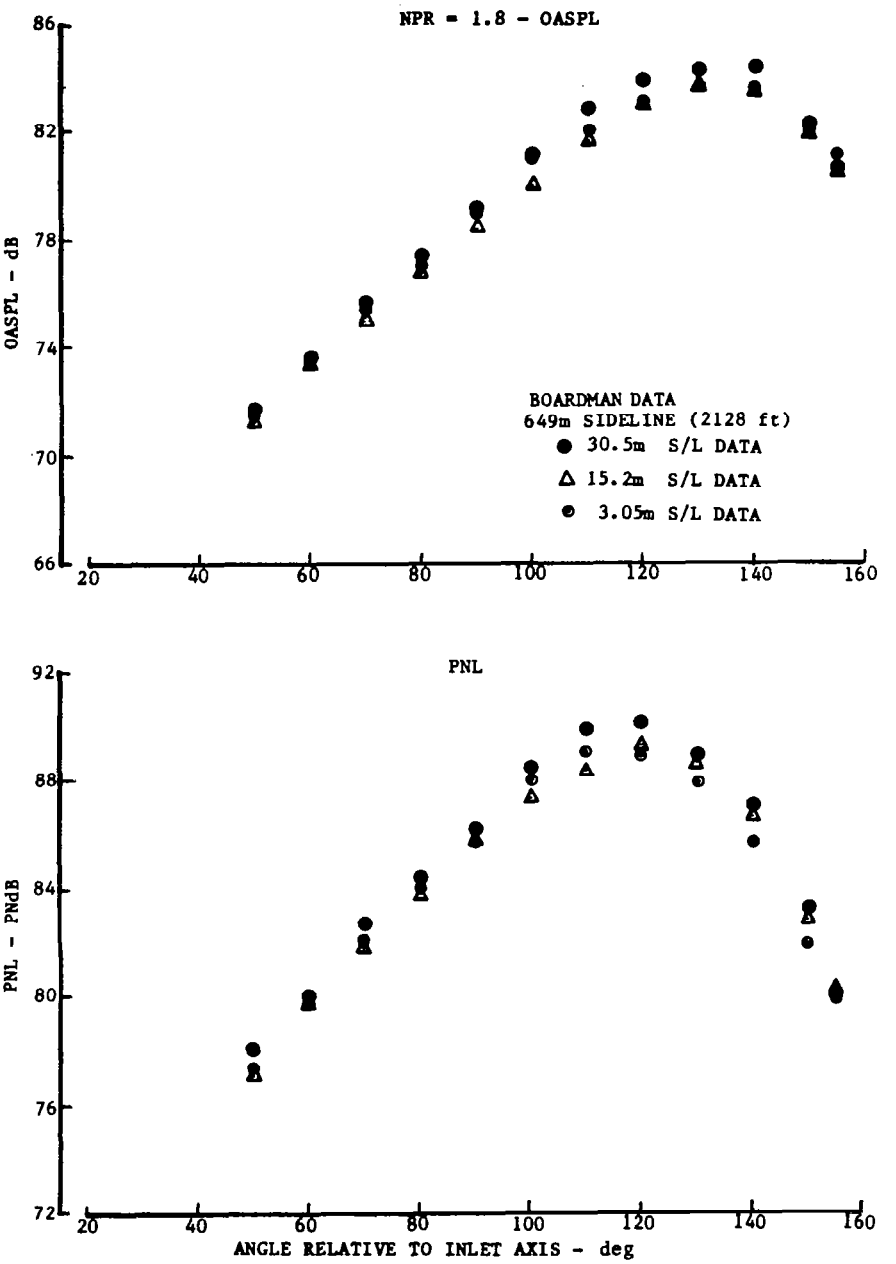

(c) NPR = 1.8

Figure 22.—(Continued)

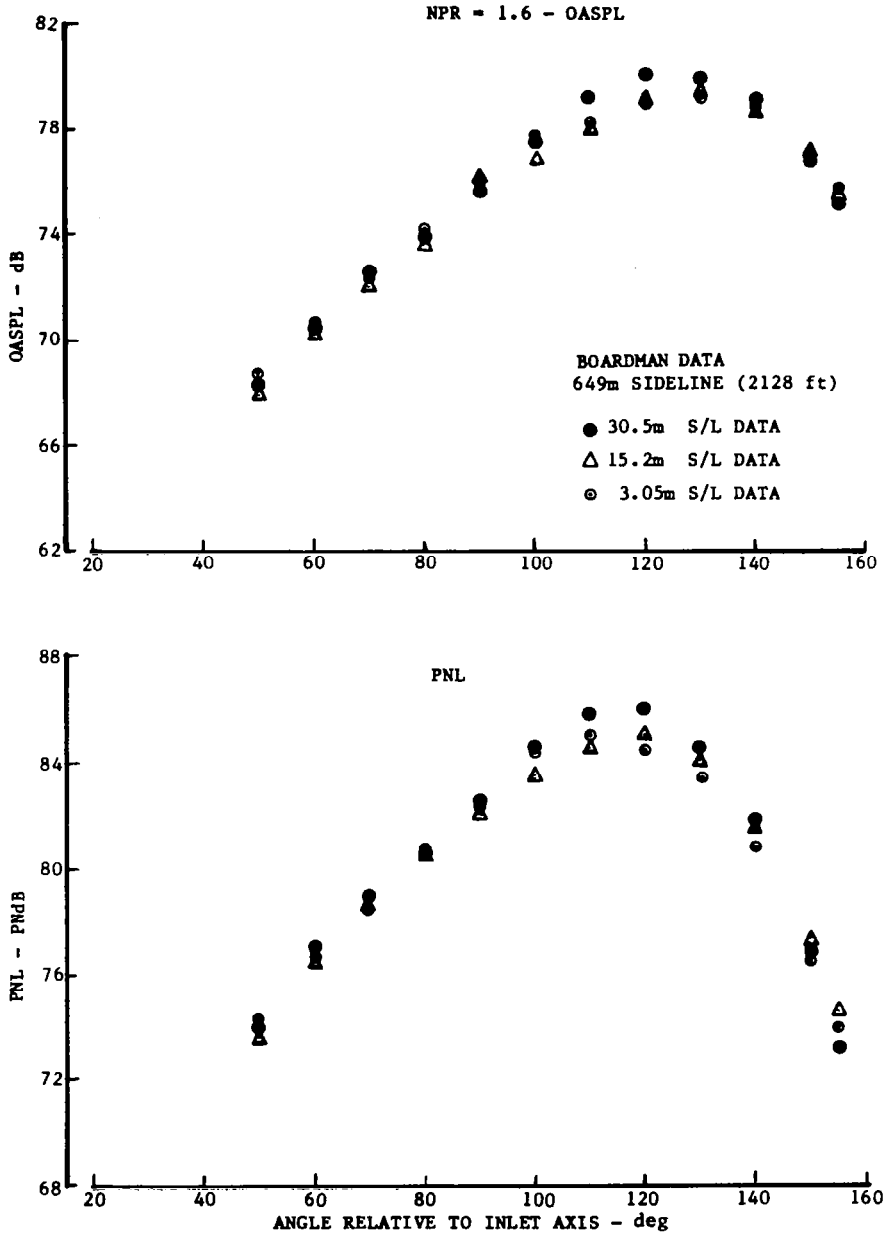

(d) NPR = 1.6

Figure 22.—(Concluded)

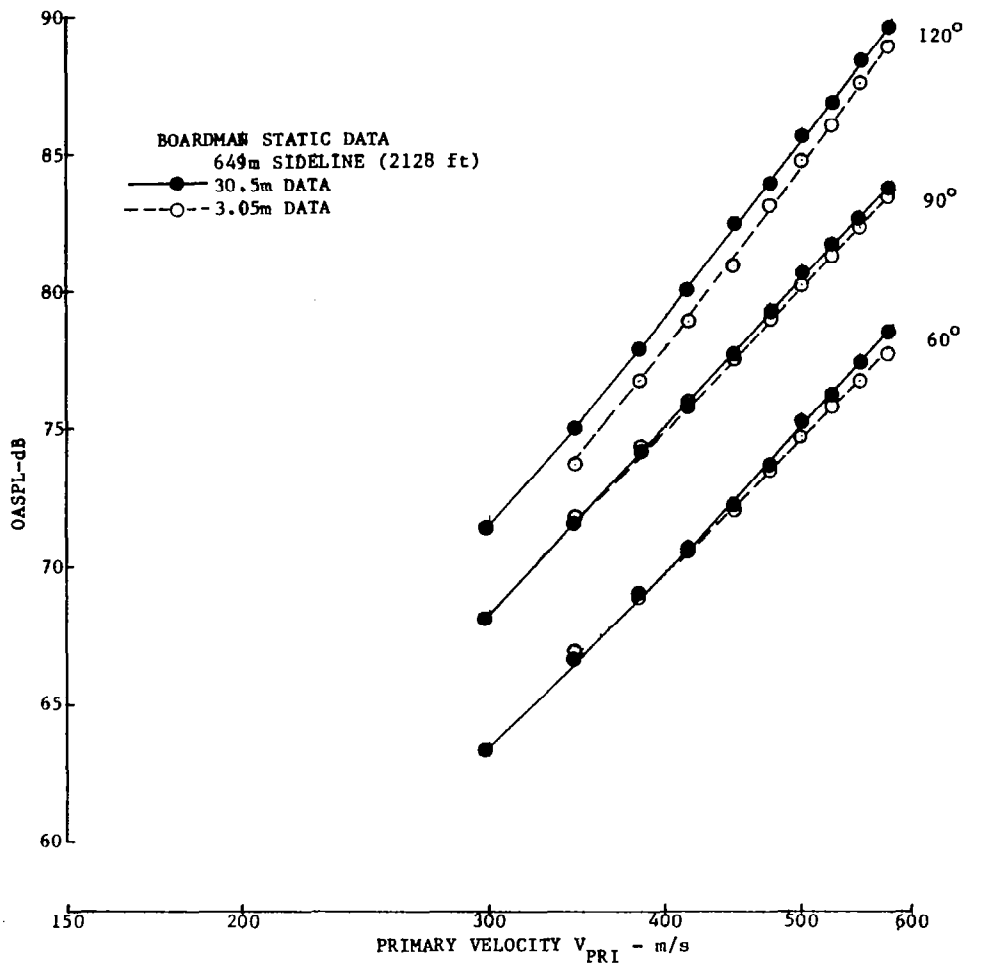

(a) 60°, 90°, 120°

Figure 23.—Comparison of OASPL versus Primary Velocity, 30.5 m and 3.05 m Data-Inverter Configuration

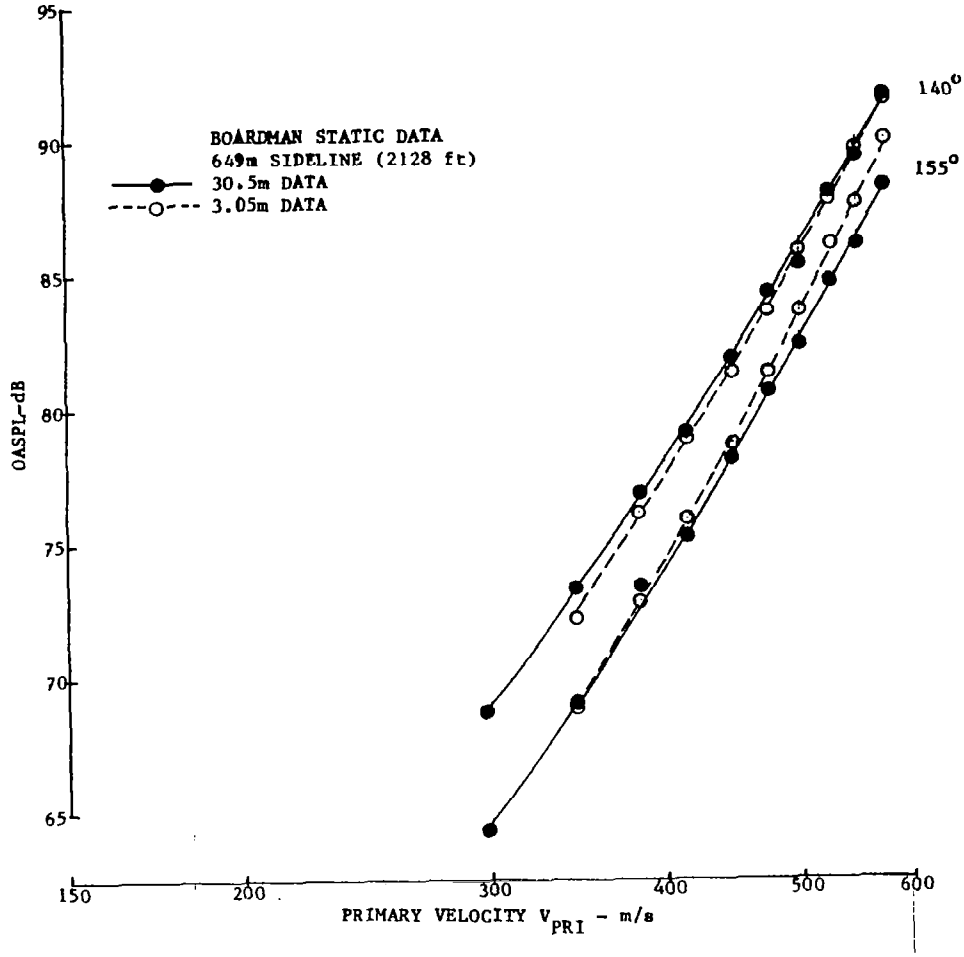

(b) 140°, 155°

Figure 23.—(Concluded)

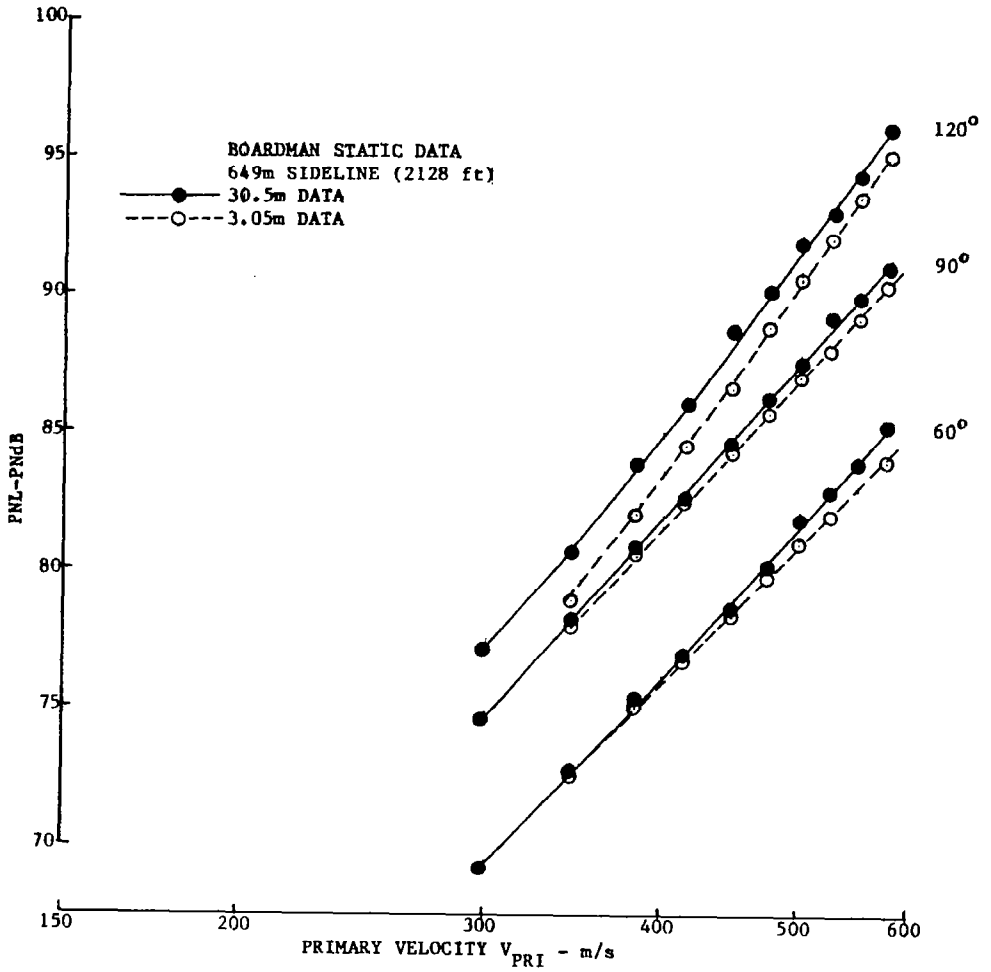

(a) 60°, 90°, 120°

Figure 24.—Comparison of PNL versus Primary Velocity, 30.5 m and 3.05 m Data-Inverter Configuration

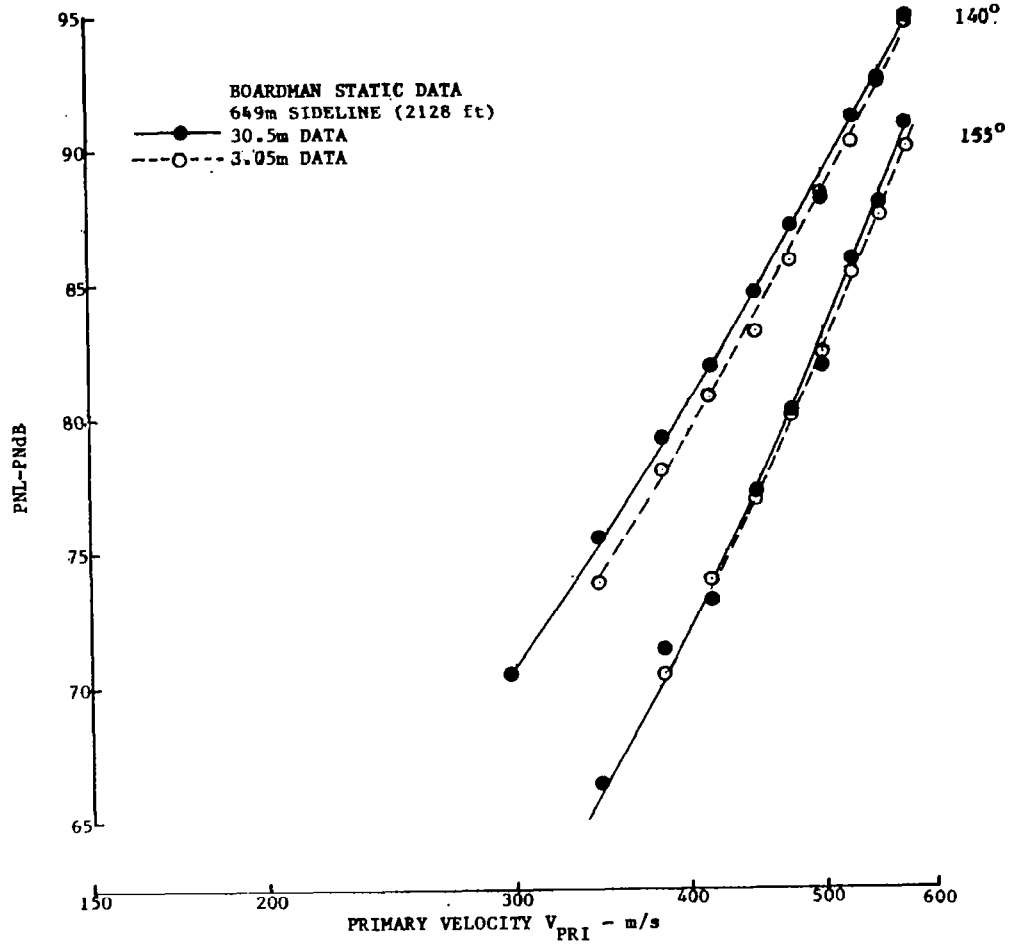

(b) 140°, 155°

Figure 24.—(Concluded)

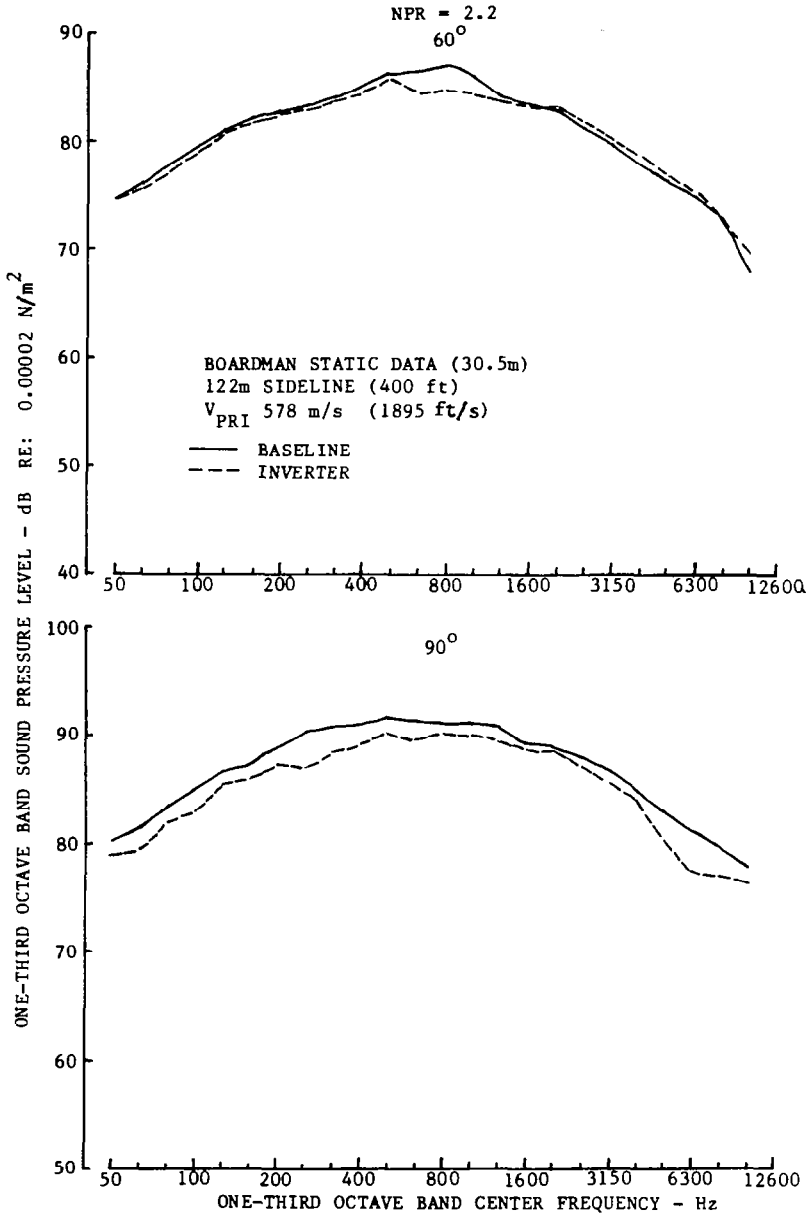

(a) 60° & 90°

Figure 25.—Comparison of Baseline and Inverter Spectra: NPR = 2.2

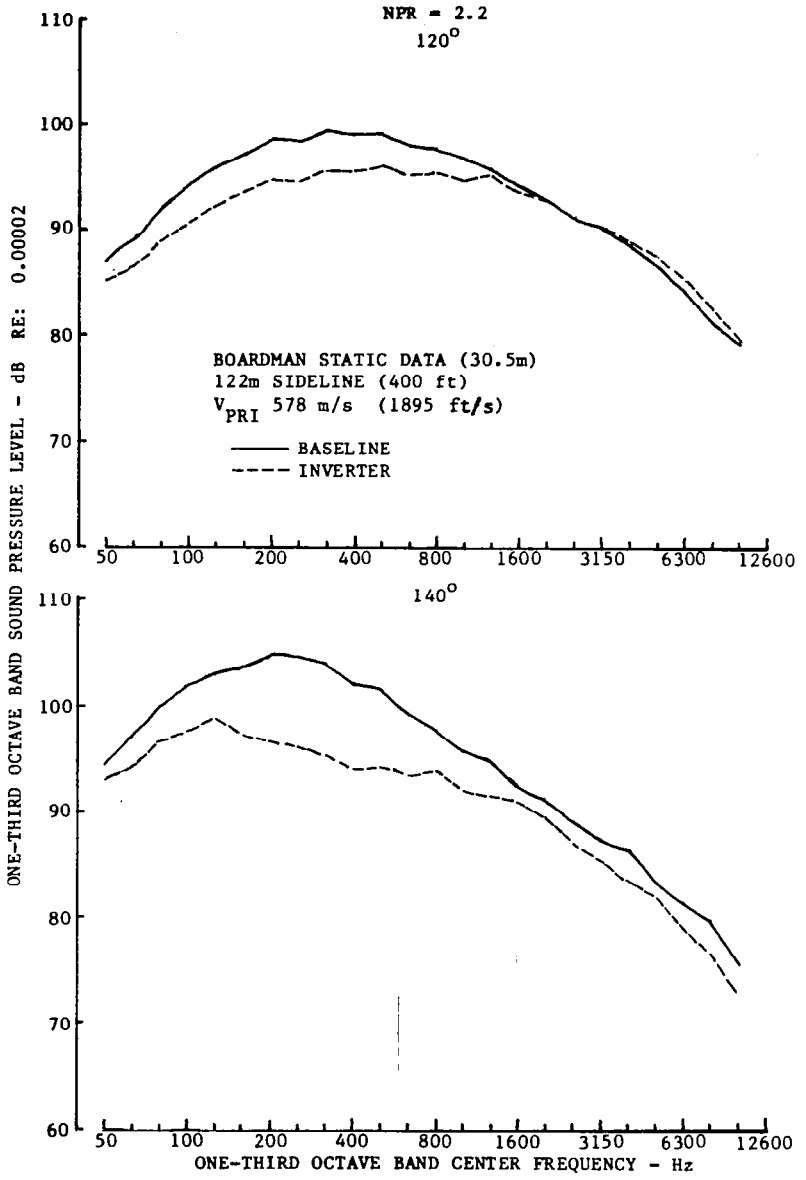

(b) 120° & 140°

Figure 25.—(Concluded)

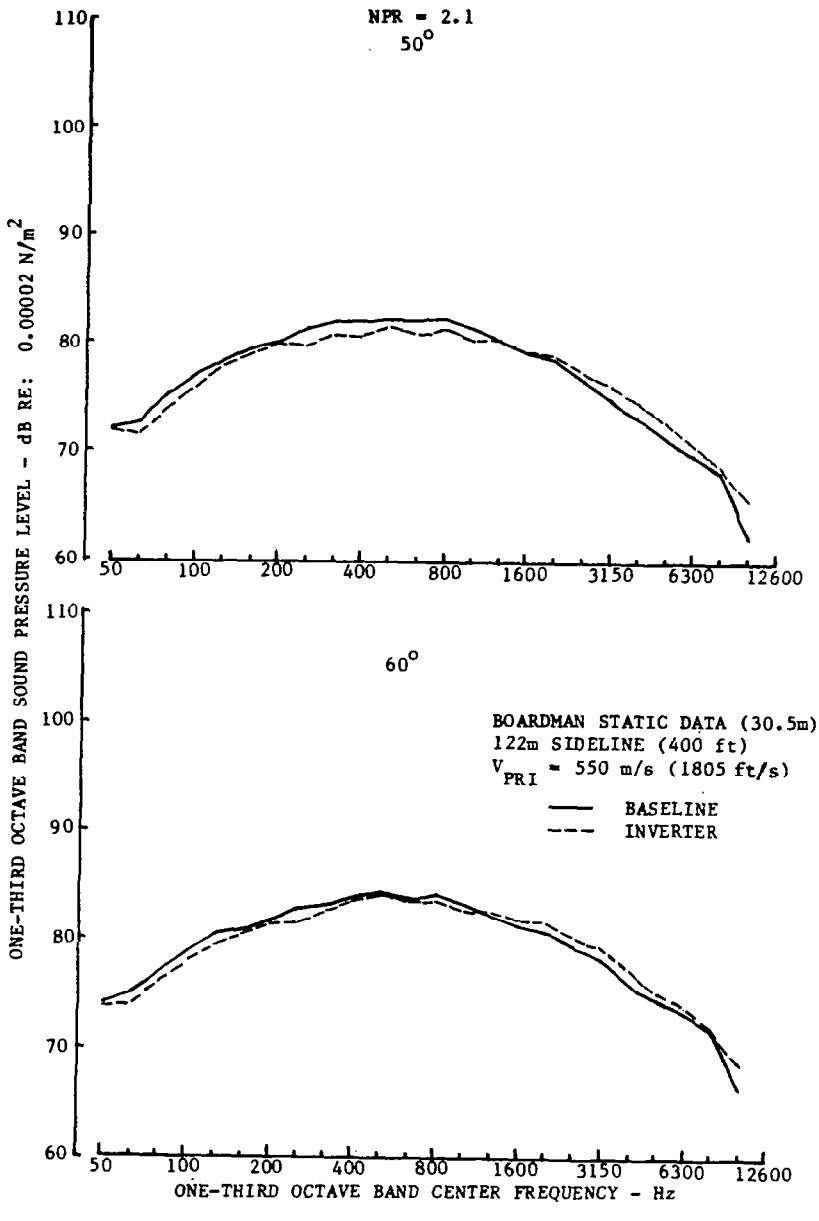

(a) 50° & 60°

Figure 26.—Comparison of Baseline and Inverter Spectra: NPR = 2.1

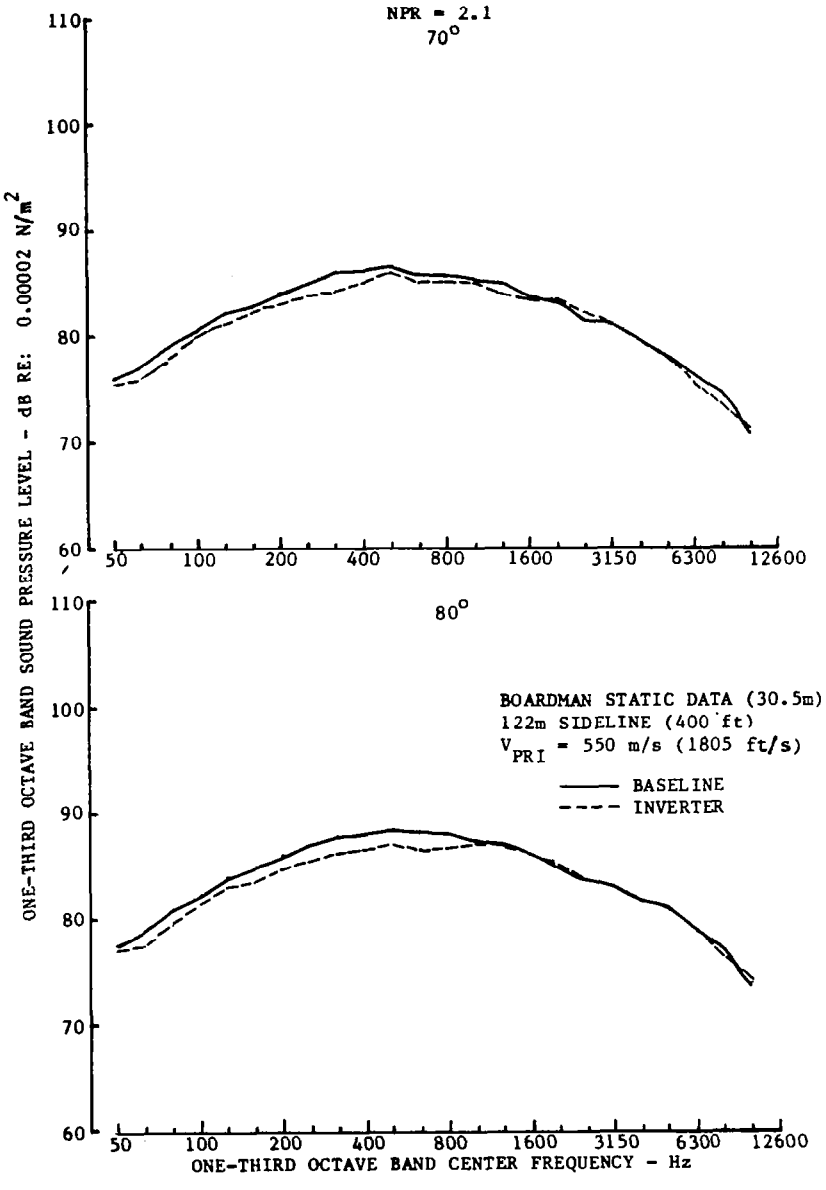

(b) 70° & 80°

Figure 26.—(Continued)

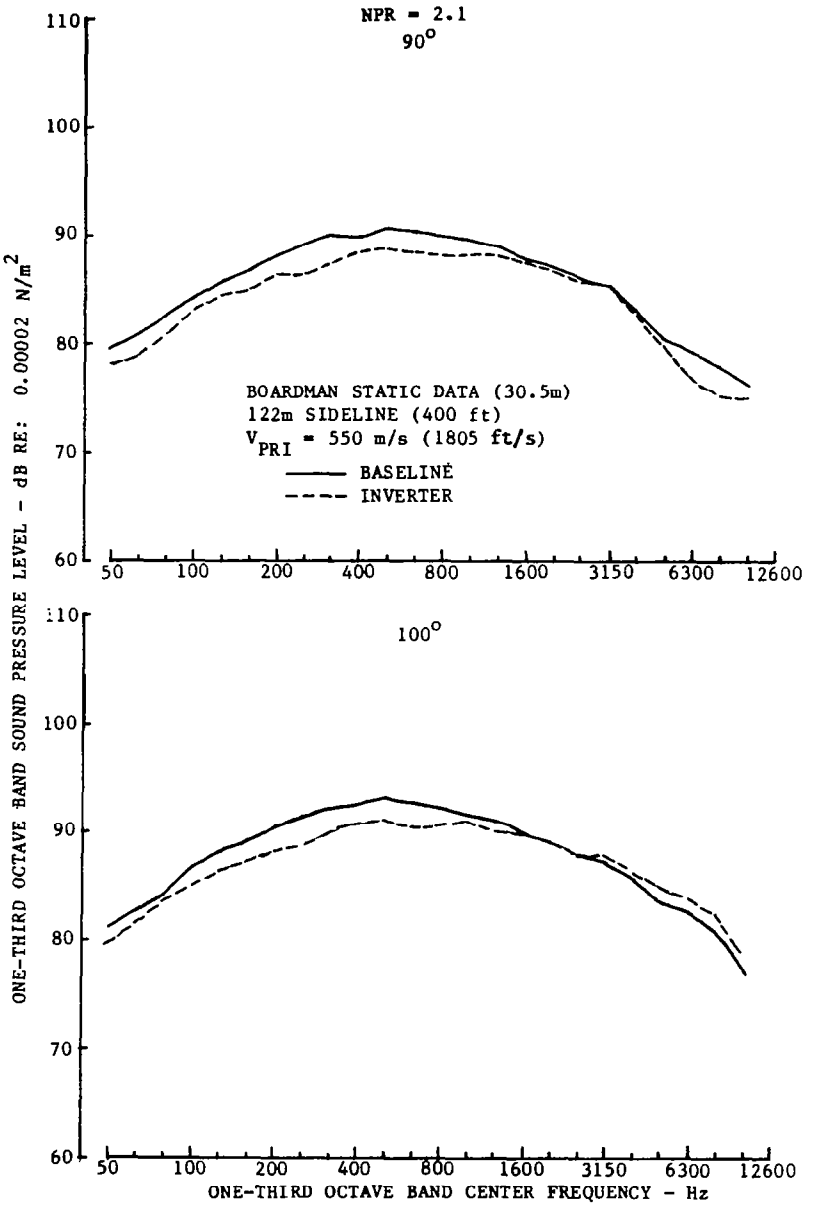

(c) 90° & 100°

Figure 26.—(Continued)

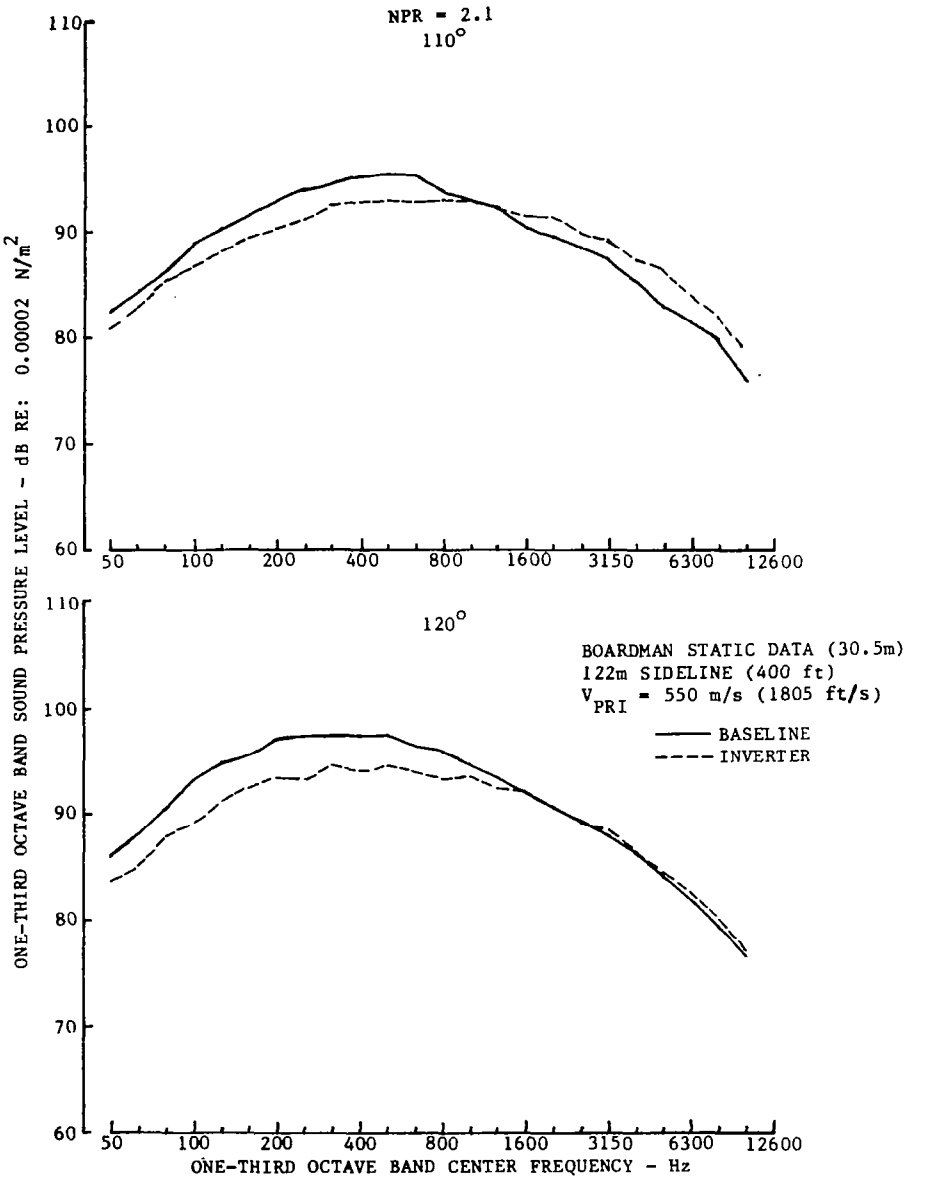

(d) 110° & 120°

Figure 26.—(Continued)

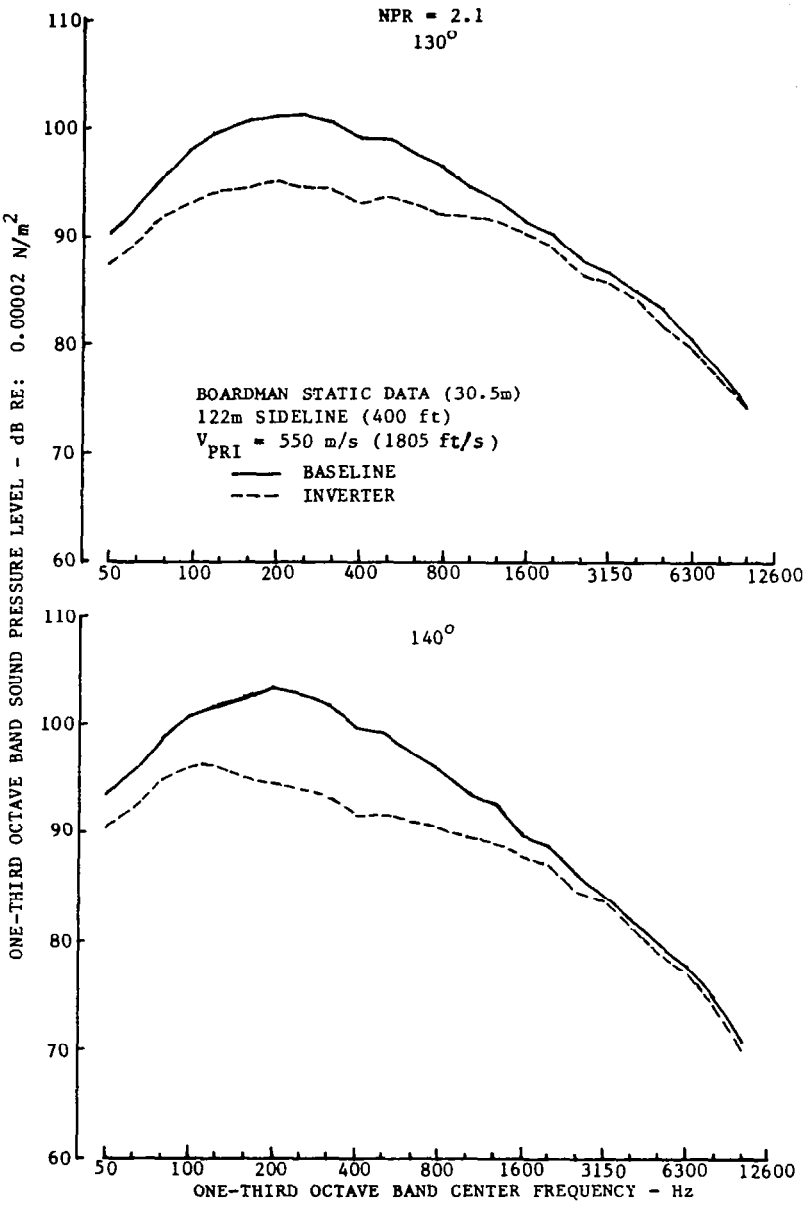

(e) 130° & 140°

Figure 26.—(Continued)

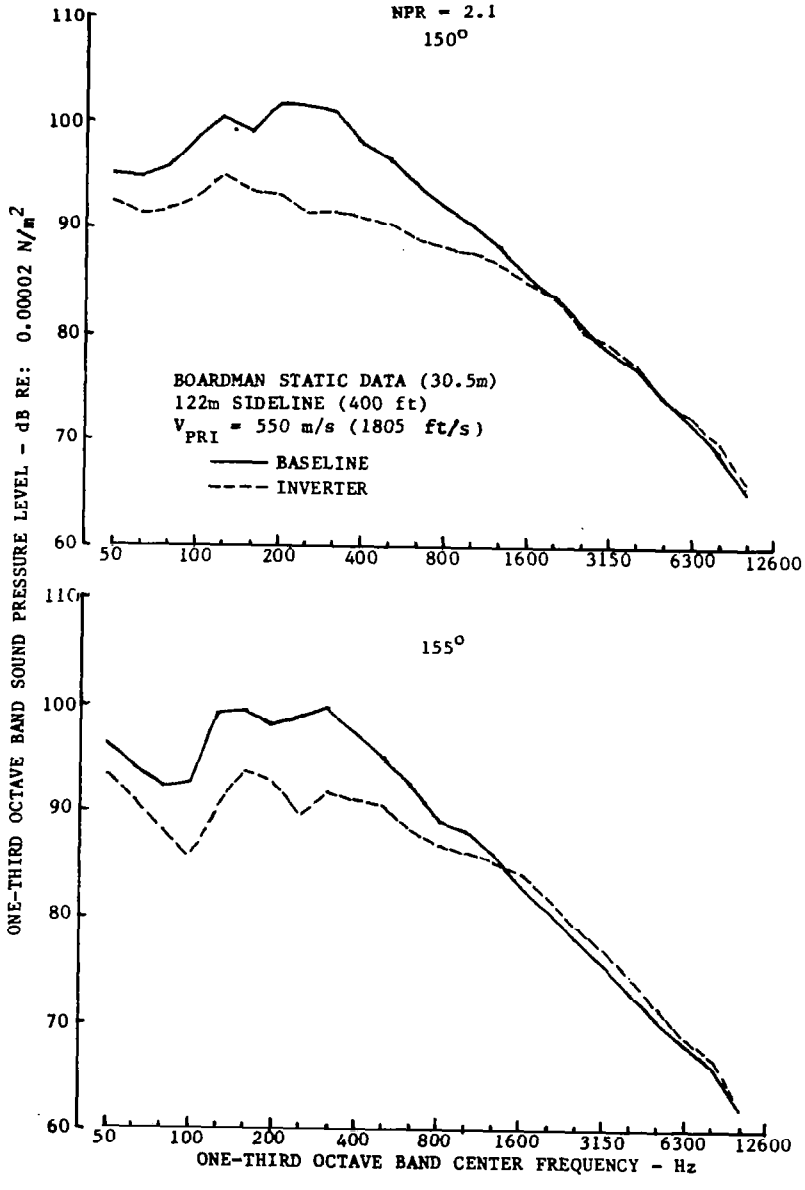

(f) 150° & 155°

Figure 26.—(Concluded)

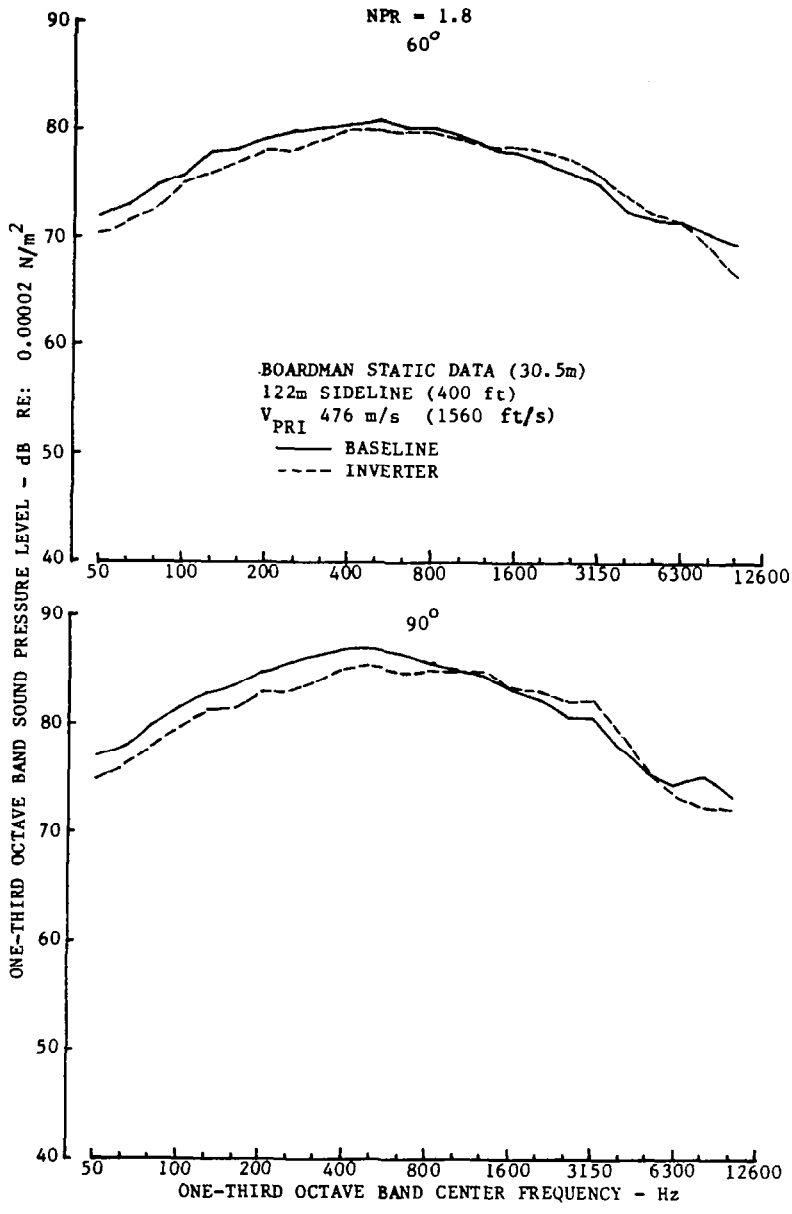

(a) 60° & 90°

Figure 27.—Comparison of Baseline and Inverter Spectra: NPR = 1.8

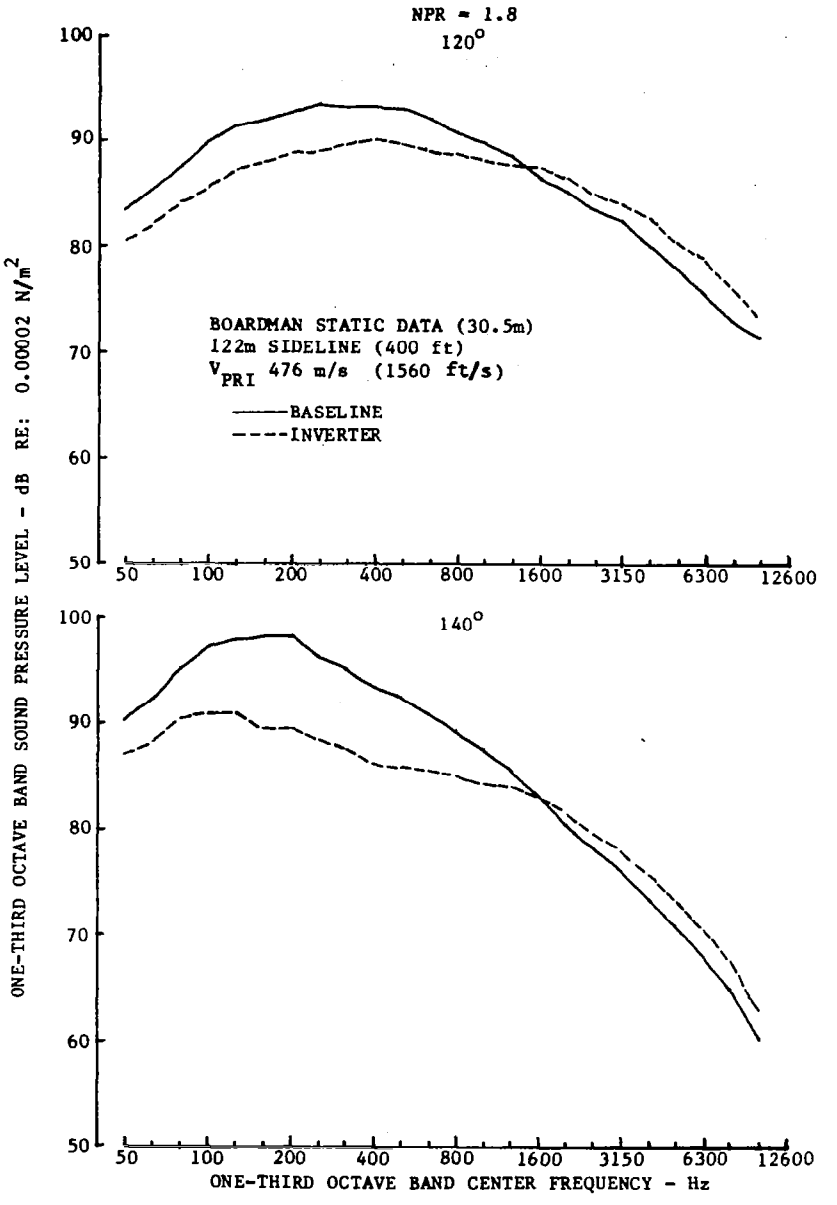

(b) 120° & 140°

Figure 27.—(Concluded)

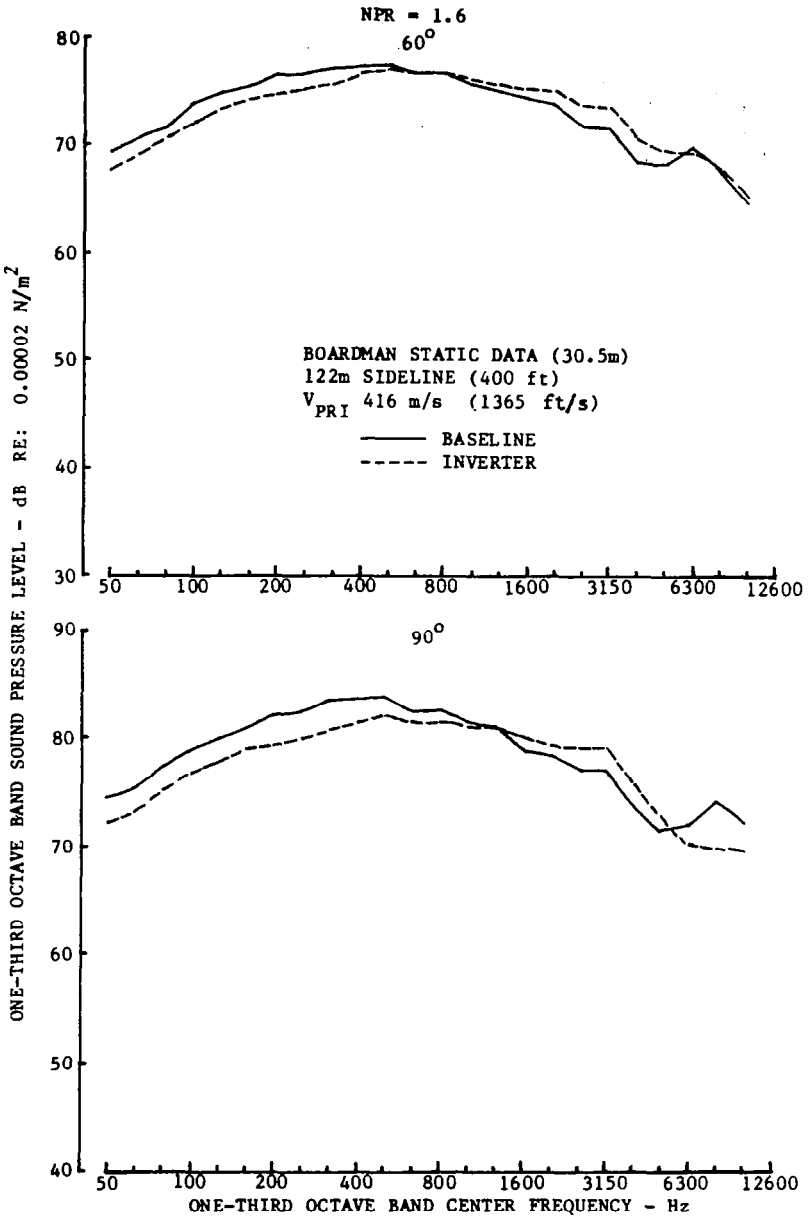

(a) 60° & 90°

Figure 28.—Comparison of Baseline and Inverter Spectra: NPR = 1.6

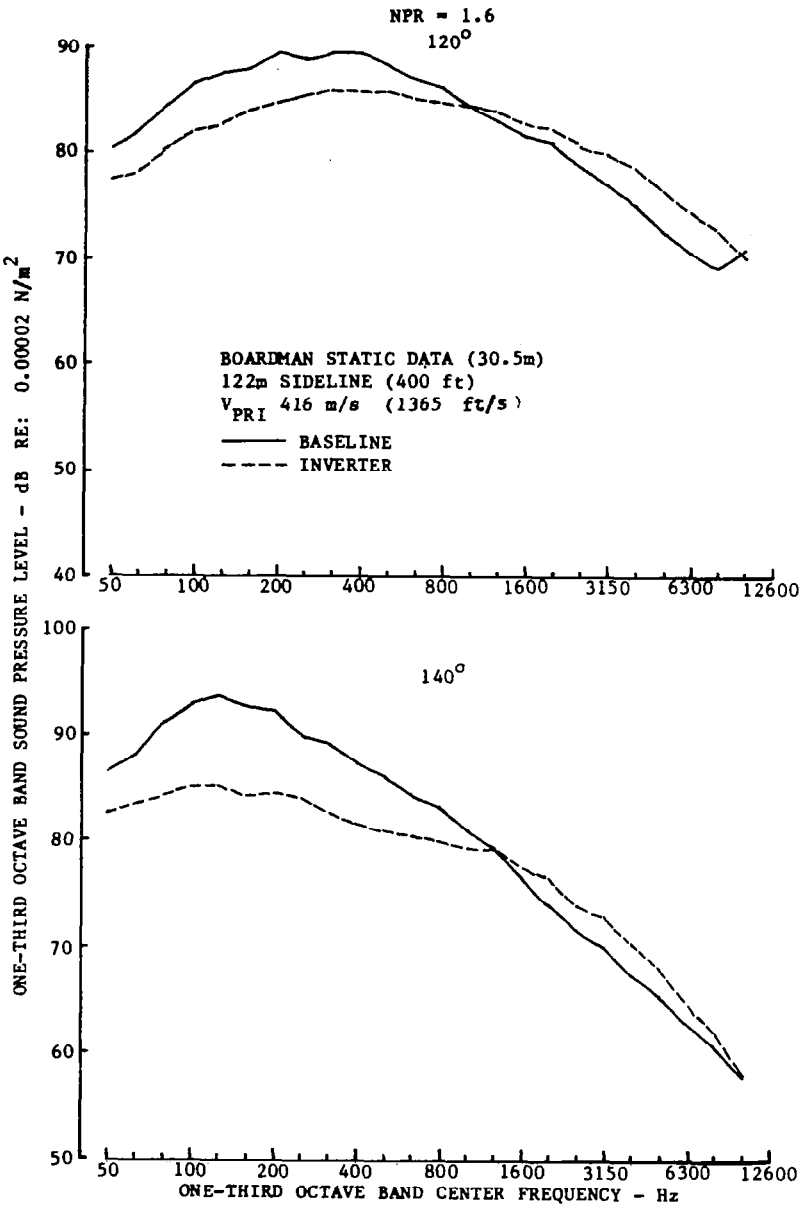

(b) 120° & 140°

Figure 28.—(Concluded)

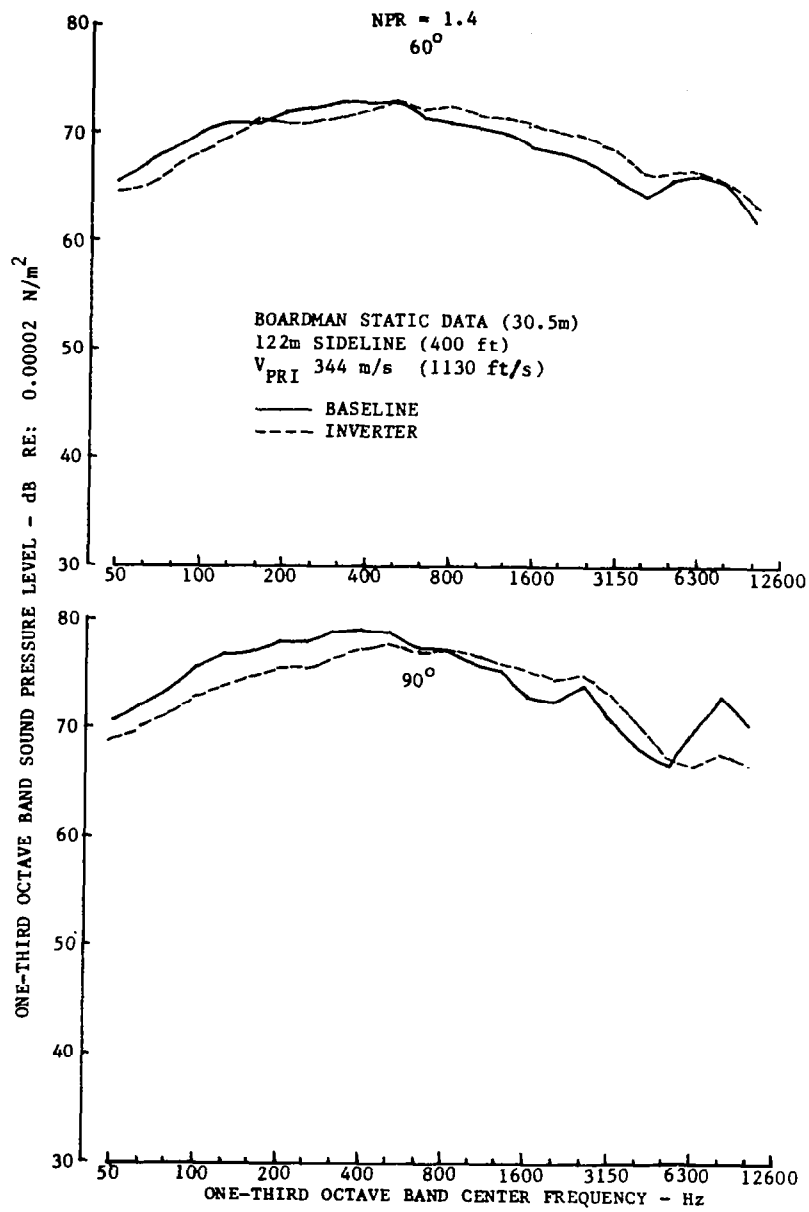

(a) 60° & 90°

Figure 29.—Comparison of Baseline and Inverter Spectra: NPR = 1.4

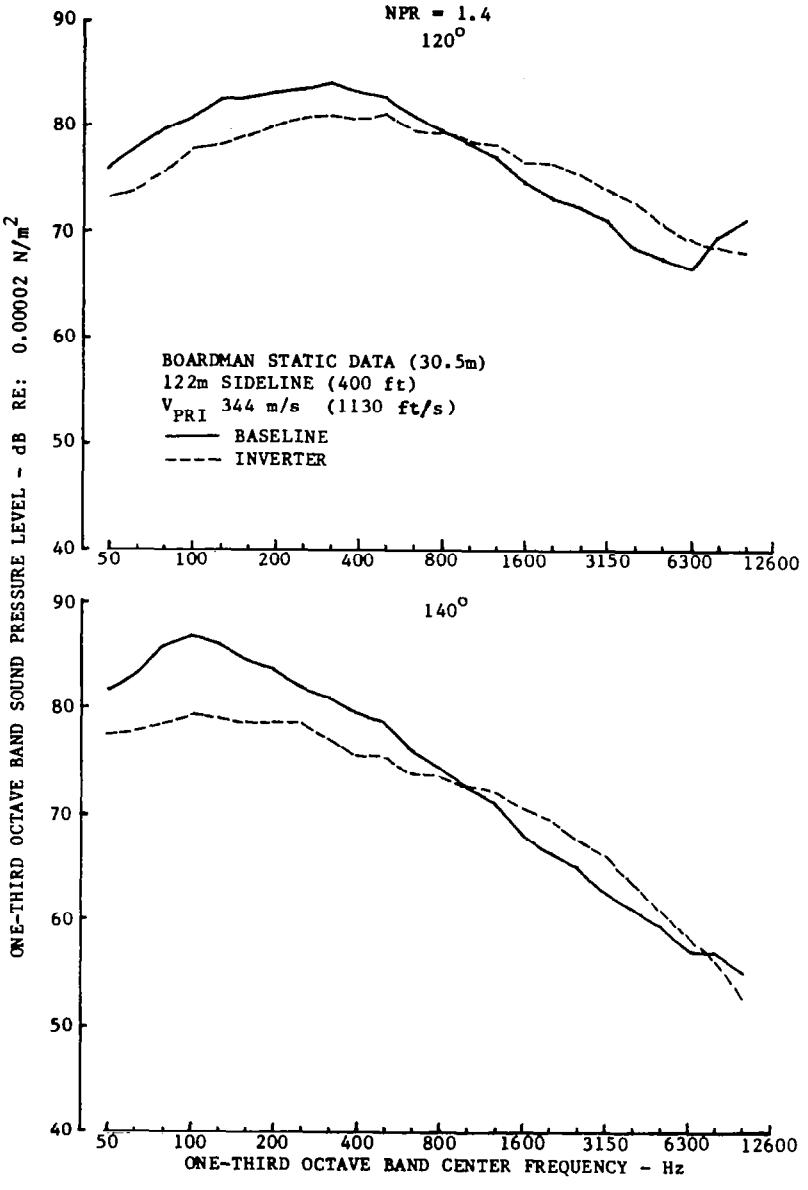

(b) 120° & 140°

Figure 29.—(Concluded)

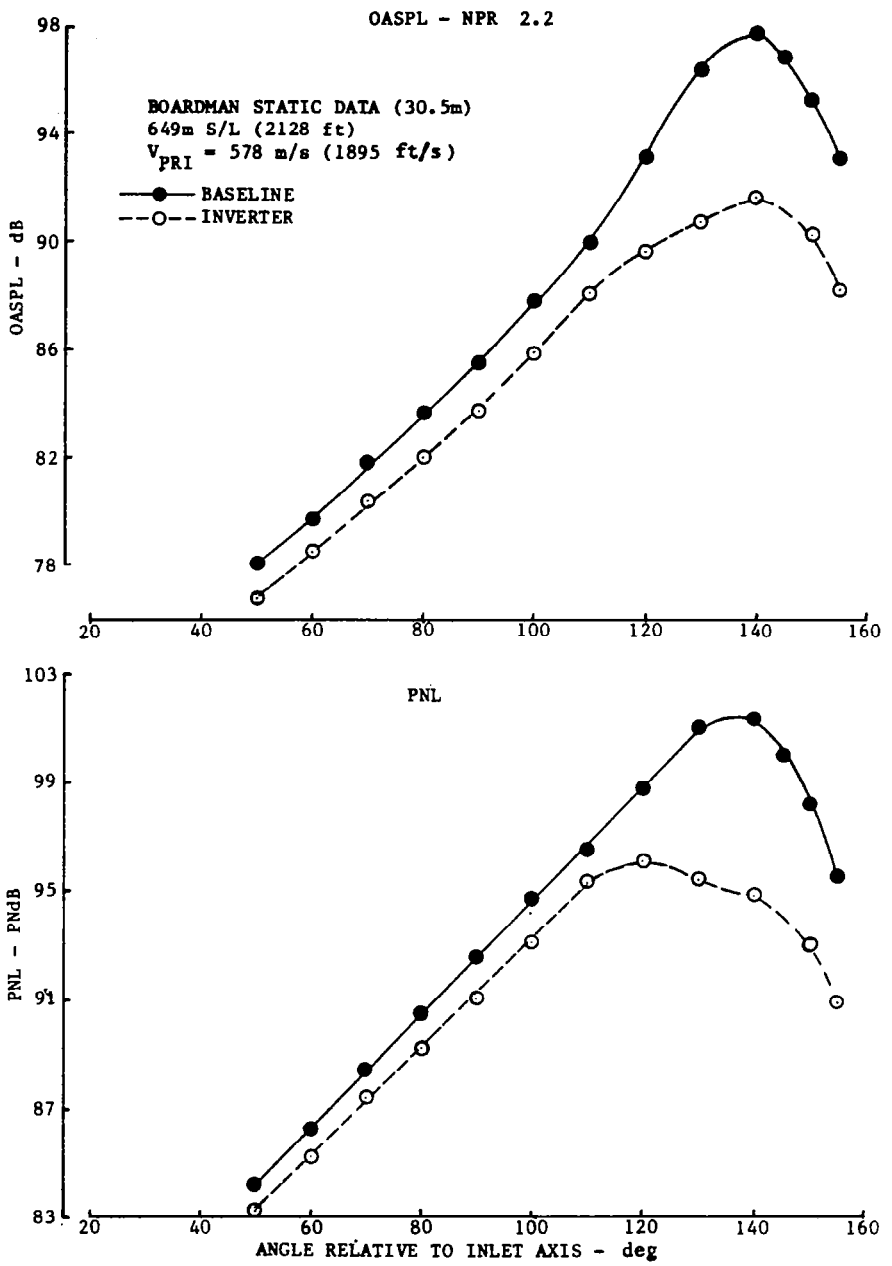

(a) NPR = 2.2

Figure 30.—Comparison of Static OASPL and PNL Directivity, Baseline versus Inverter

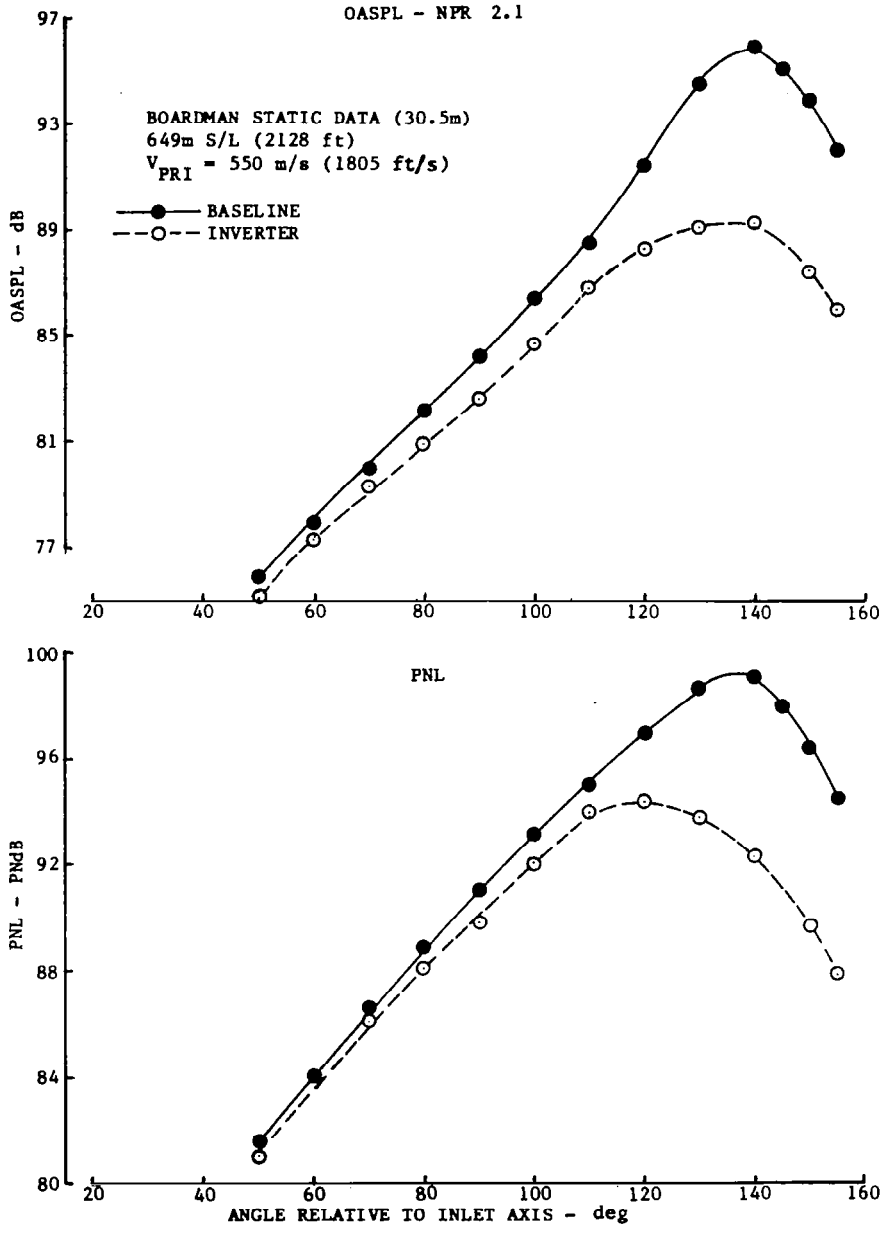

(b) NPR = 2.1

Figure 30.—(Continued)

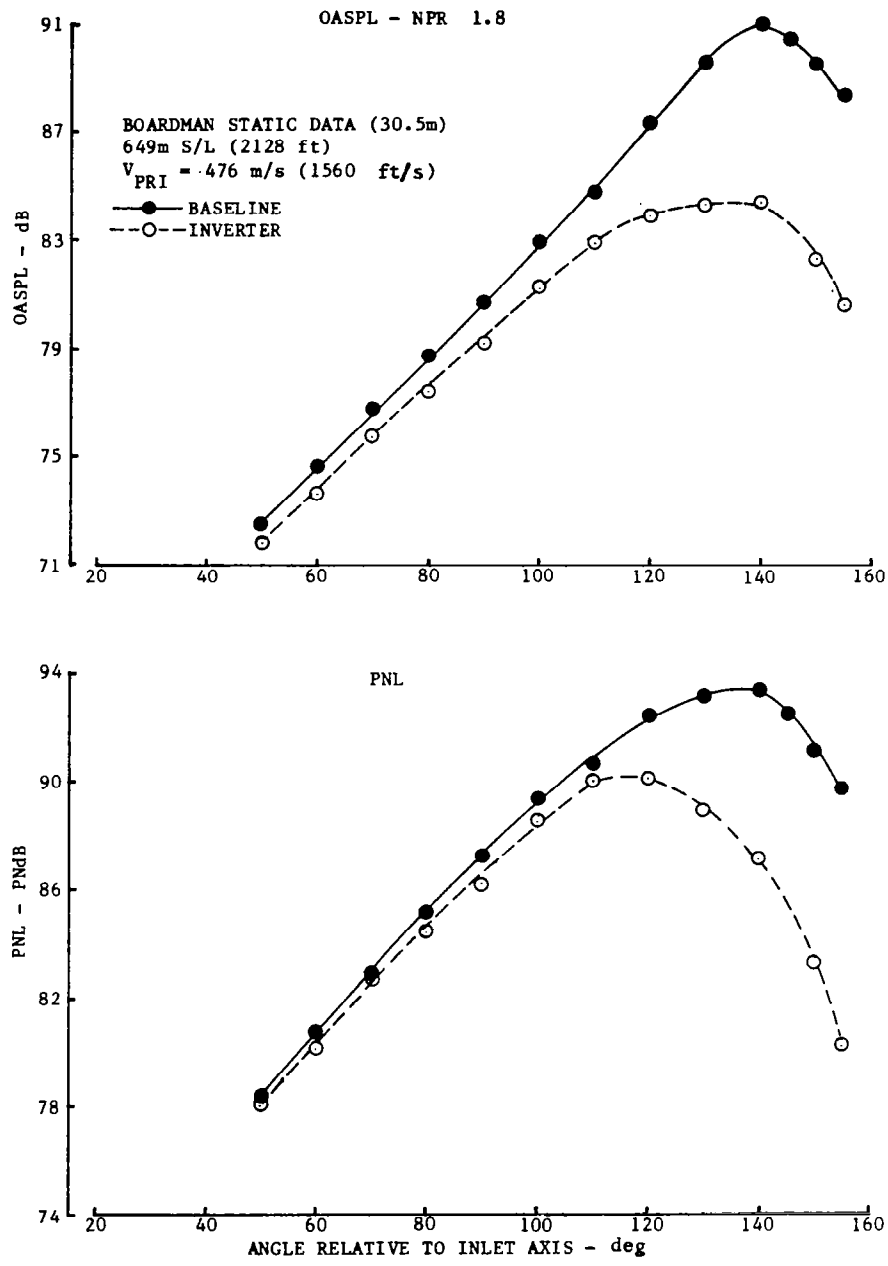

(c) NPR = 1.8

Figure 30.—(Continued)

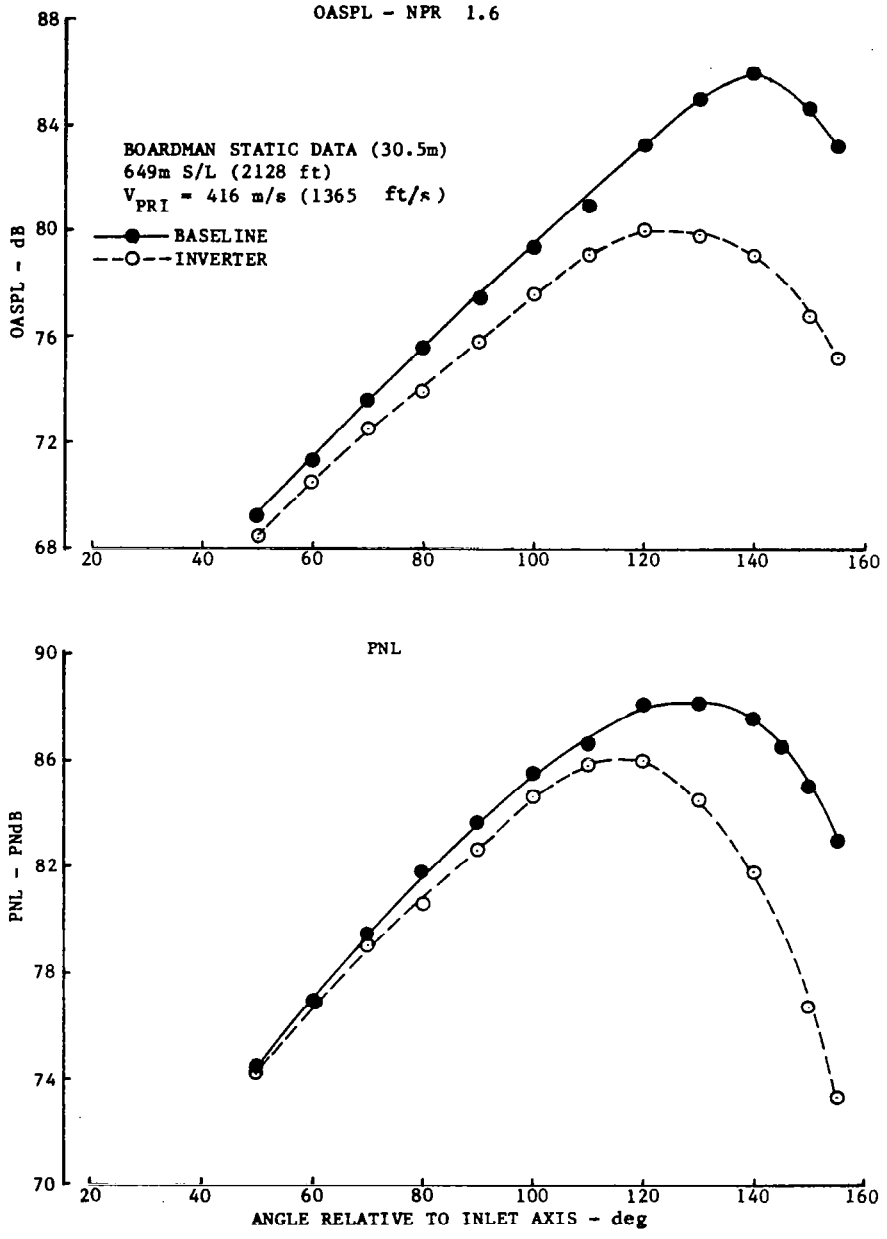

(d) NPR = 1.6

Figure 30.—(Continued)

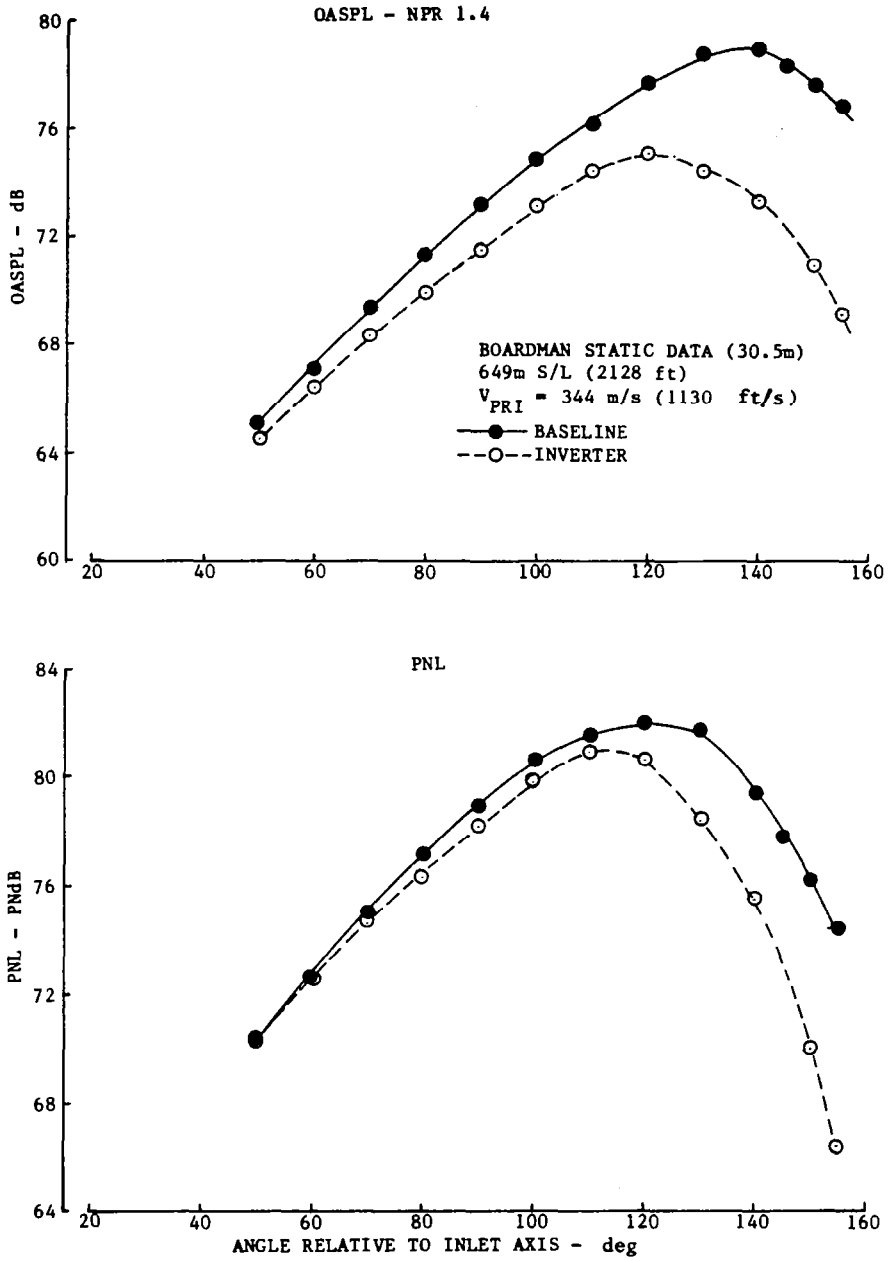

(e) NPR = 1.4

Figure 30.—(Concluded)

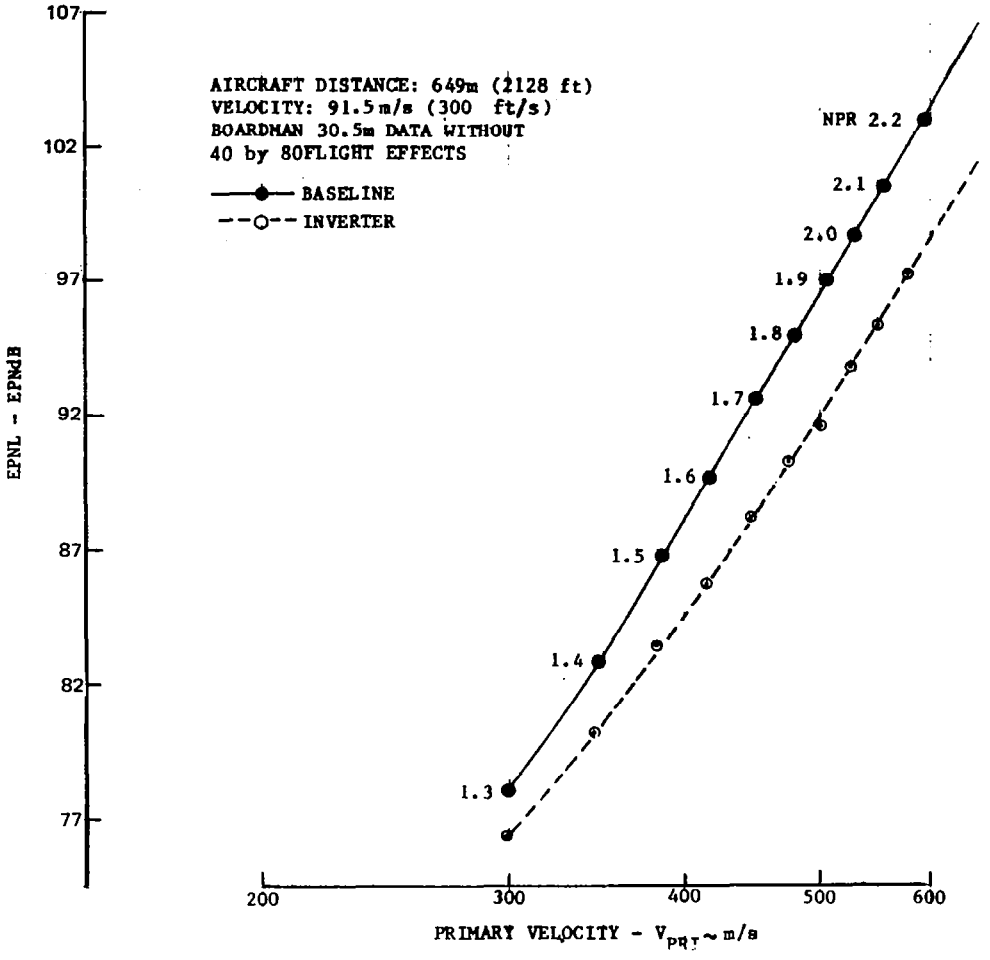

Figure 31.—Comparison of Baseline and Inverter EPNL, Static Levels

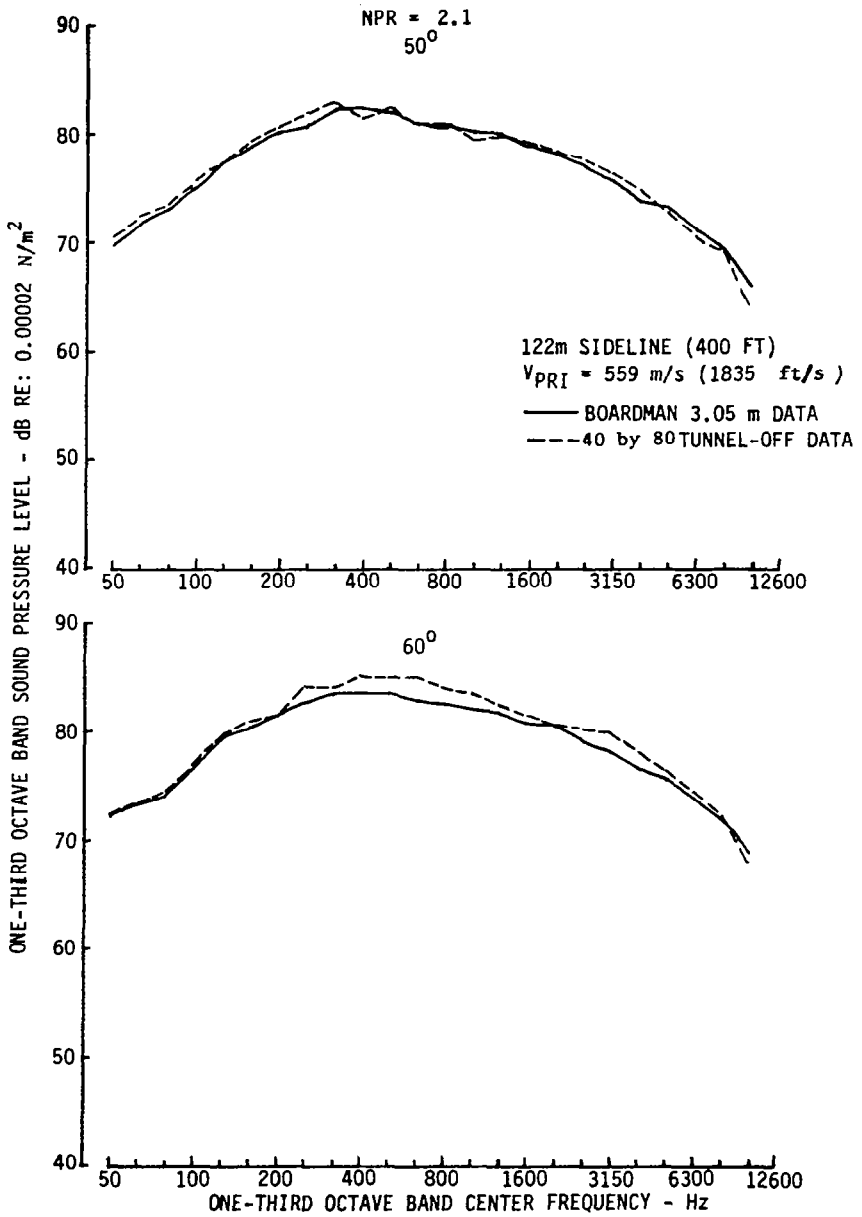

(a) 50° & 60°

Figure 32.—Comparison of Boardman and 40 by 80 Spectra, Inverter Configuration

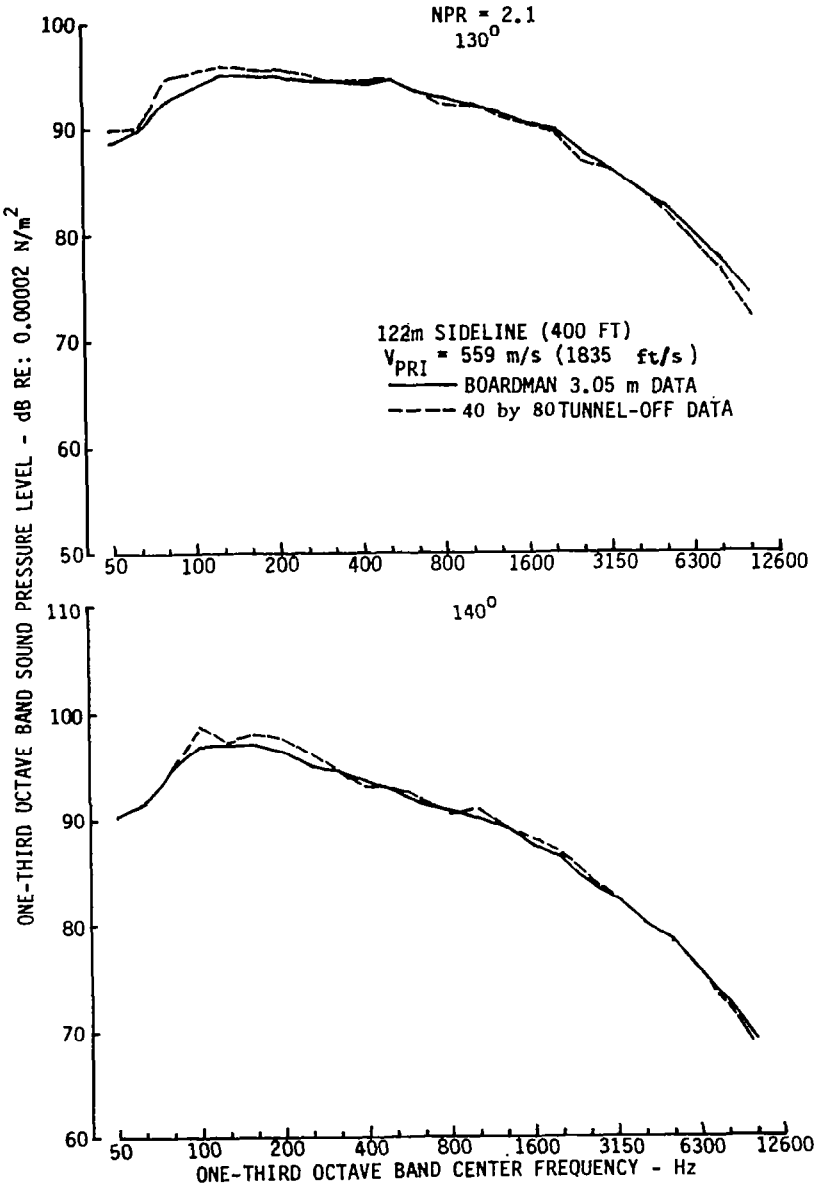

(b) 130° & 140°

Figure 32.—(Concluded)

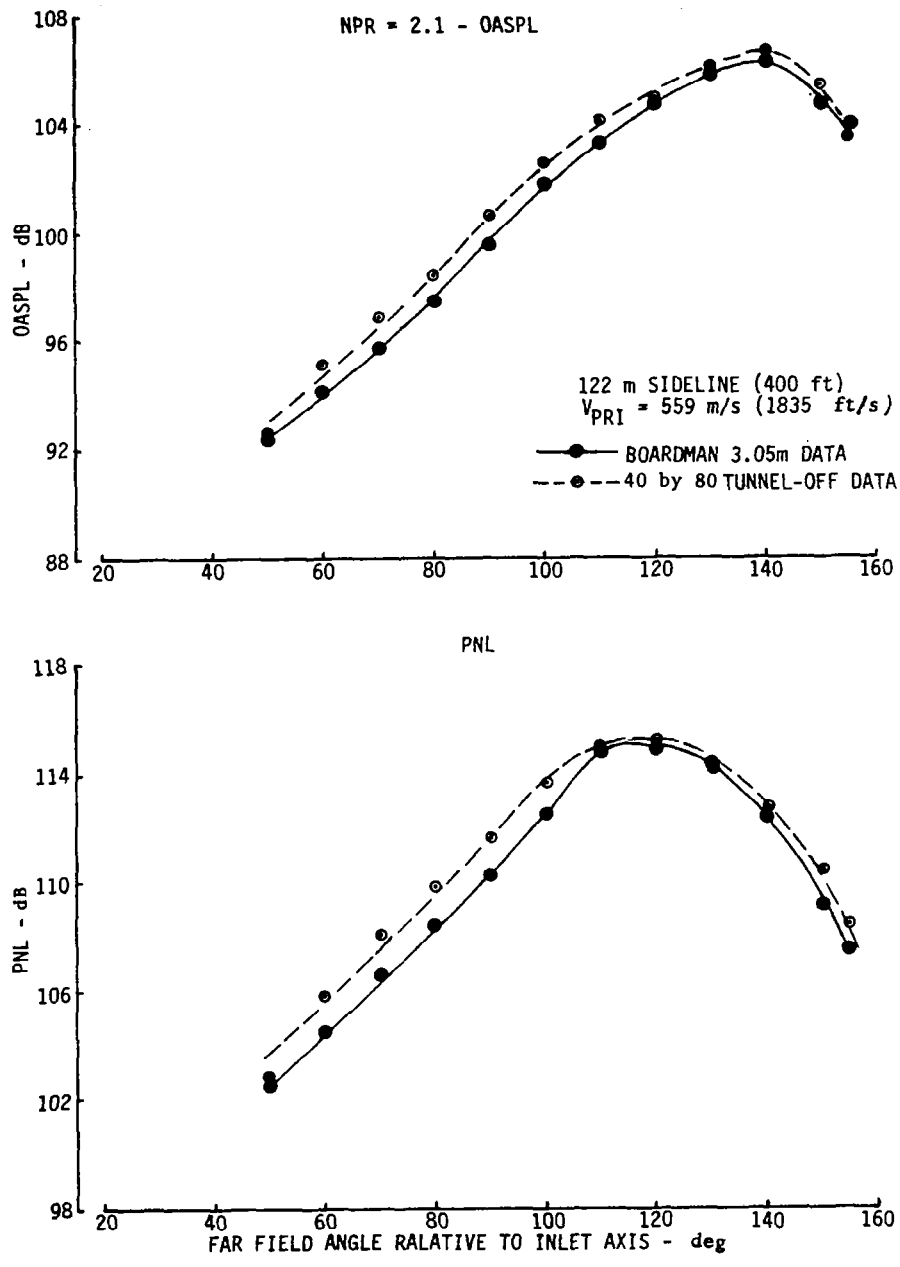

Figure 33.—Comparison of Boardman and 40 by 80 OASPL and PNL Directivities, Inverter Configuration

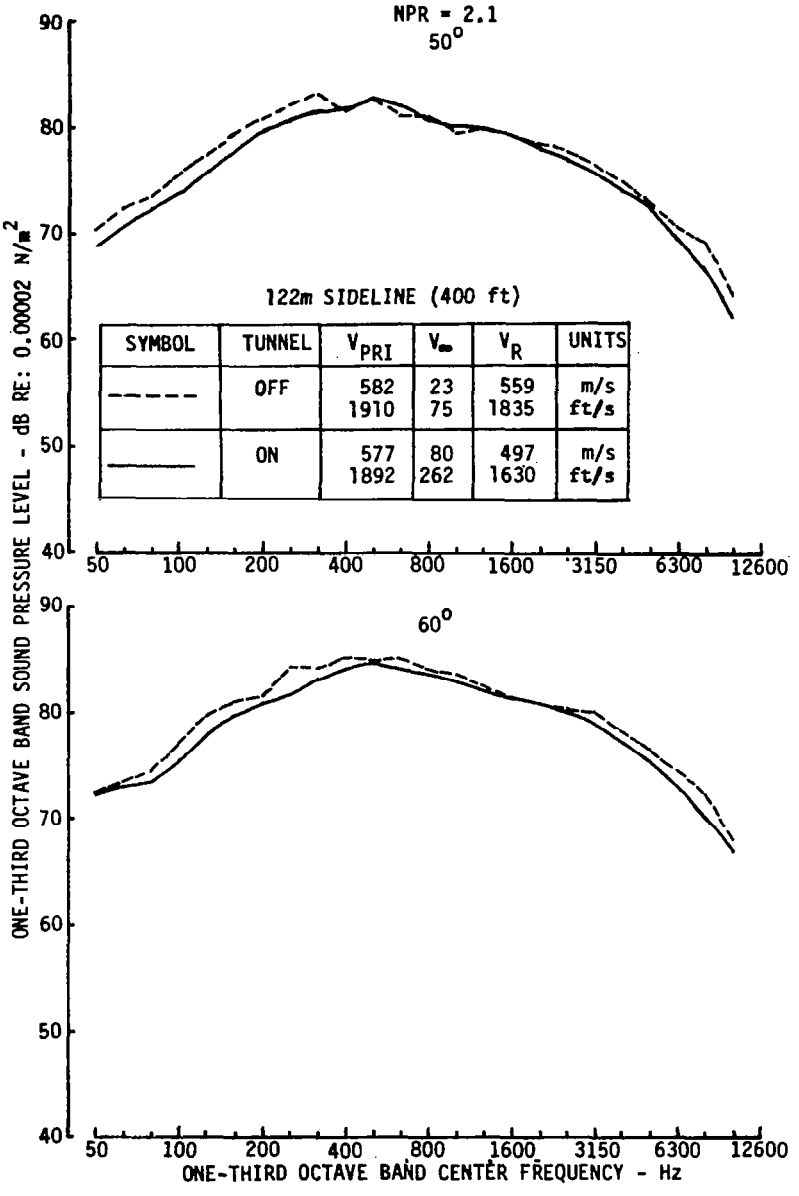

(a) 50° & 60°

Figure 34.—Comparison of Tunnel-Off and -On Spectra, Inverter Configuration: NPR = 2.1

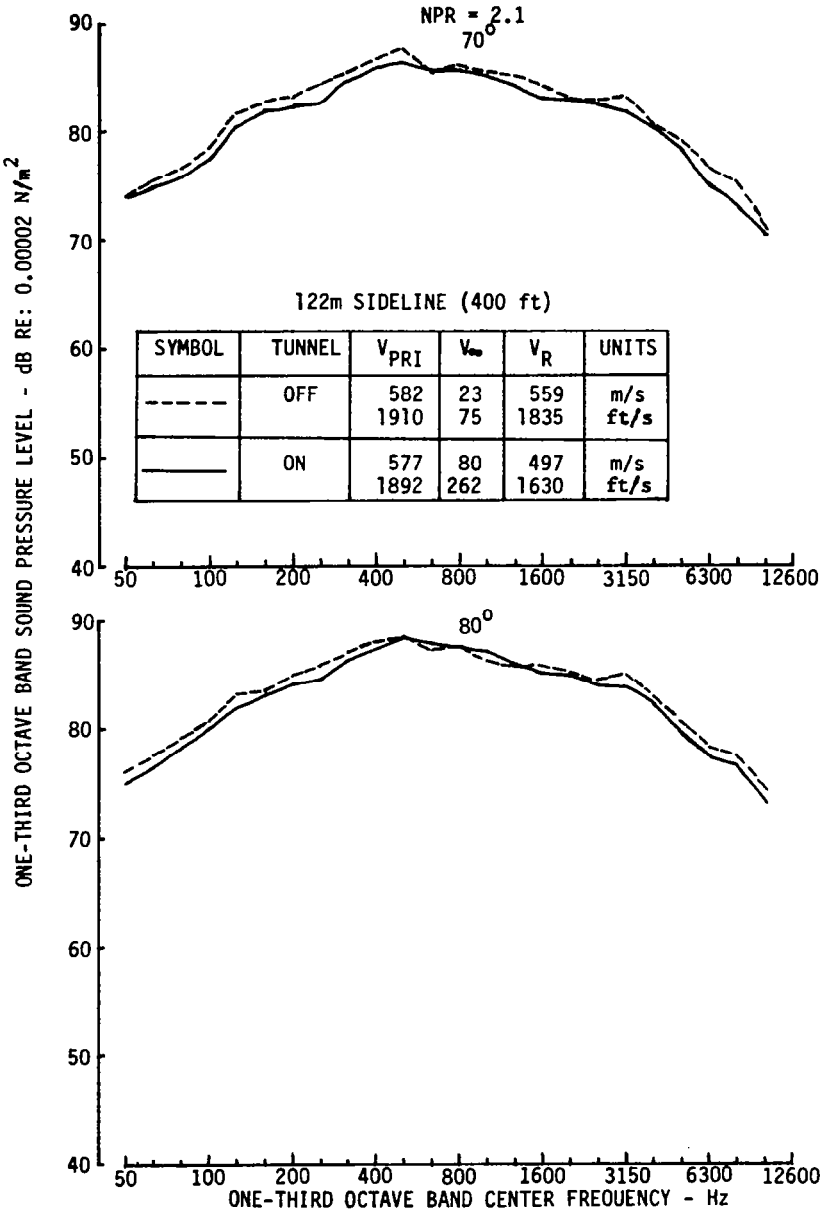

(b) 70° & 80°

Figure 34.—(Continued)

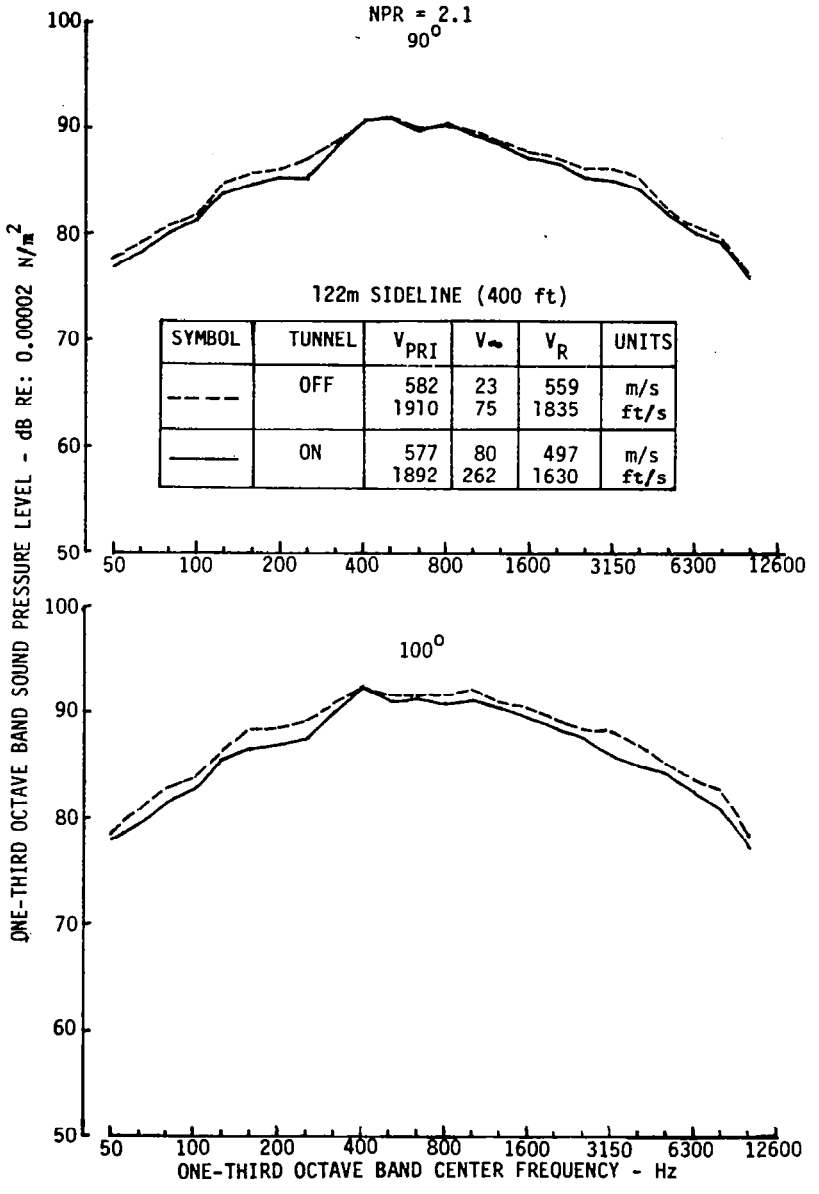

(c) 90° & 100°

Figure 34.—(Continued)

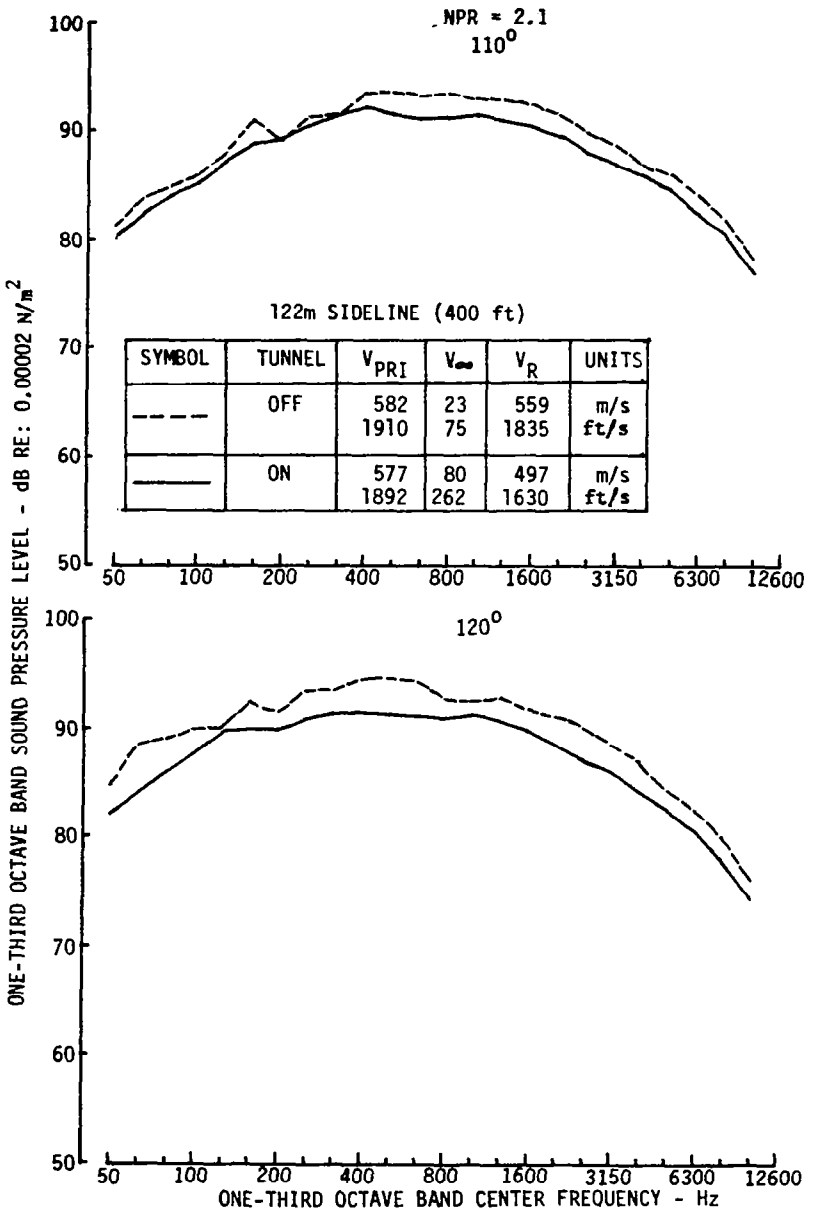

(d) 110° & 120°

Figure 34.—(Continued)

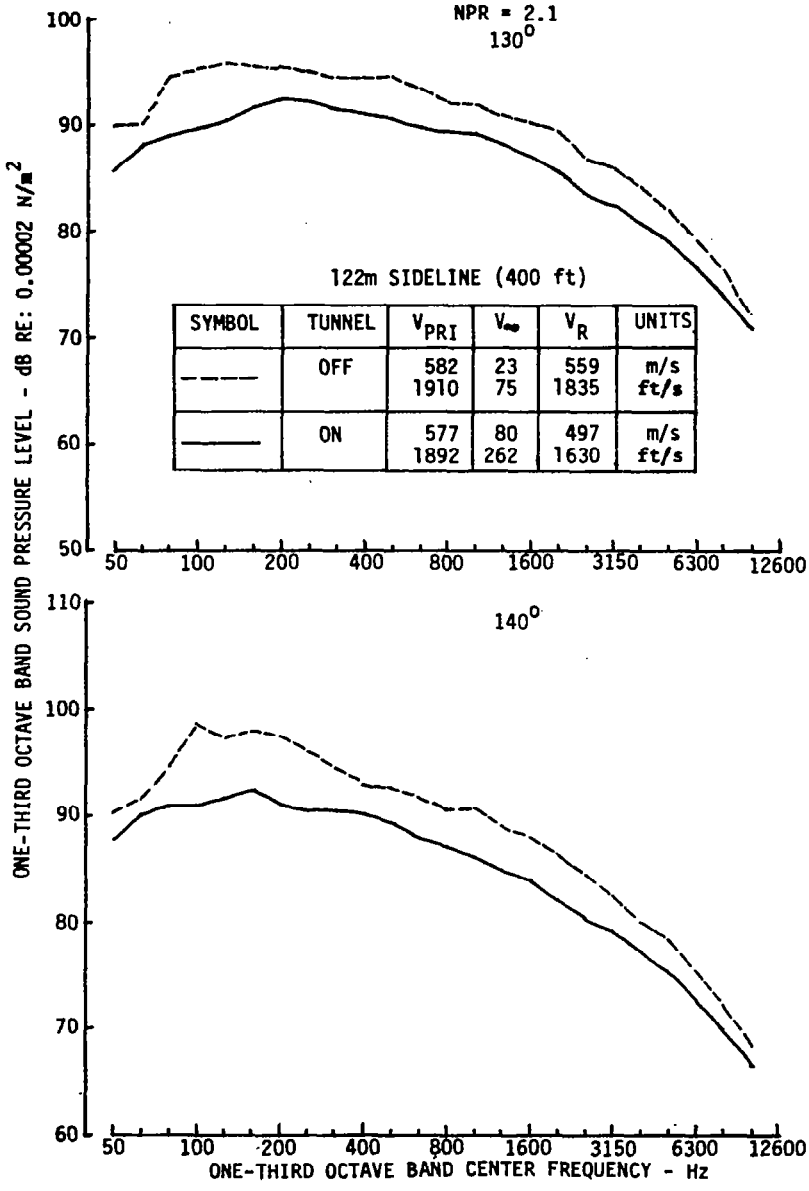

(e) 130° & 140°

Figure 34.—(Continued)

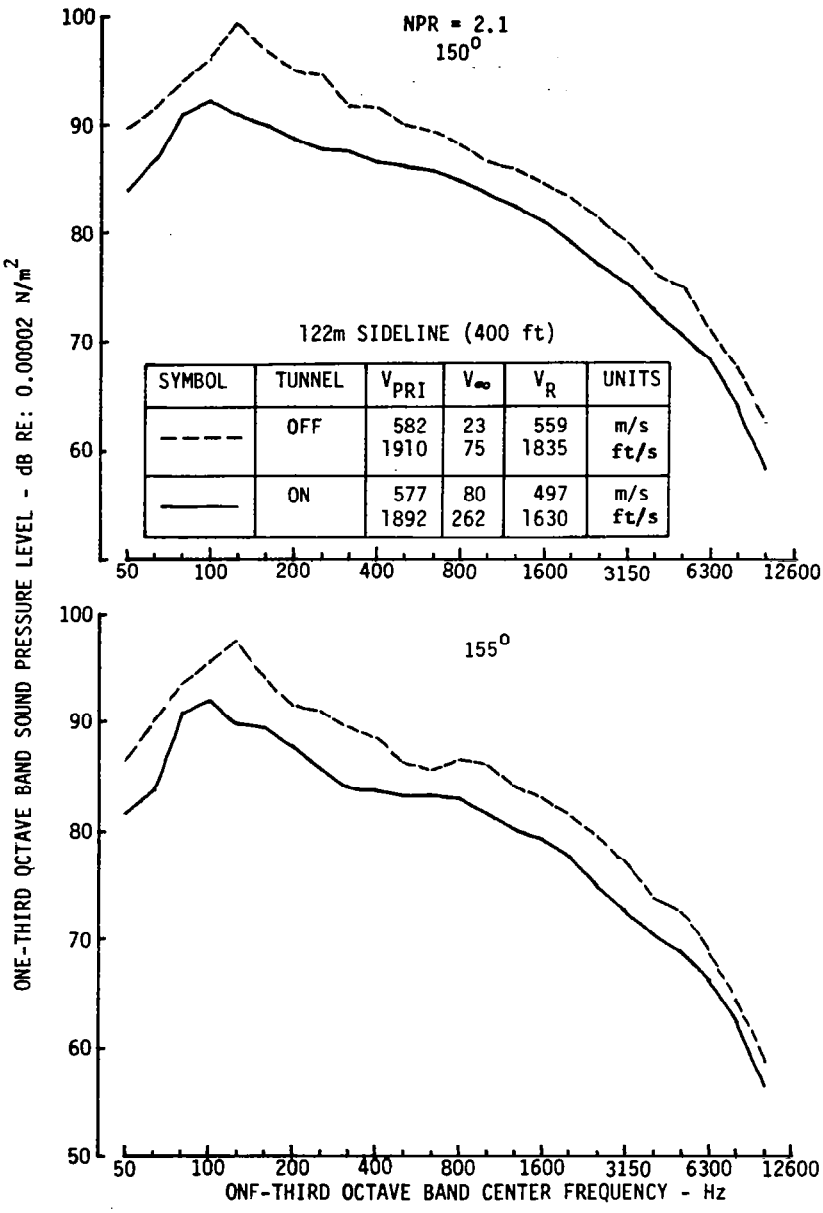

(f) 150° & 155°

Figure 34.—(Concluded)

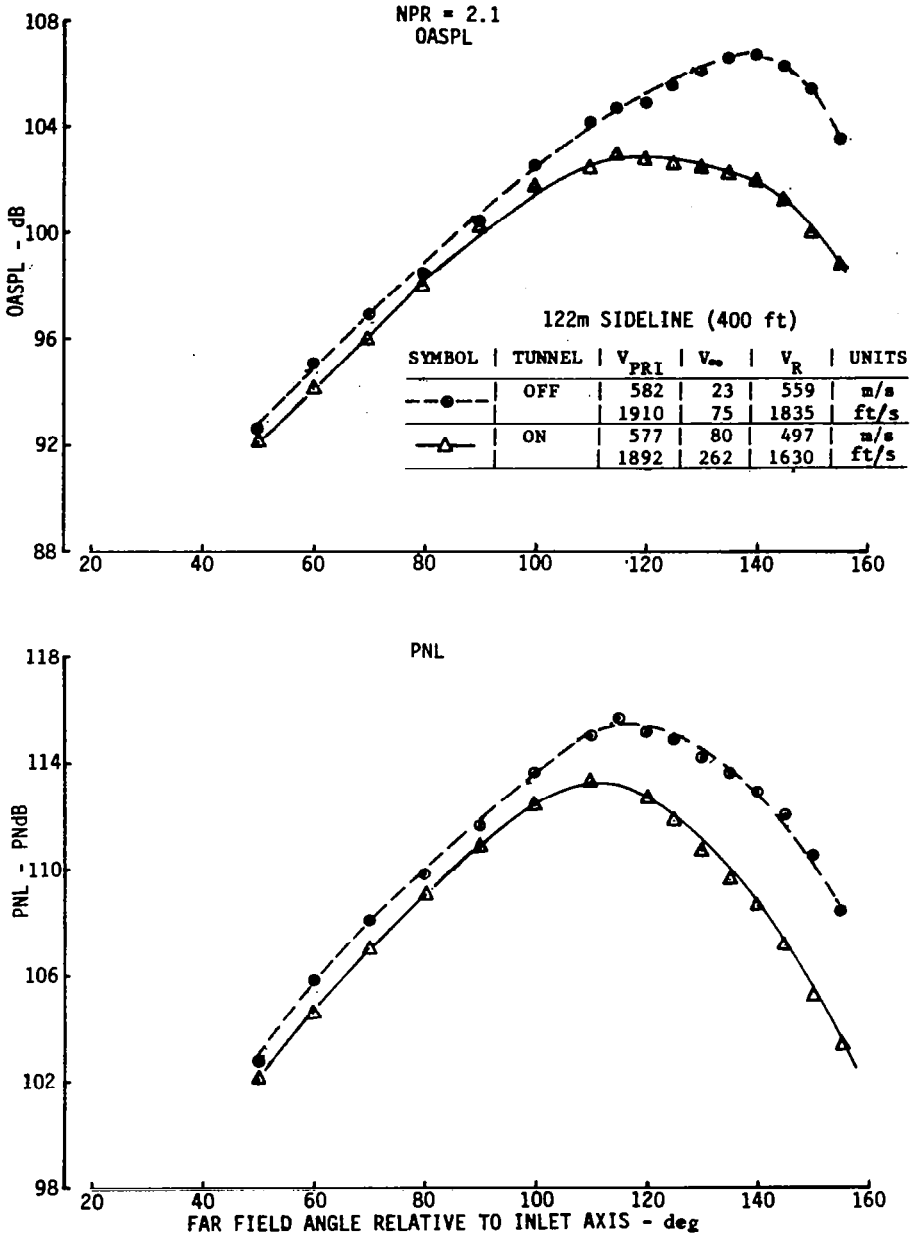

(a) 122m Sideline

Figure 35.—Comparison of Tunnel-Off and -On OASPL and PNL Directivities, Inverter Configuration: NPR = 2.1

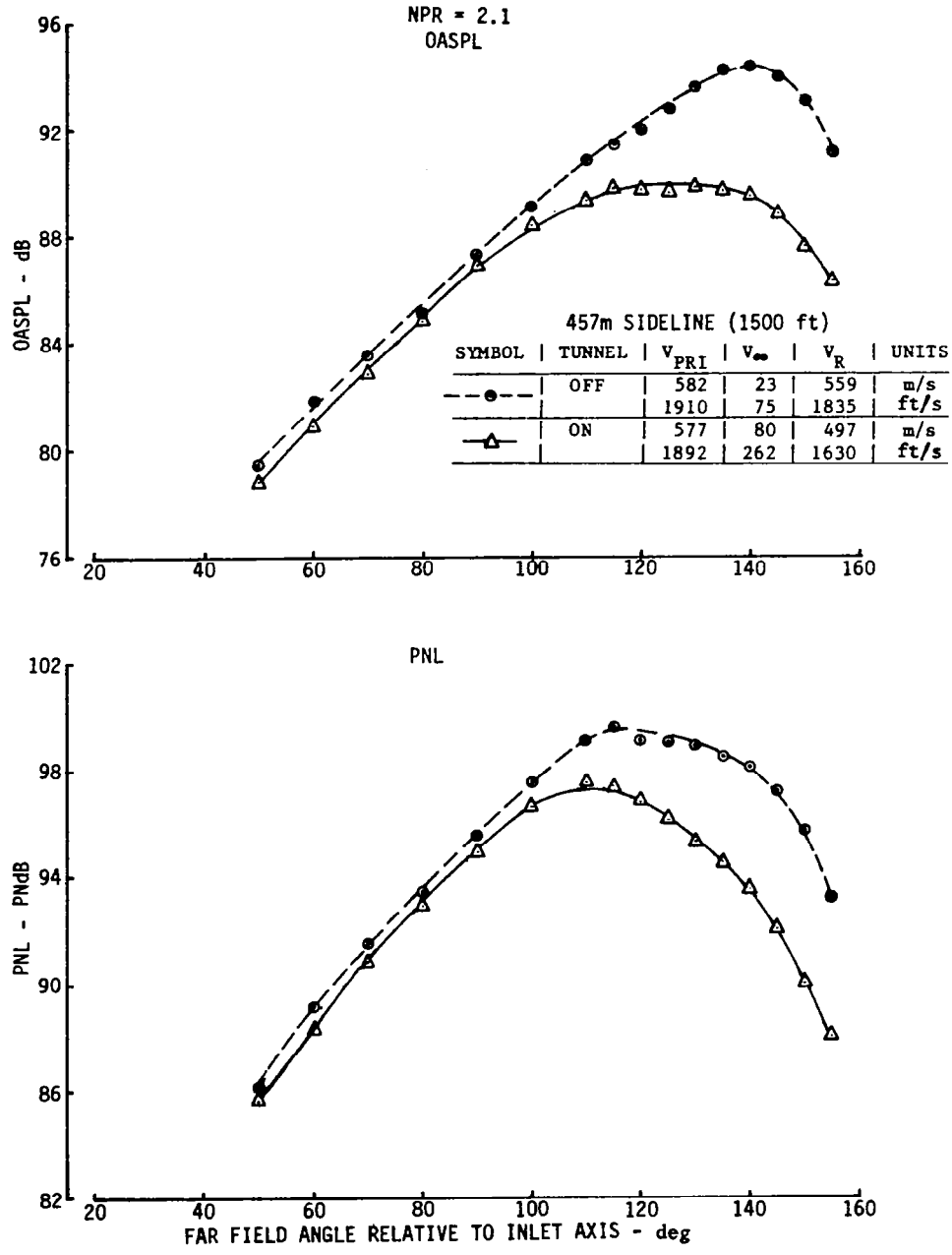

(b) 457m Sideline

Figure 35.—(Continued)

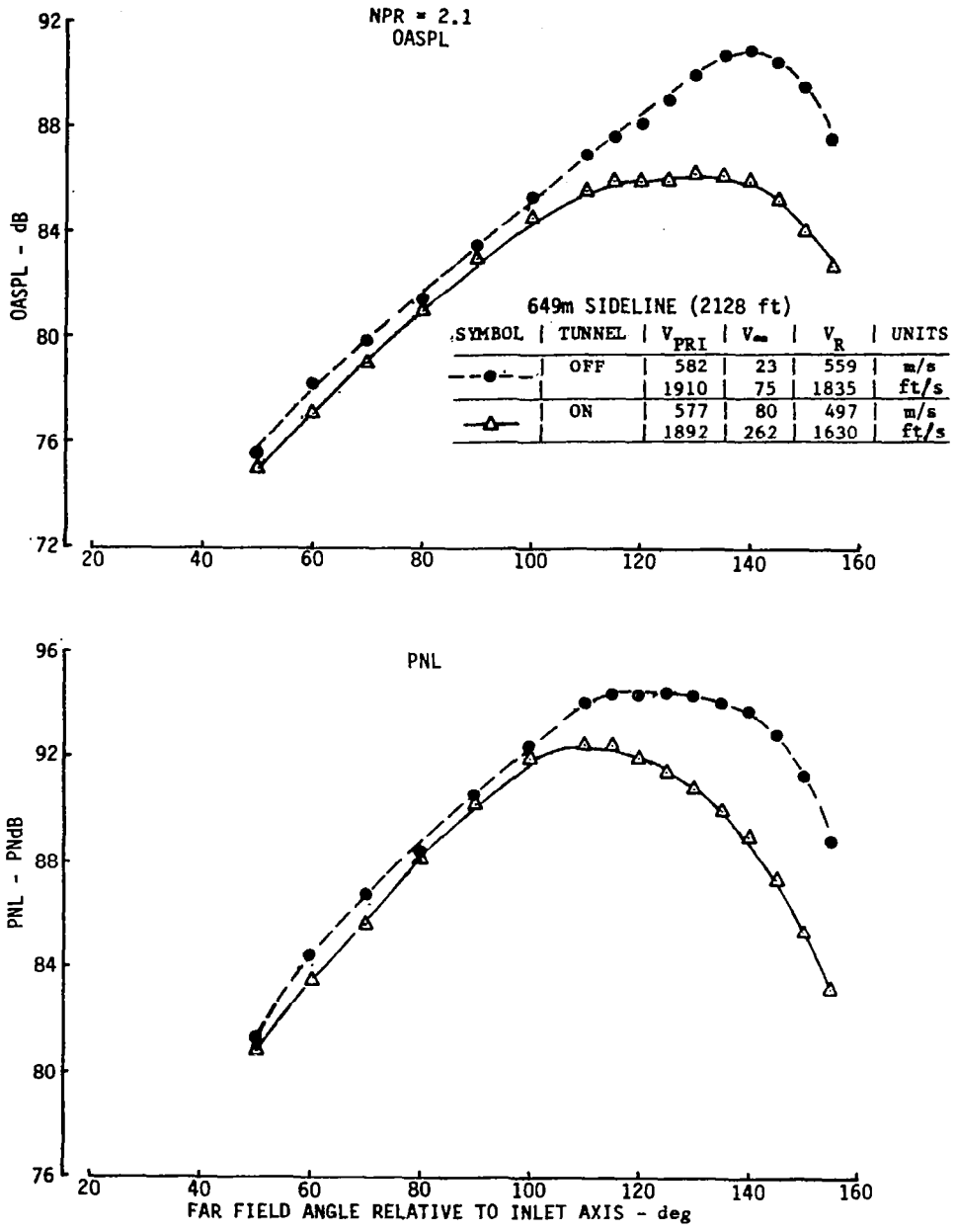

(c) 649m Sideline

Figure 35.—(Concluded)

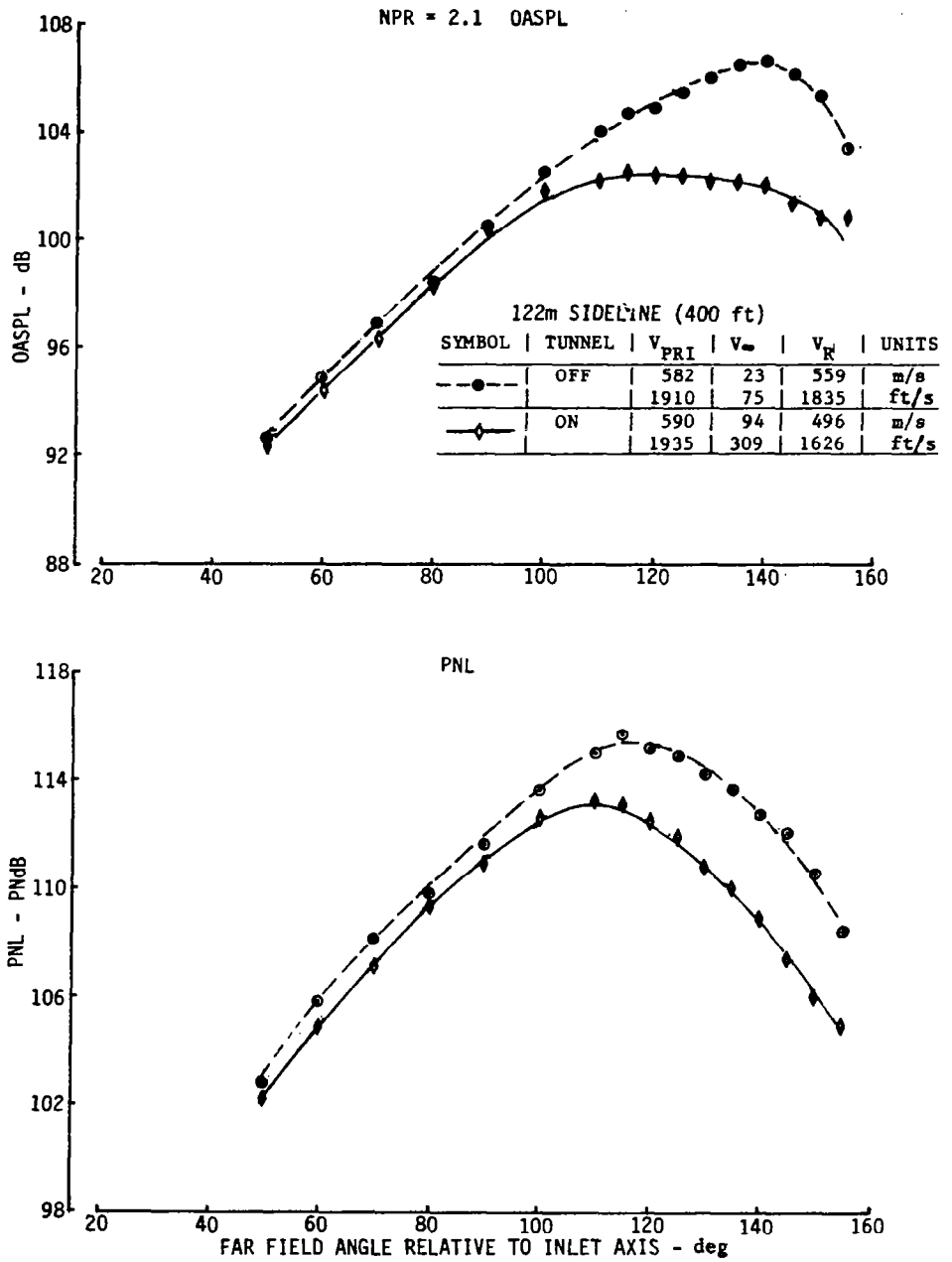

(a) 122m Sideline

Figure 36.—Comparison of Tunnel-Off and -On OASPL and PNL Directivities, Inverter Configuration: NPR = 2.1

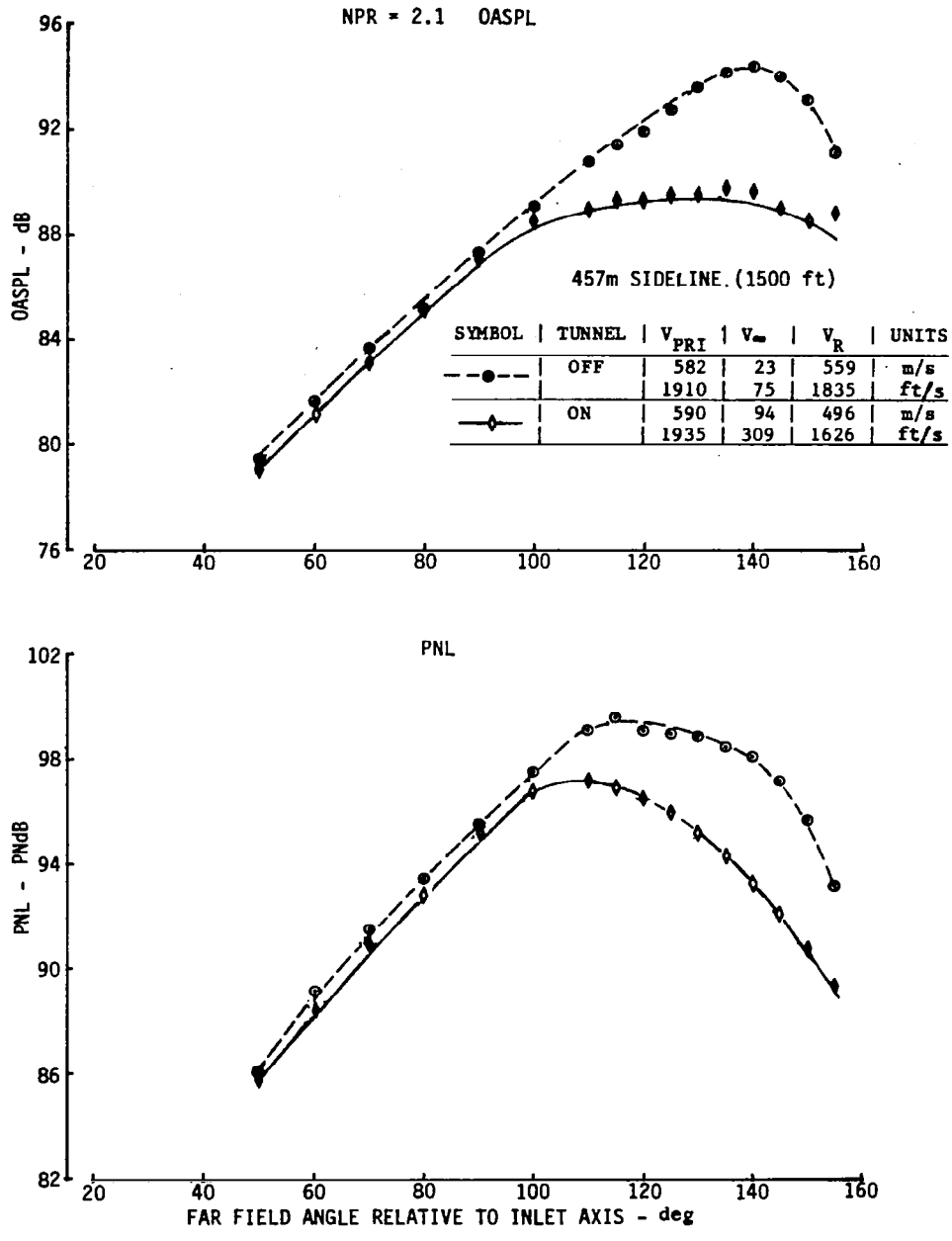

(b) 457m Sideline

Figure 36.—(Continued)

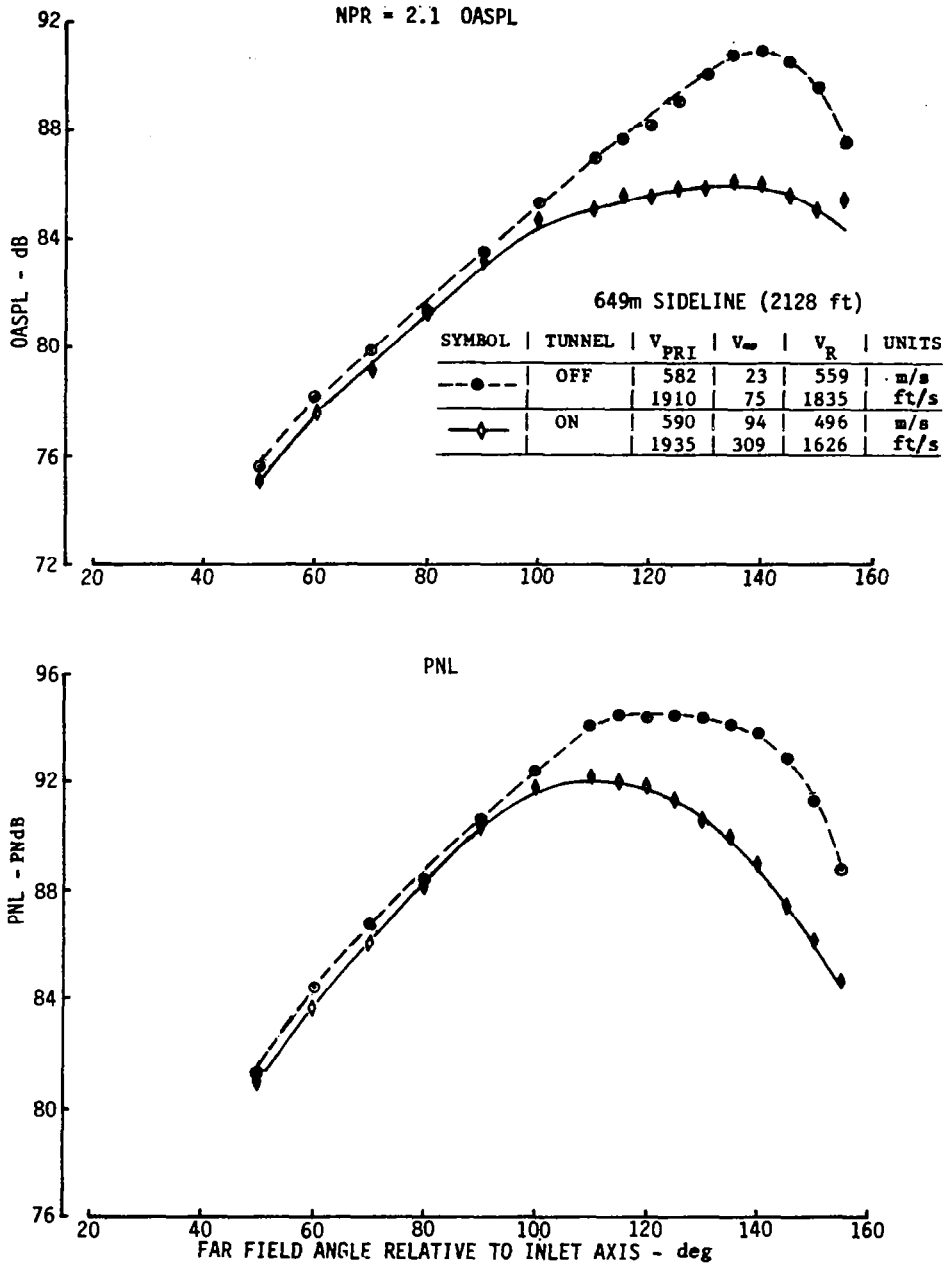

(c) 649m Sideline

Figure 36.—(Concluded)

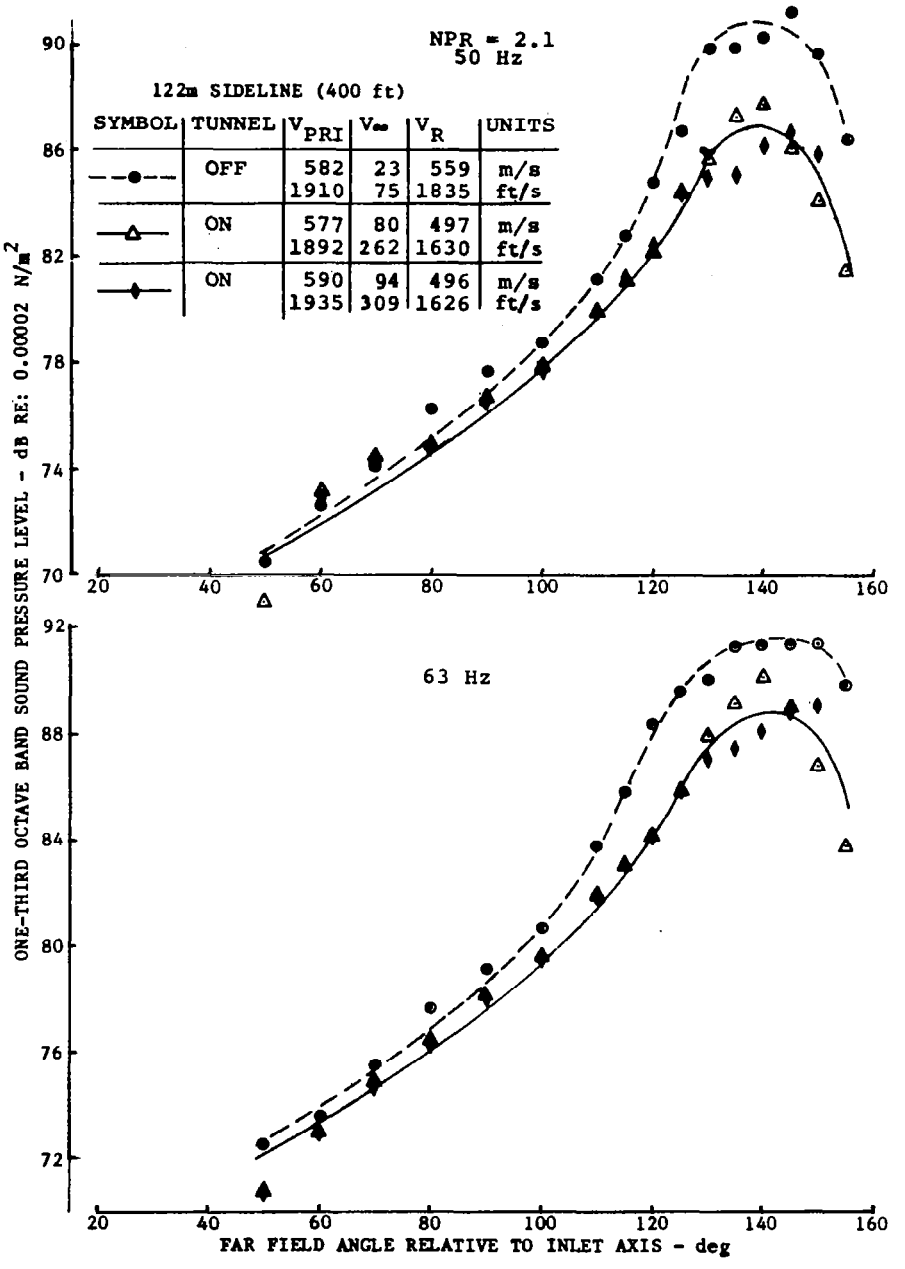

(a) 50 Hz & 63 Hz

Figure 37.—Comparison of Tunnel-Off and -On SPL Directivity, Inverter Configuration: NPR = 2.1

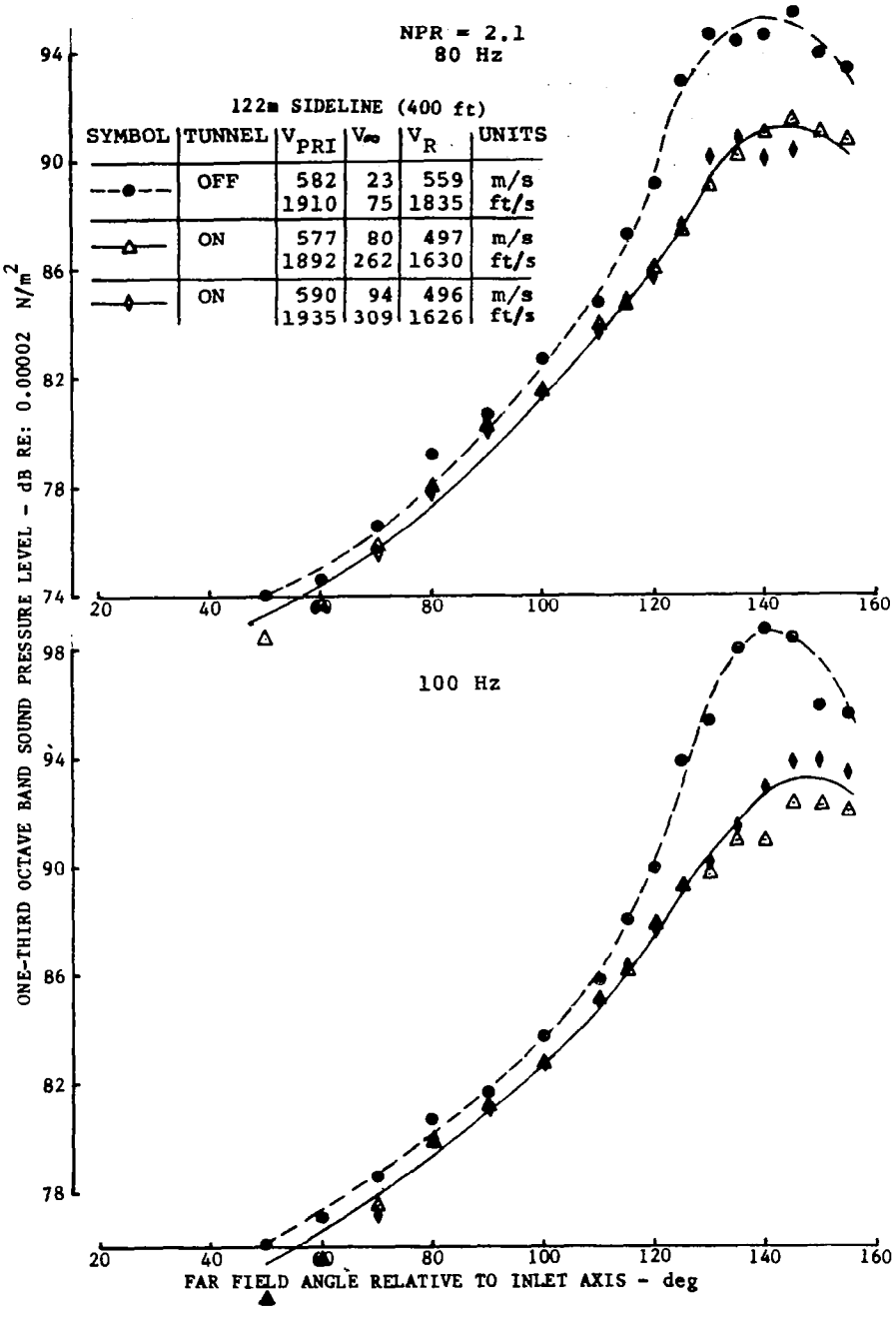

(b) 80 Hz & 100 Hz

Figure 37.—(Continued)

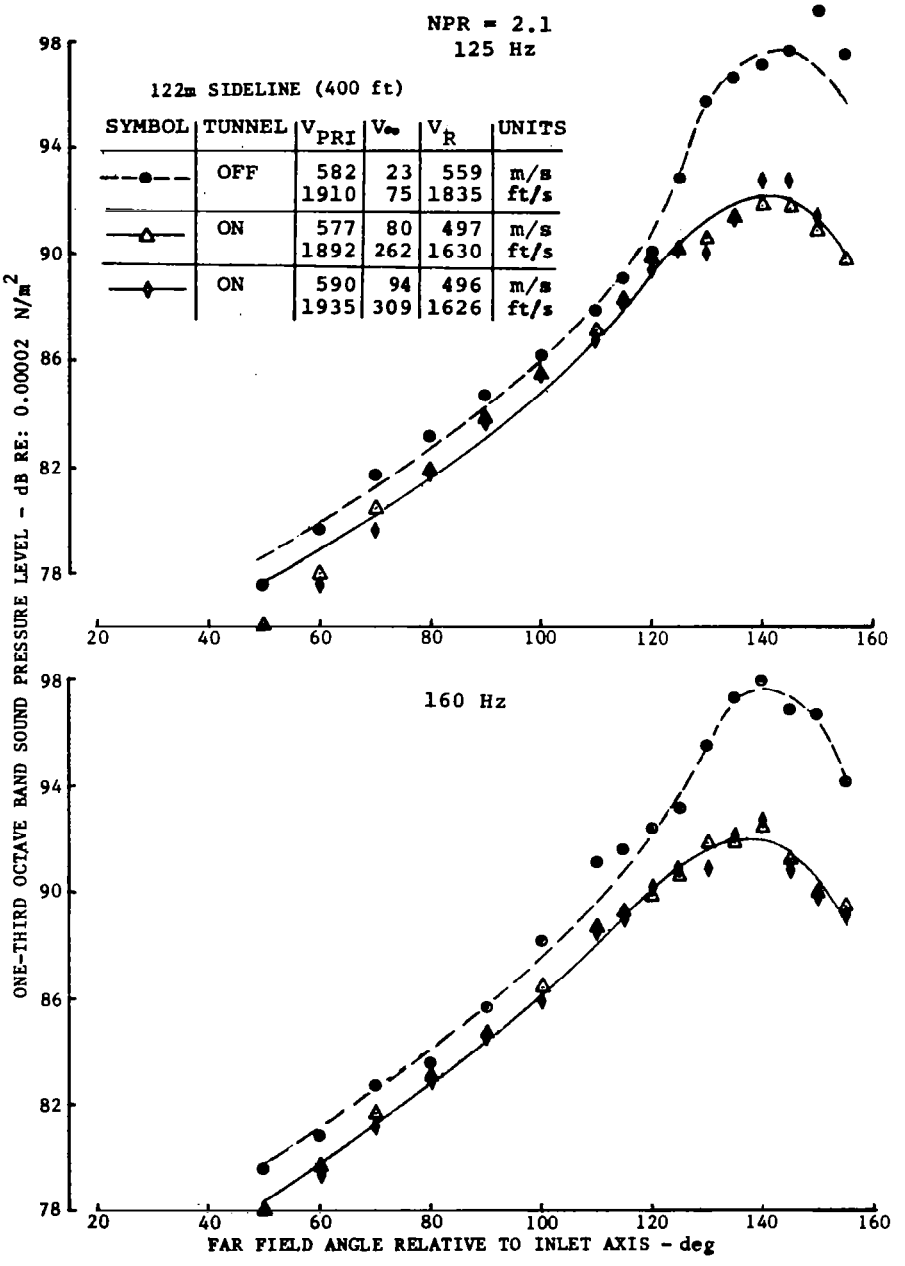

(c) 125 Hz & 160 Hz

Figure 37.—(Continued)

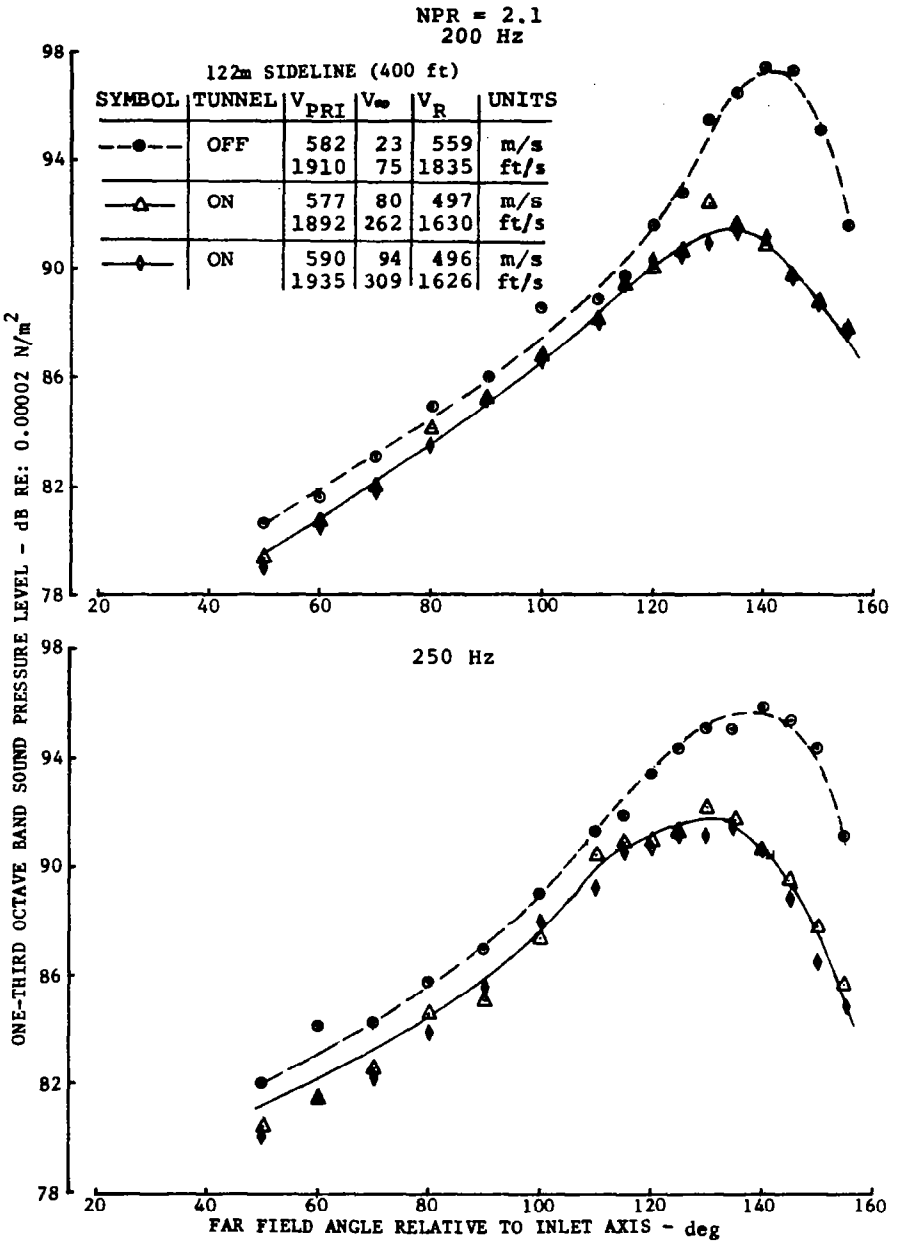

(d) 200 Hz & 250 Hz

Figure 37.—(Continued)

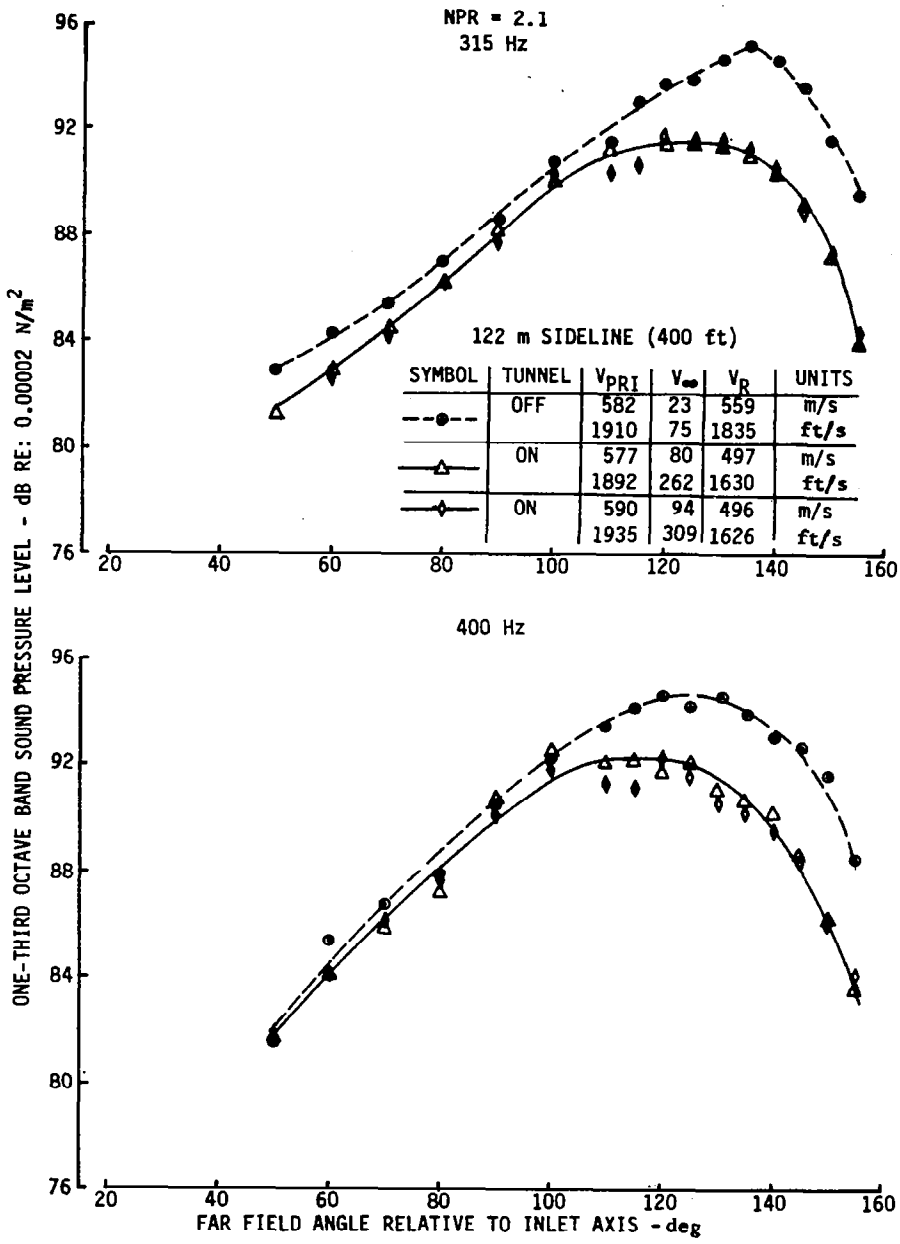

(e) 315 Hz & 400 Hz

Figure 37.—(Continued)

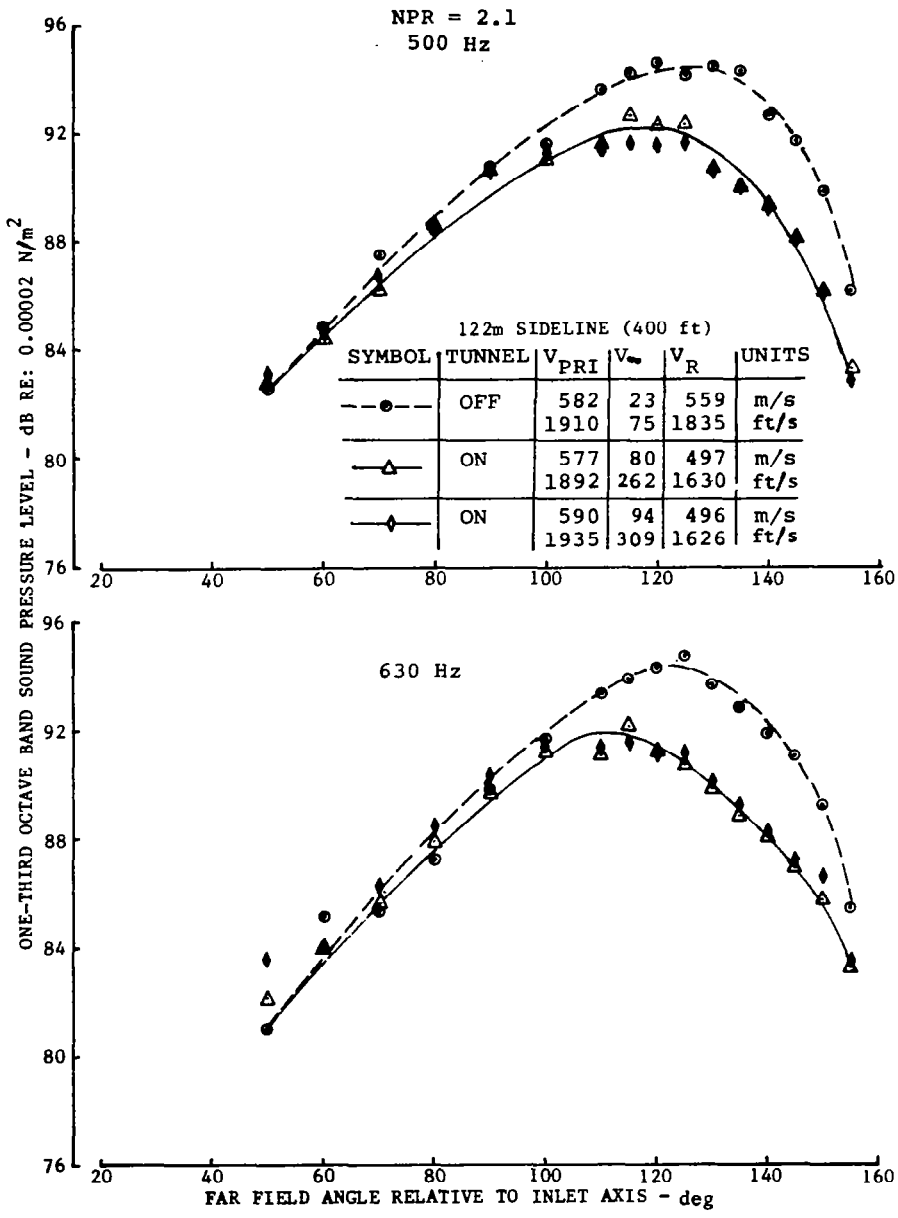

(f) 500 Hz & 630 Hz

Figure 37.—(Continued)

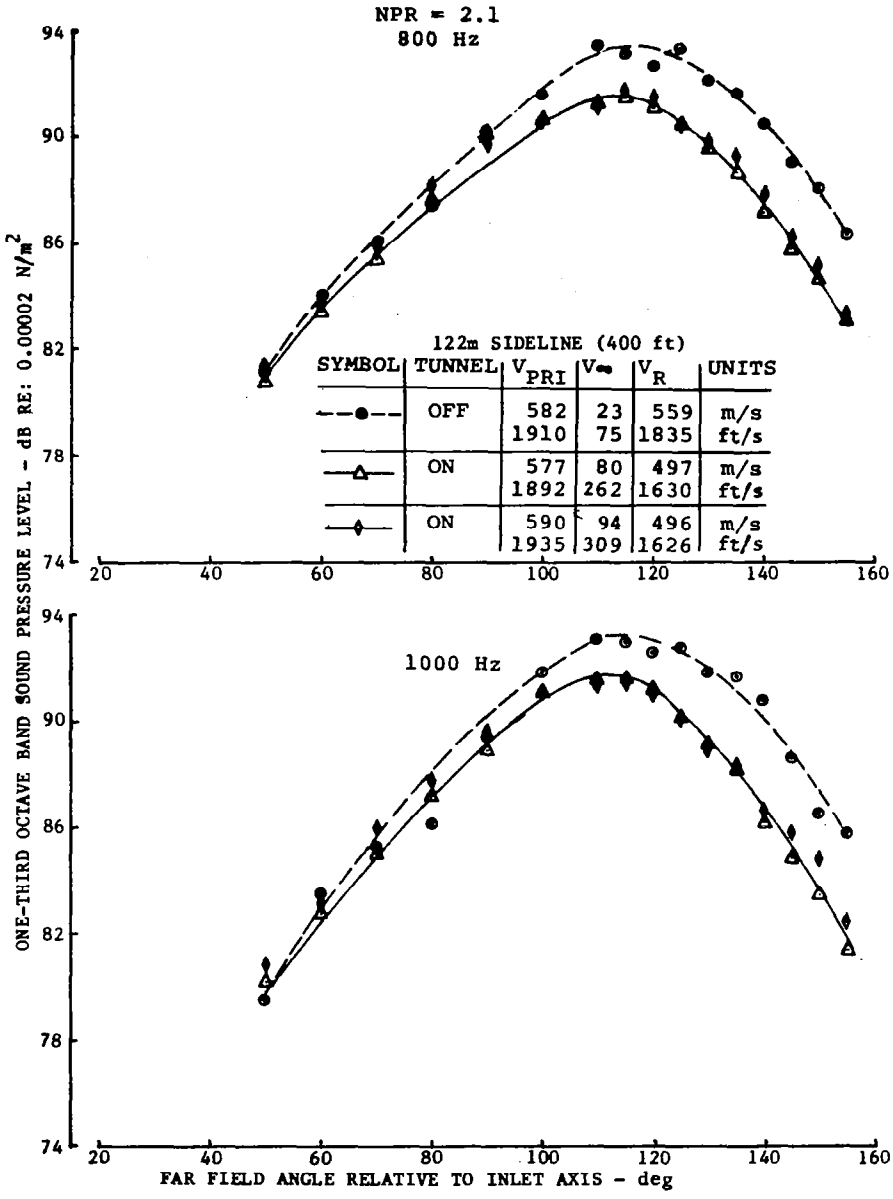

(g) 800 Hz & 1000 Hz

Figure 37.—(Continued)

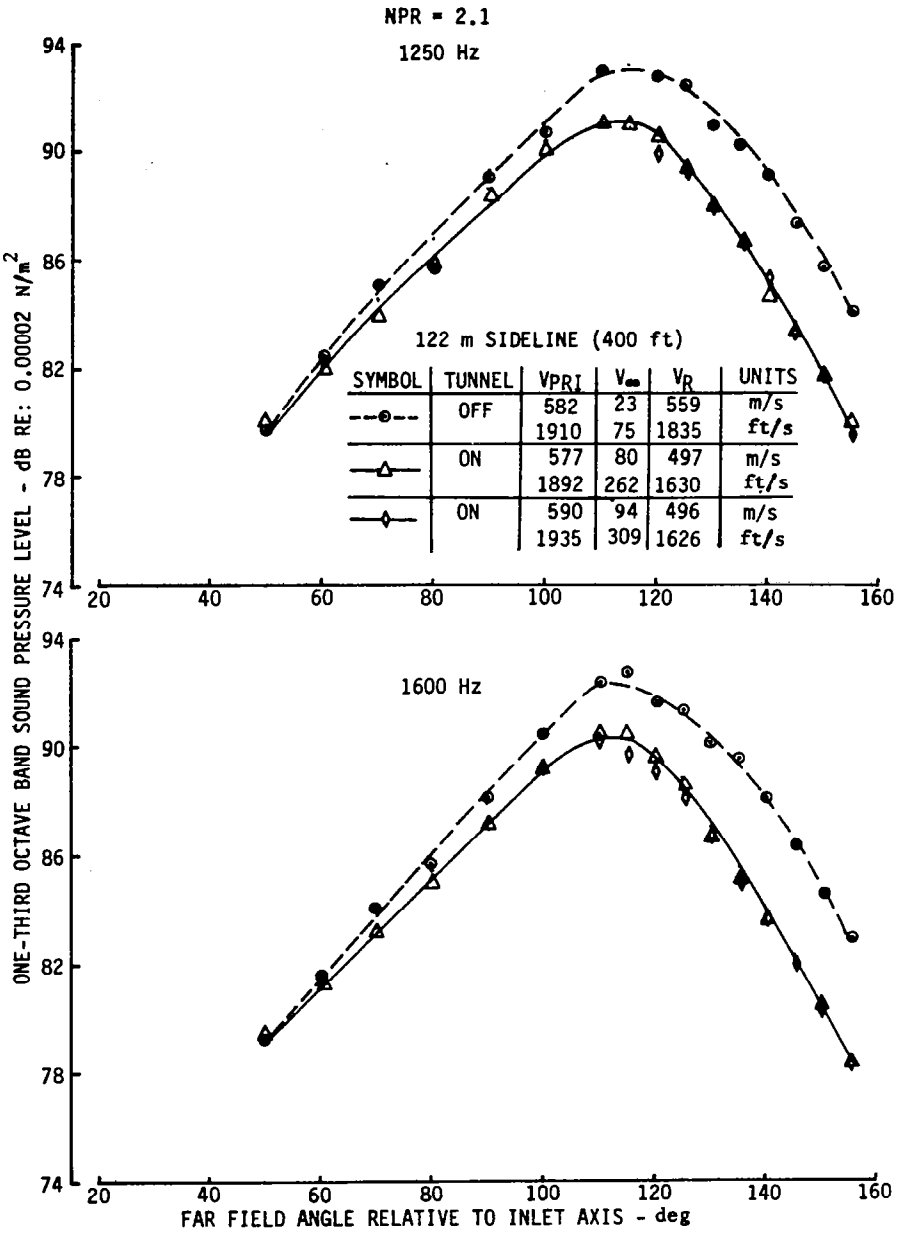

(h) 1250 Hz & 1600 Hz

Figure 37.—(Continued)

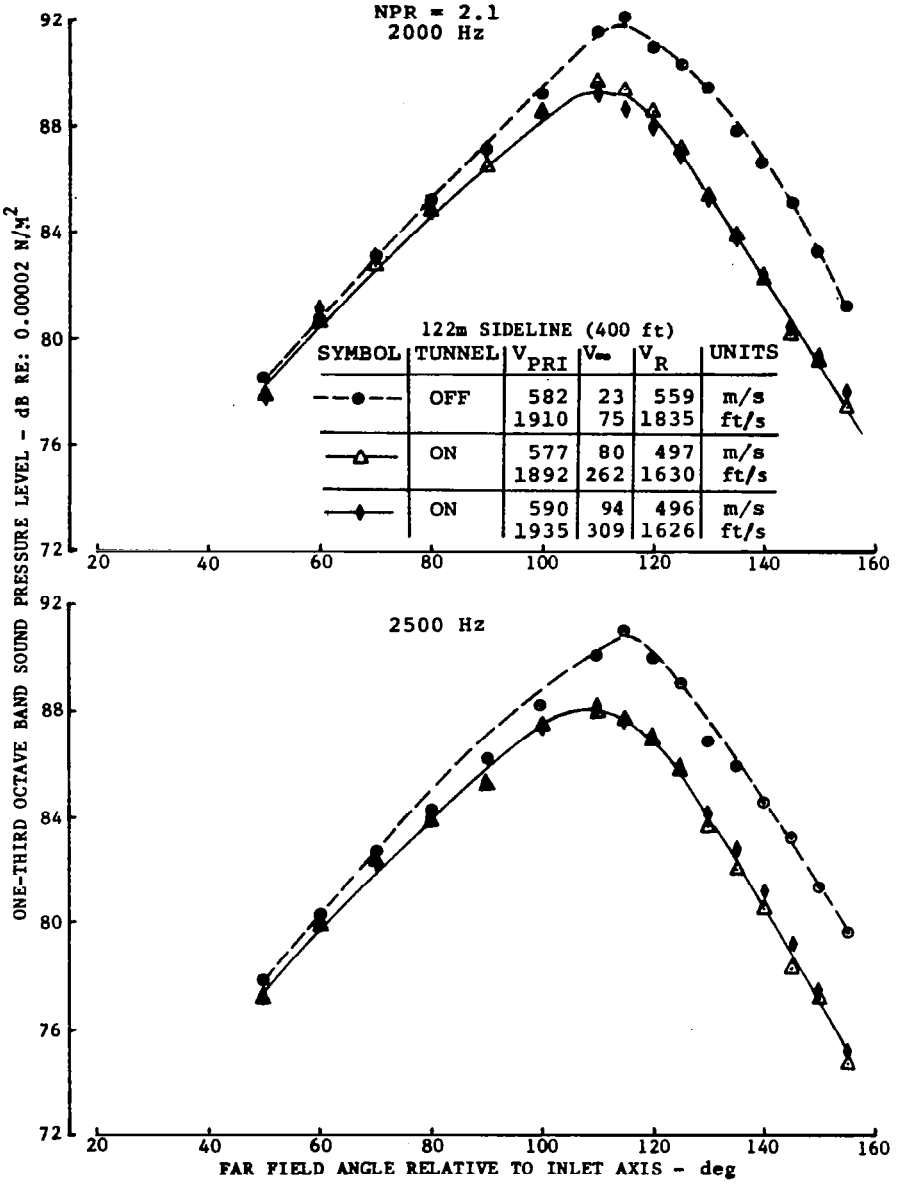

(i) 2000 Hz & 2500 Hz

Figure 37.—(Continued)

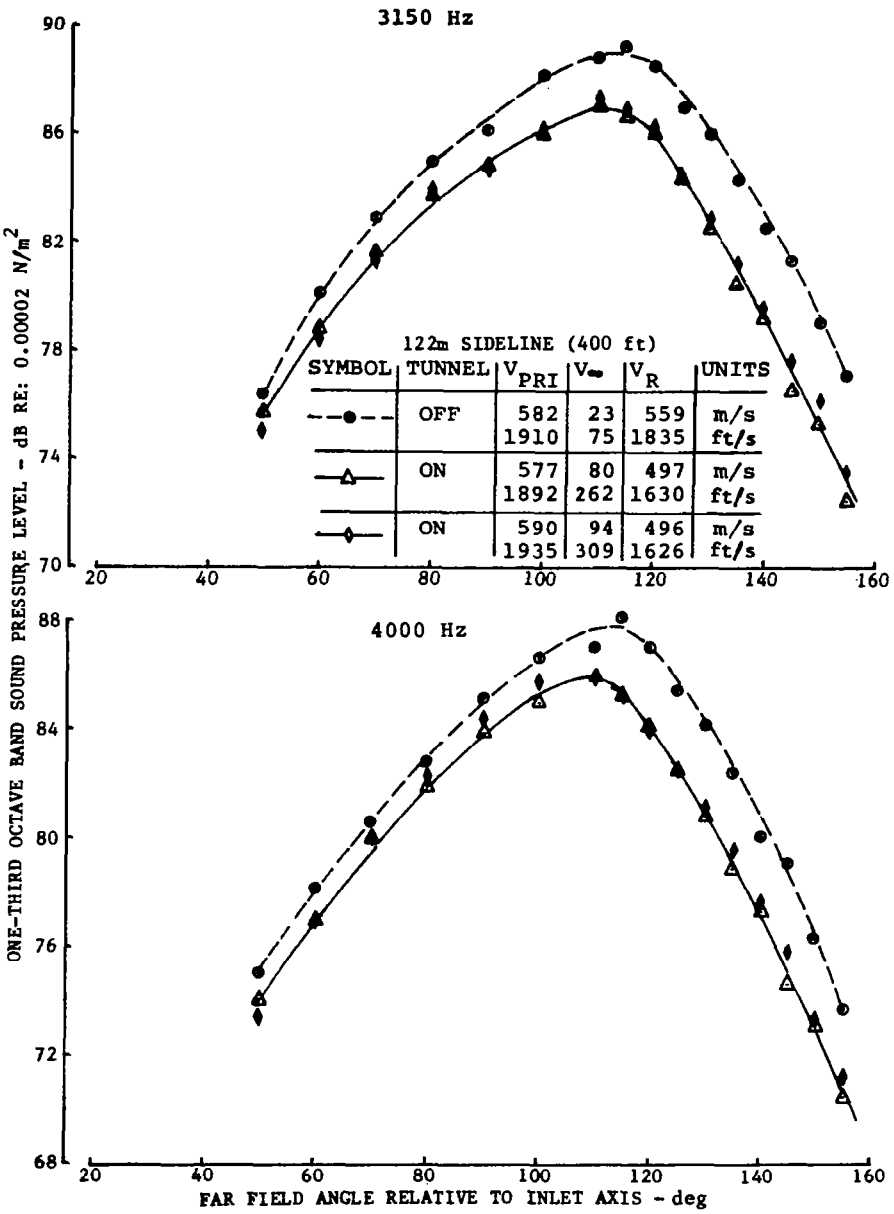

(j) 3150 Hz & 4000 Hz

Figure 37.—(Continued)

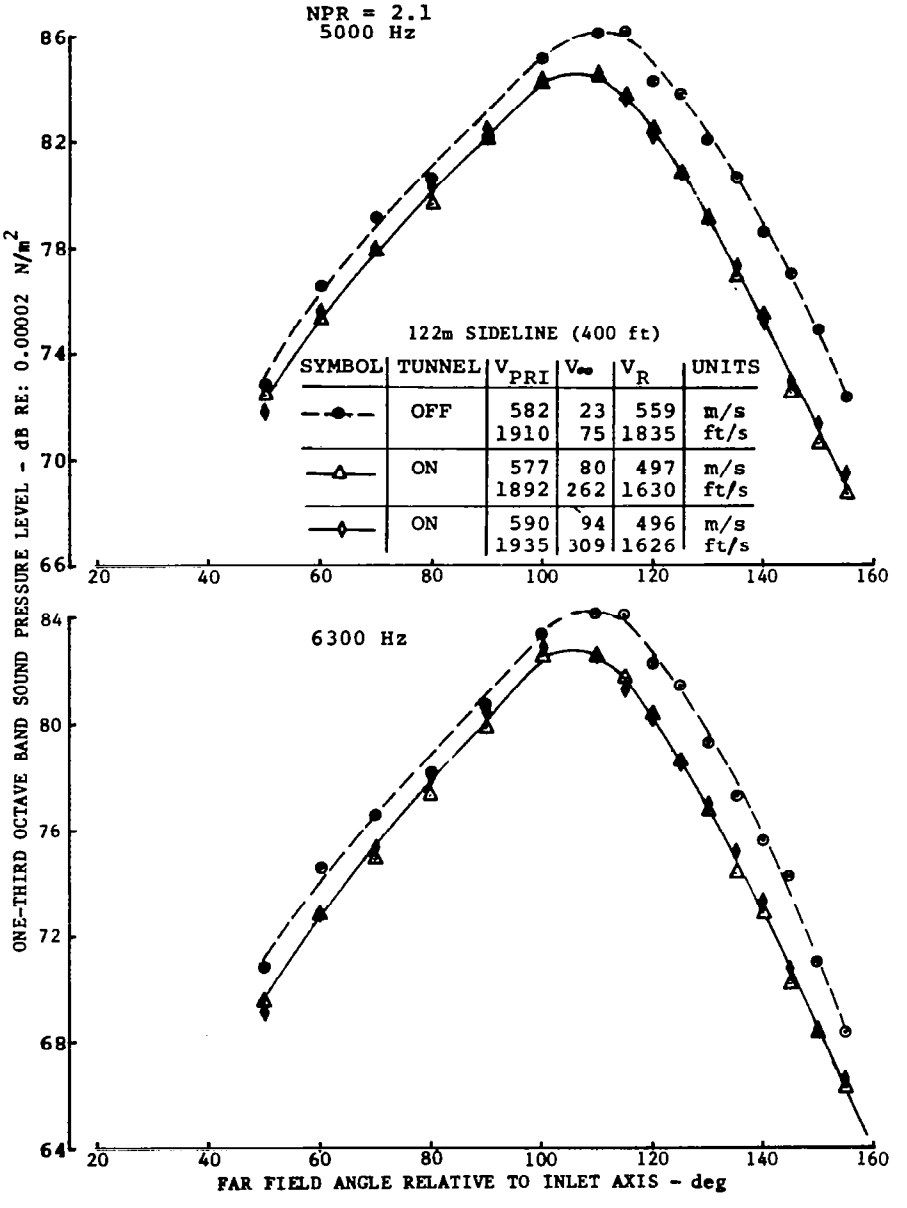

(k) 5000 Hz & 6300 Hz

Figure 37.—(Continued)

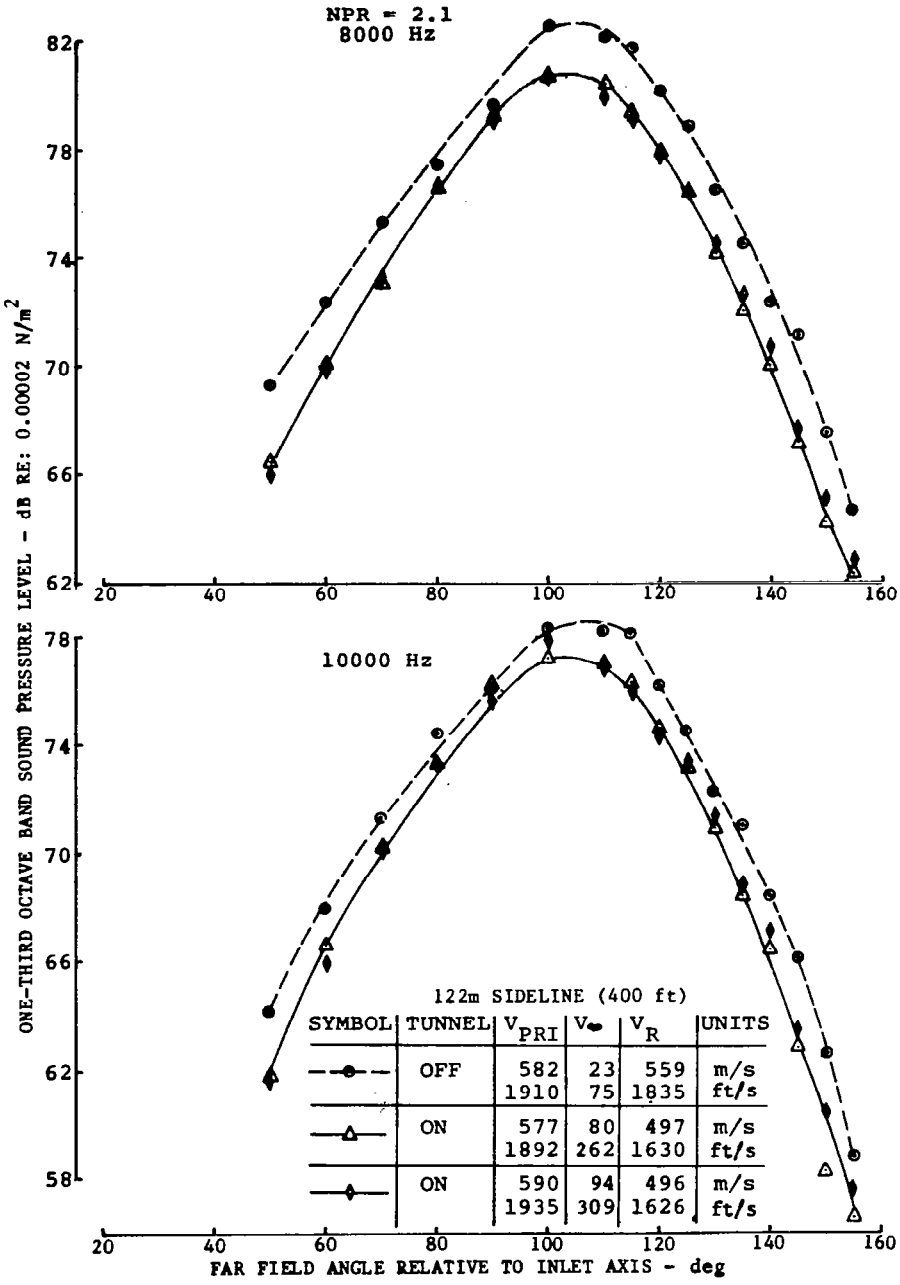

(l) 8000 Hz & 10000 Hz

Figure 37.—(Concluded)

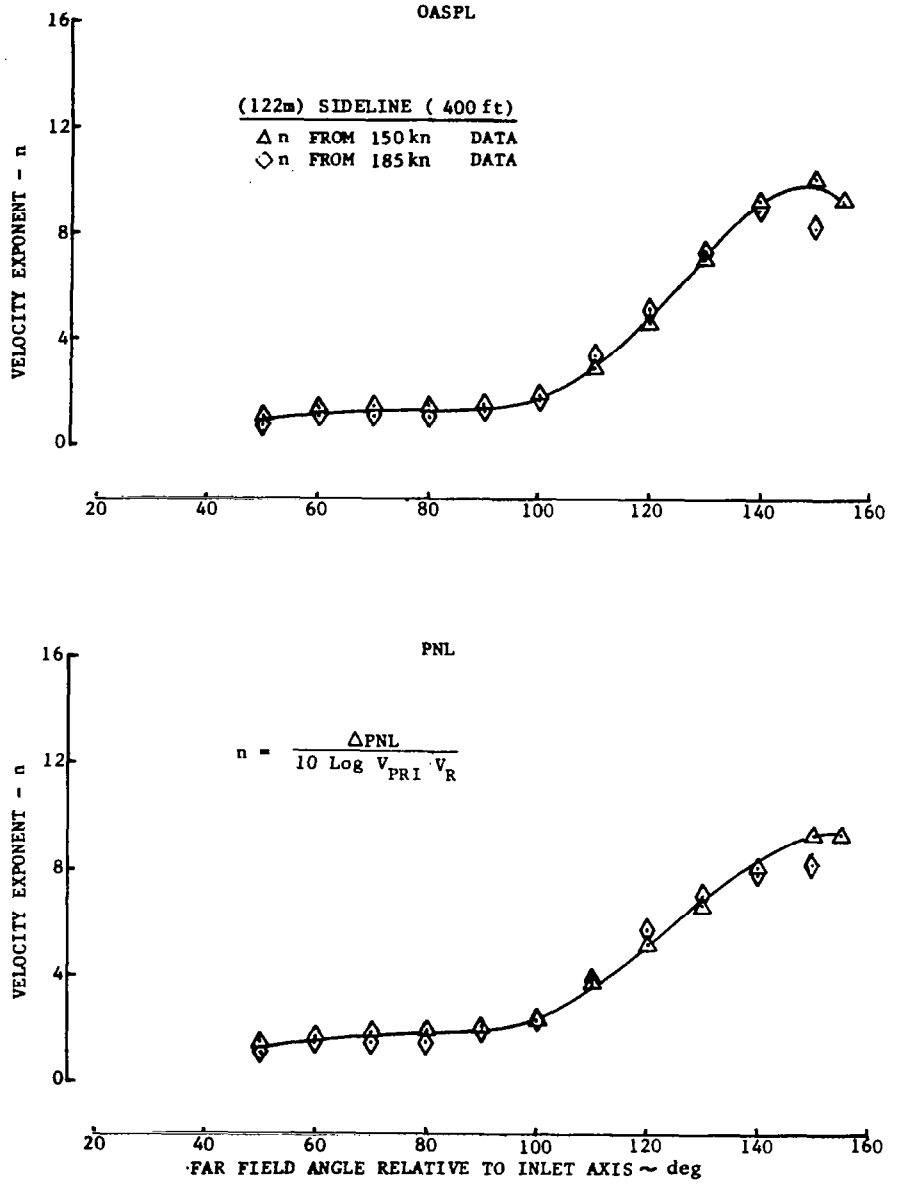

(a) 122m Sideline

Figure 38.—Velocity Exponents for OASPL and PNL, Inverter Configuration: NPR = 2.1

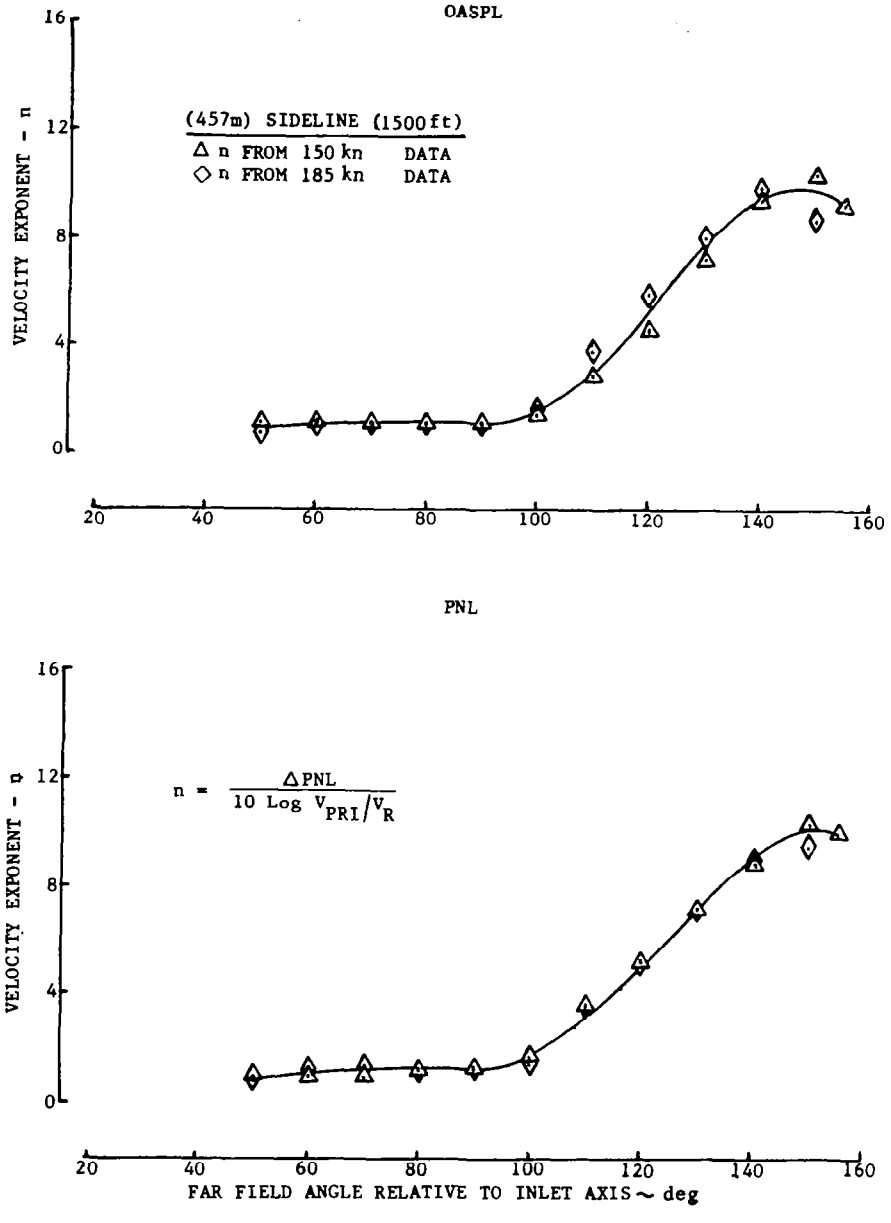

(b) 457m Sideline

Figure 38.—(Continued)

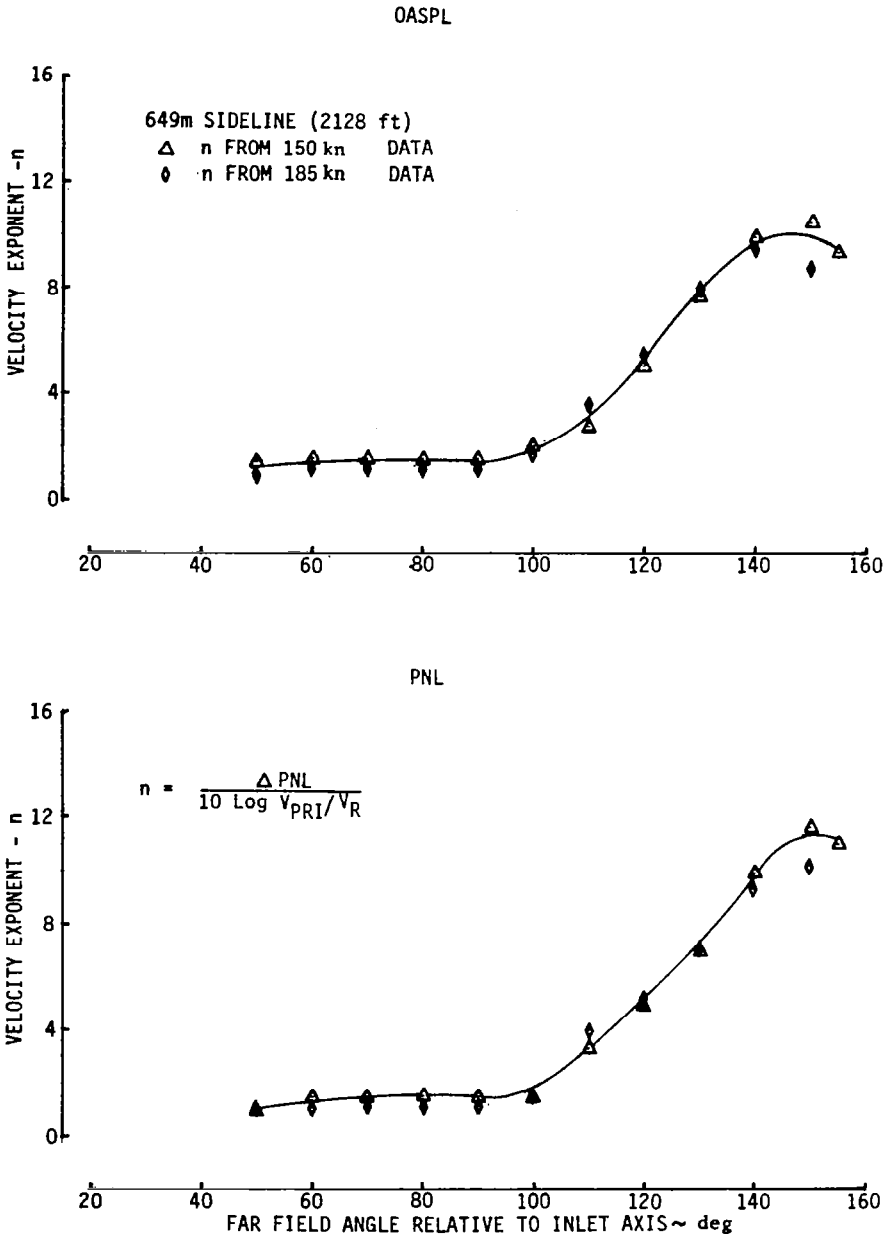

(c) 649m Sideline

Figure 38.—(Concluded)

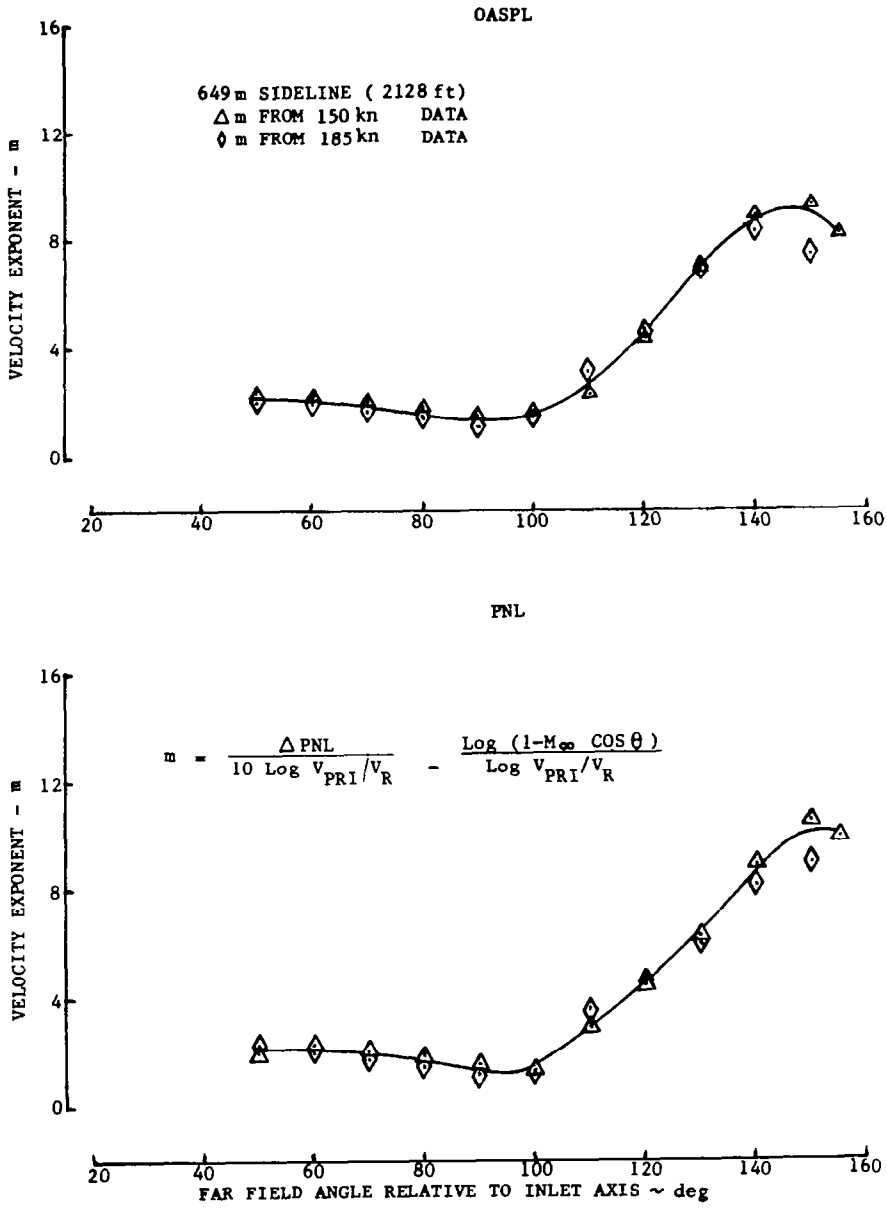

Figure 39.—Velocity Exponents for OASPL and PNL, Inverter Configuration: NPR = 2.1

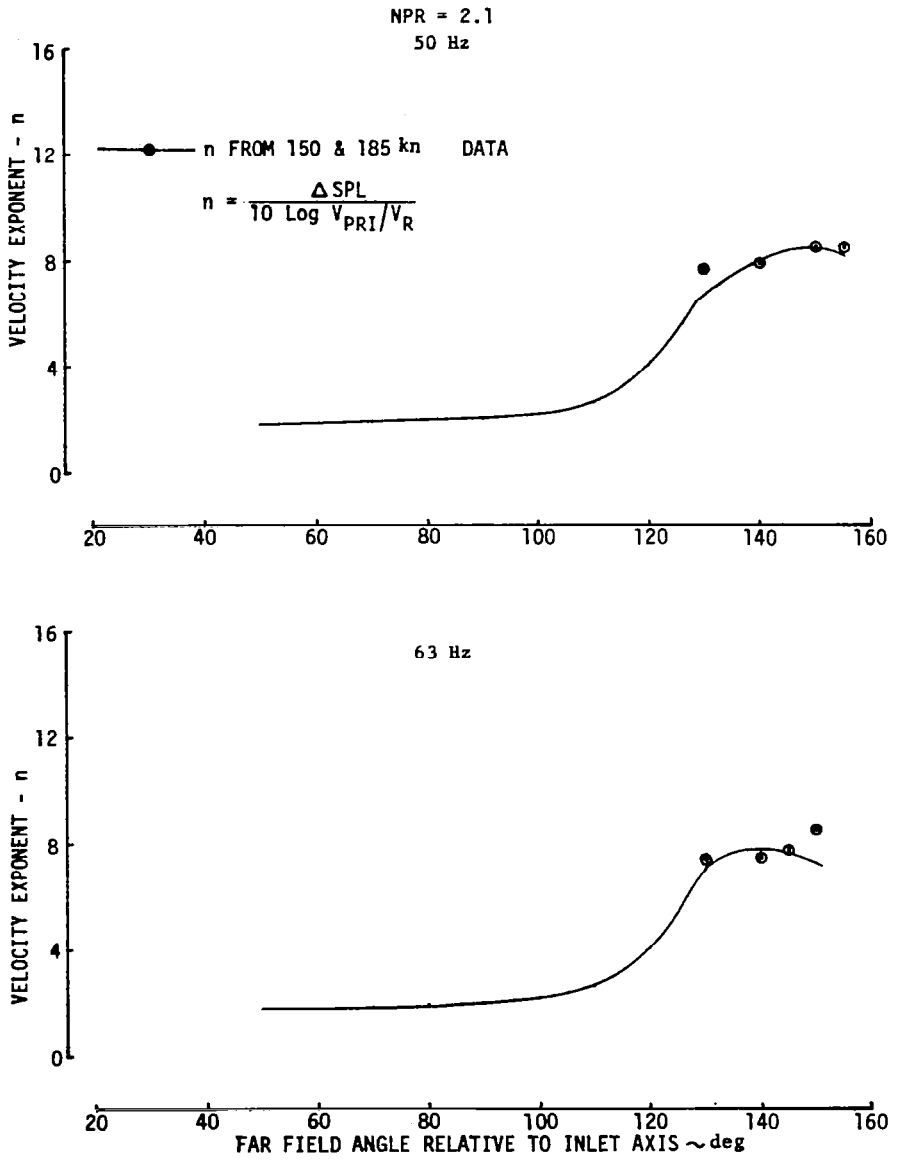

(a) 50 Hz & 63 Hz

Figure 40.—Velocity Exponents for SPL, Inverter Configuration: NPR = 2.1

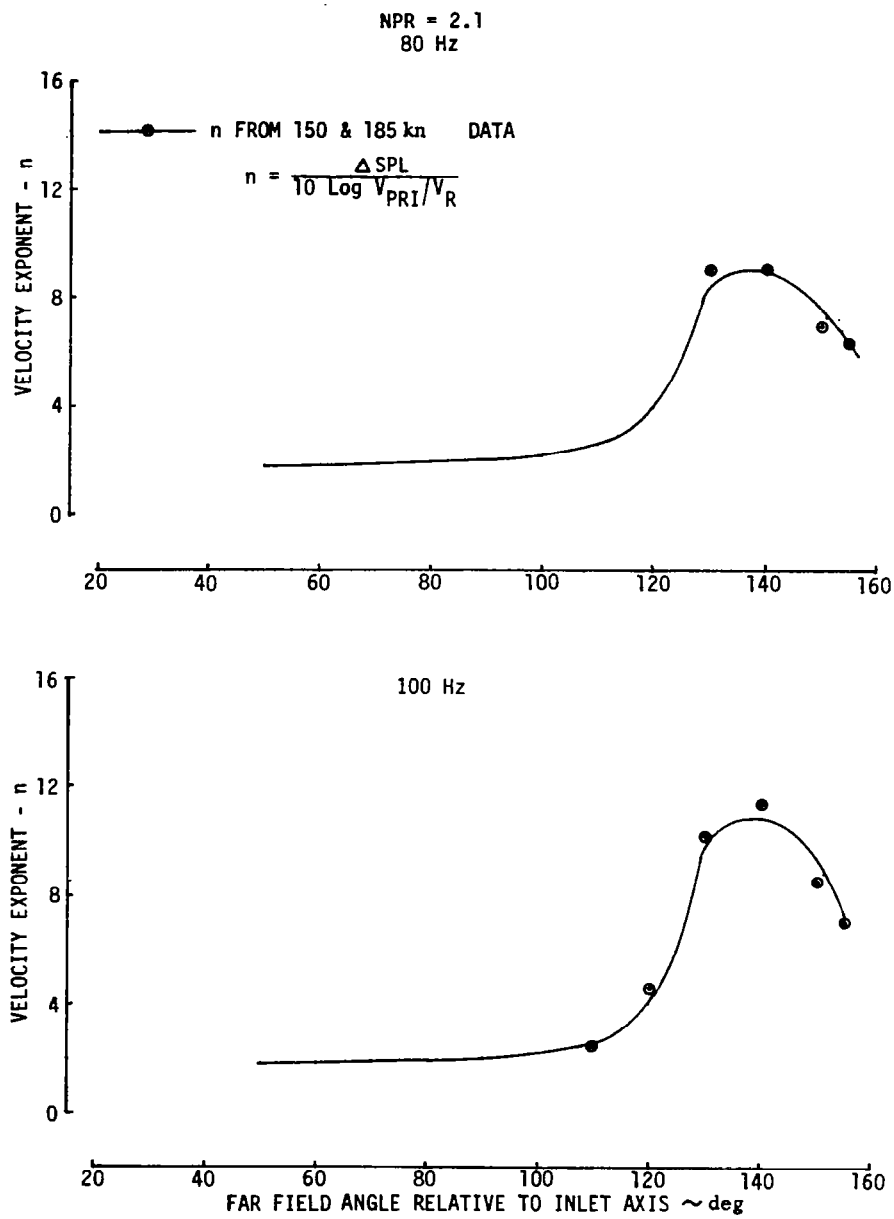

(b) 80 Hz & 100 Hz

Figure 40.—(Continued)

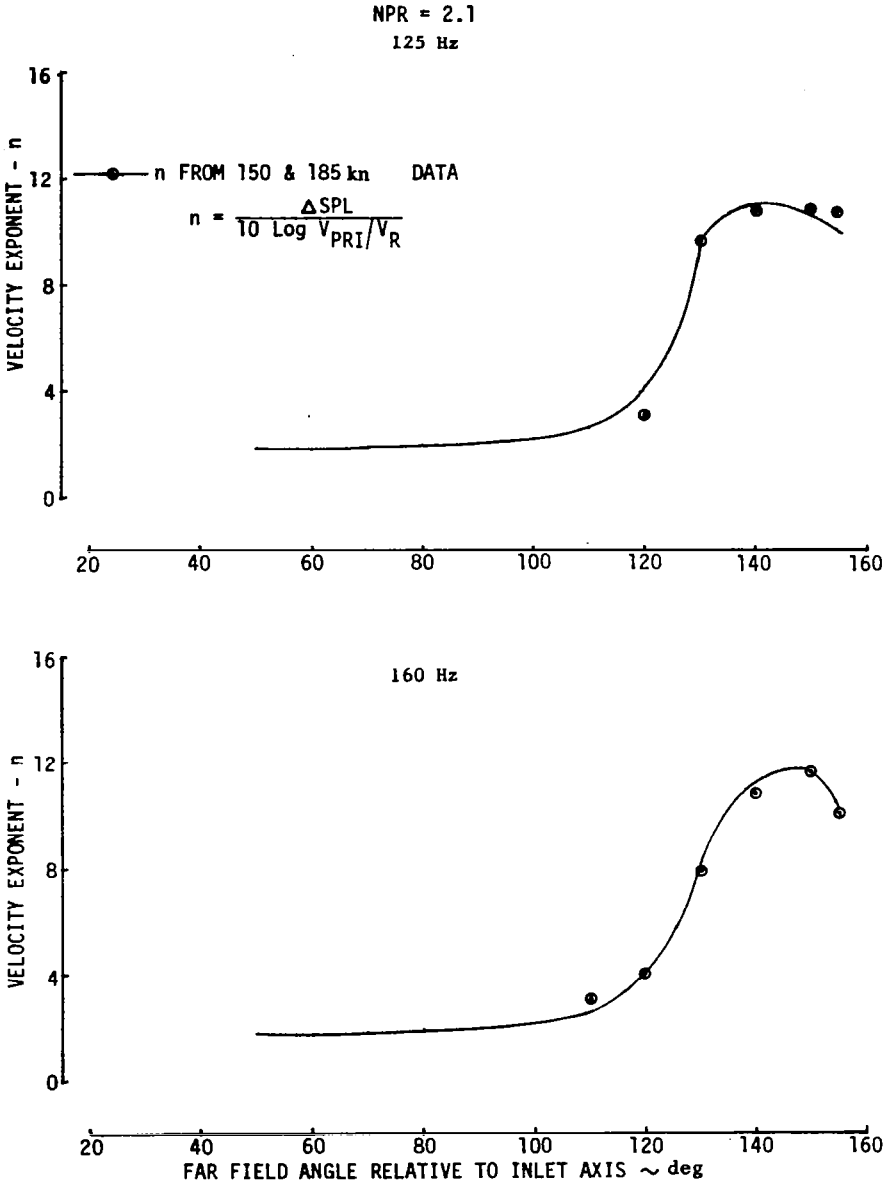

(c) 125 Hz & 160 Hz

Figure 40.—(Continued)

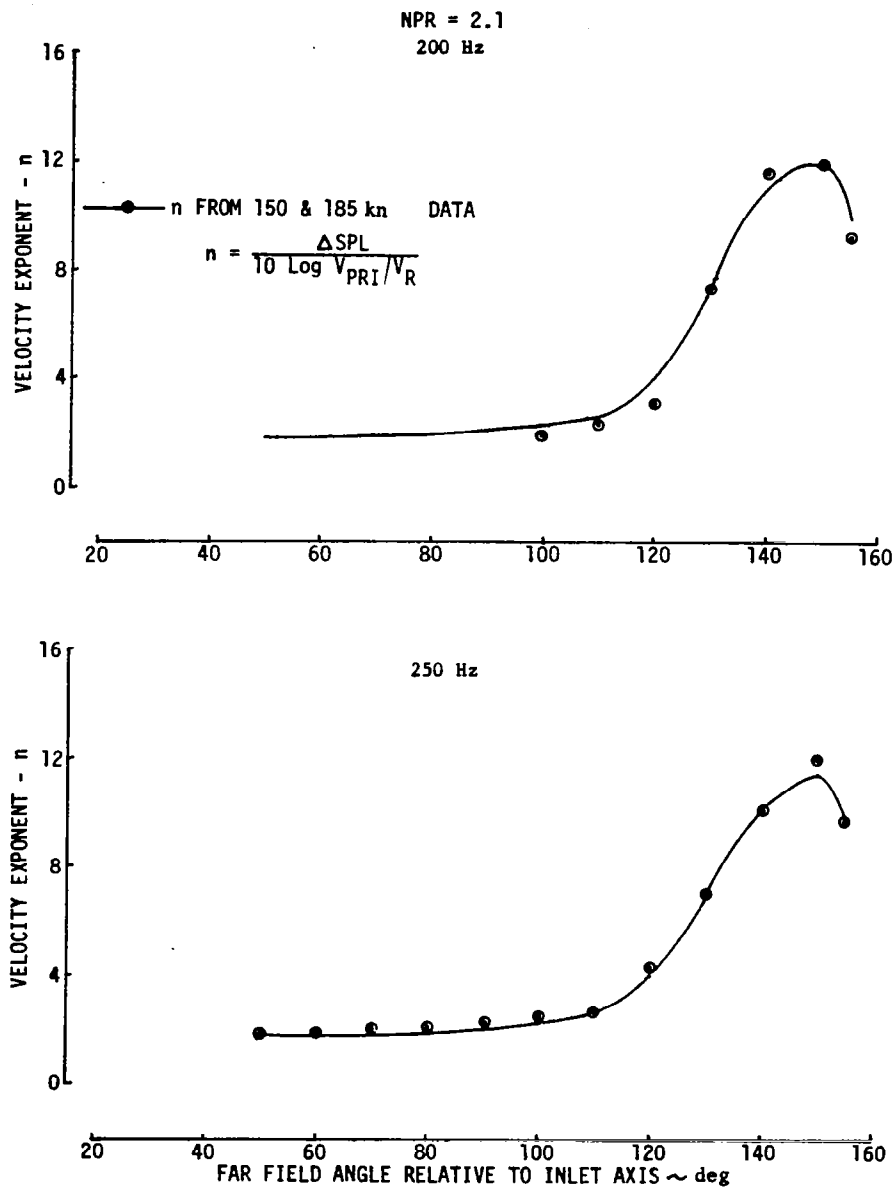

(d) 200 Hz & 250 Hz

Figure 40.—(Continued)

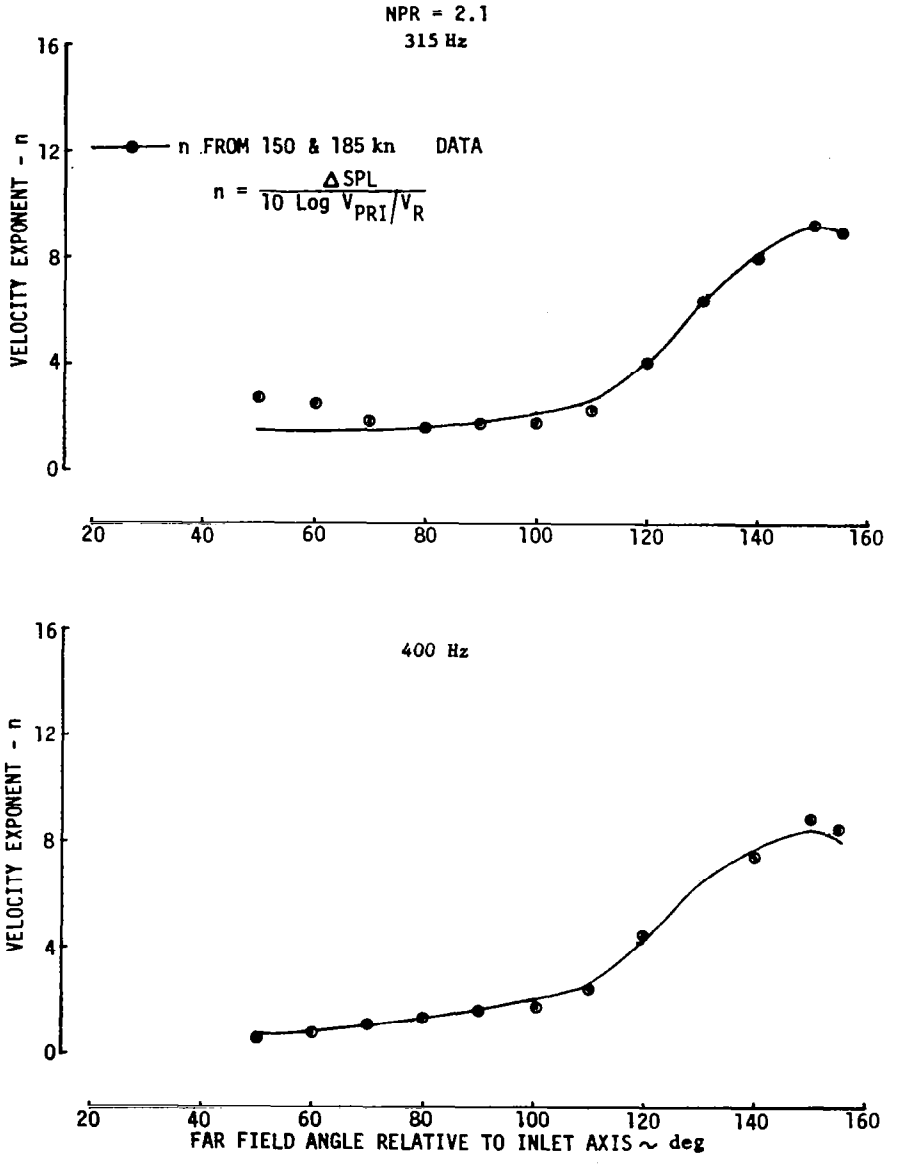

(e) 315 Hz & 400 Hz

Figure 40.—(Continued)

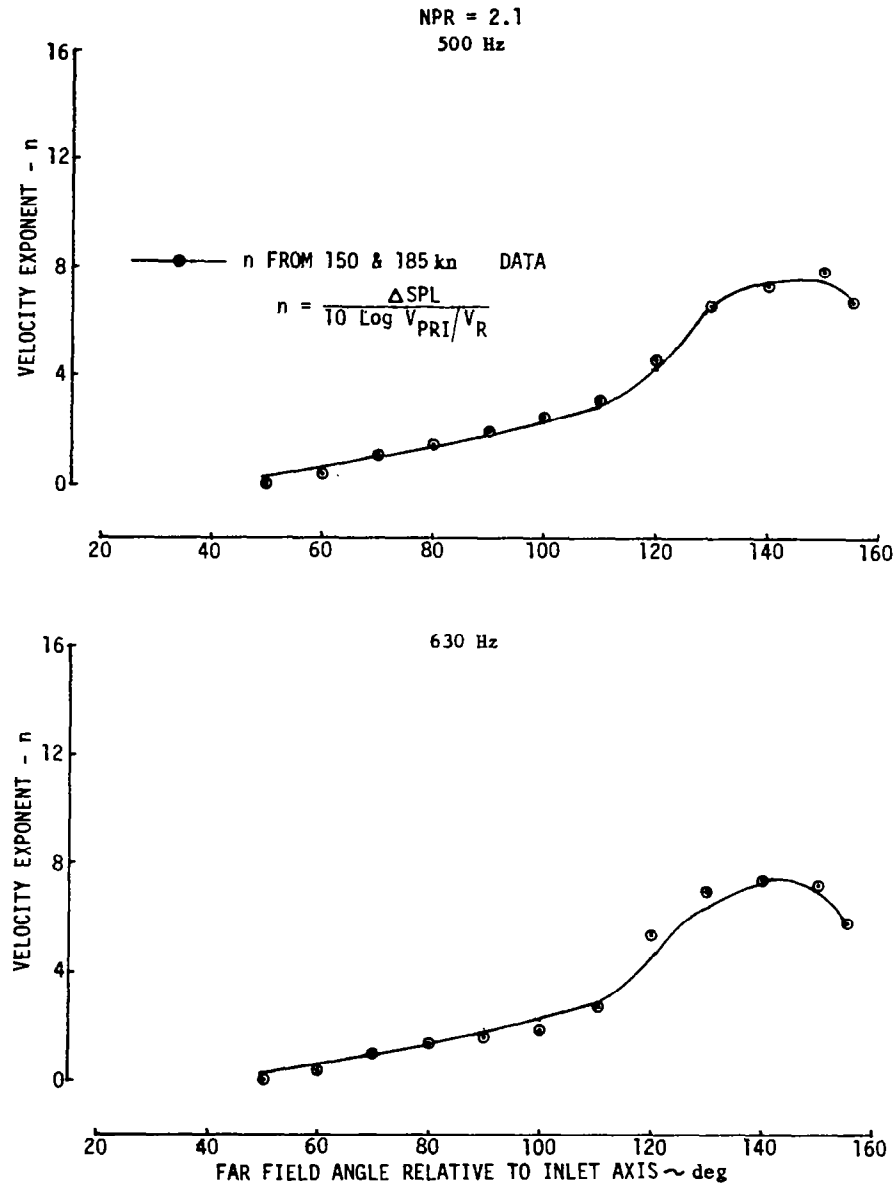

(f) 500 Hz & 630 Hz

Figure 40.—(Continued)

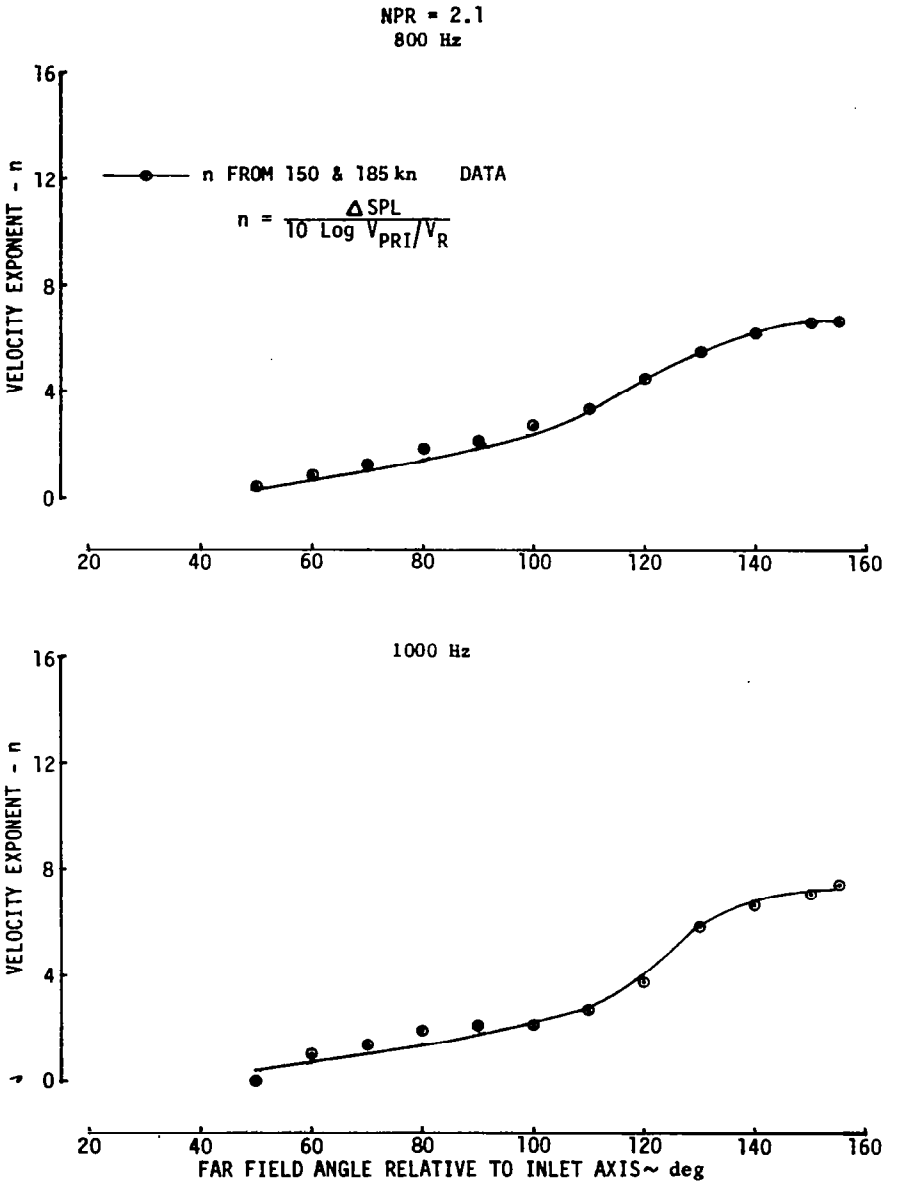

(g) 800 Hz & 1000 Hz

Figure 40.—(Continued)

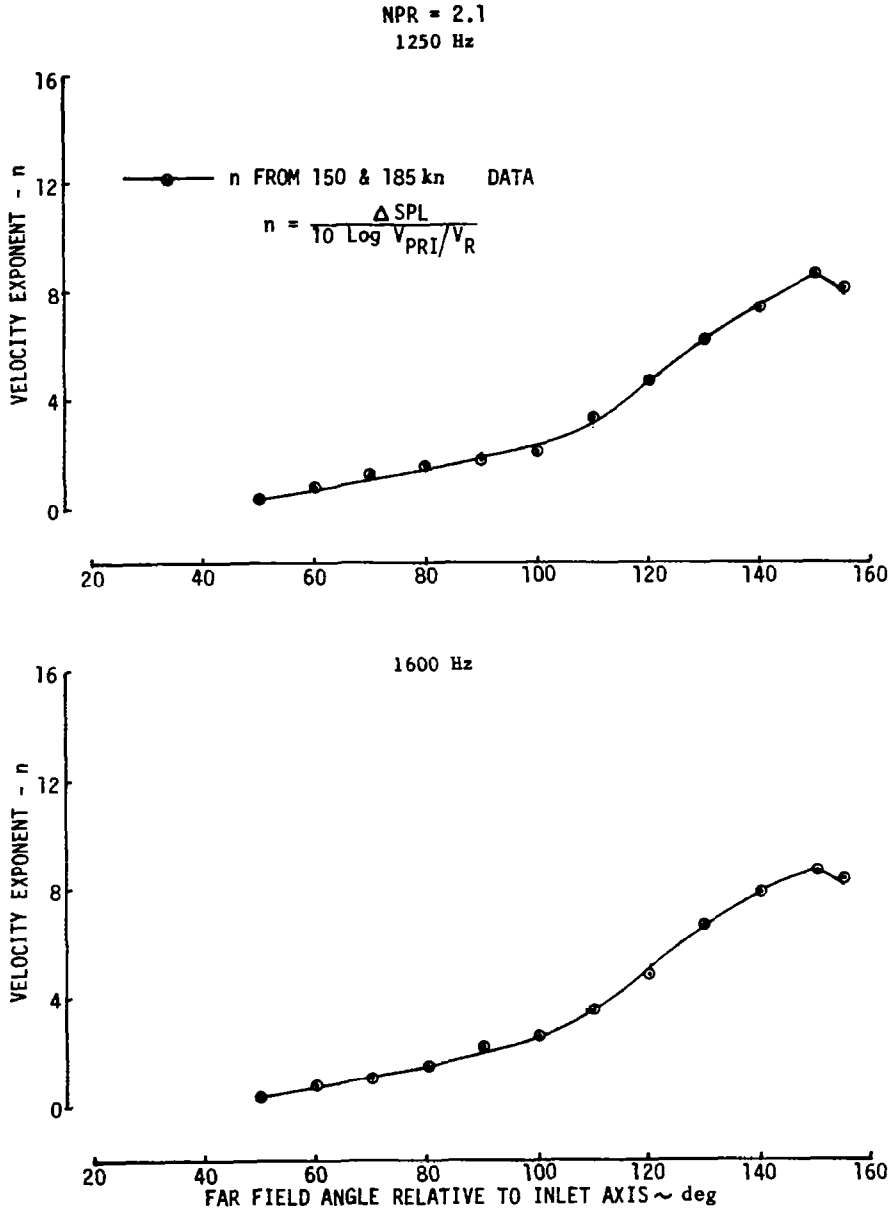

(h) 1250 Hz & 1600 Hz

Figure 40.—(Continued)

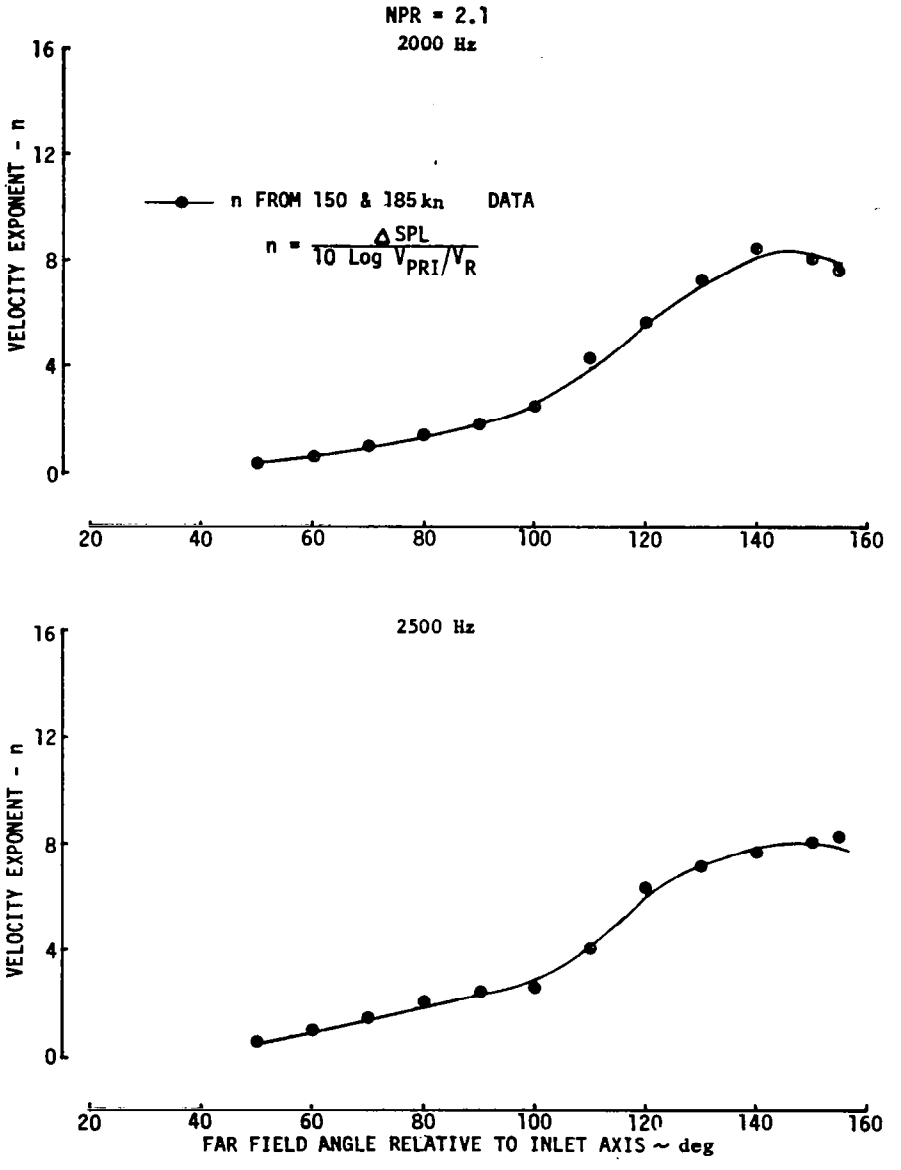

(i) 2000 Hz & 2500 Hz

Figure 40.—(Continued)

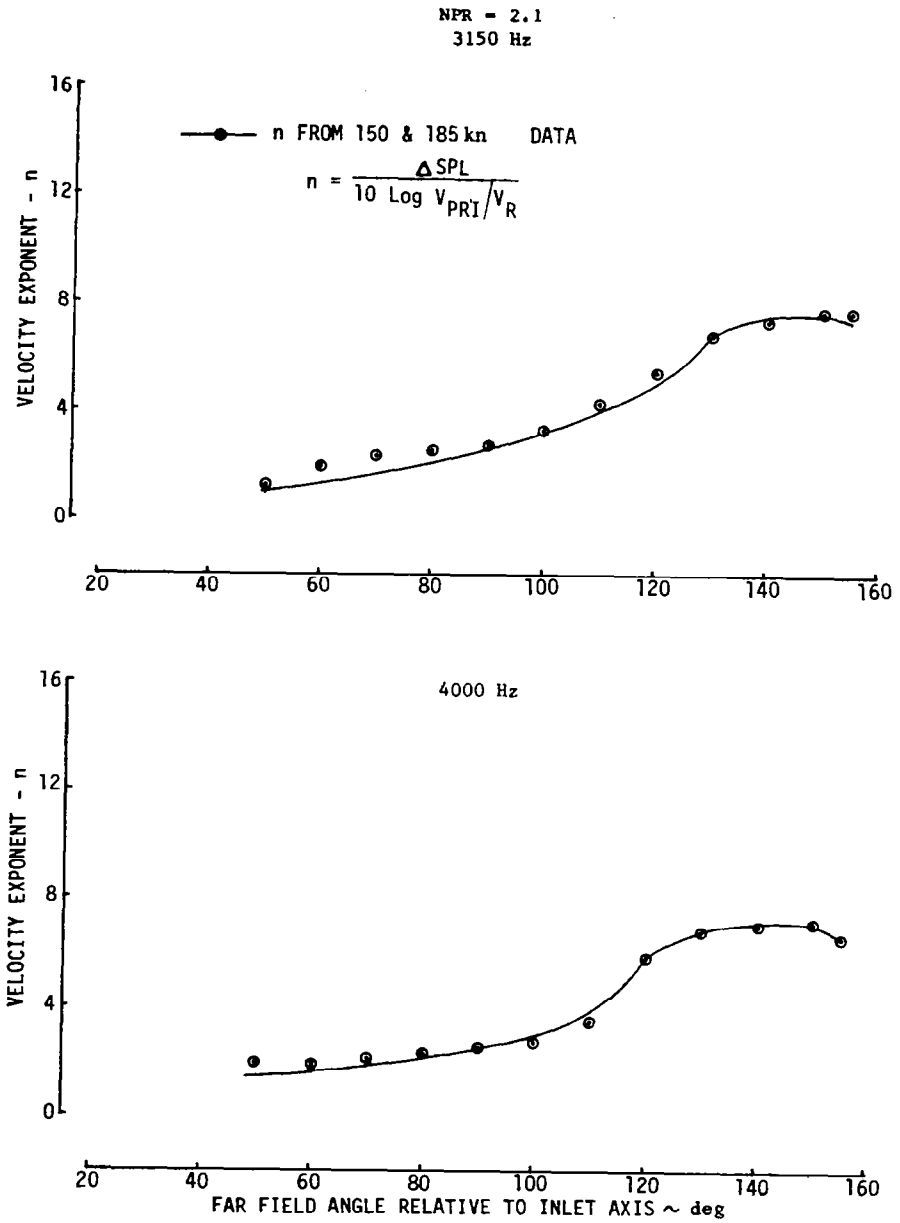

(j) 3150 Hz & 4000 Hz

Figure 40.—(Continued)

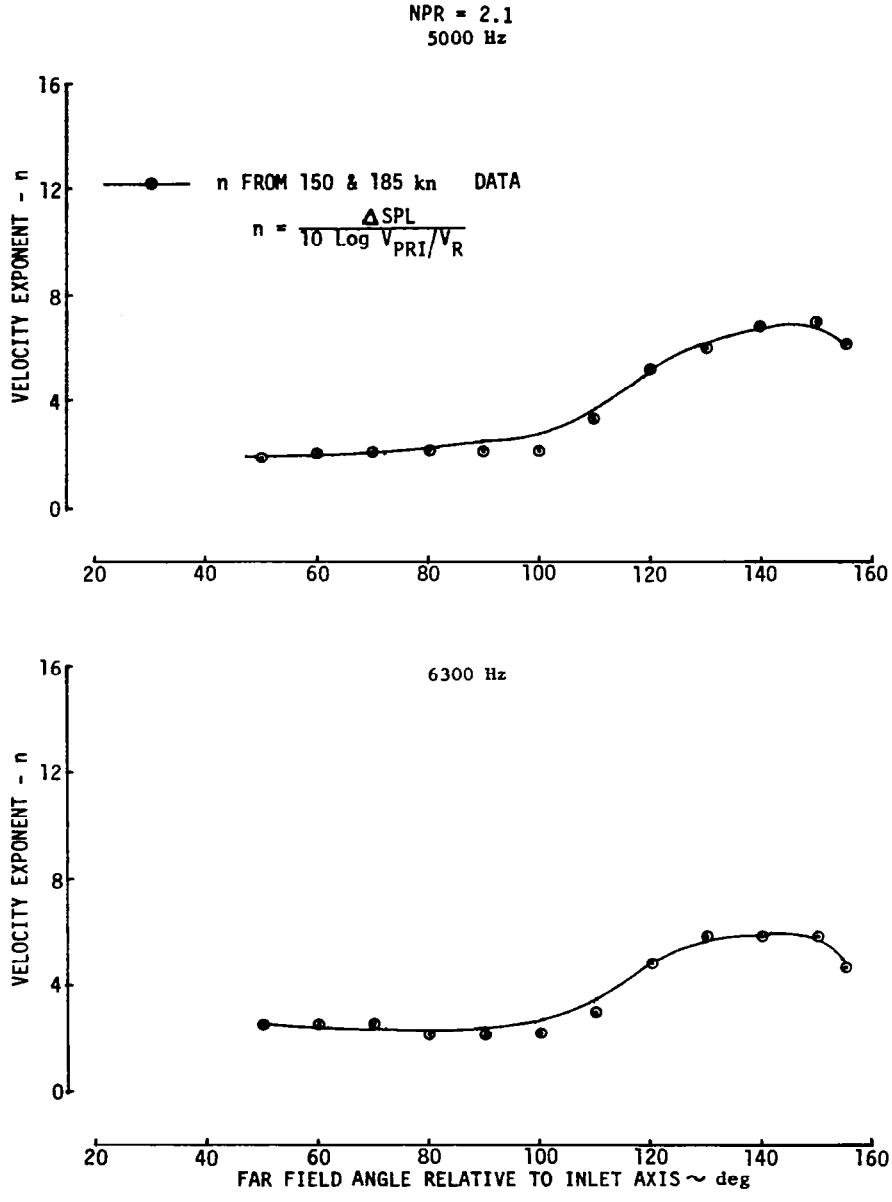

(k) 5000 Hz & 6300 Hz

Figure 40.—(Continued)

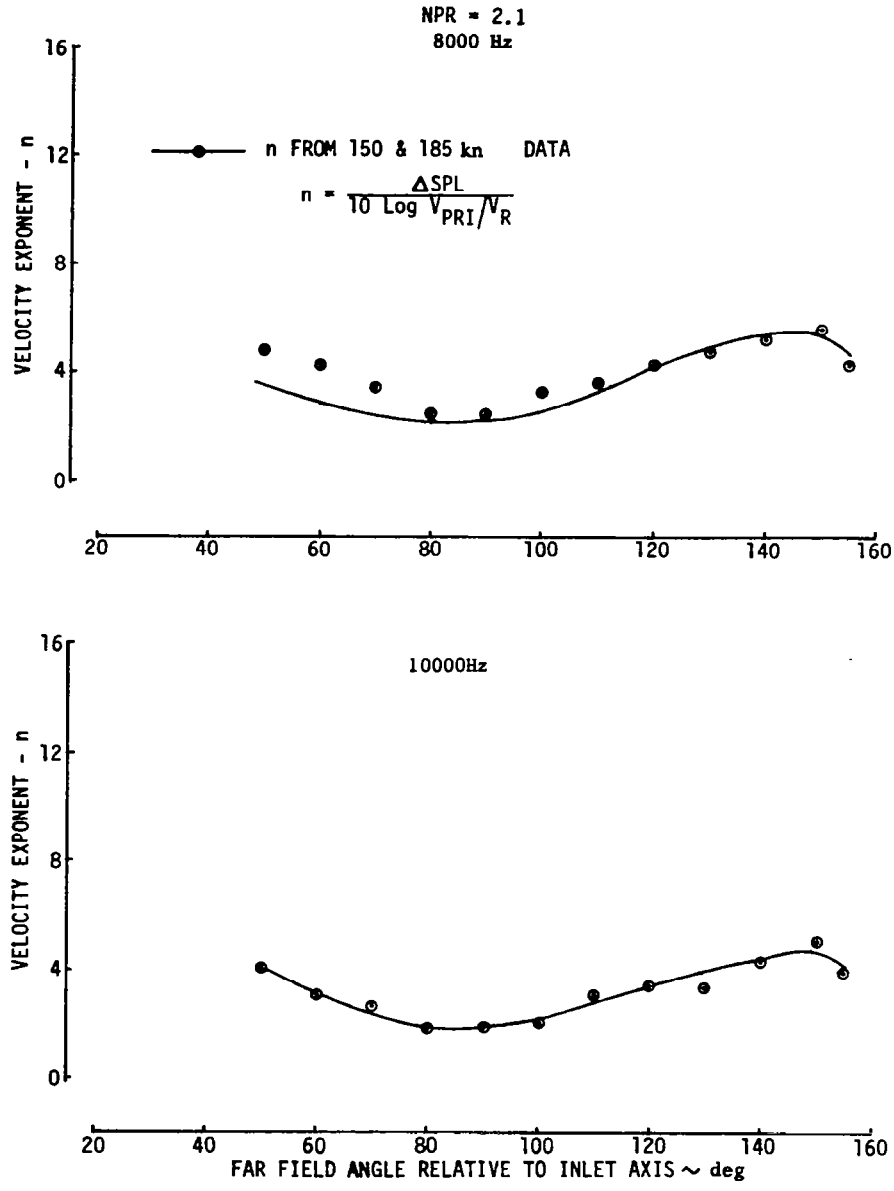

(l) 8000 Hz & 10000 Hz

Figure 40.—(Concluded)

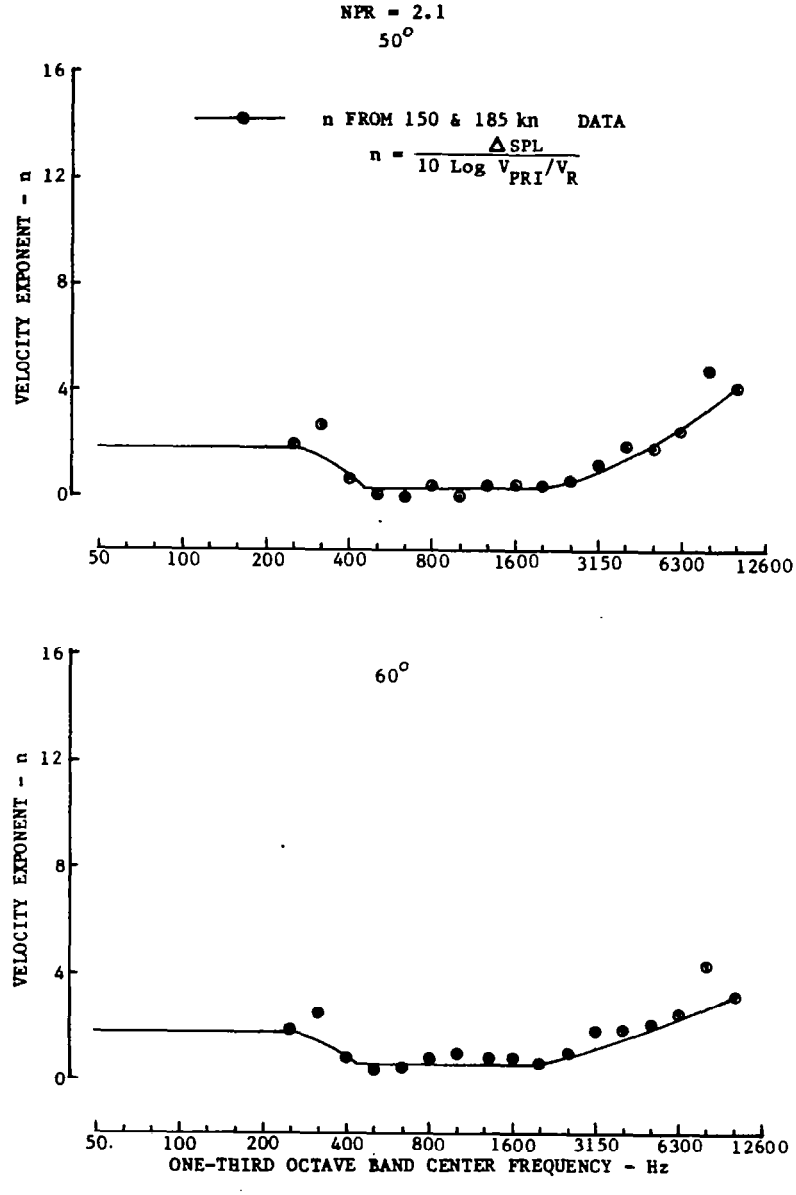

(a) 50° & 60°

Figure 41.—Velocity Exponent versus Frequency, Inverter Configuration: NPR = 2.1

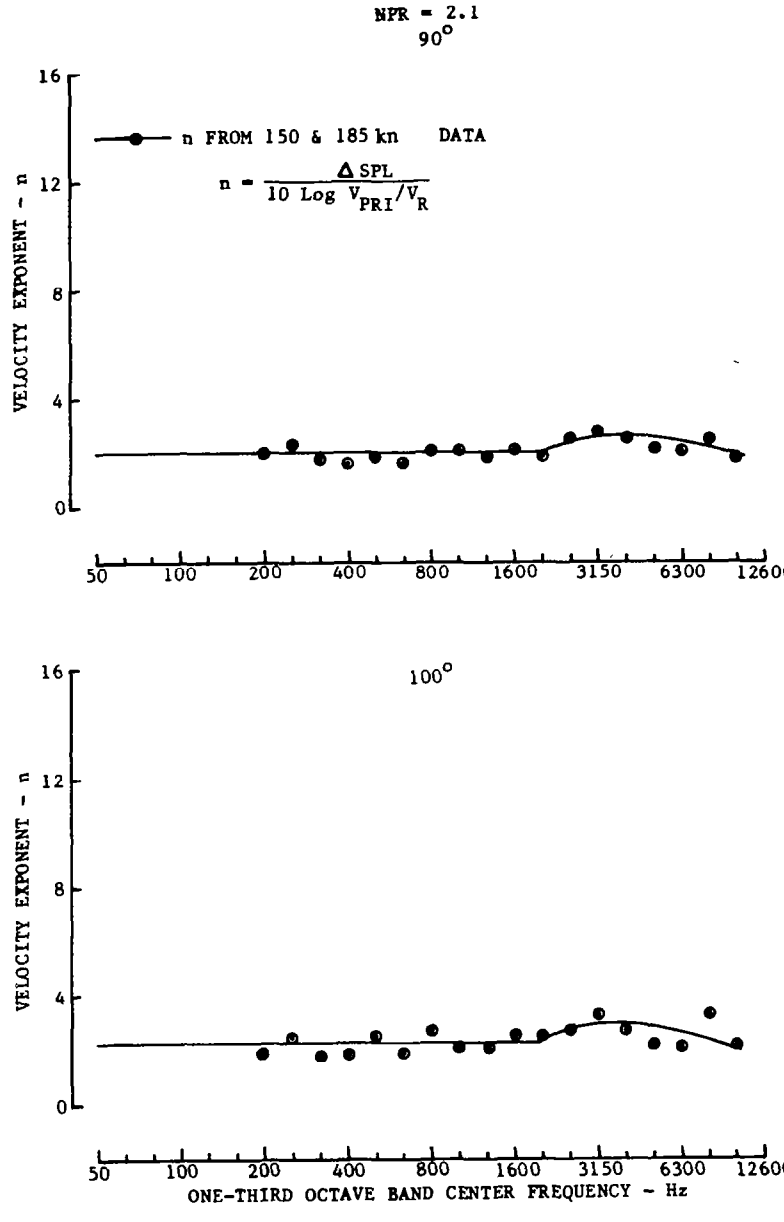

(b) 90° & 100°

Figure 41.—(Continued)

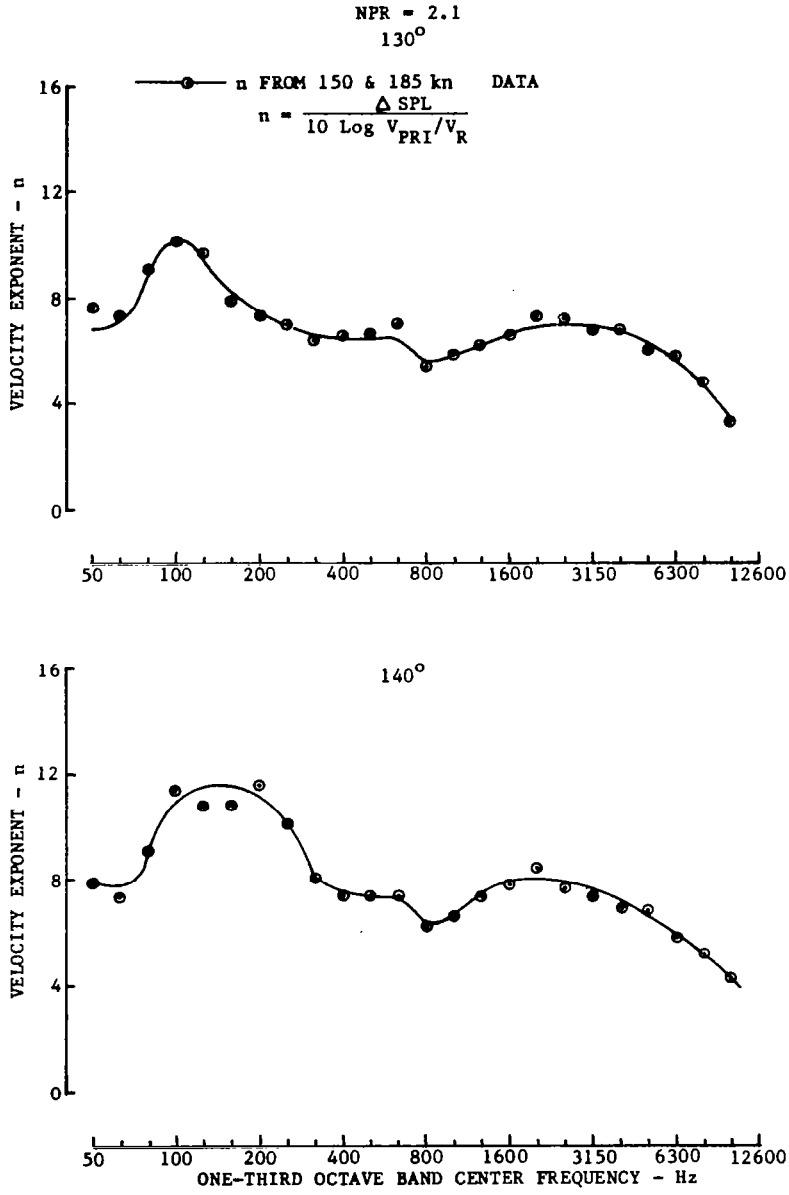

(c) 130° & 140°

Figure 41.—(Concluded)

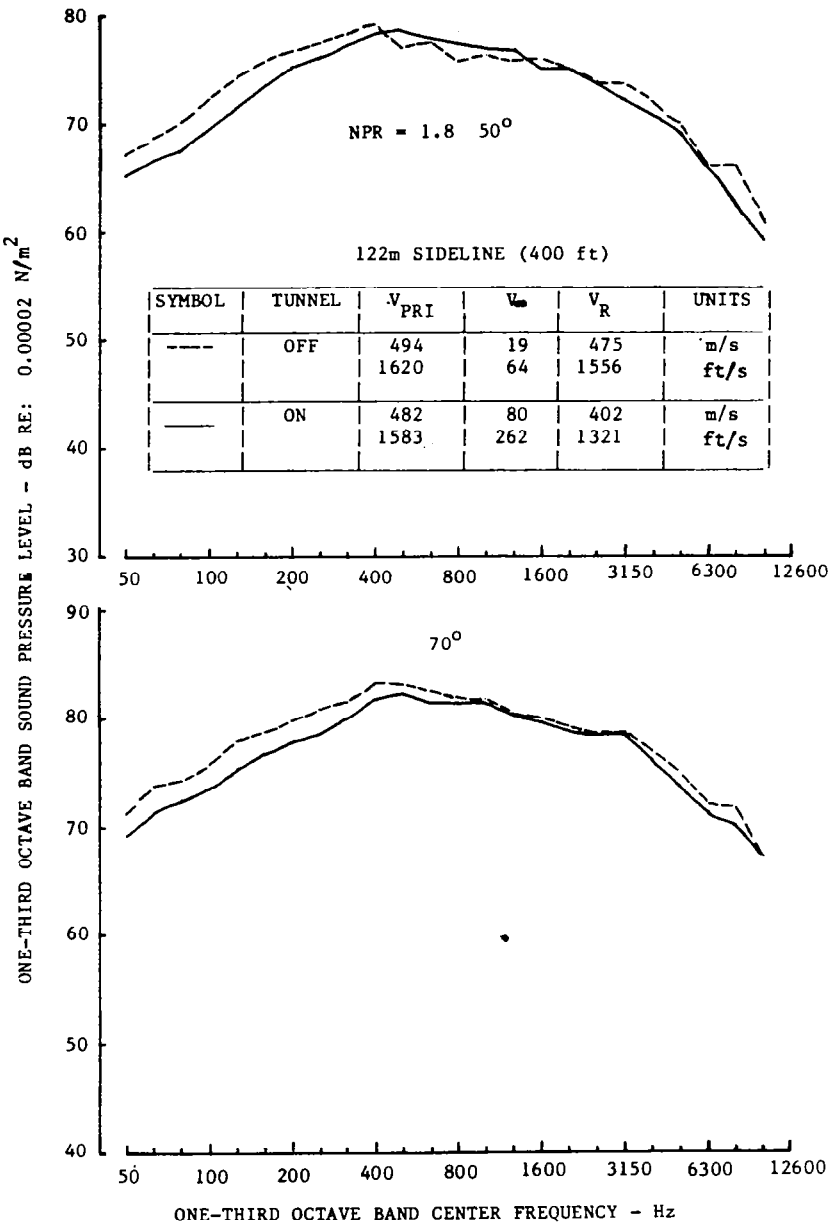

(a) 50° & 70°

Figure 42.—Comparison of Tunnel-Off and -On Spectra, Inverter Configuration: NPR = 1.8

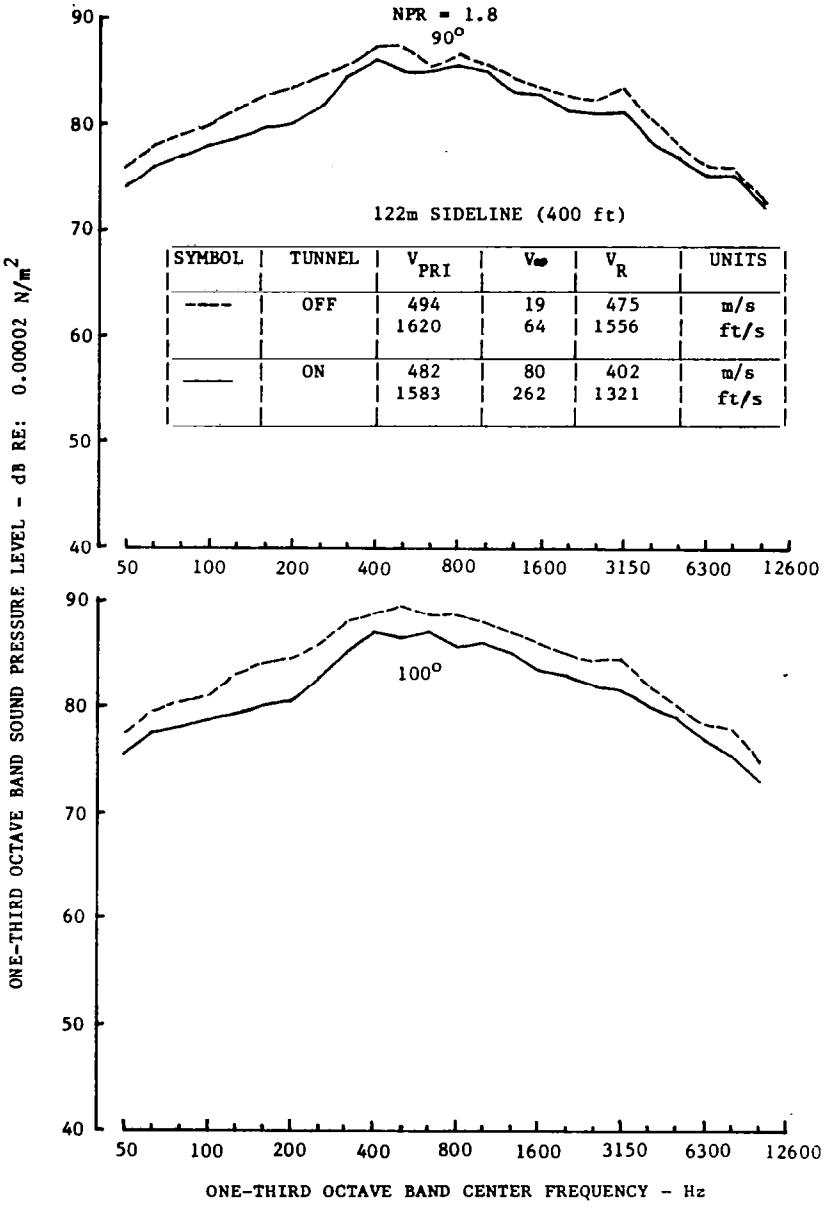

(b) 90° & 100°

Figure 42.—(Continued)

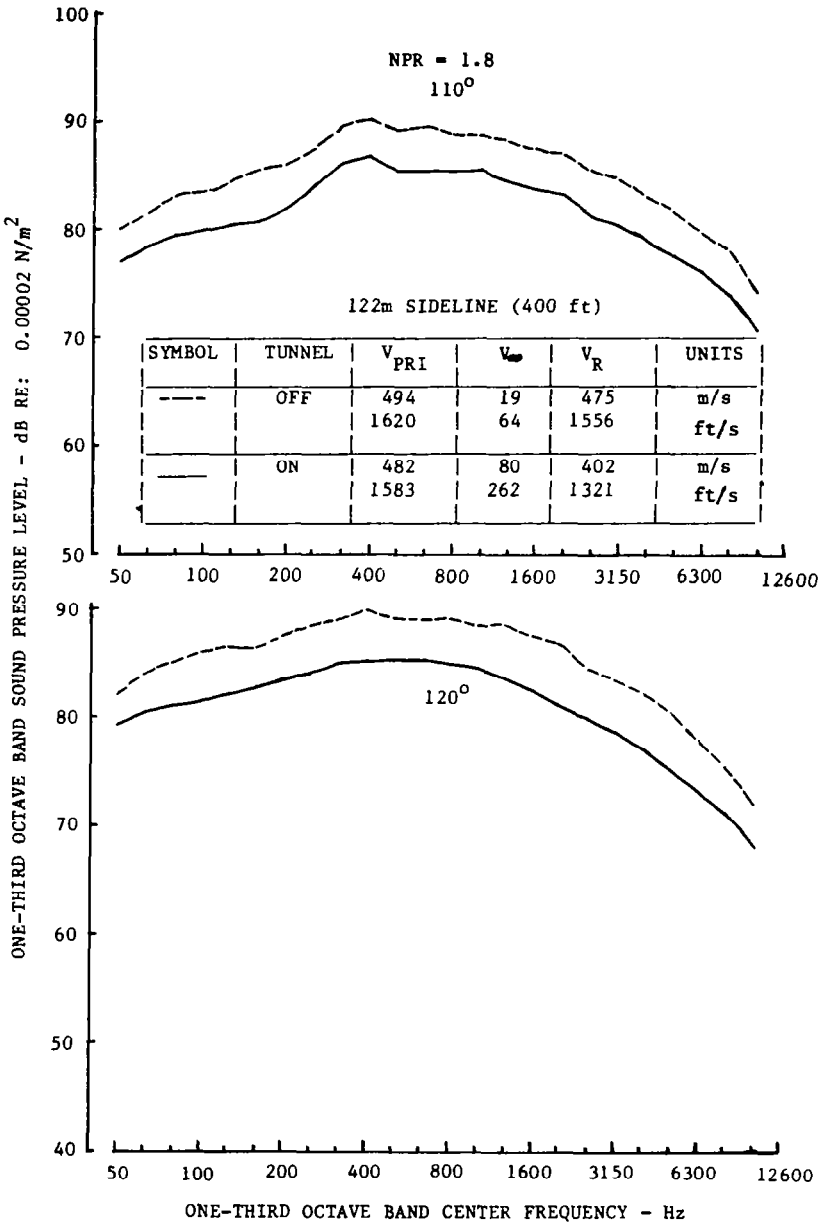

(c) 110° & 120°

Figure 42.—(Continued)

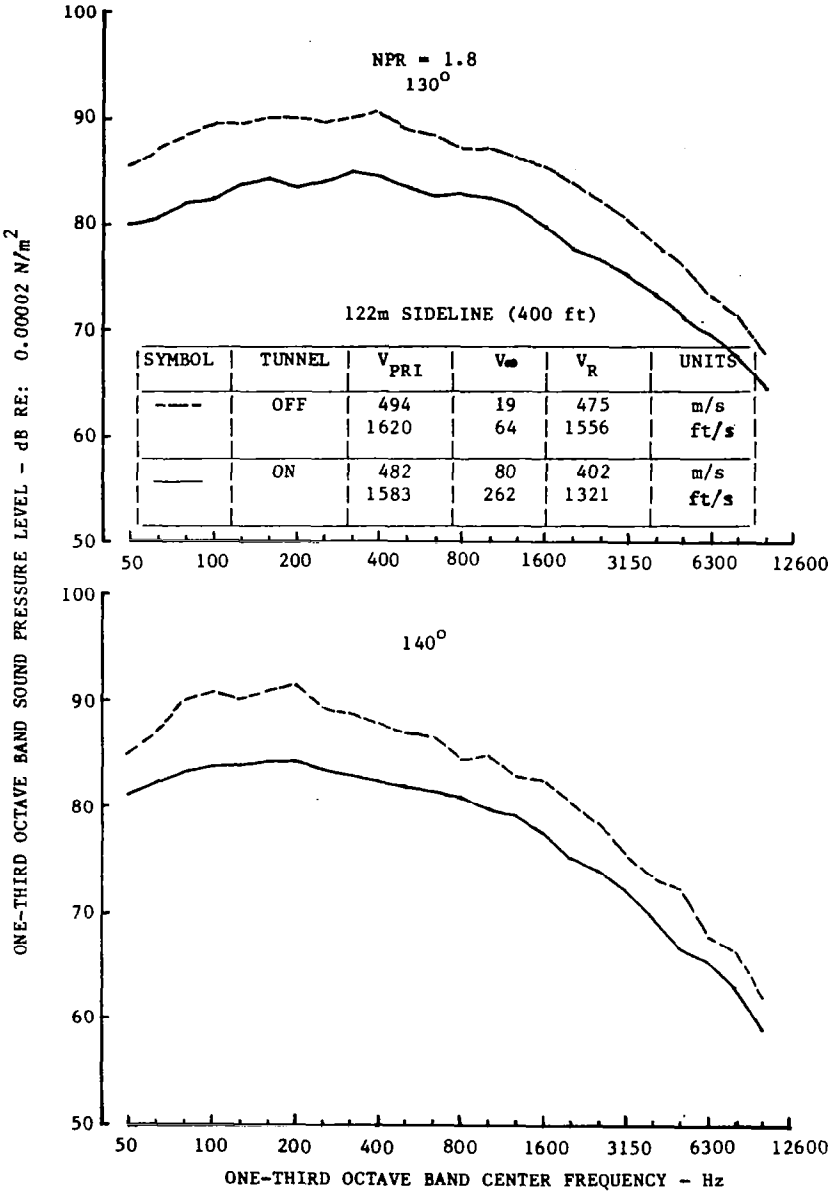

(d) 130° & 140°

Figure 42.—(Continued)

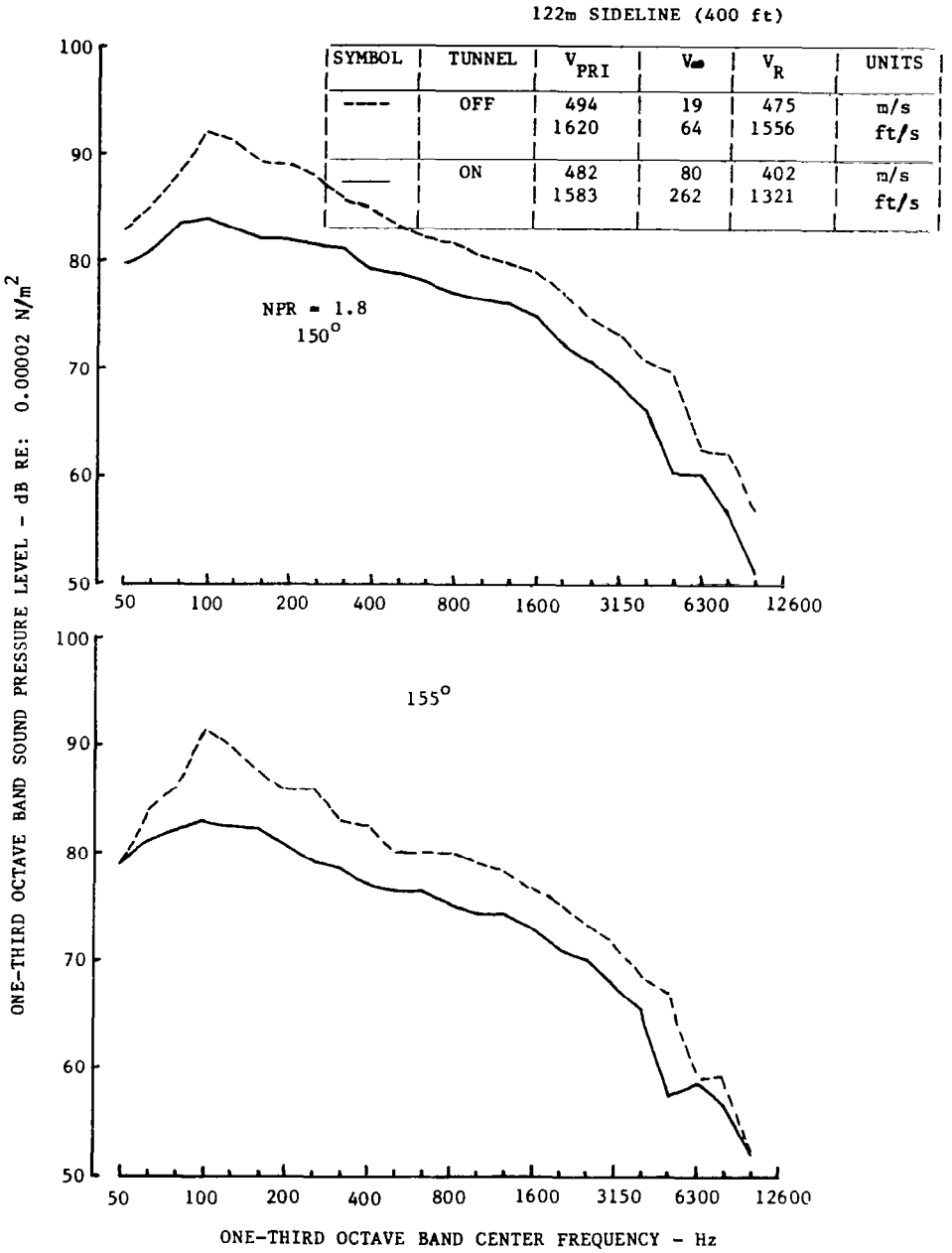

(e) 150° & 155°

Figure 42.—(Concluded)

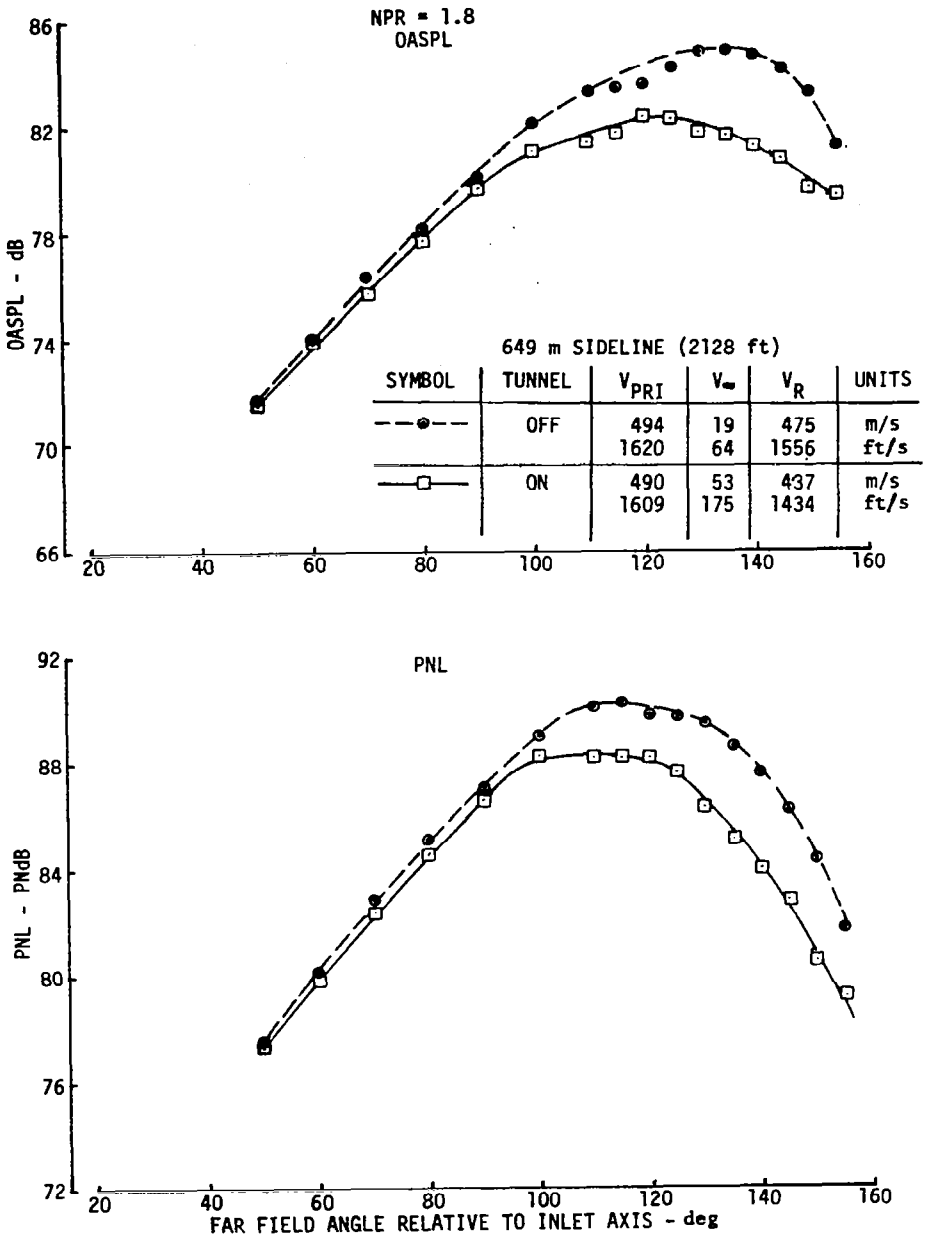

(a) 100 kn

Figure 43.—Comparison of Tunnel-Off and -On OASPL and PNL Directivities, Inverter Configuration: NPR = 1.8

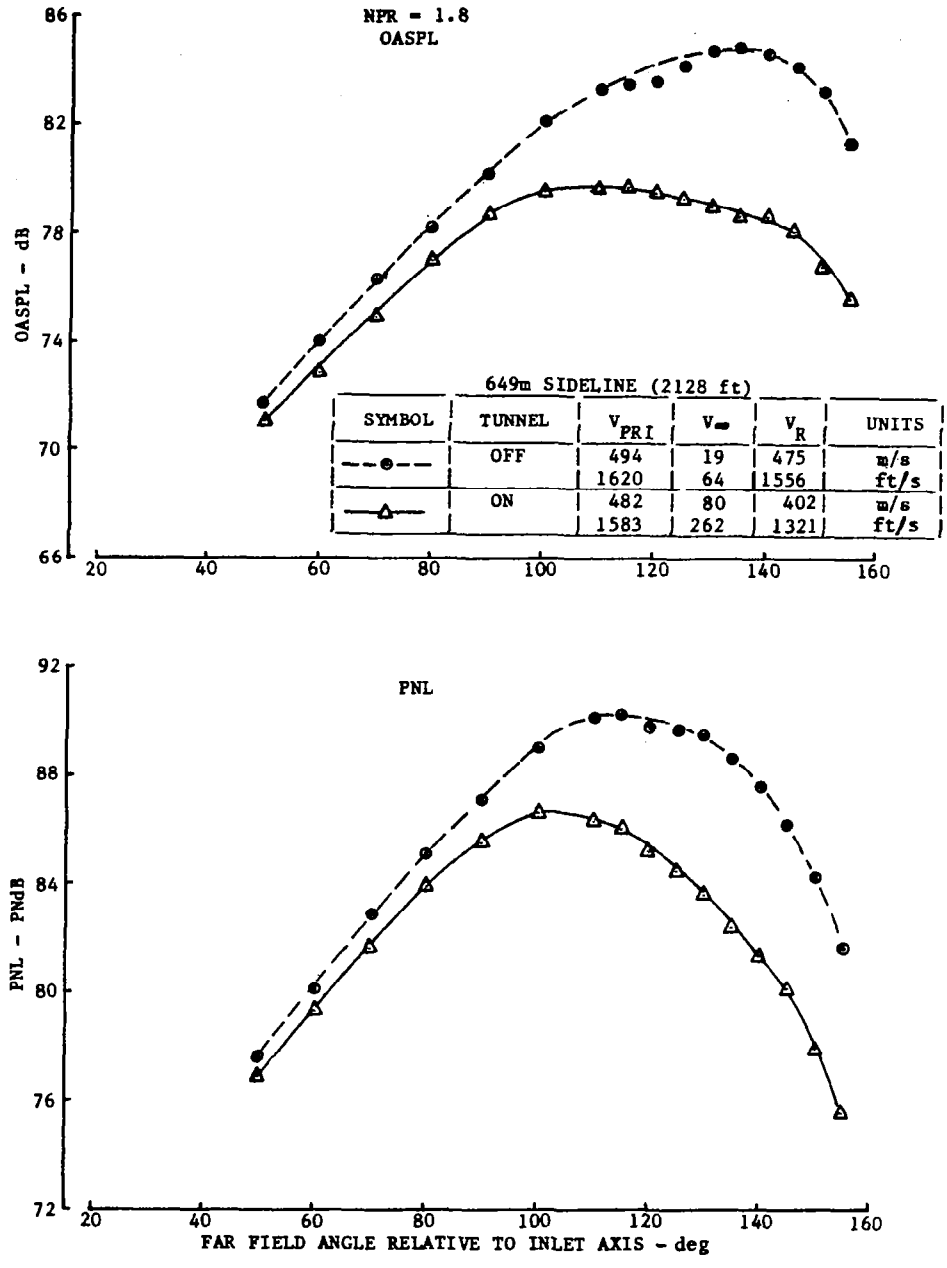

(b) 150 kn

Figure 43.—(Concluded)

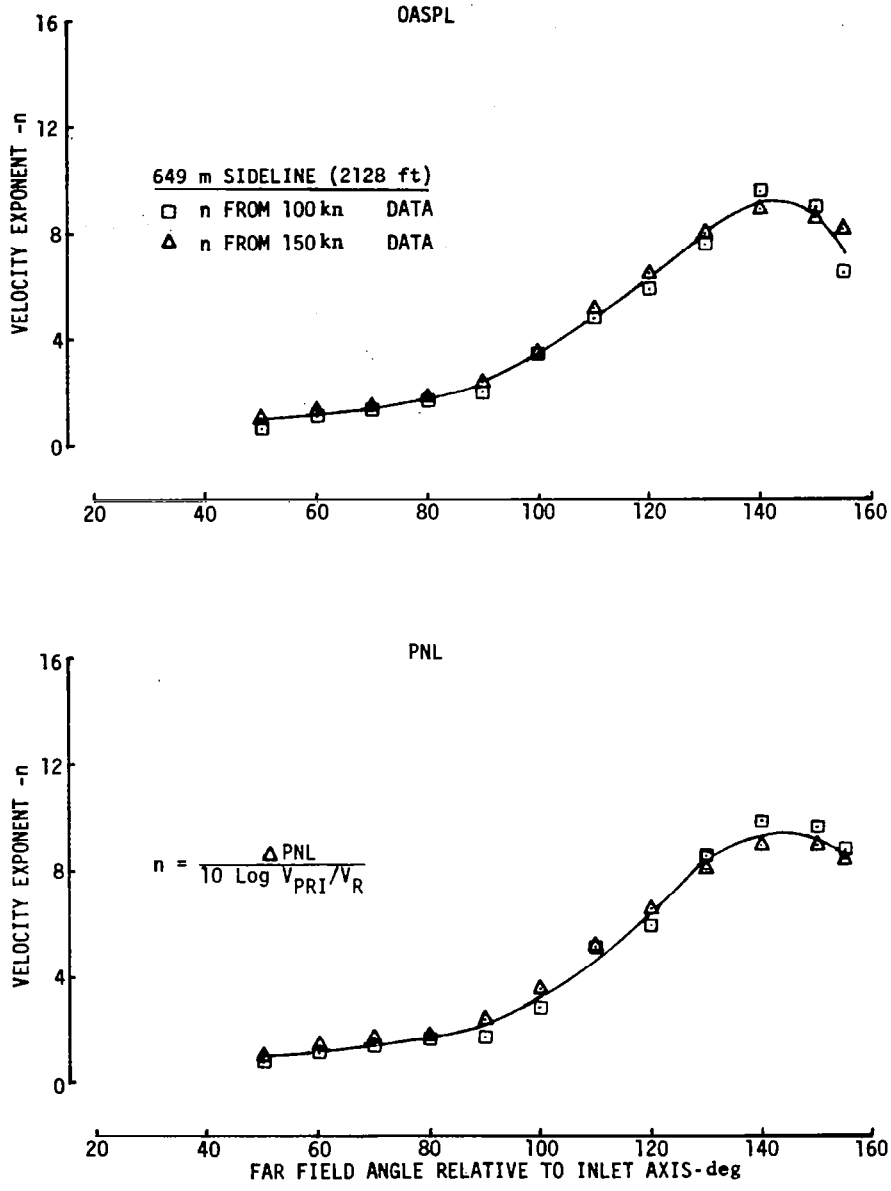

Figure 44.—Velocity Exponents for OASPL and PNL, Inverter Configuration: NPR = 1.8

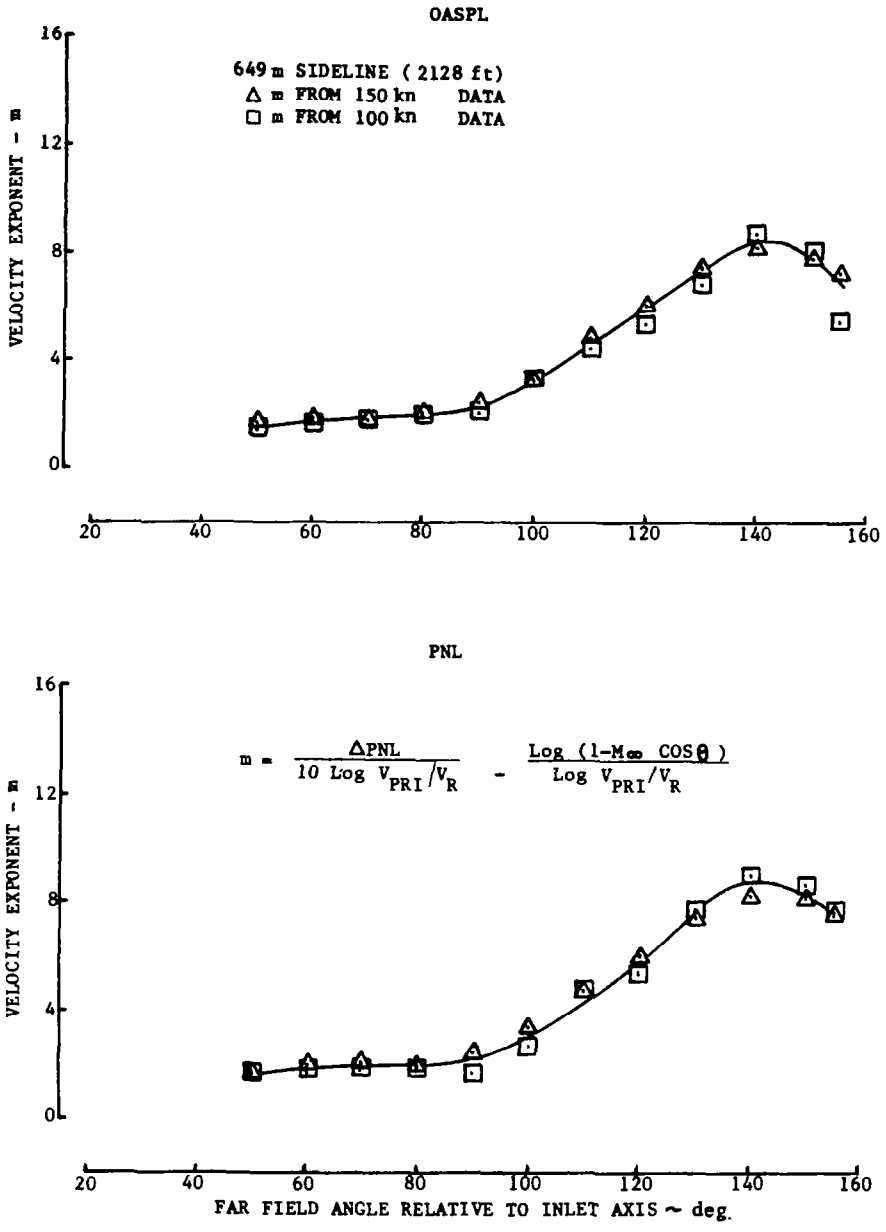

Figure 45.—Velocity Exponents for OASPL and PNL, Inverter Configuration: NPR = 1.8

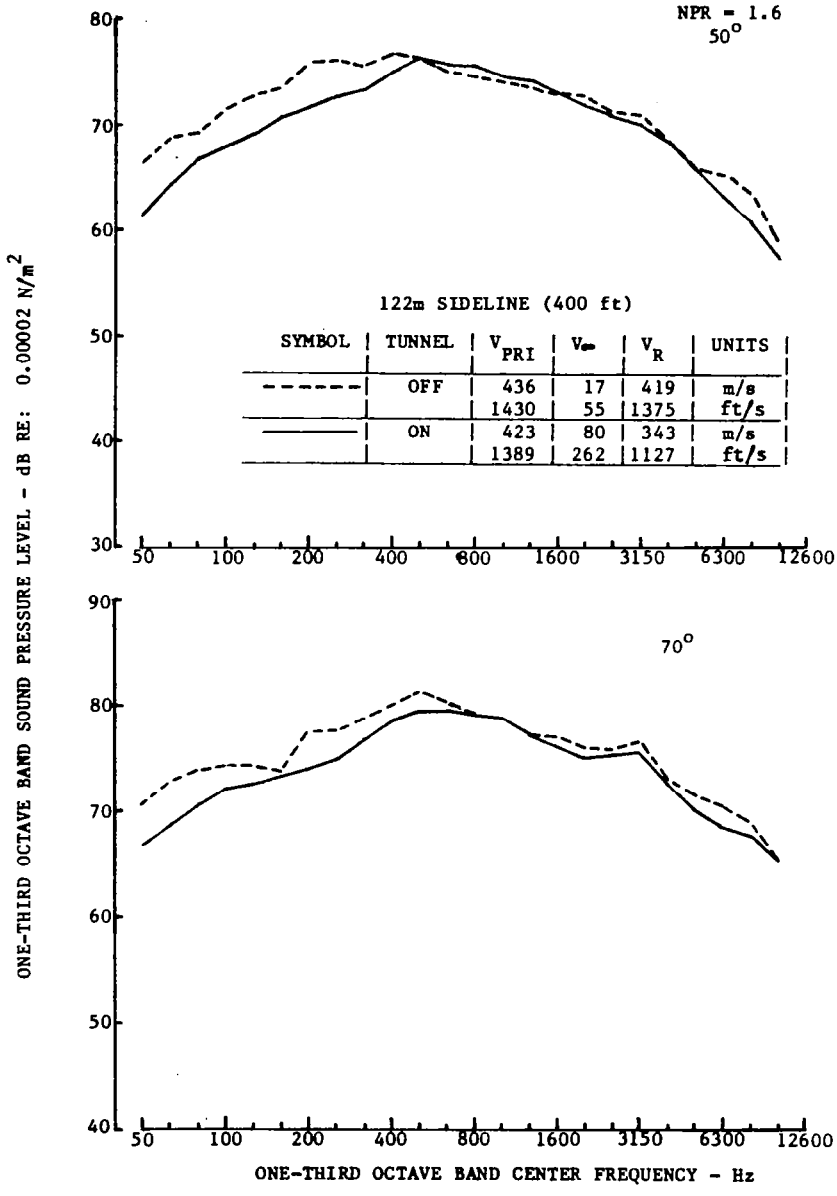

(a) 50° & 70°

Figure 46.—Comparison of Tunnel-Off and -On Spectra, Inverter Configuration: NPR = 1.6

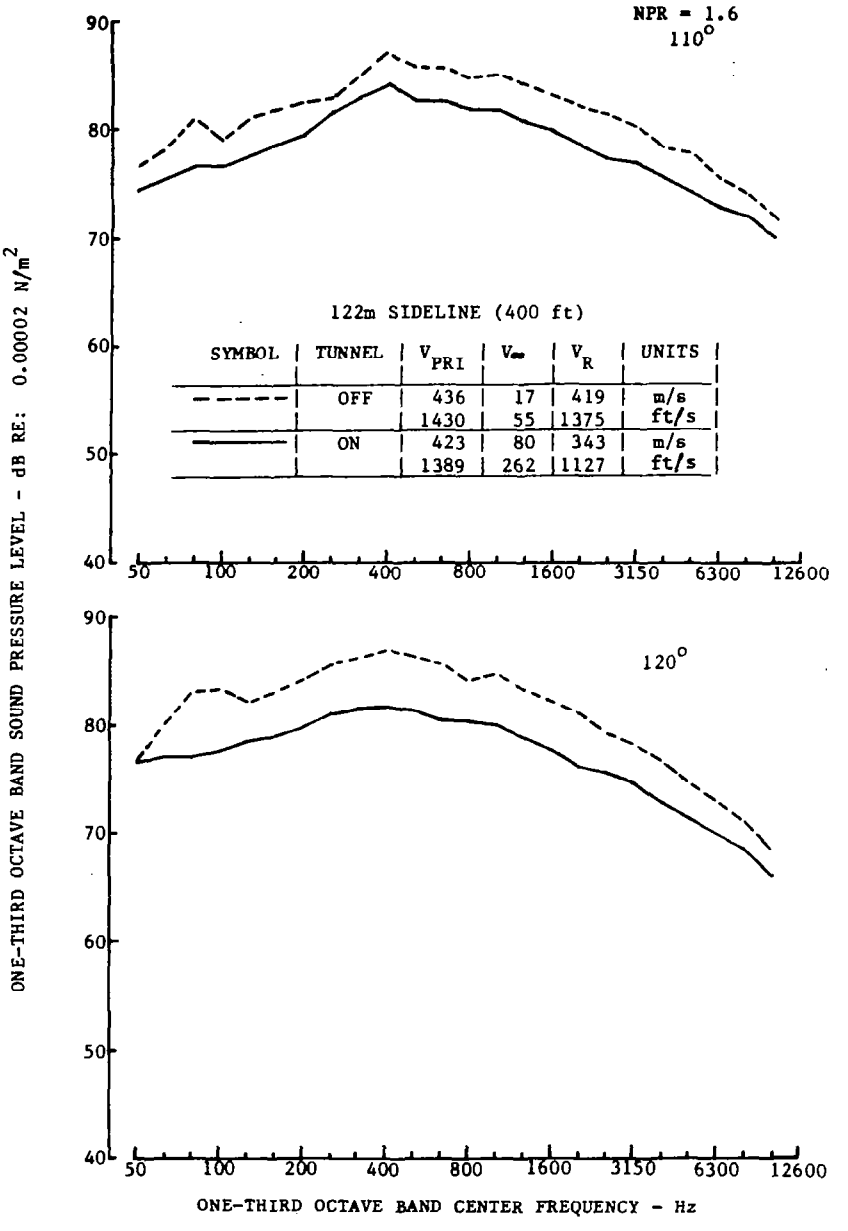

(b) 110° & 120°

Figure 46.–(Continued)

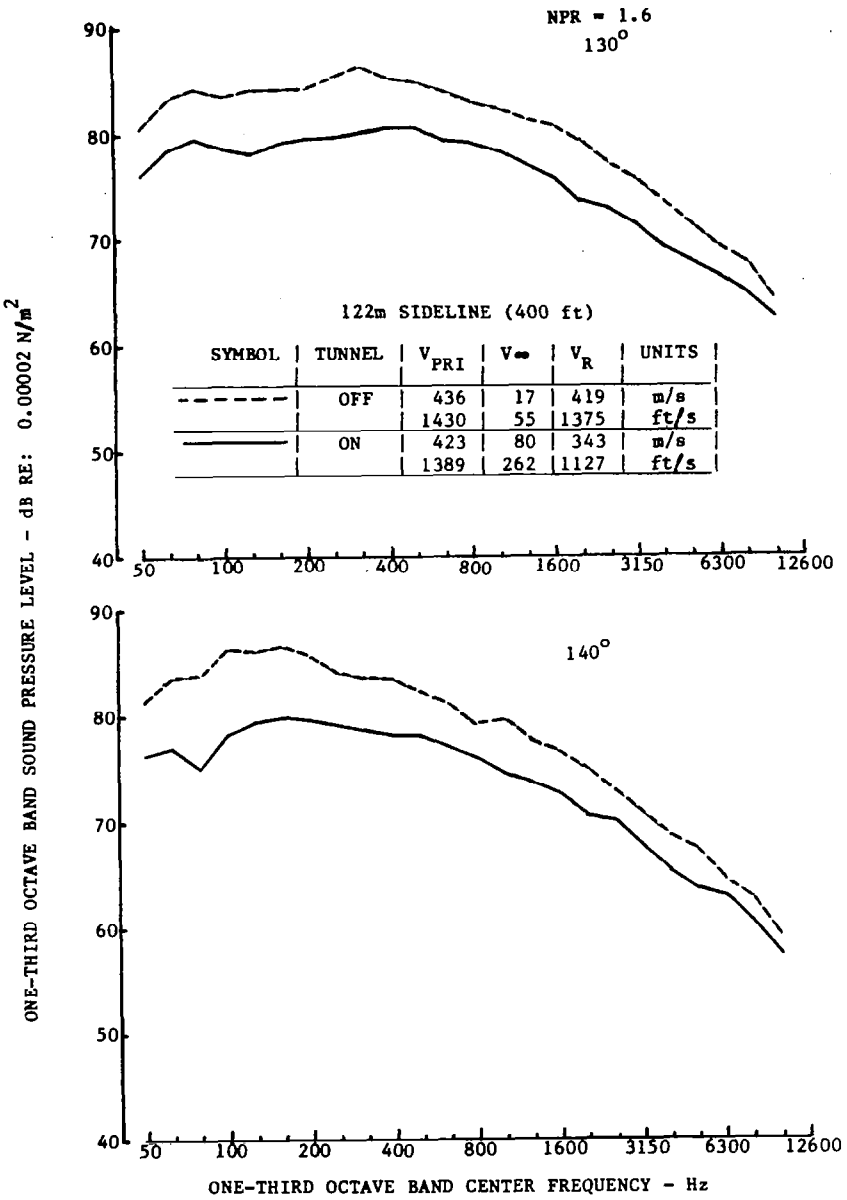

(c) 130° & 140°

Figure 46.—(Concluded)

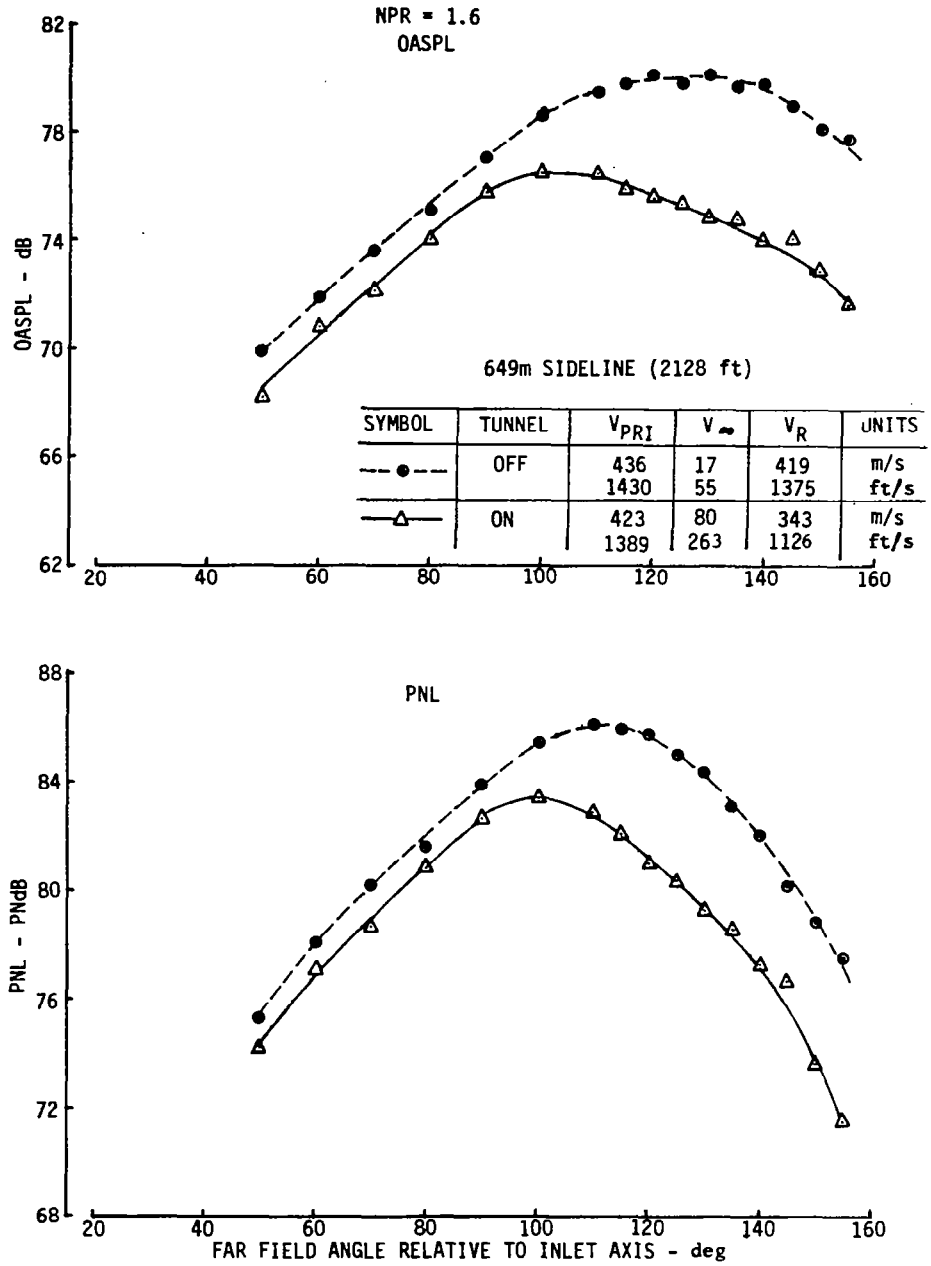

Figure 47.—Comparison of Tunnel-Off and -On OASPL and PNL Directivities, Inverter Configuration: NPR = 1.6

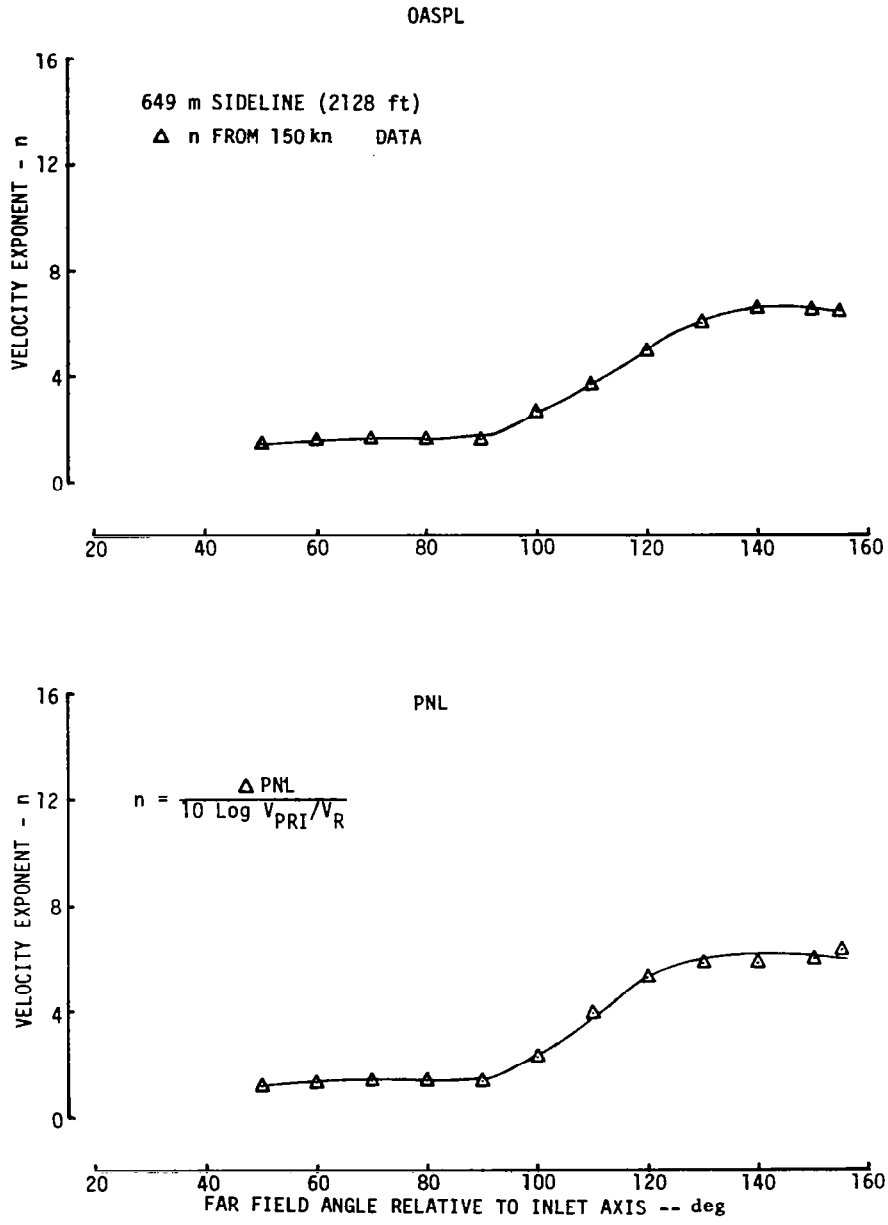

Figure 48.—Velocity Exponents for OASPL and PNL, Inverter Configuration: NPR = 1.6

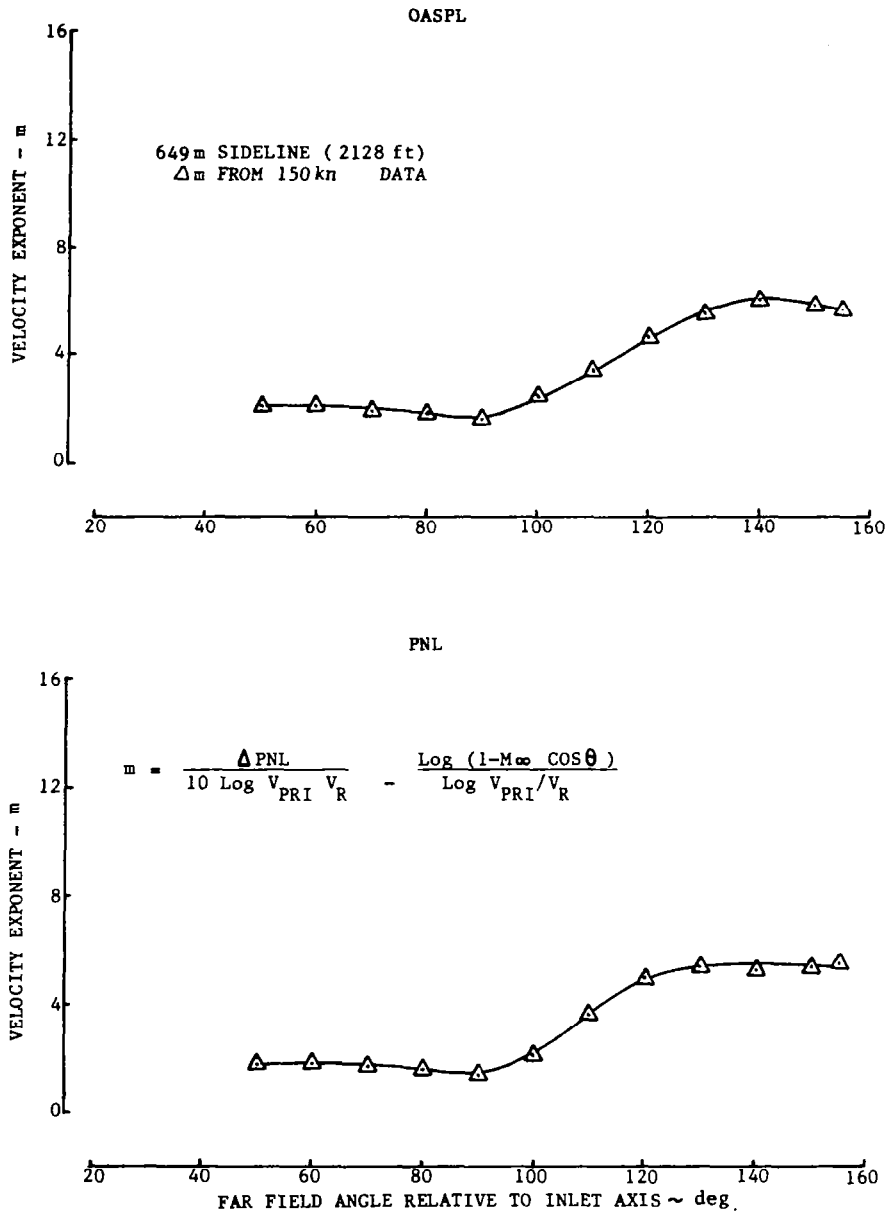

Figure 49.—Velocity Exponents for OASPL and PNL, Inverter Configuration: NPR = 1.6

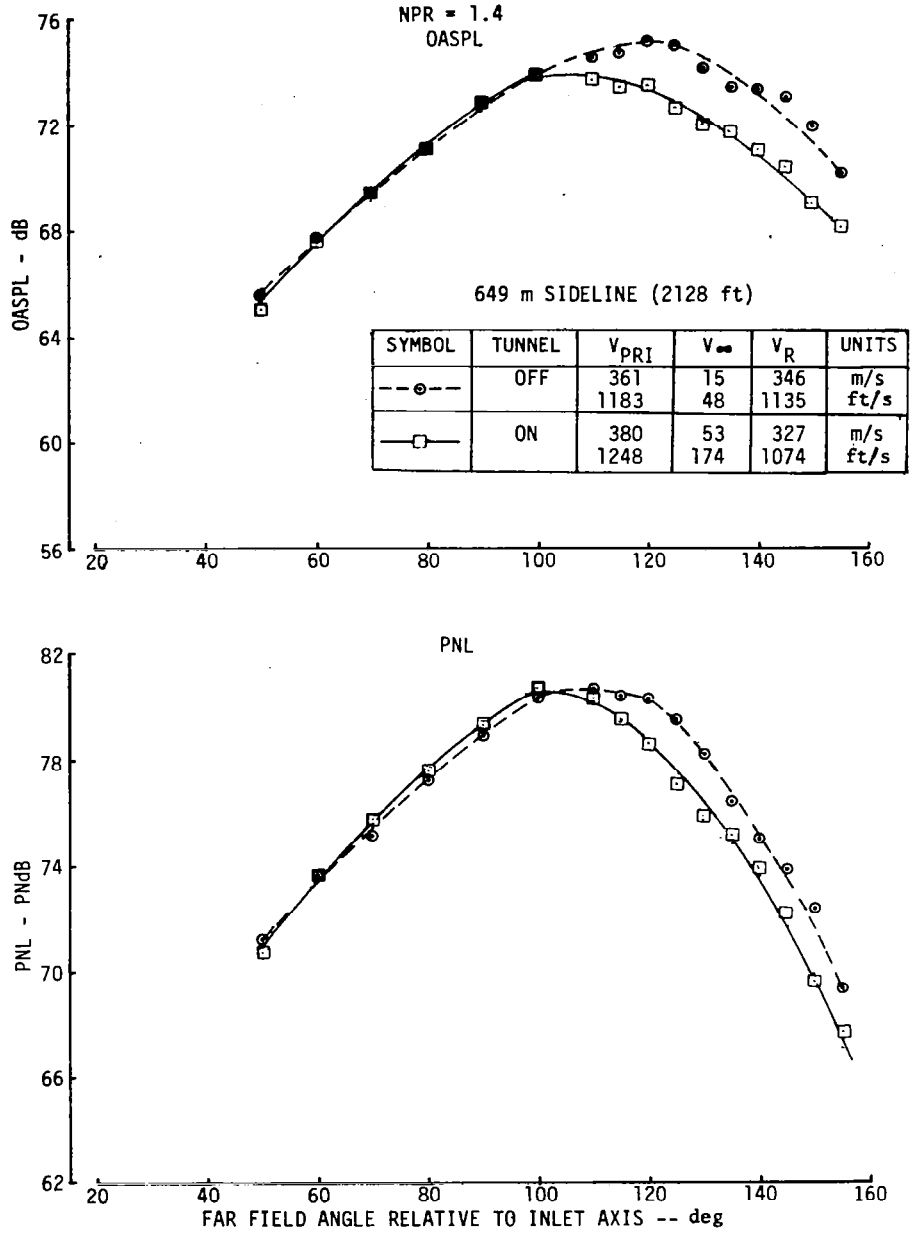

Figure 50.—Comparison of Tunnel-Off and -On OASPL and PNL Directivities, Inverter Configuration: NPR = 1.4

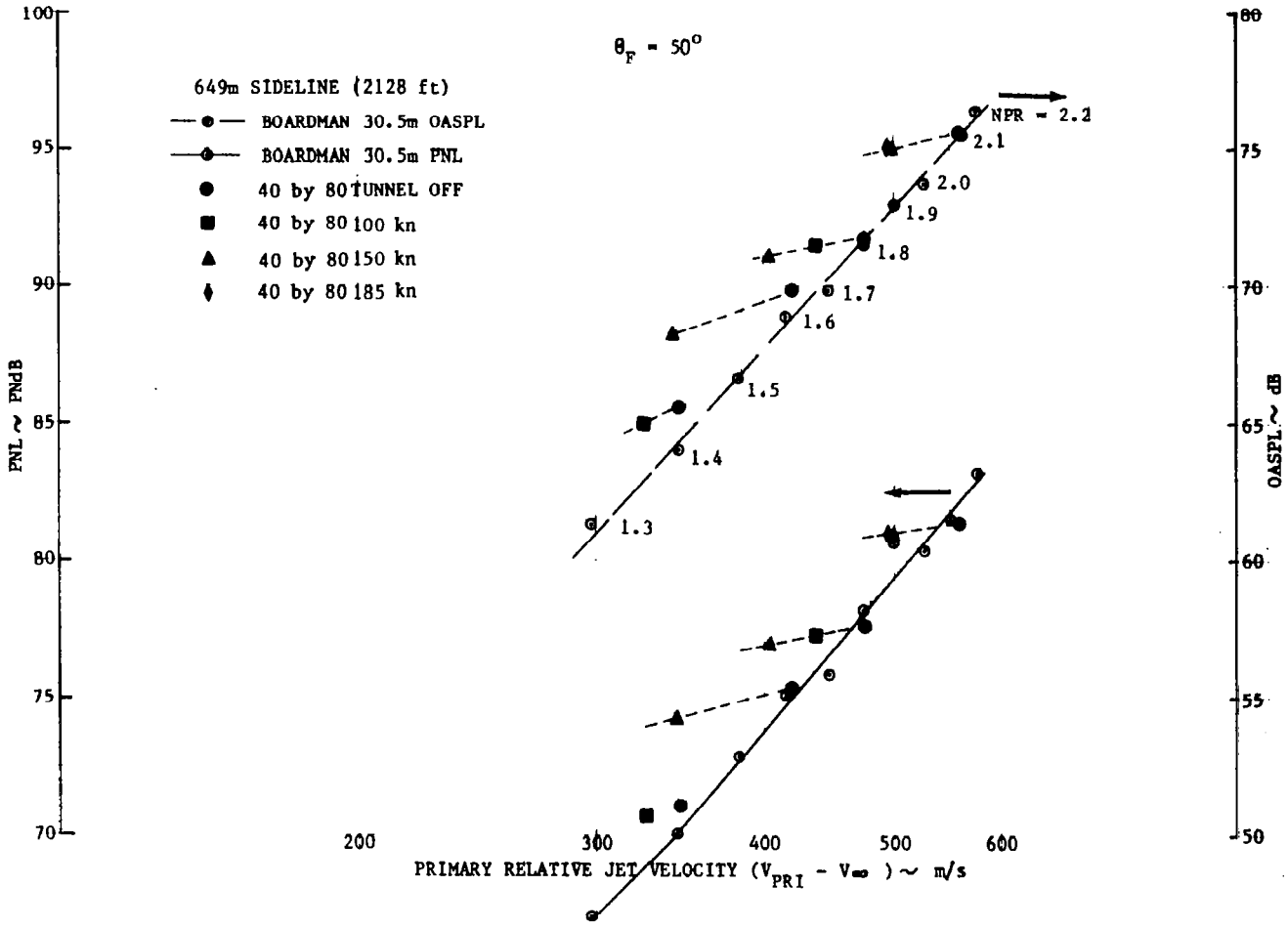

(a) 50°

Figure 51.—Tunnel-Off and -On OASPL and PNL versus Primary Velocity, Inverter Configuration

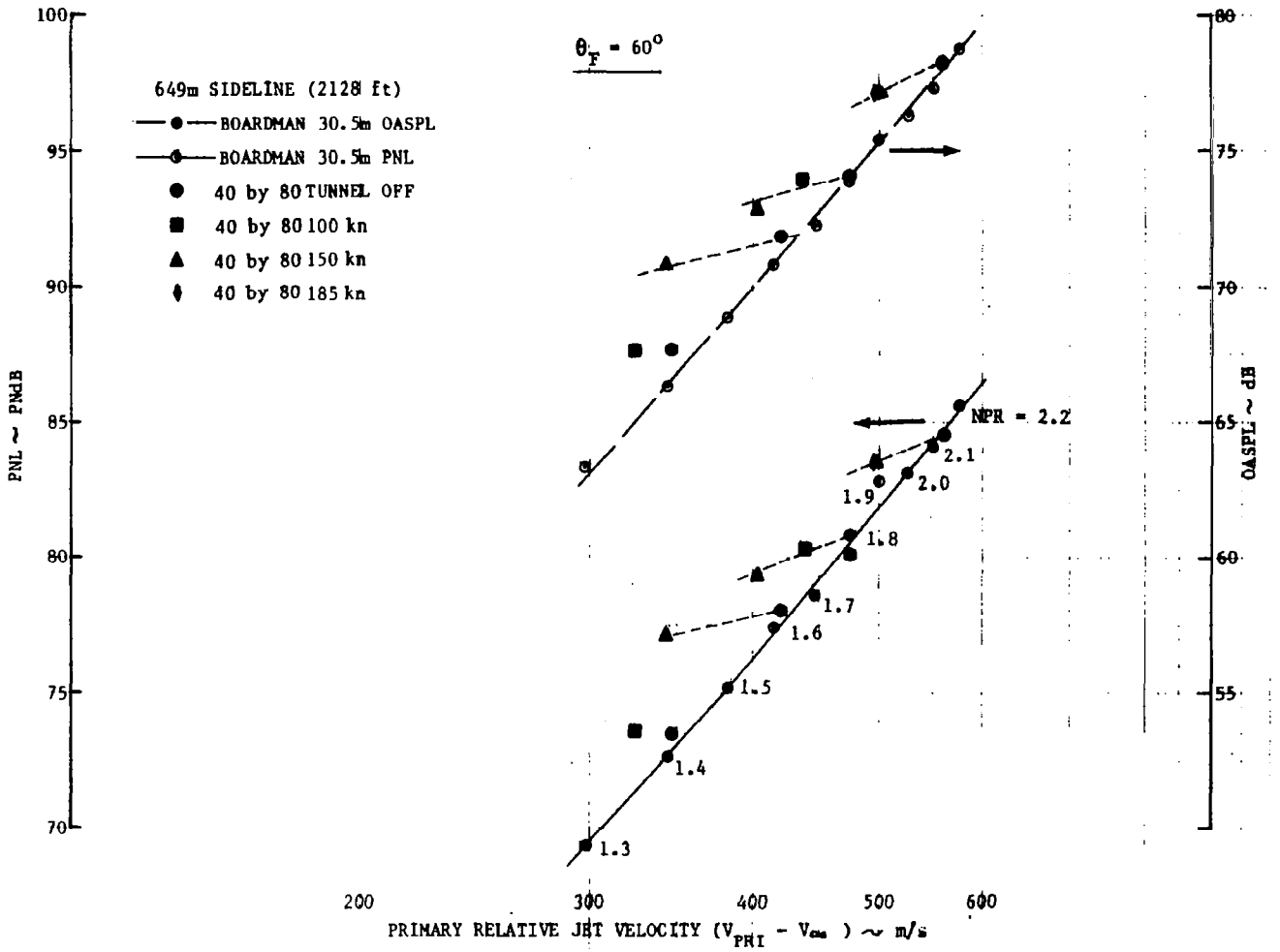

(b) 60°

Figure 51.—(Continued)

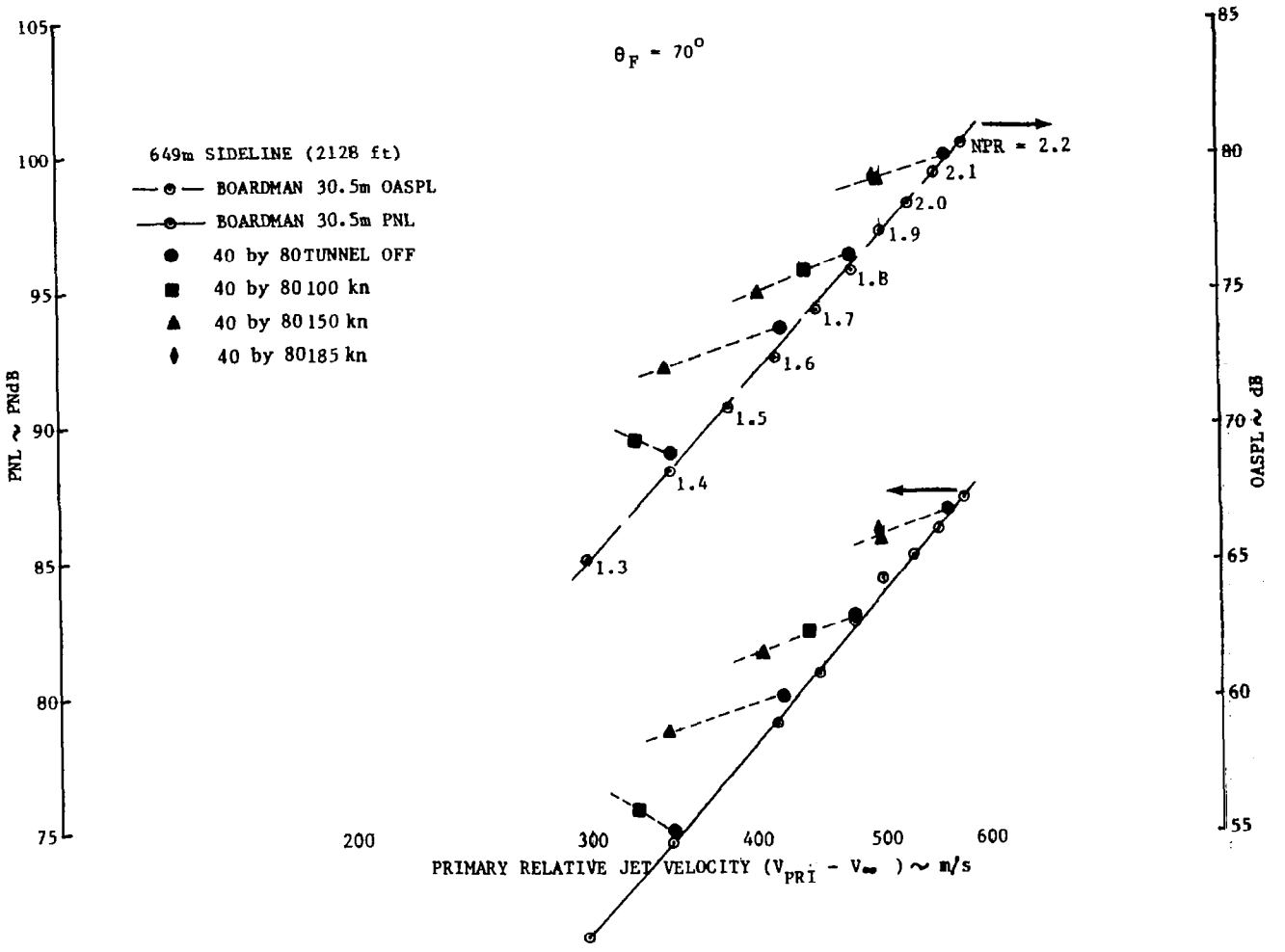

(c) 70°

Figure 51.—(Continued)

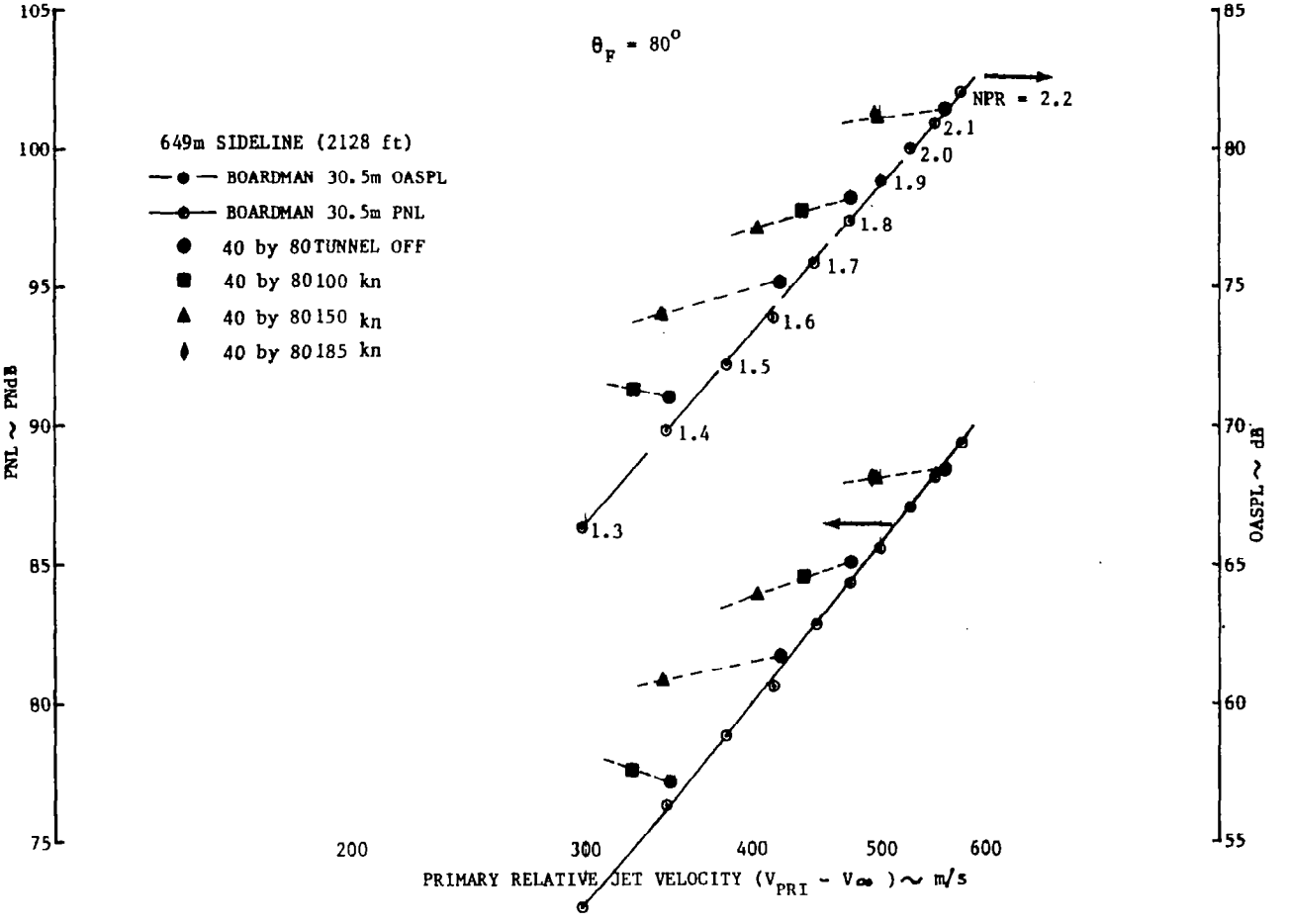

(d) 80°

Figure 51.—(Continued

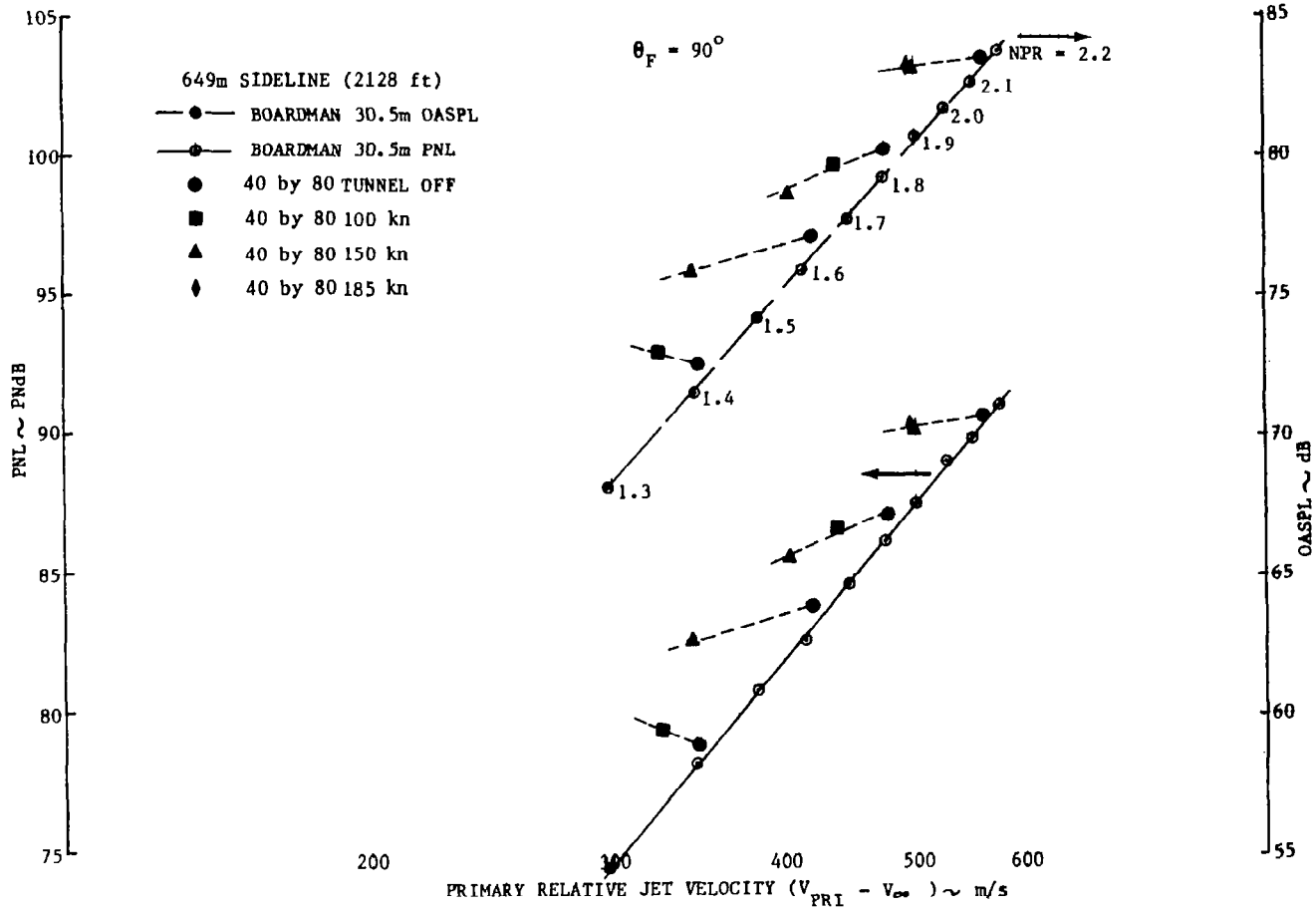

(e) 90°

Figure 51.—(Continued)

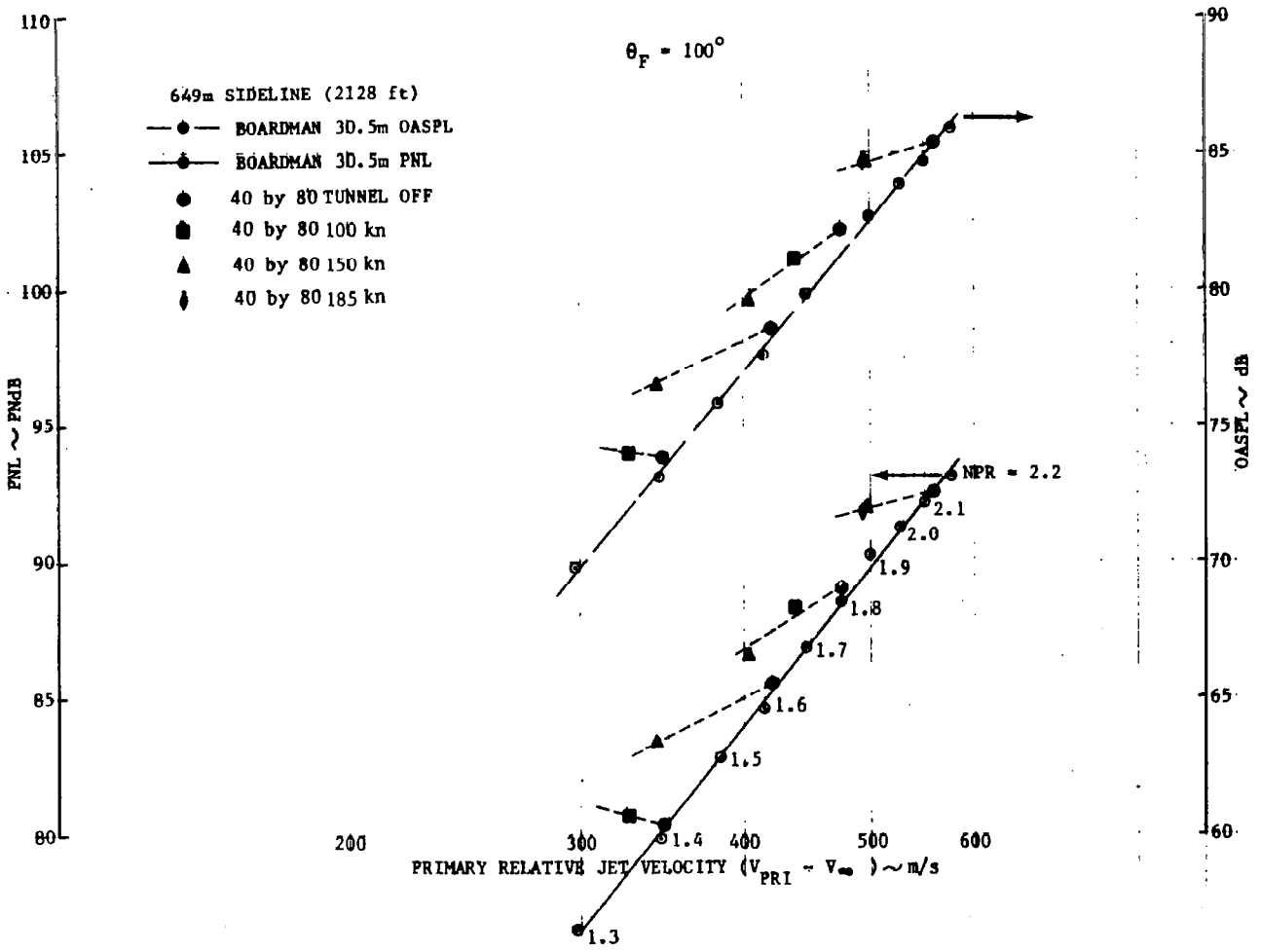

(f) 100°

Figure 51.—(Continued)

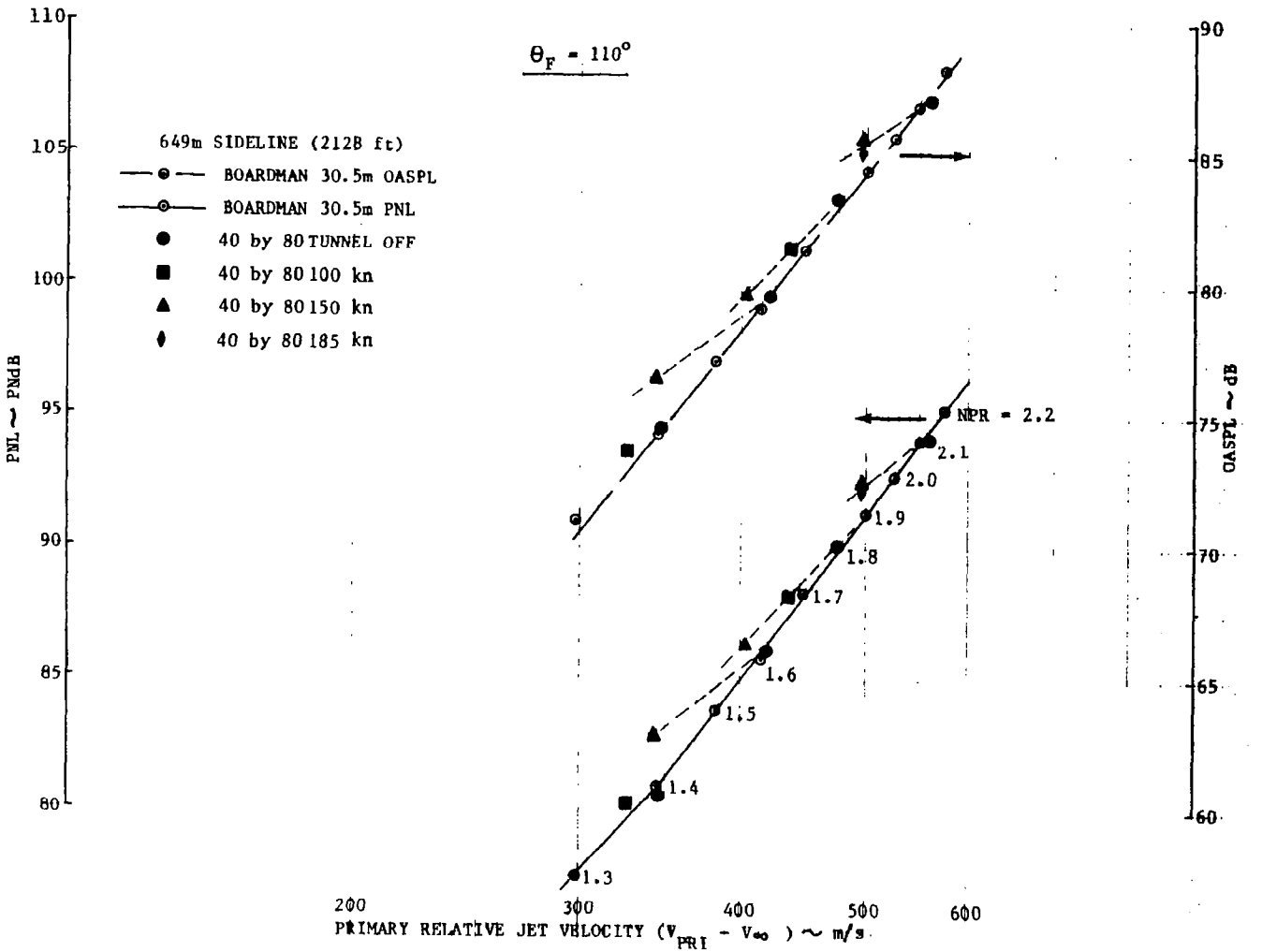

(g) 110°

Figure 51.—(Continued)

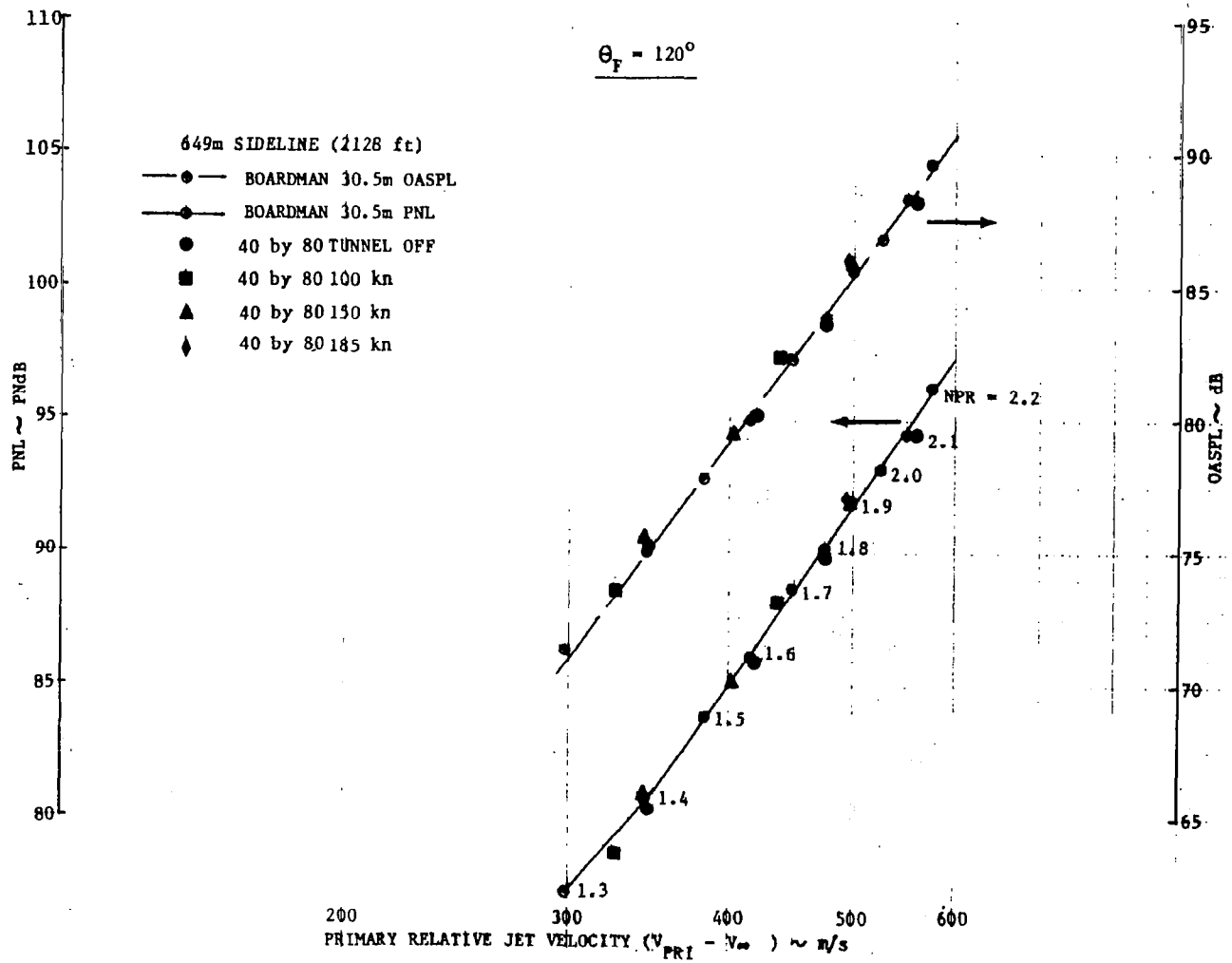

(h) 120°

Figure 51.—(Continued)

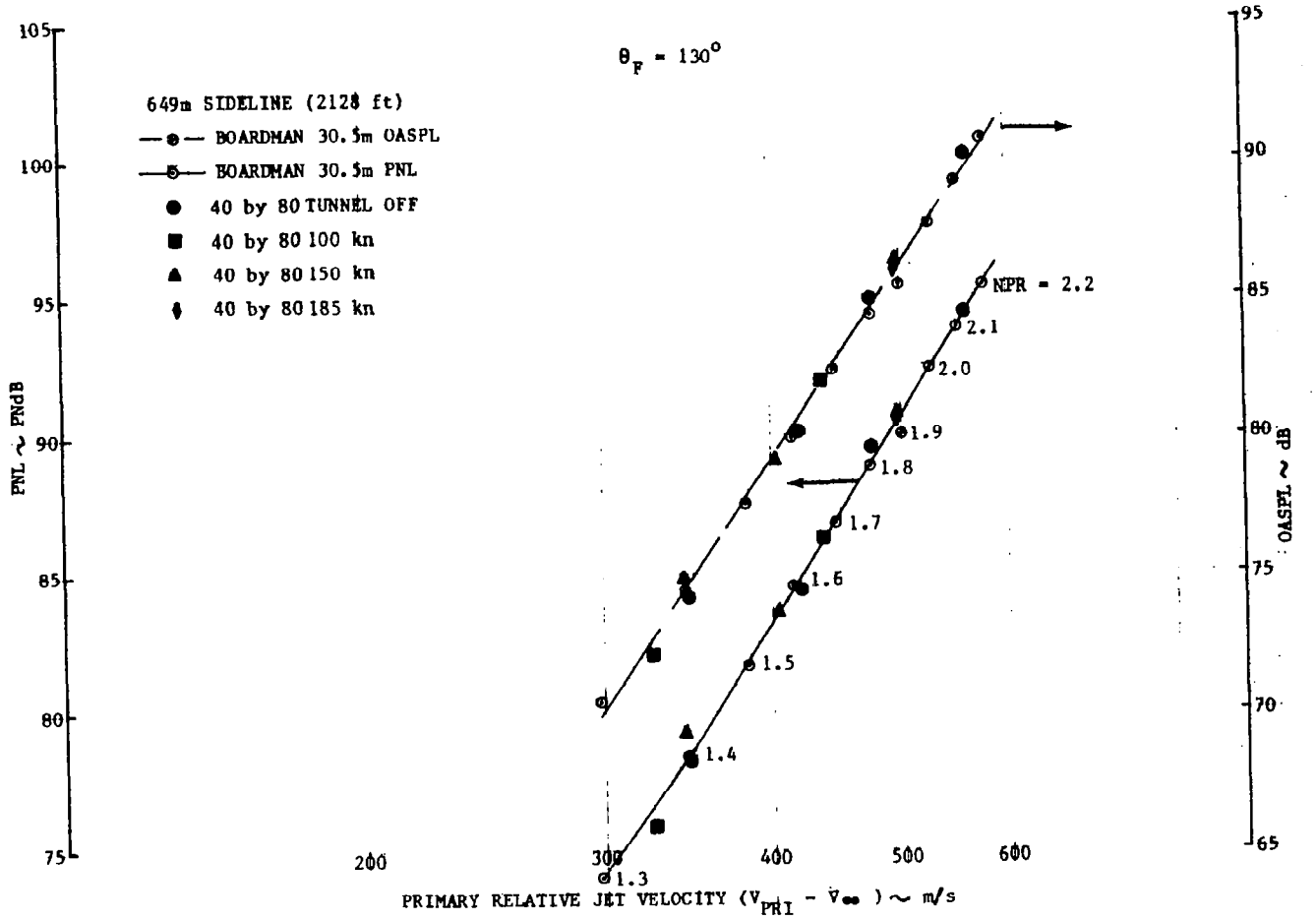

(i) 130°

Figure 51.—(Continued)

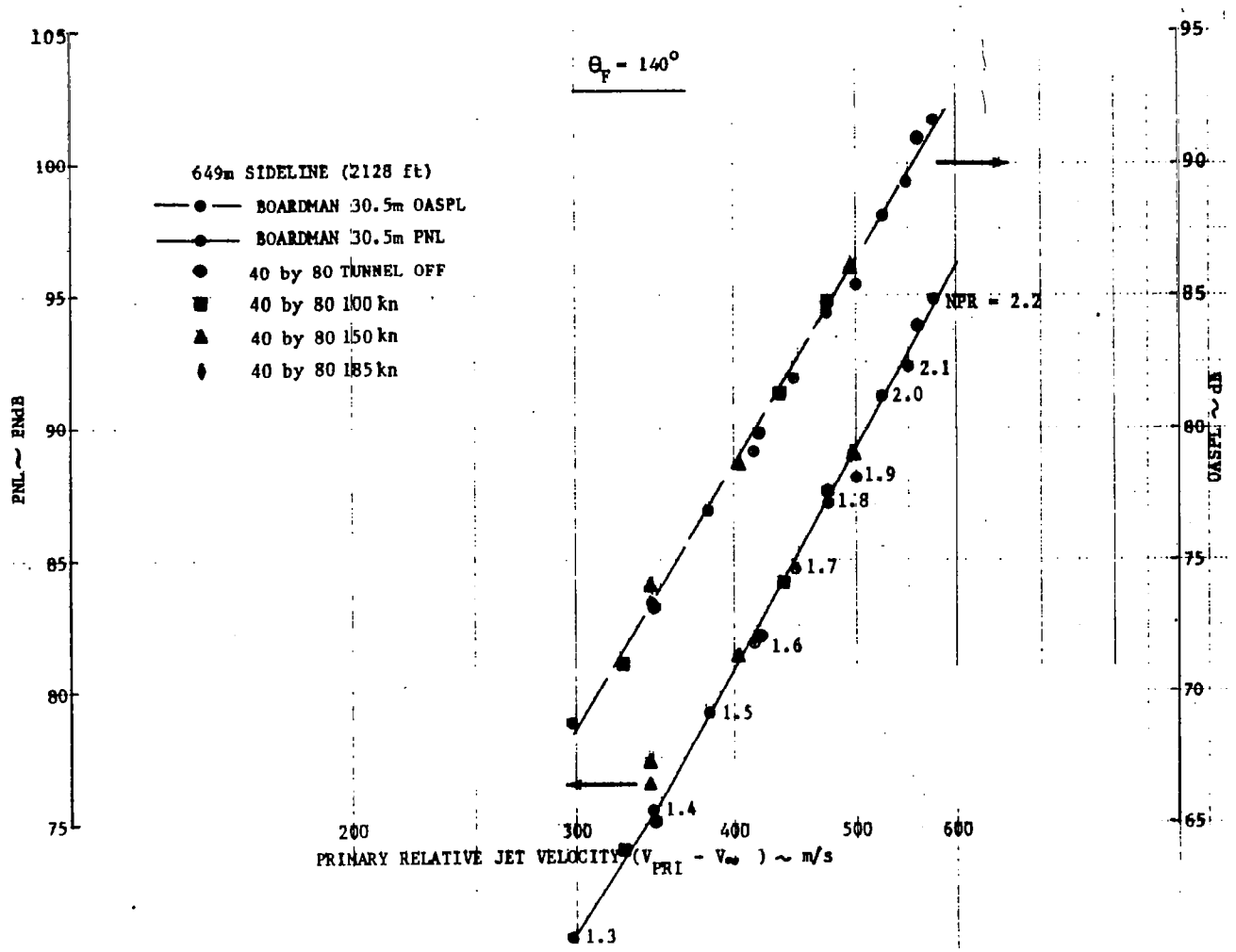

(j) 140°

Figure 51.—(Continued)

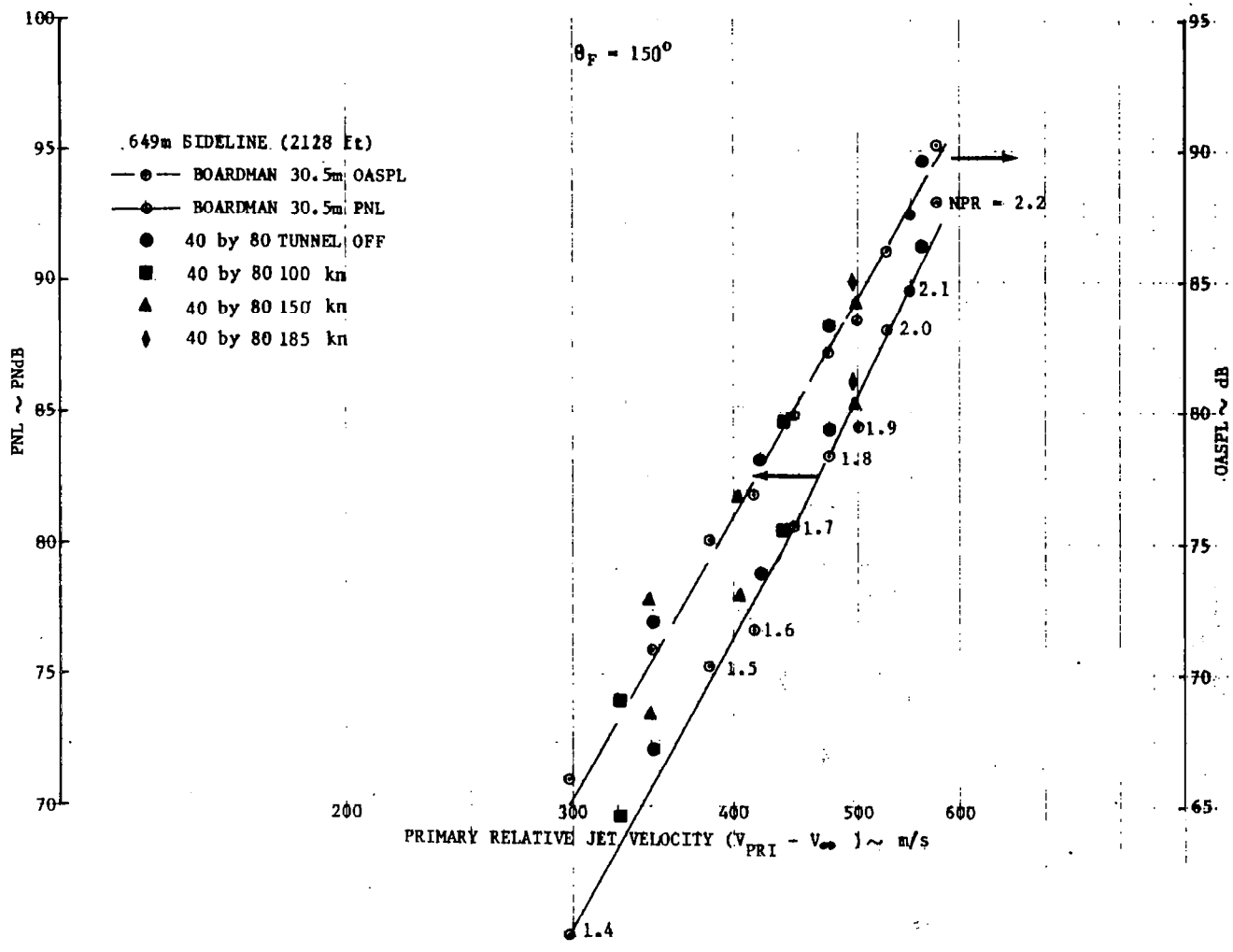

(k) 150°

Figure 51.—(Continued)

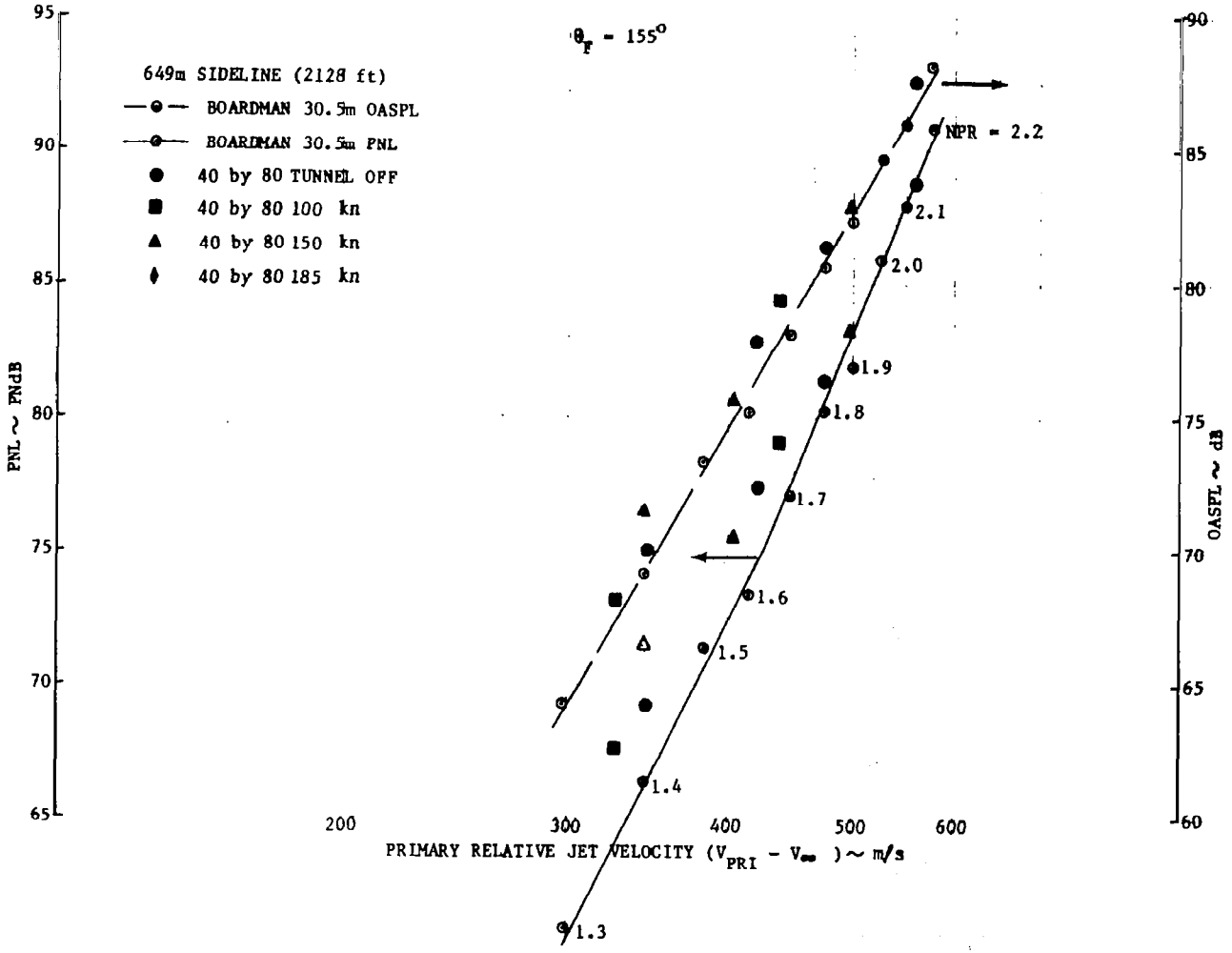

(l) 155°

Figure 51.—(Concluded)

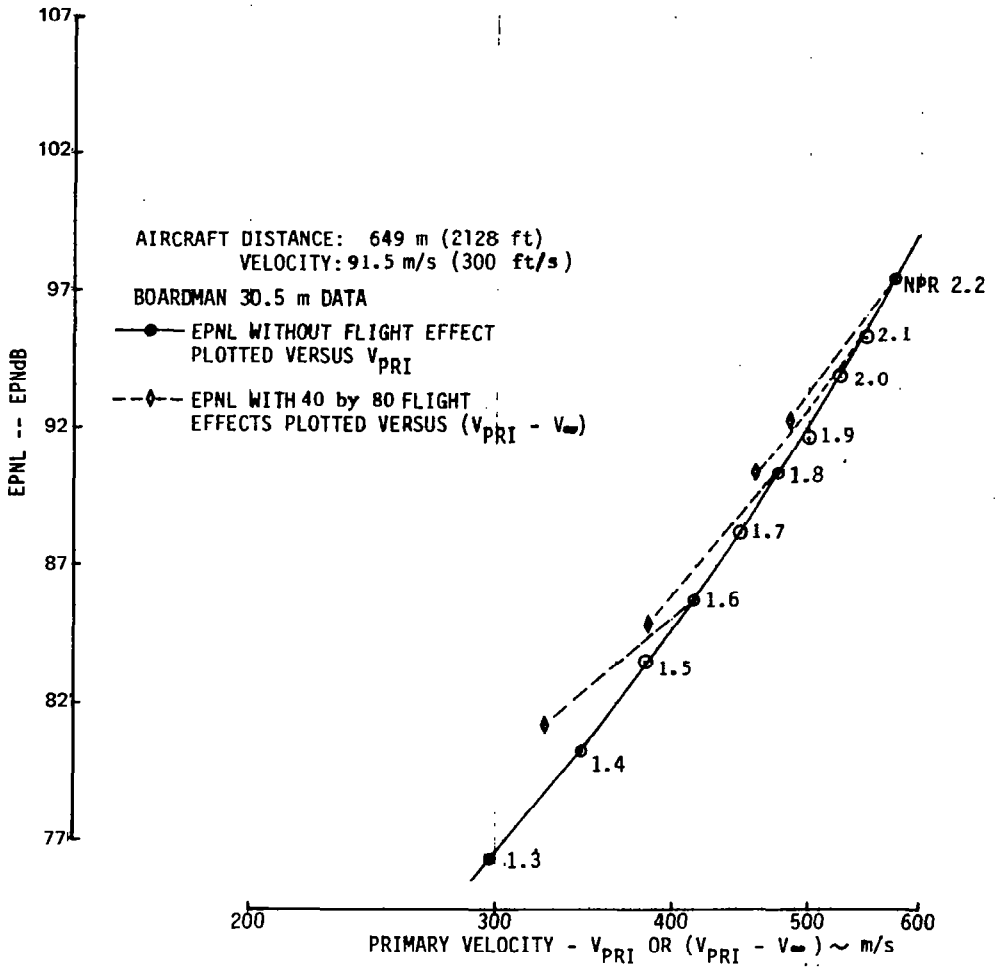

Figure 52.—Static and Estimated Flight EPNL Characteristics, Inverter Configuration

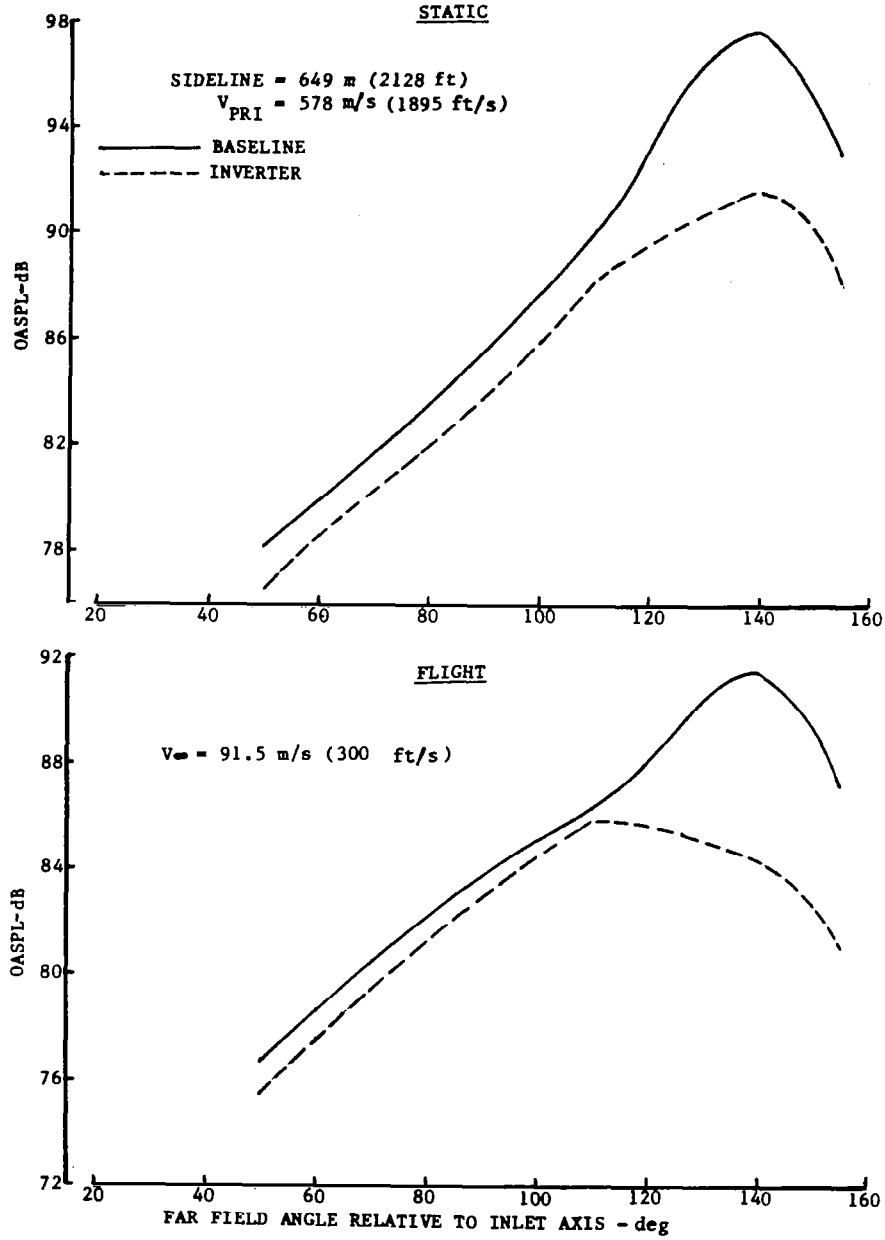

Figure 53.—Comparison of Static and Flight OASPL Directivity for Baseline and Inverter

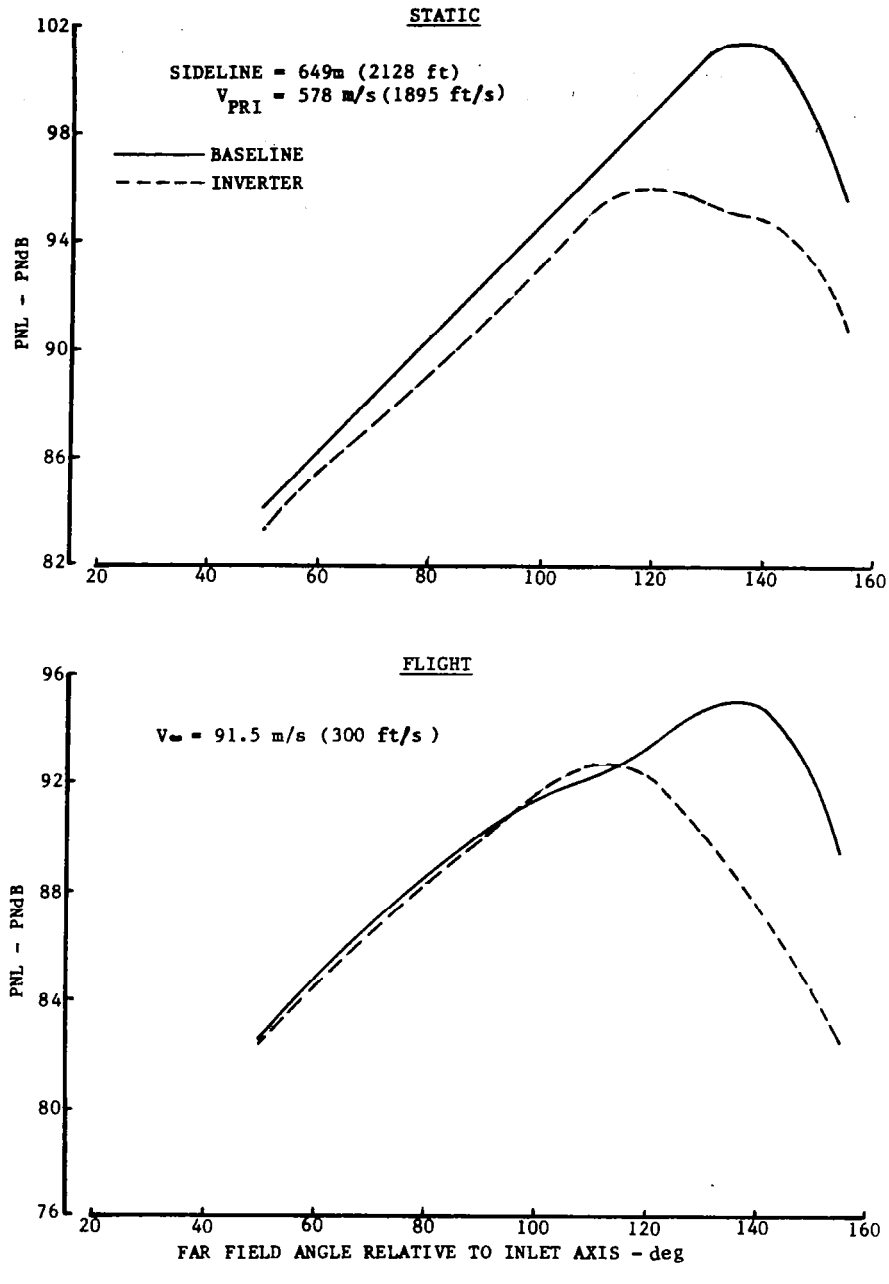

Figure 54.—Comparison of Static and Flight PNL Directivity for Baseline and Inverter

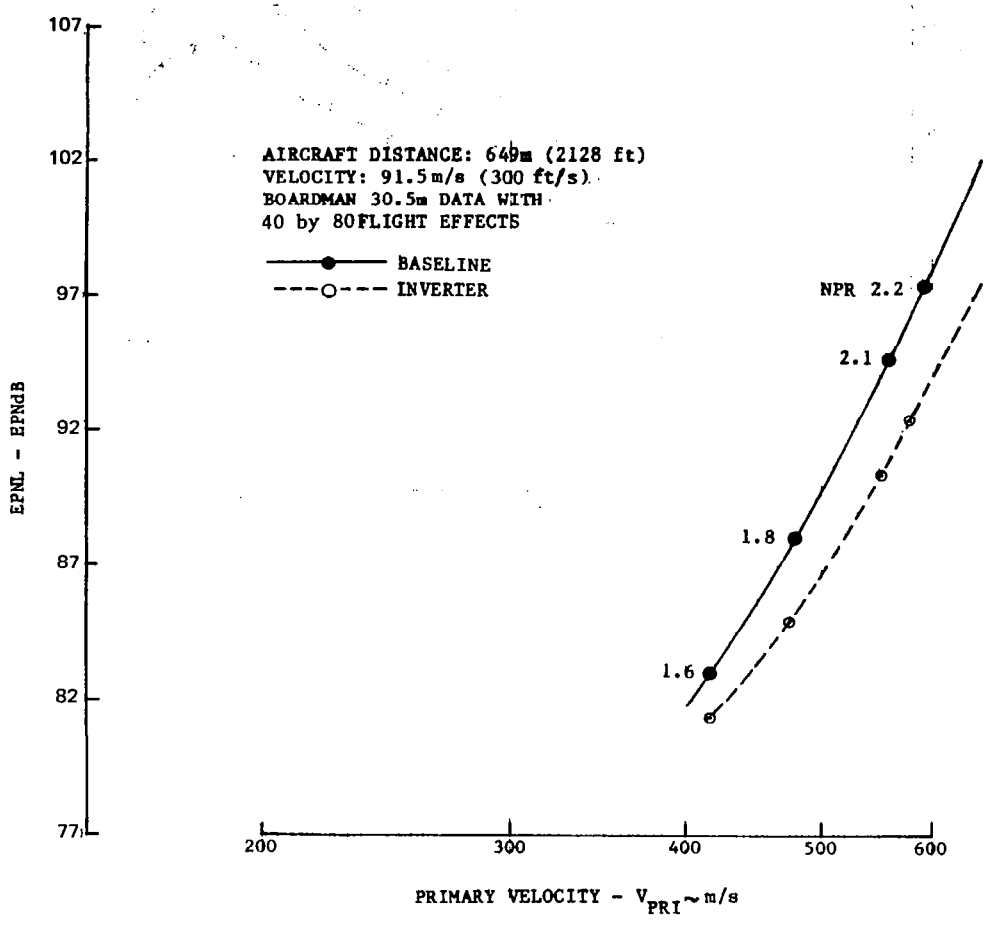

Figure 55.—Comparison of Baseline and Inverter EPNL, Flight Levels

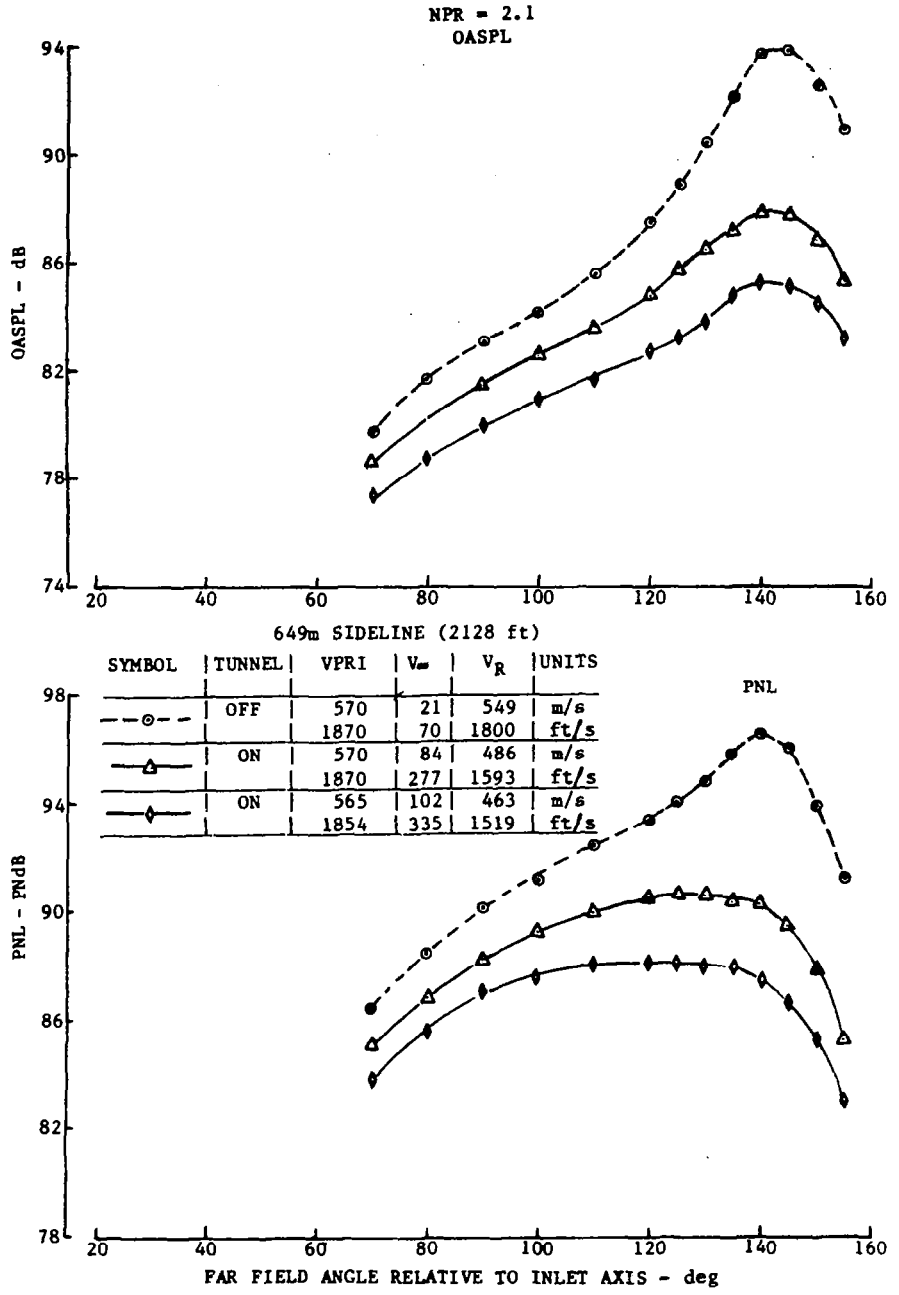

(a) NPR = 2.1

Figure 56.–Comparison of Tunnel-Off and -On OASPL and PNL Directivities, Internal Mixer Configuration

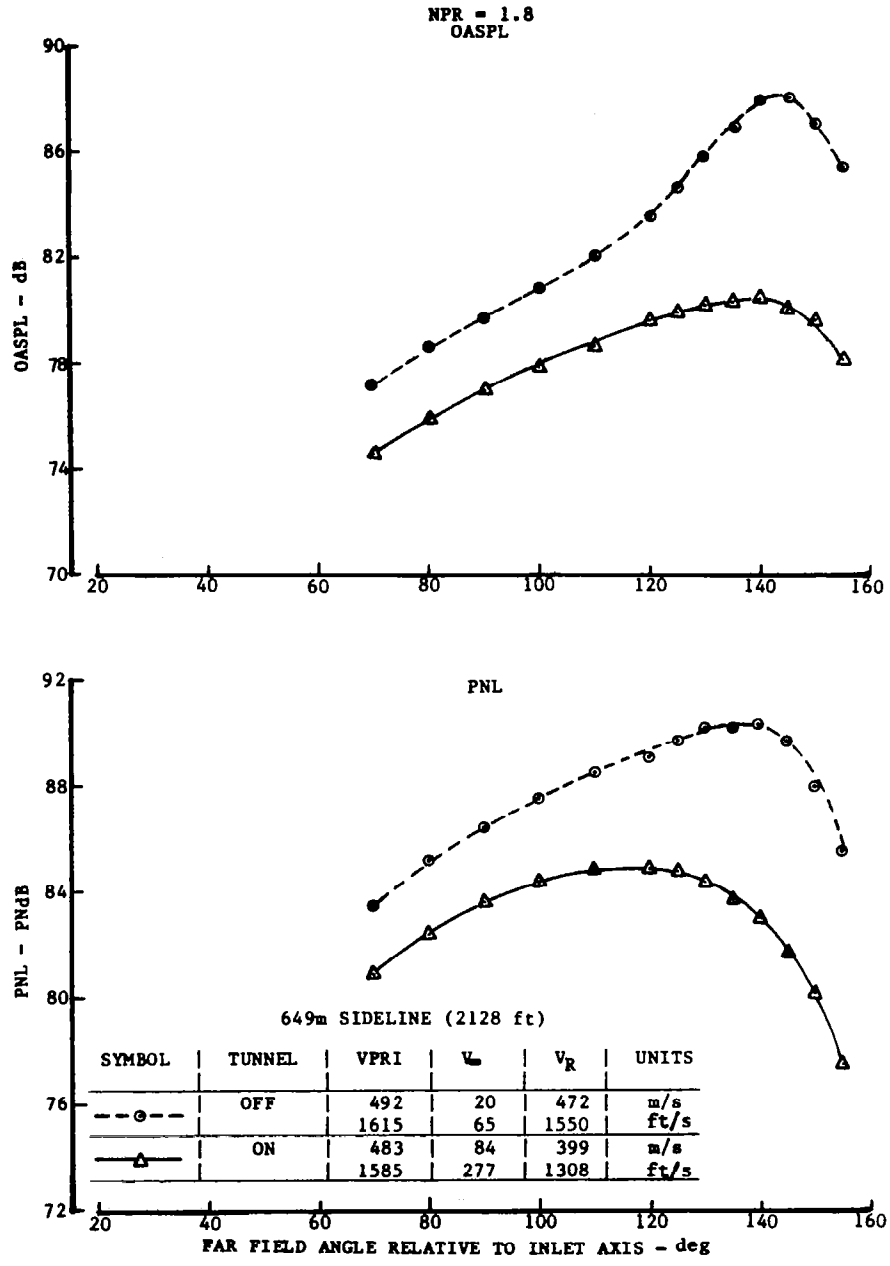

(b) NPR = 1.8

Figure 56.—(Concluded)

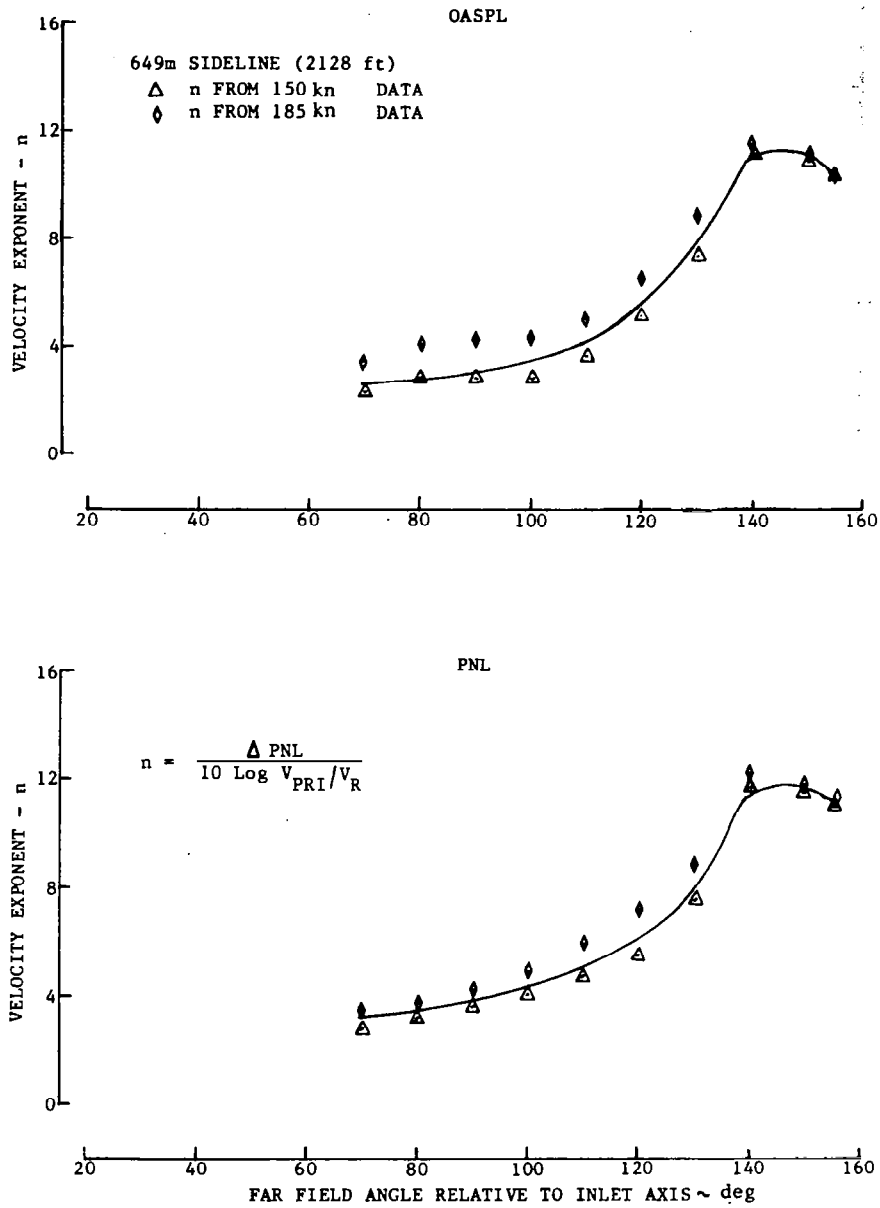

(a) NPR = 2.1

Figure 57.—Velocity Exponents for OASPL and PNL, Internal Mixer Configuration

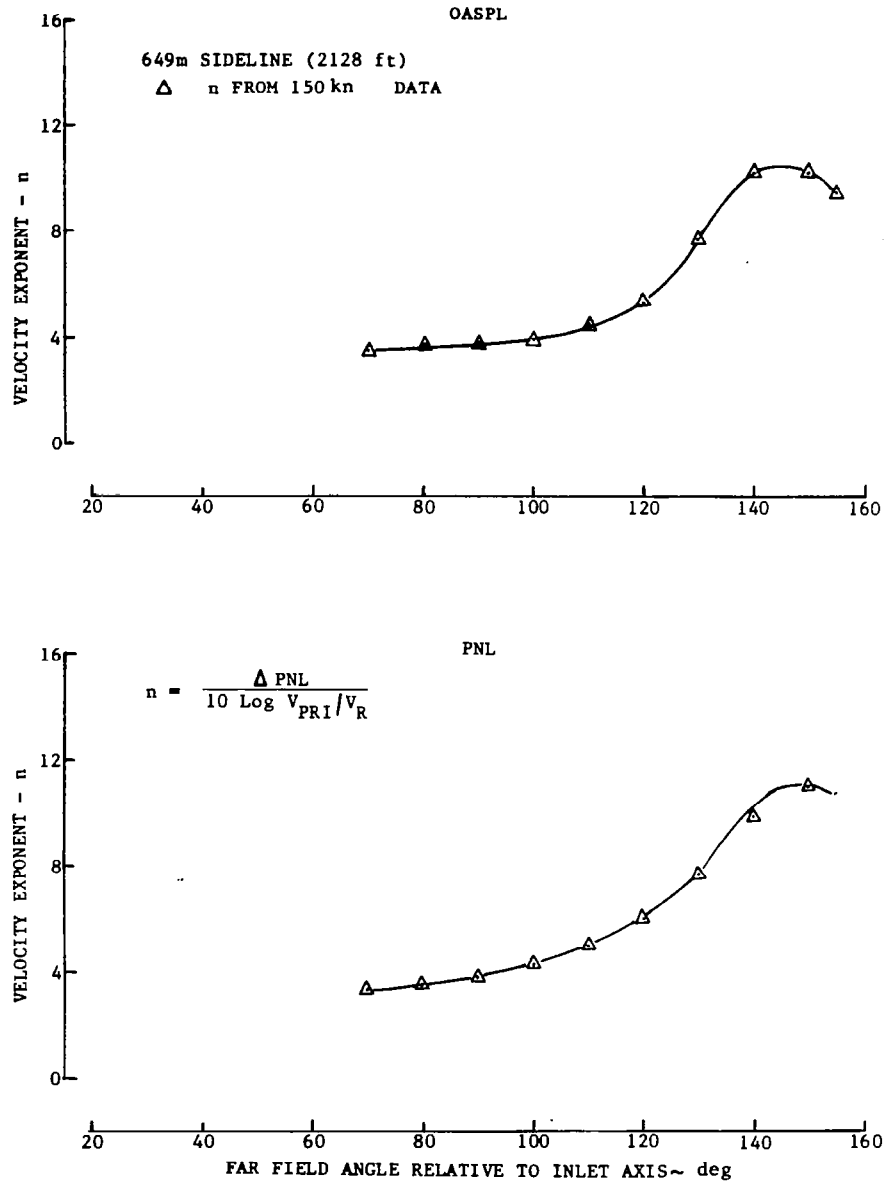

(b) NPR = 1.8

Figure 57.—(Concluded)

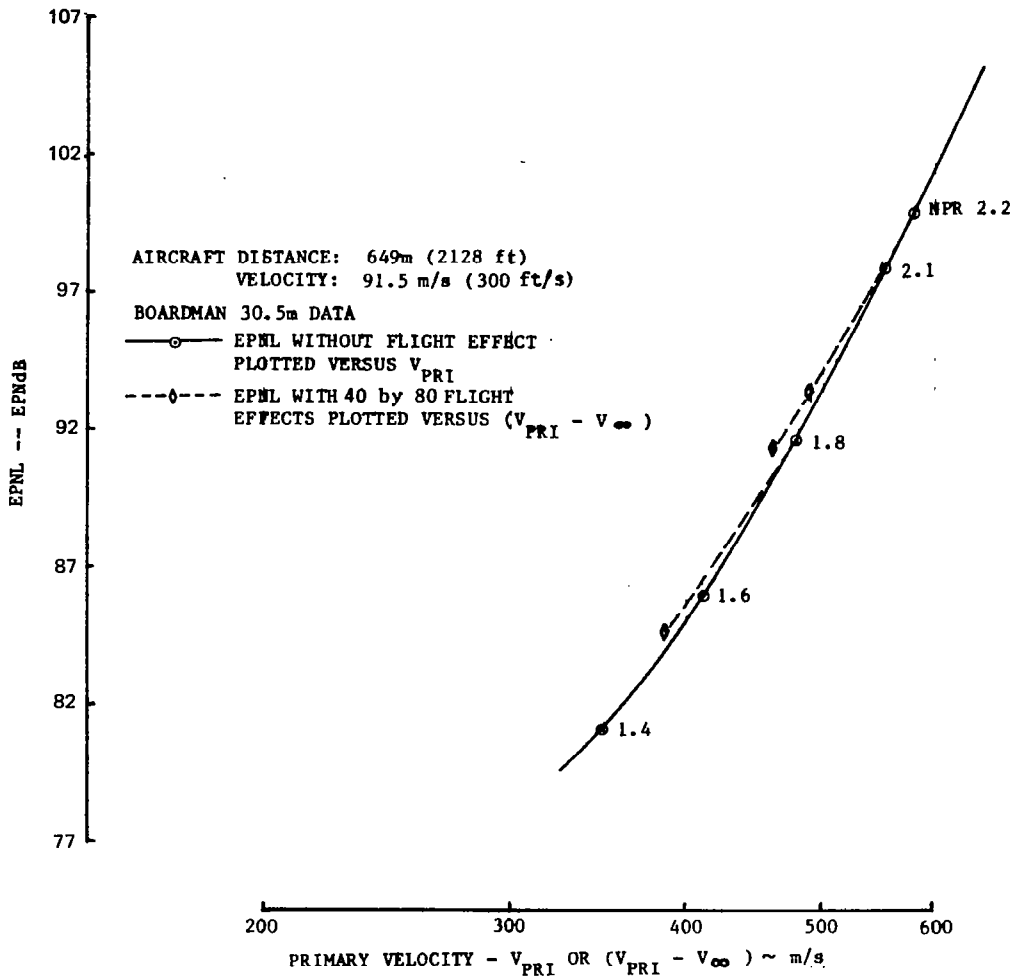

Figure 58. –Static and Estimated Flight EPNL Characteristics, Internal Mixer Configuration

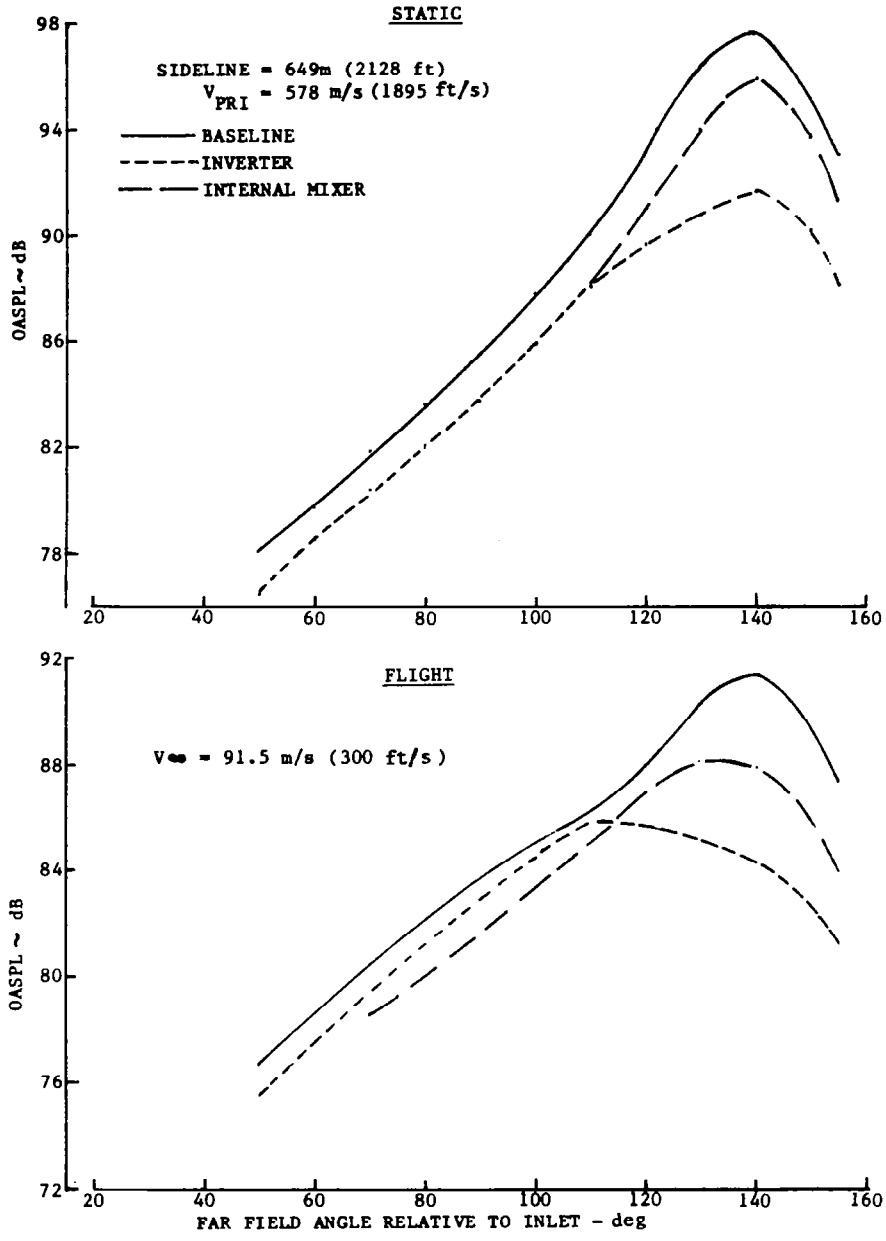

Figure 59.—Comparison of Static and Flight OASPL Directivity for Baseline, Inverter, and Internal Mixer

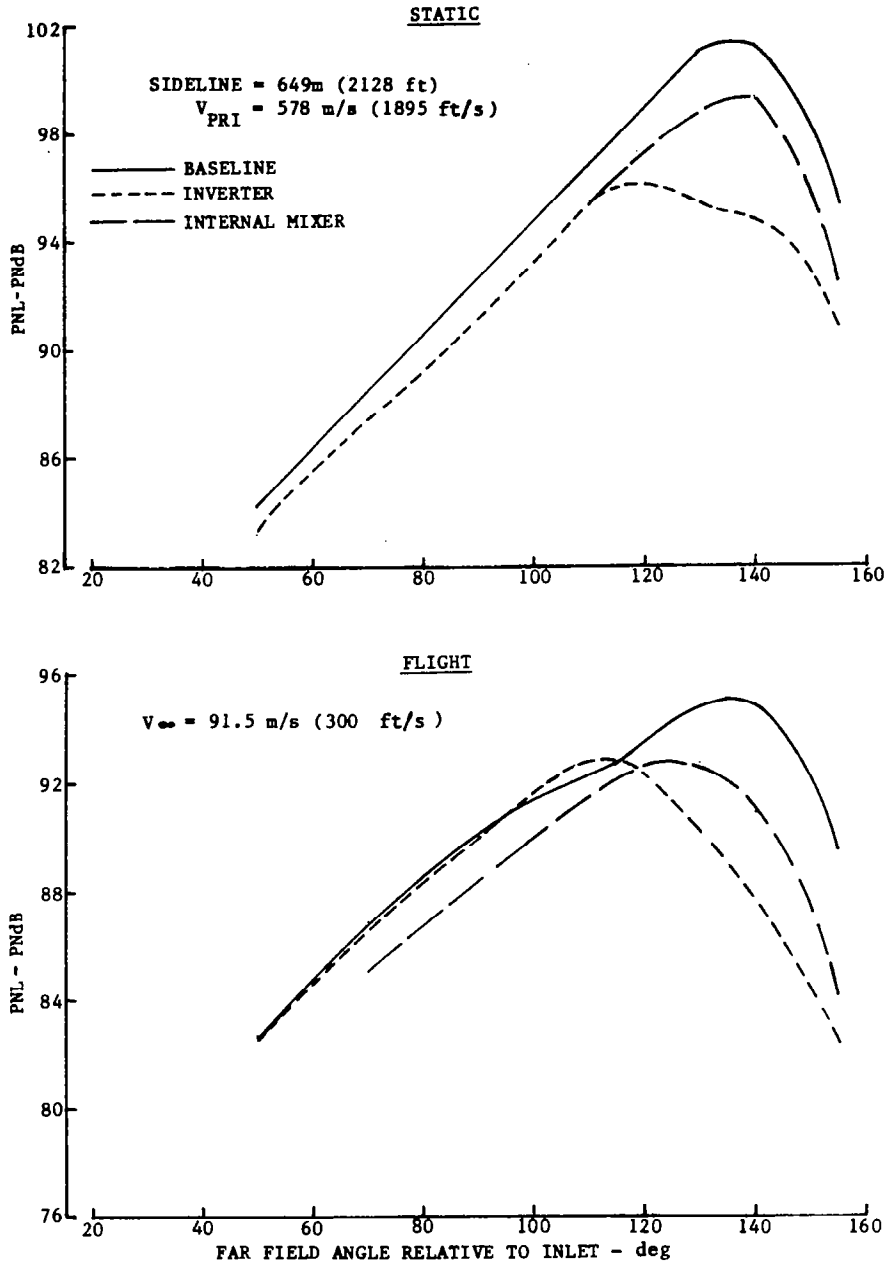

Figure 60.—Comparison of Static and Flight PNL Directivity for Baseline, Inverter, and Internal Mixer

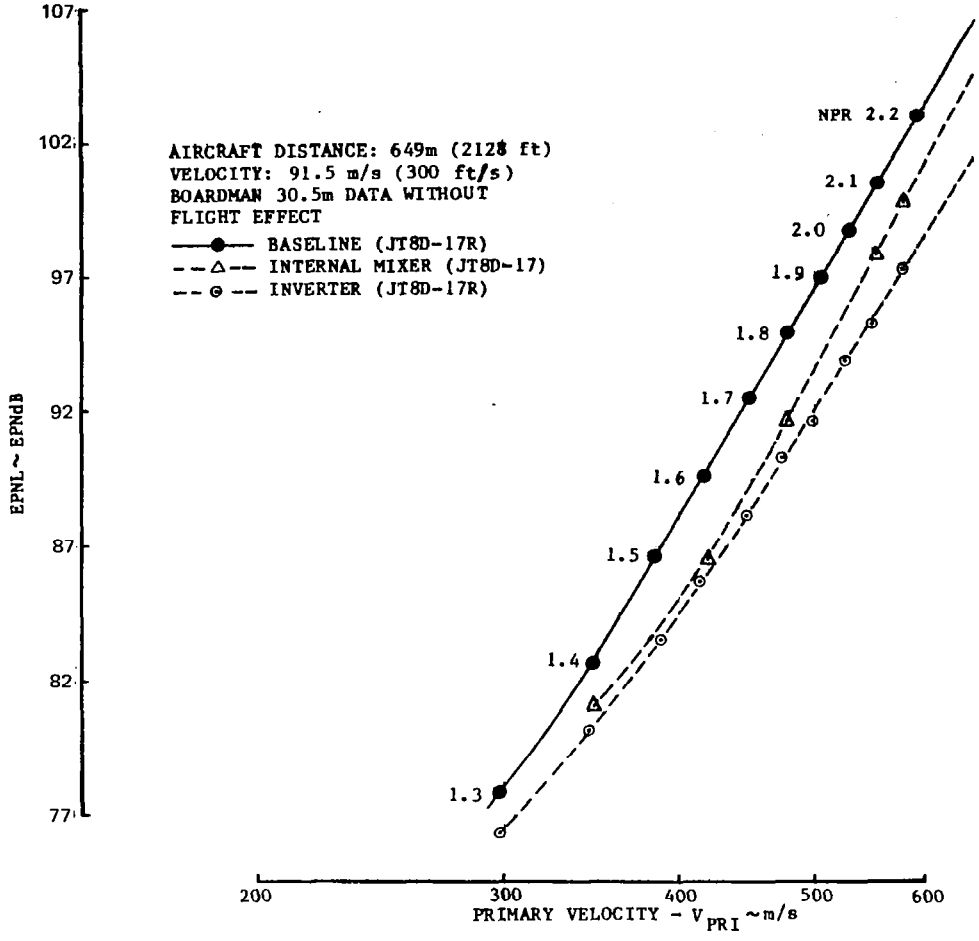

Figure 61.—Comparison of Baseline, Inverter and Internal Mixer EPNL, Static Levels

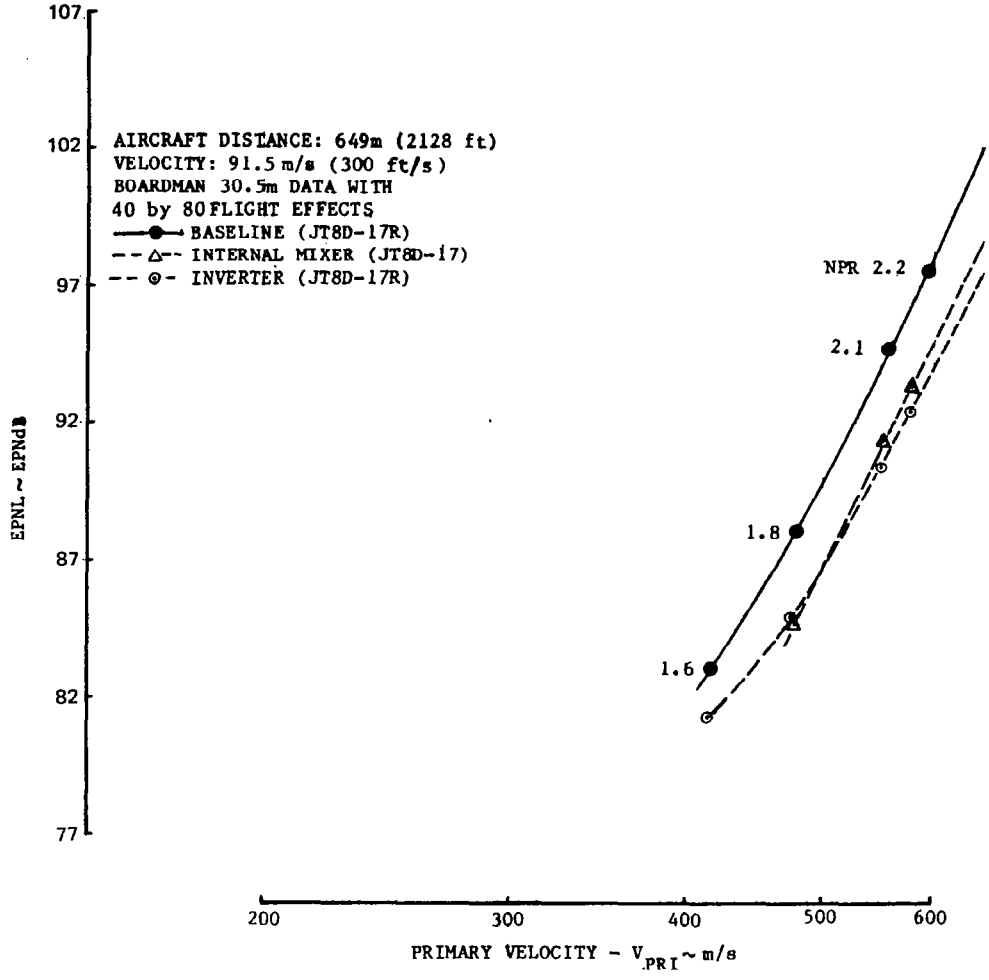

Figure 62.—Comparison of Baseline, Inverter and Internal Mixer EPNL, Flight Levels

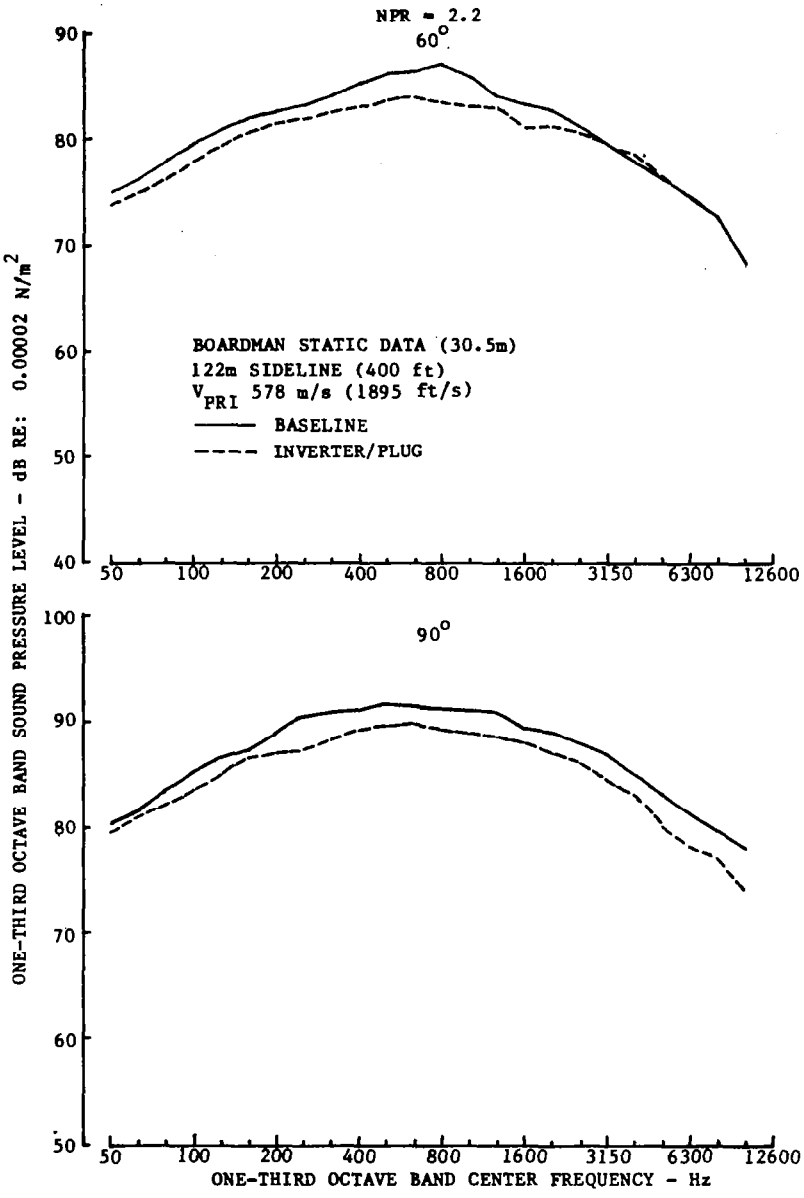

Figure 63.—Comparison of Baseline and Inverter/Plug Spectra

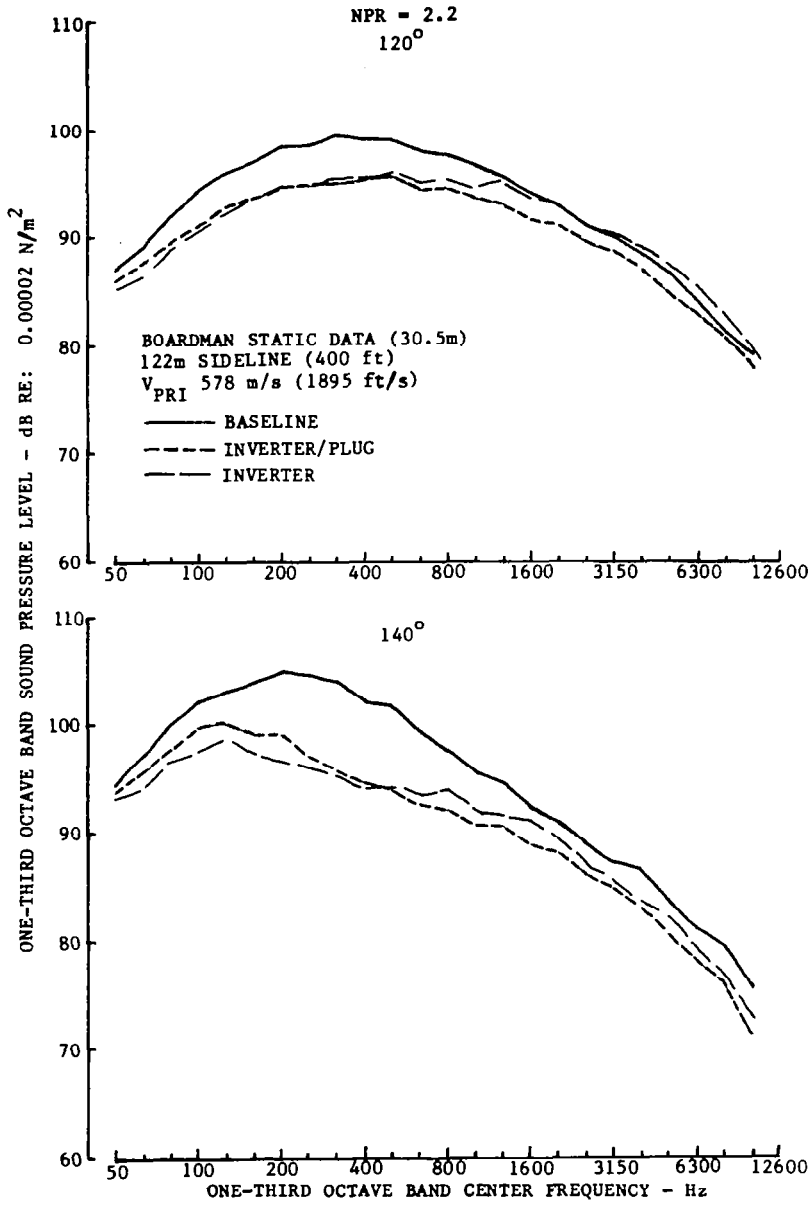

Figure 64.—Comparison of Baseline and Inverter/Plug and Inverter Spectra

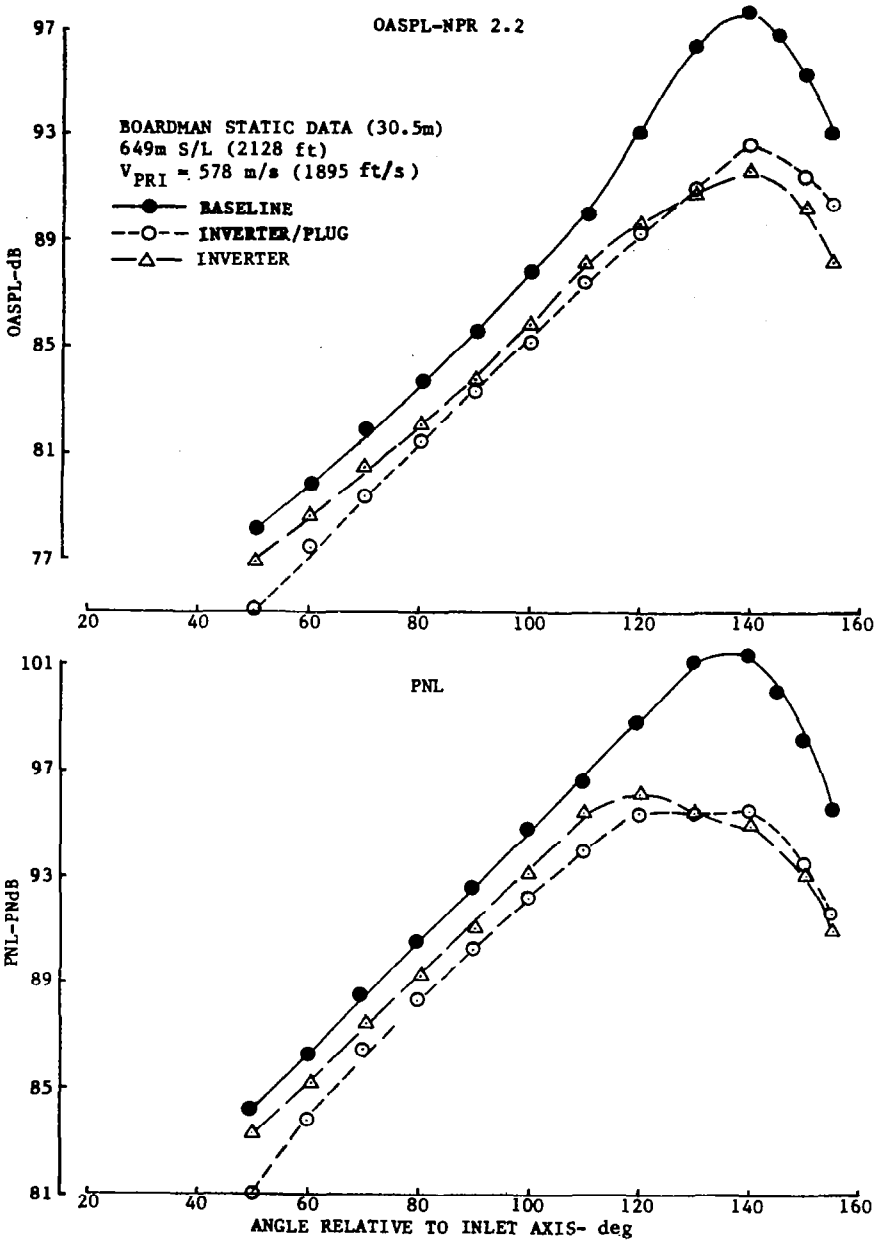

Figure 65.—Comparison of Static OASPL and PNL Directivity, Baseline versus Inverter/Plug and Inverter

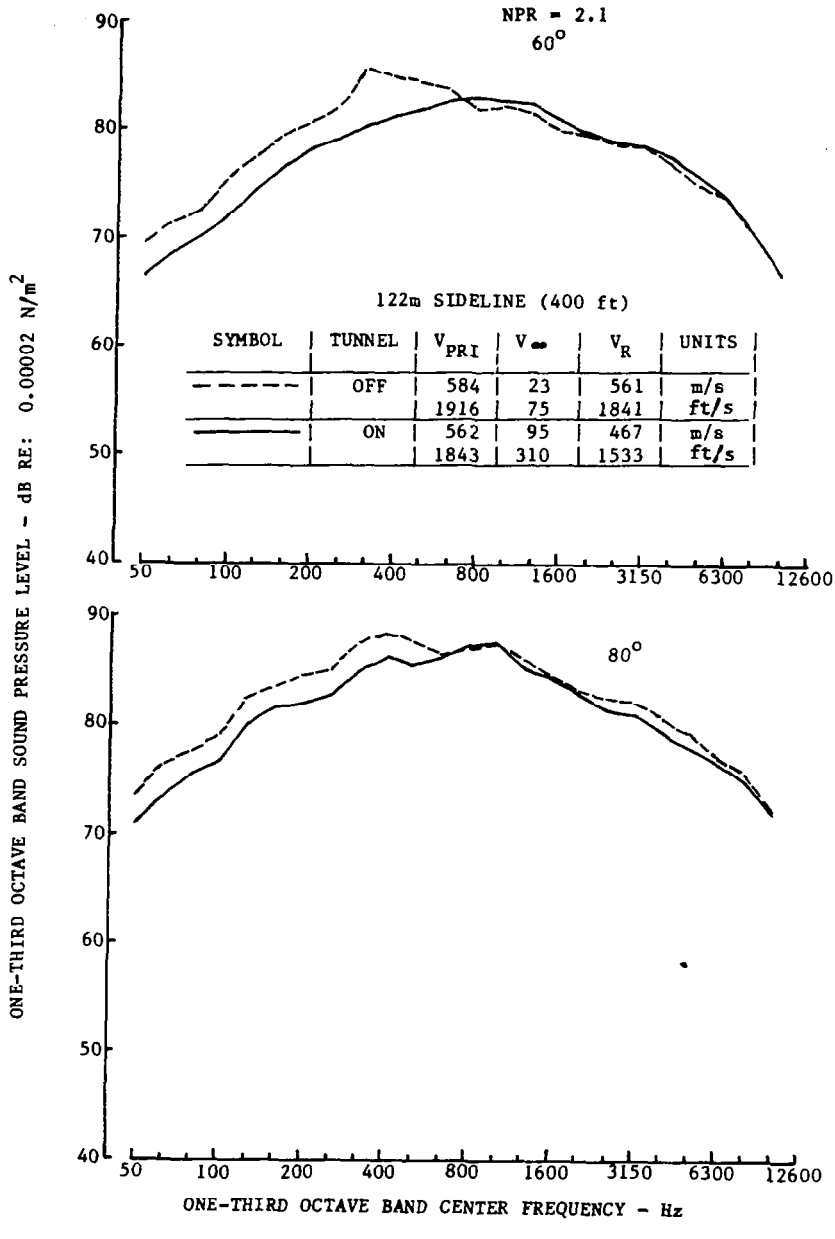

(a) 60° & 80°

Figure 66.—Comparison of Tunnel-Off and -On Spectra, Inverter/Plug Configuration

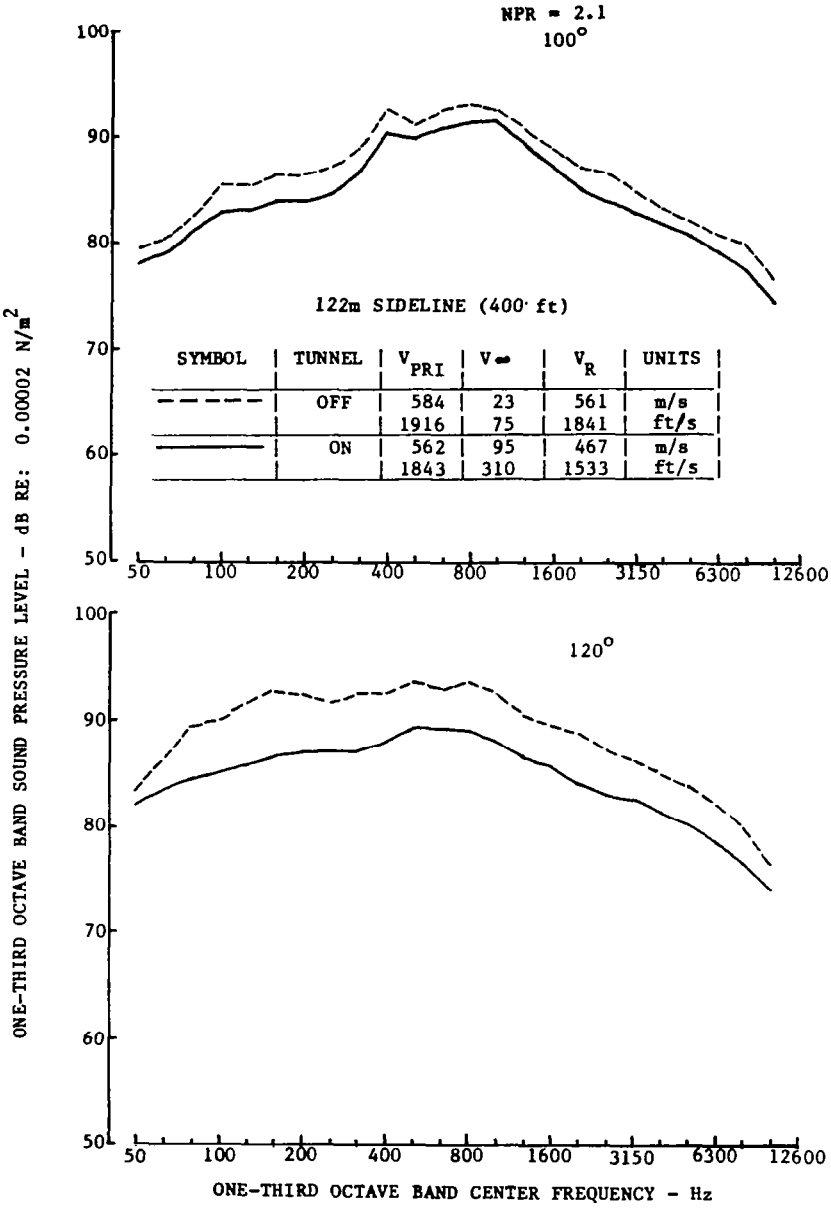

(b) 100° & 120°

Figure 66.—(Continued)

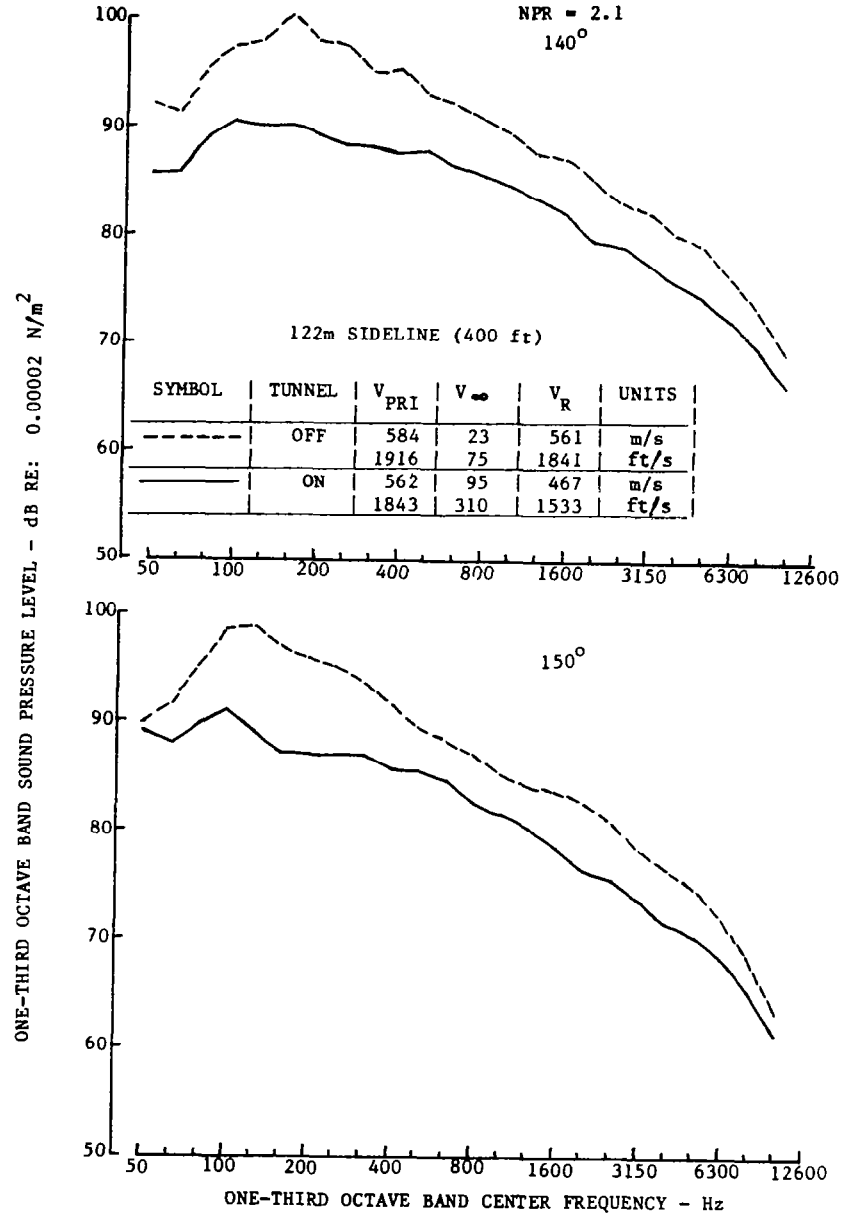

(c) 140° & 150°

Figure 66.—(Concluded)

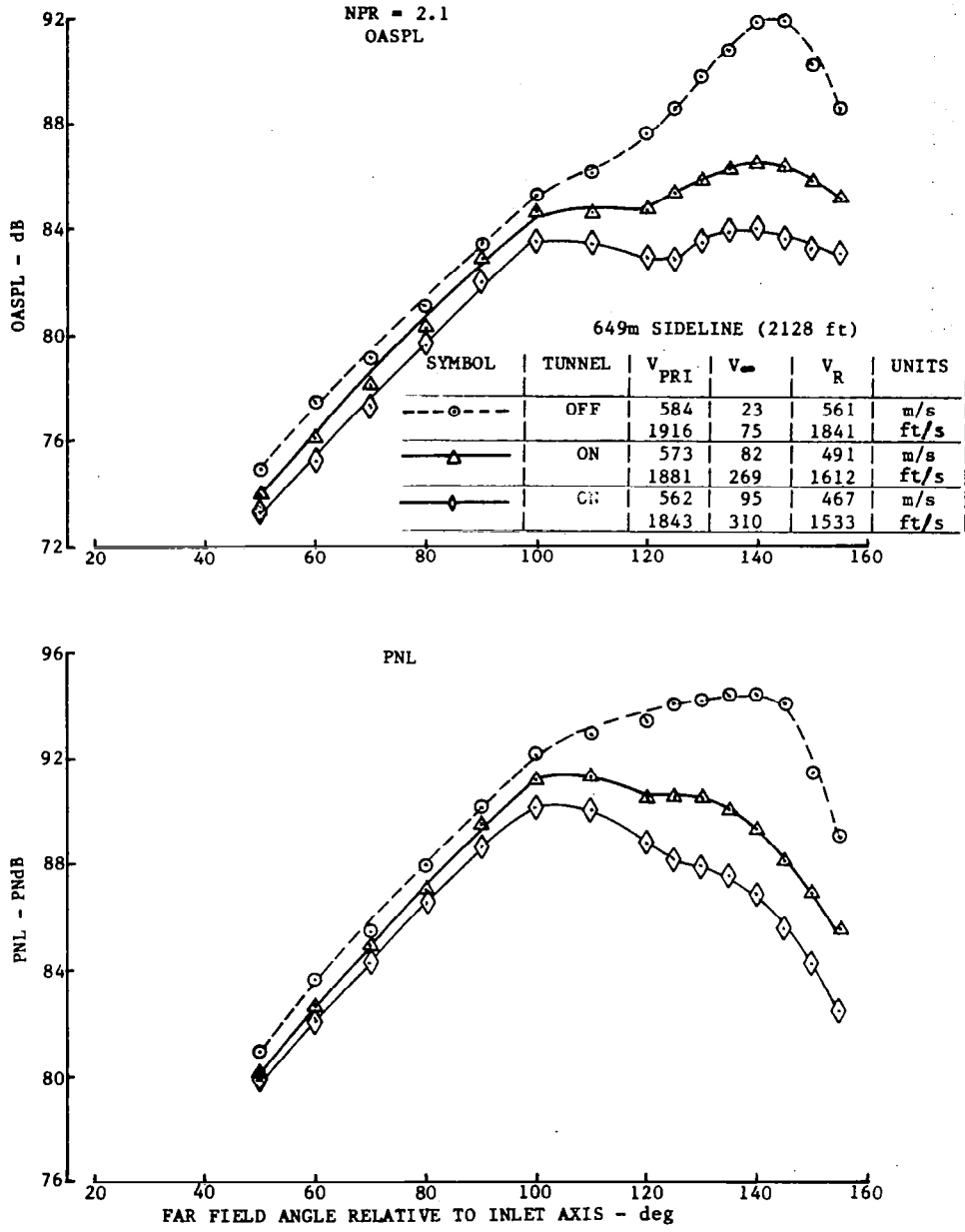

(a) NPR = 2.1

Figure 67.—Comparison of Tunnel-Off and -On OASPL and PNL Directivities, Inverter/Plug Configuration

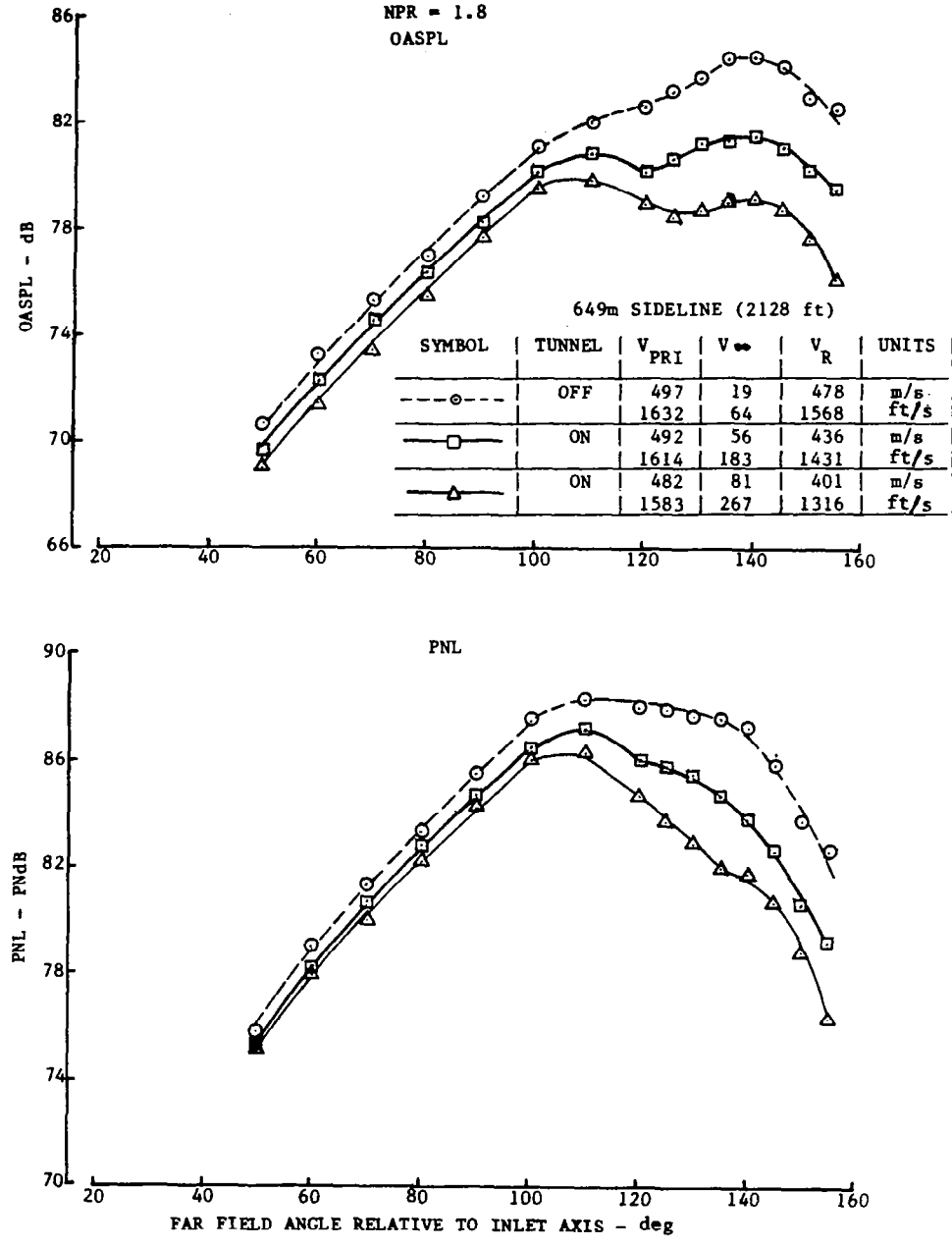

(b) NPR = 1.8

Figure 67.—(Concluded)

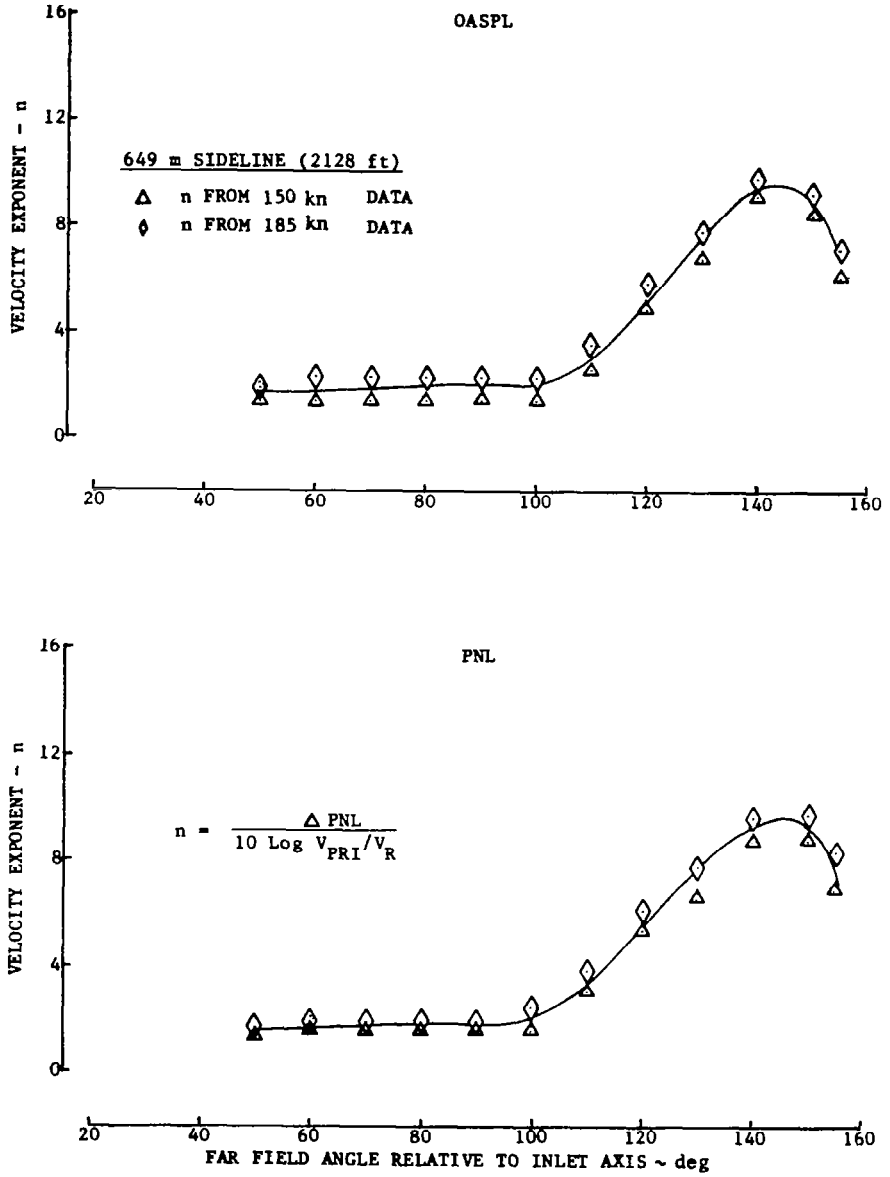

(a) NPR = 2.1

Figure 68.—Velocity Exponents for OASPL and PNL, Inverter/Plug Configuration

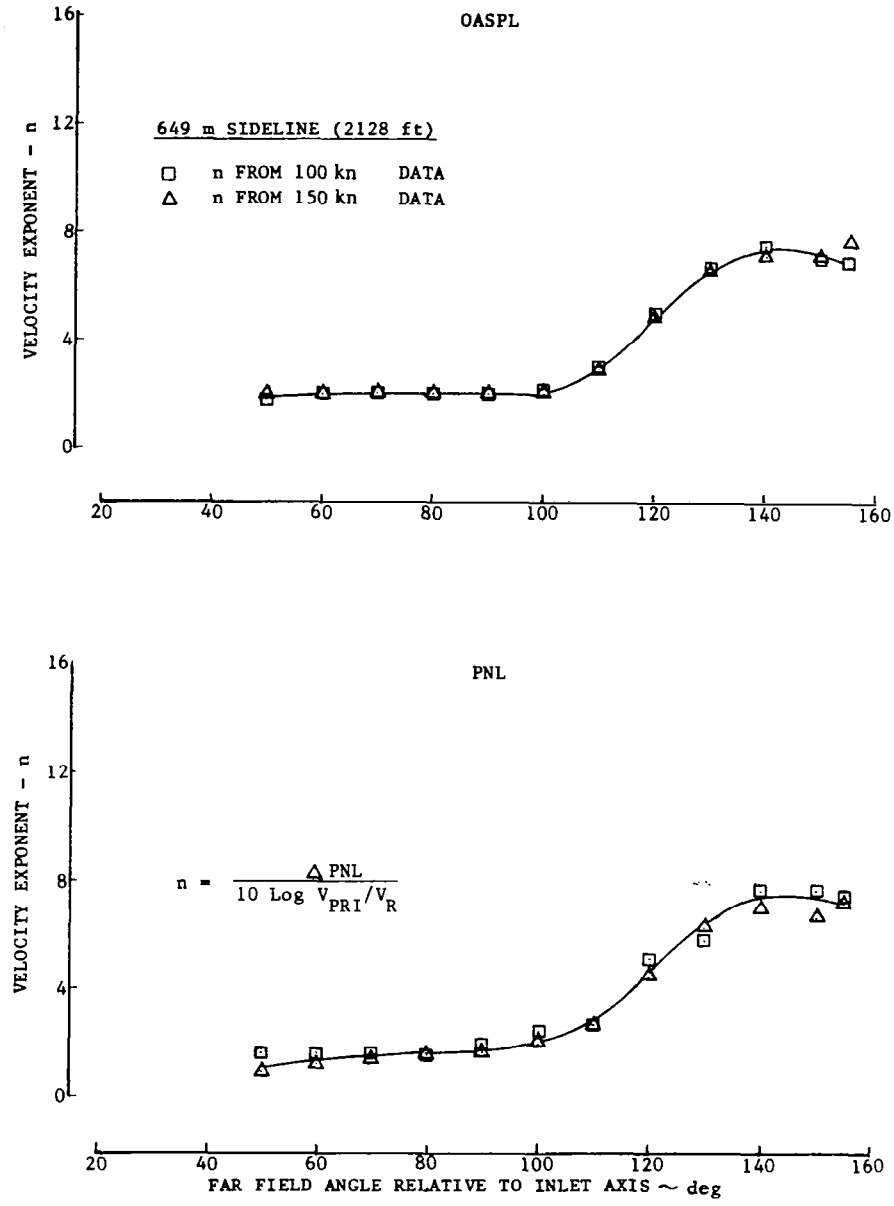

(b) NPR = 1.8

Figure 68.—(Concluded)

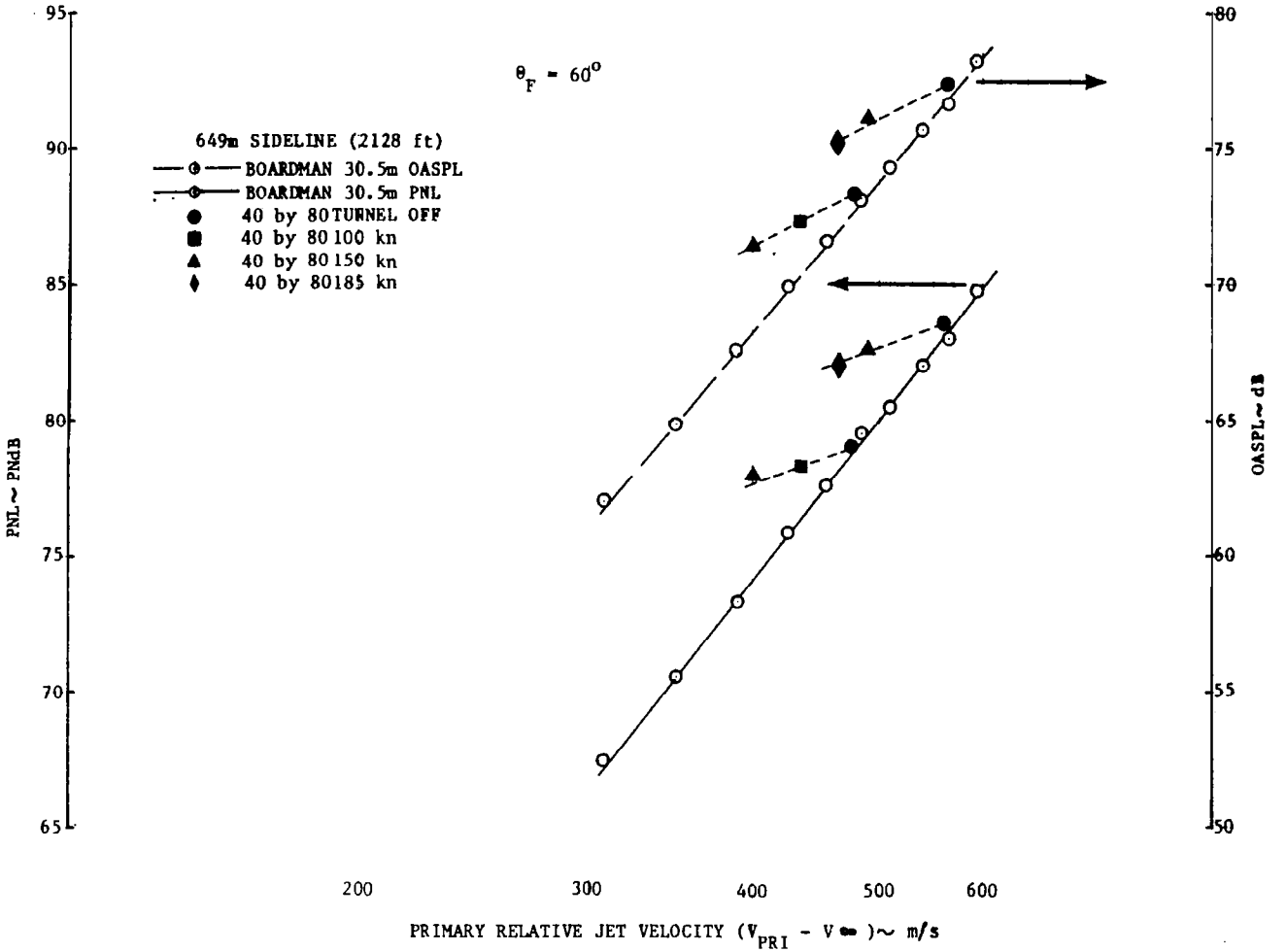

(a) 60°

Figure 69.—Tunnel-Off and -On OASPL and PNL versus Primary Velocity, Inverter/Plug Configuration

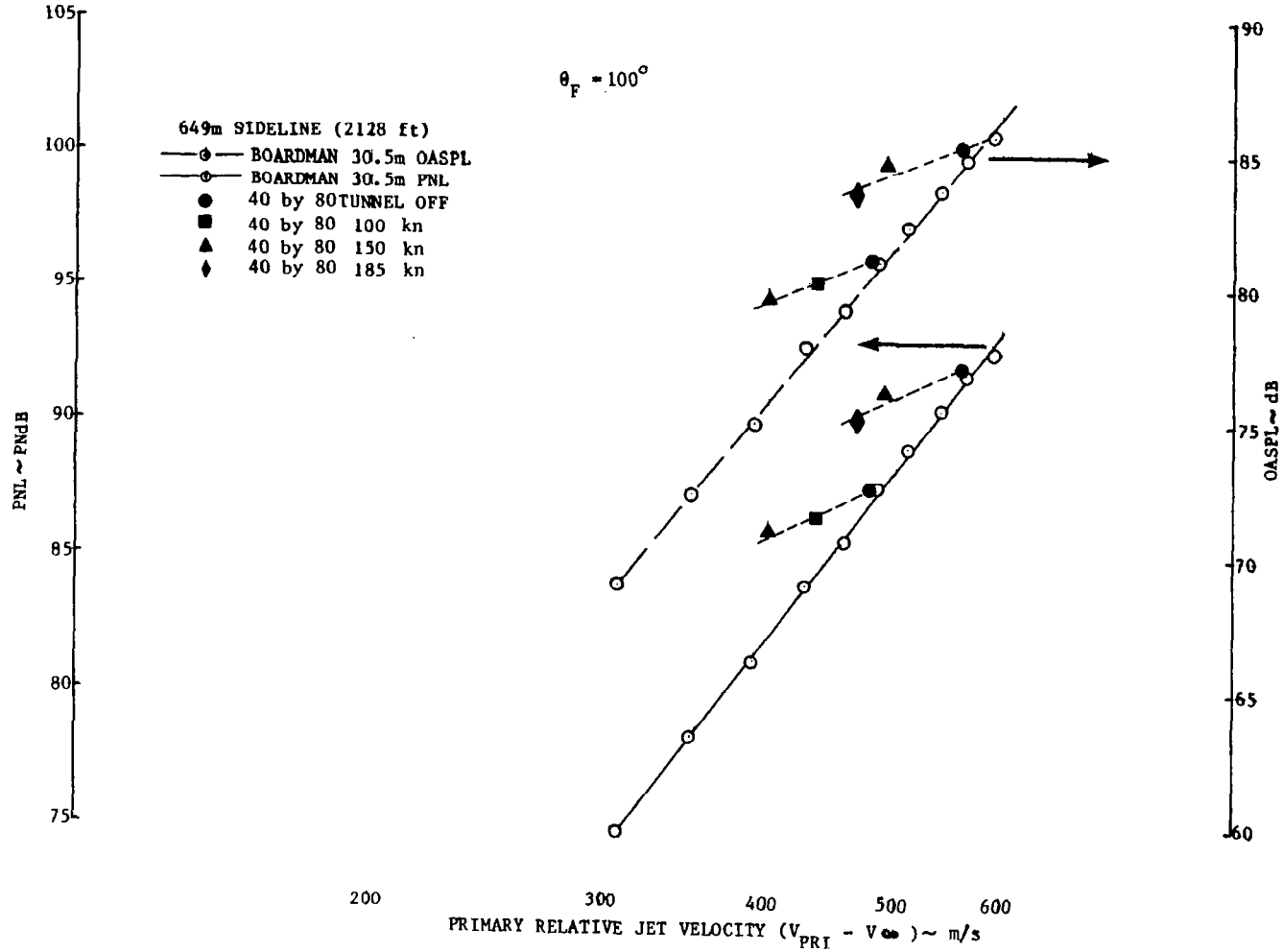

(b) 100°

Figure 69.—(Continued)

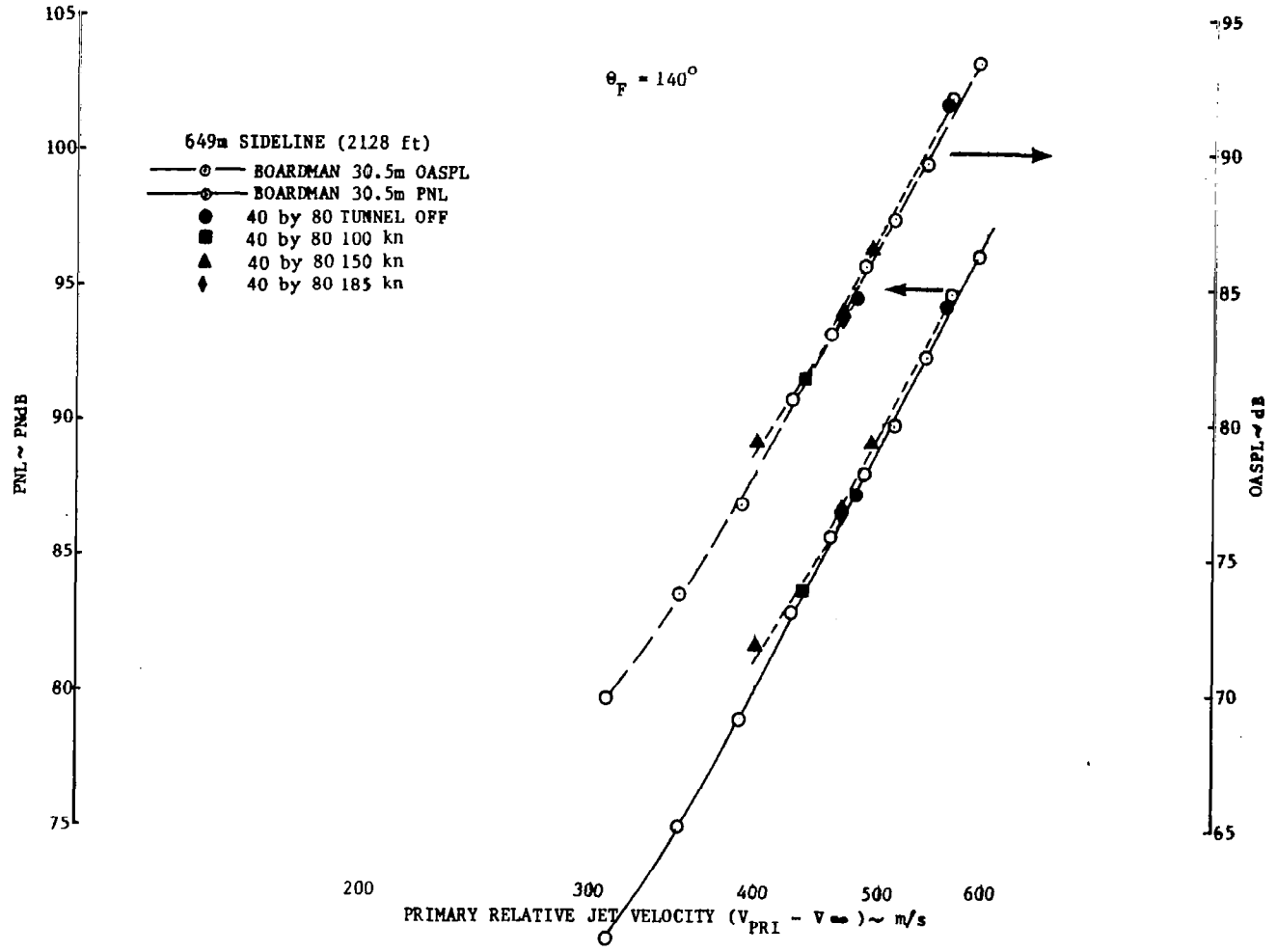

(c) 140°

Figure 69.—(Concluded)

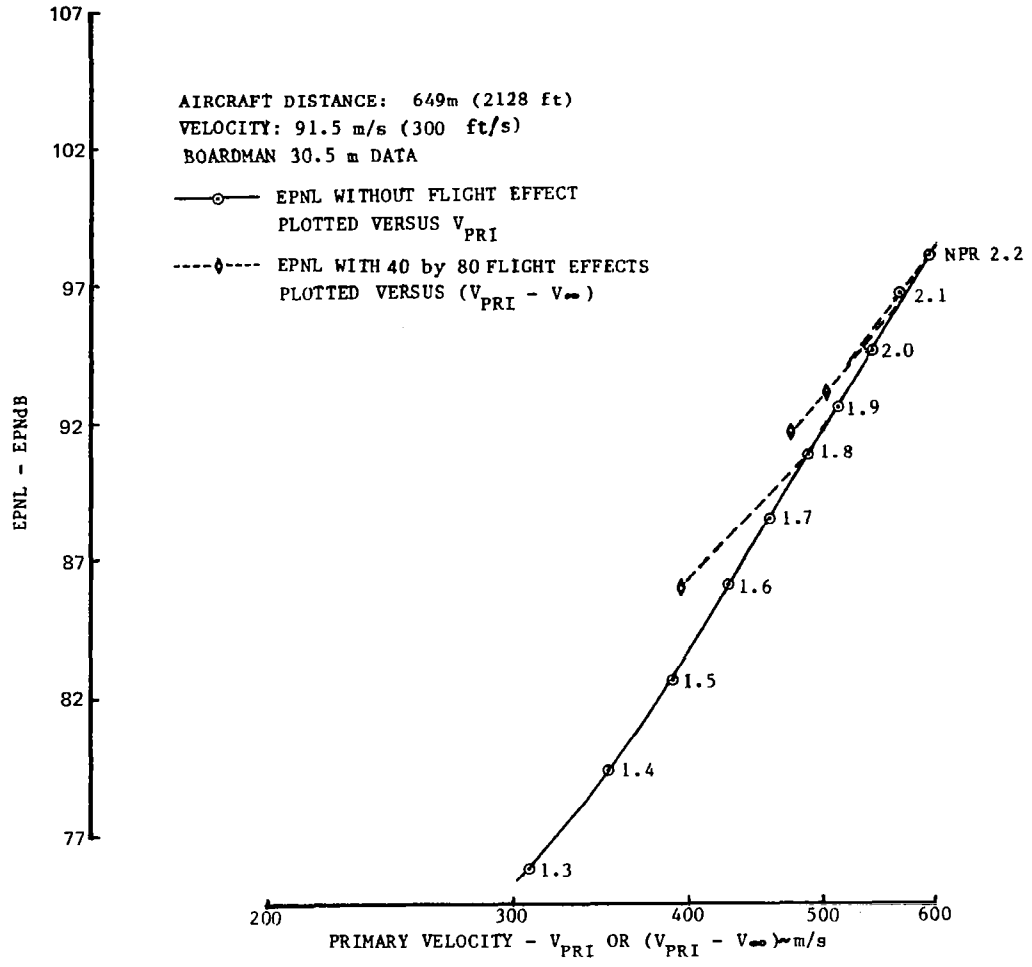

Figure 70.—Static and Estimated Flight EPNL Characteristics, Inverter/Plug Configuration

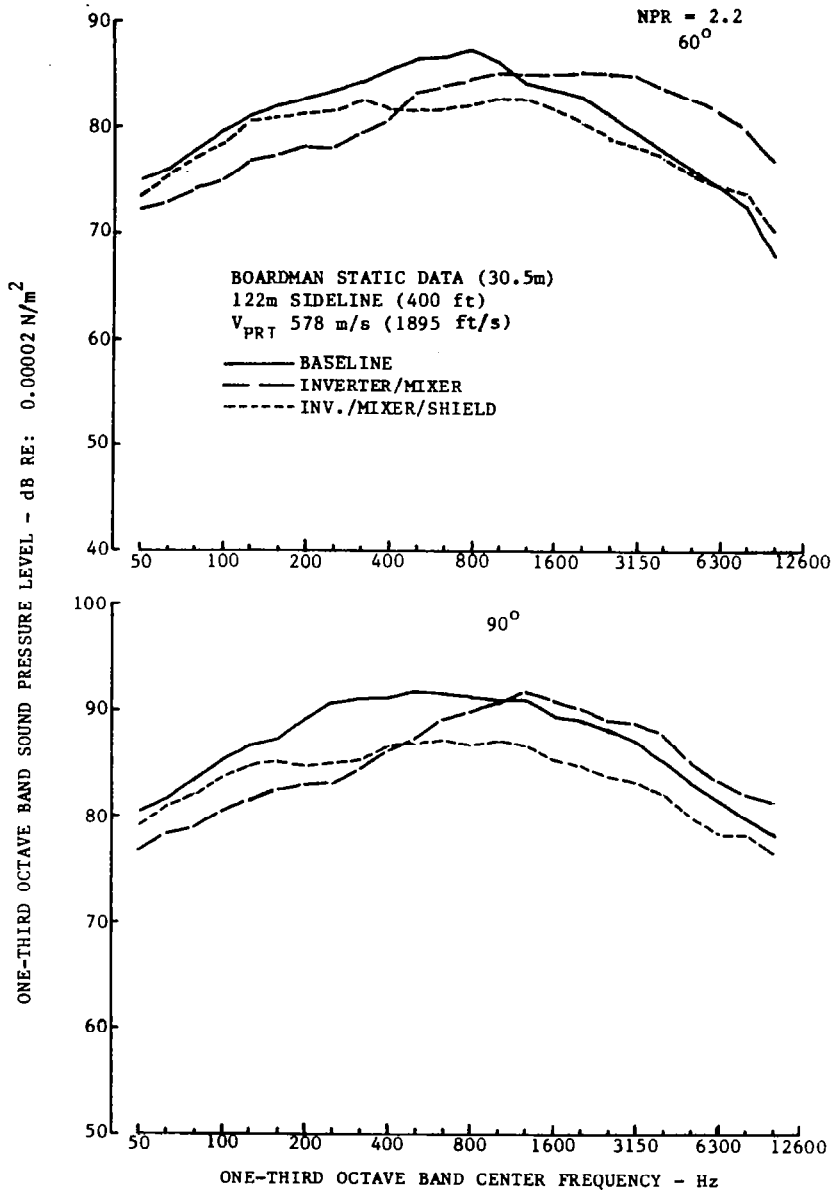

(a) 60° & 90°

Figure 71.—Comparison of Baseline; Inverter/Mixer with and without Shield Spectra

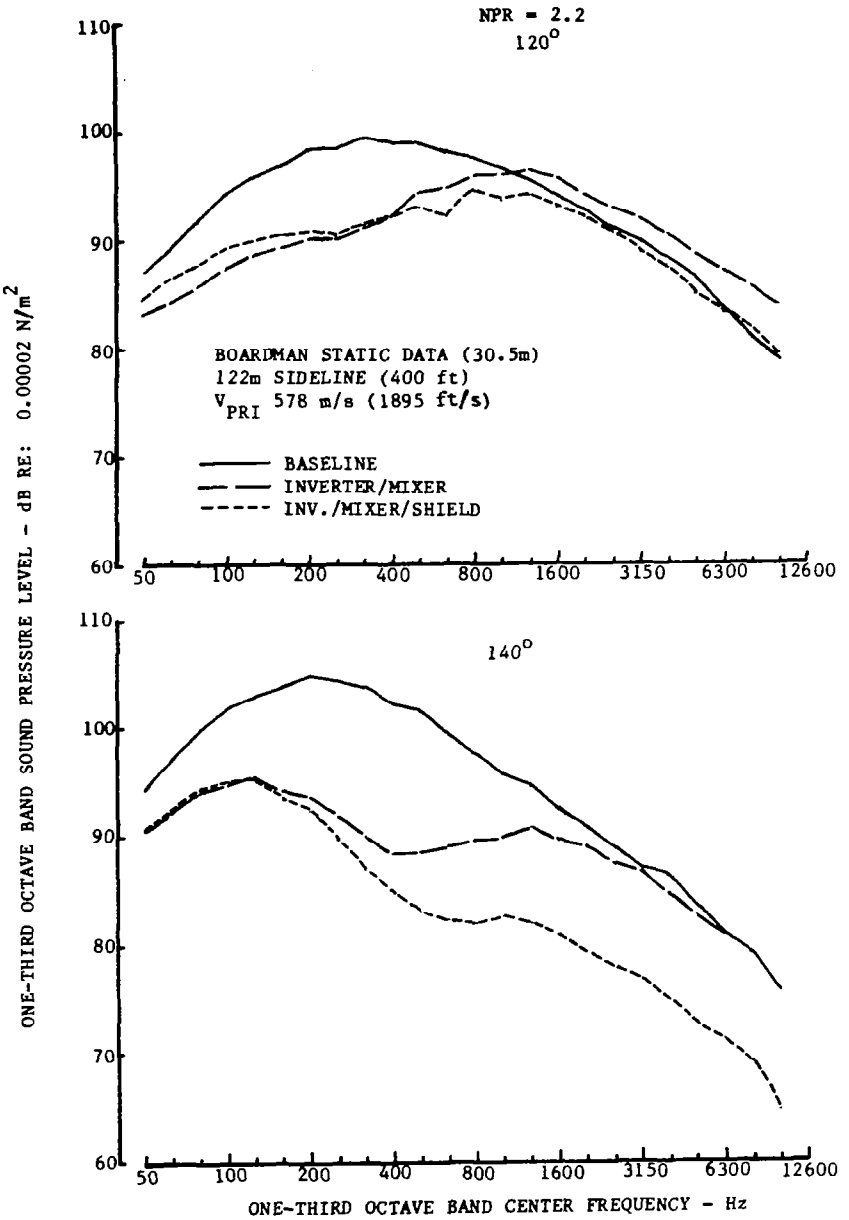

(b) 120° & 140°

Figure 71.—(Concluded)

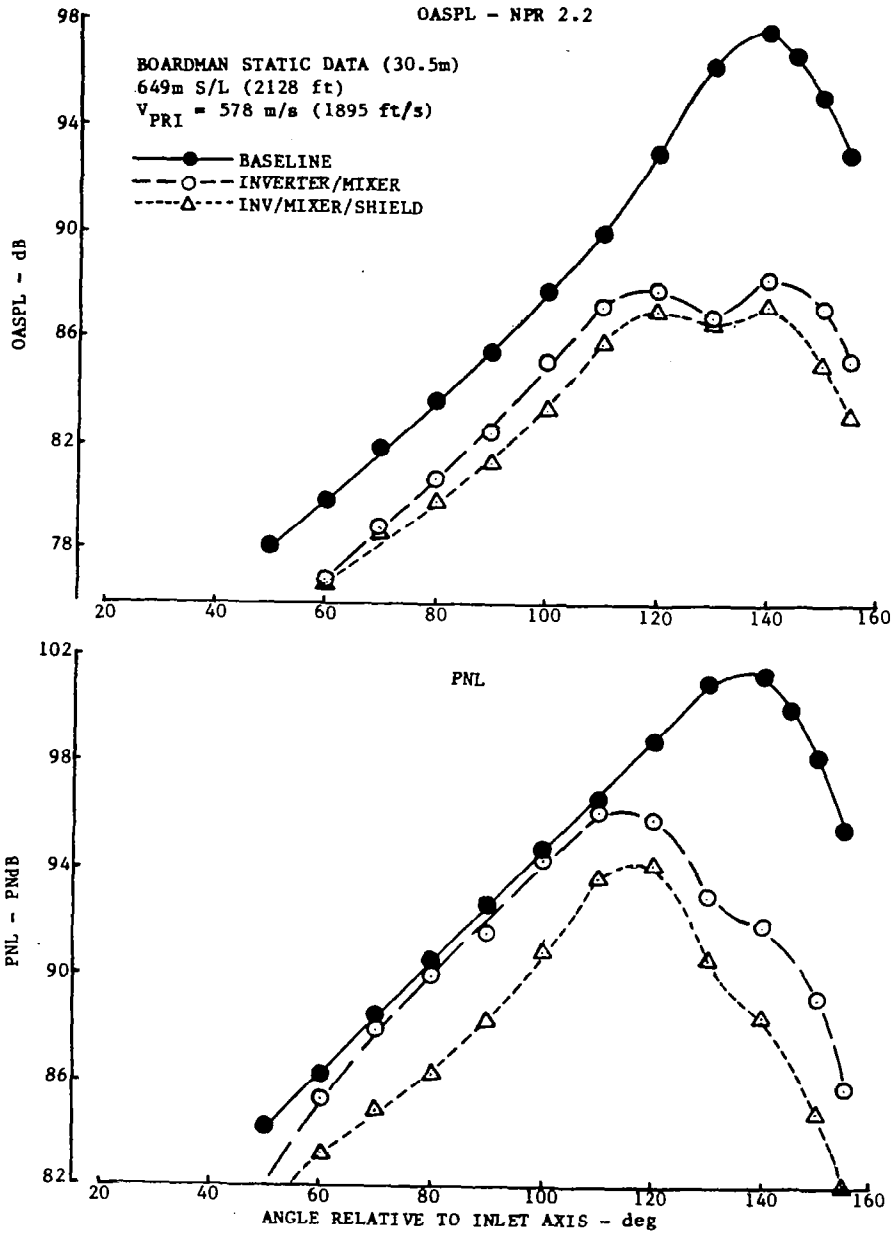

Figure 72.—Comparison of Static OASPL and PNL Directivity, Baseline versus Inverter/ Mixer with and without Shield

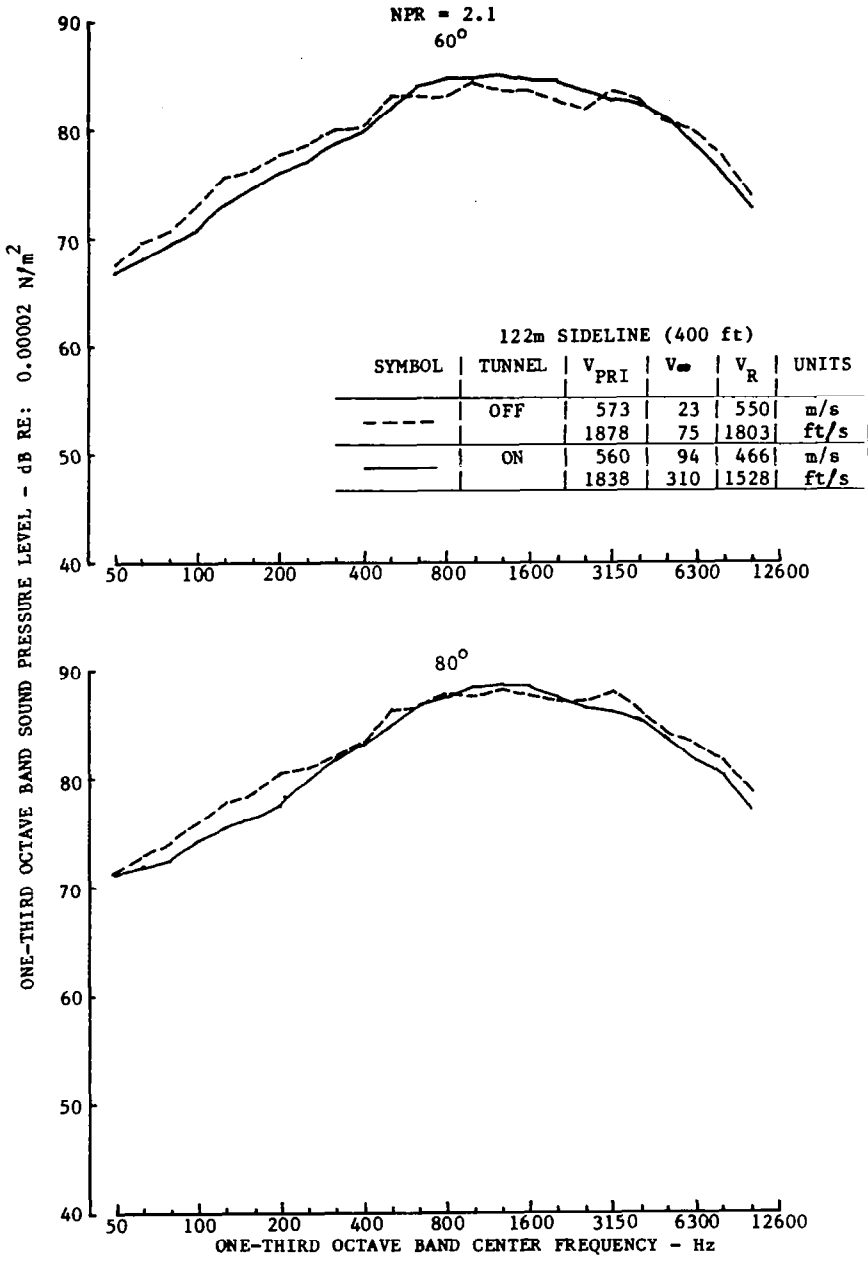

(a) 60° & 80°

Figure 73.—Comparison of Tunnel-Off and -On Spectra, Inverter/Mixer Configuration

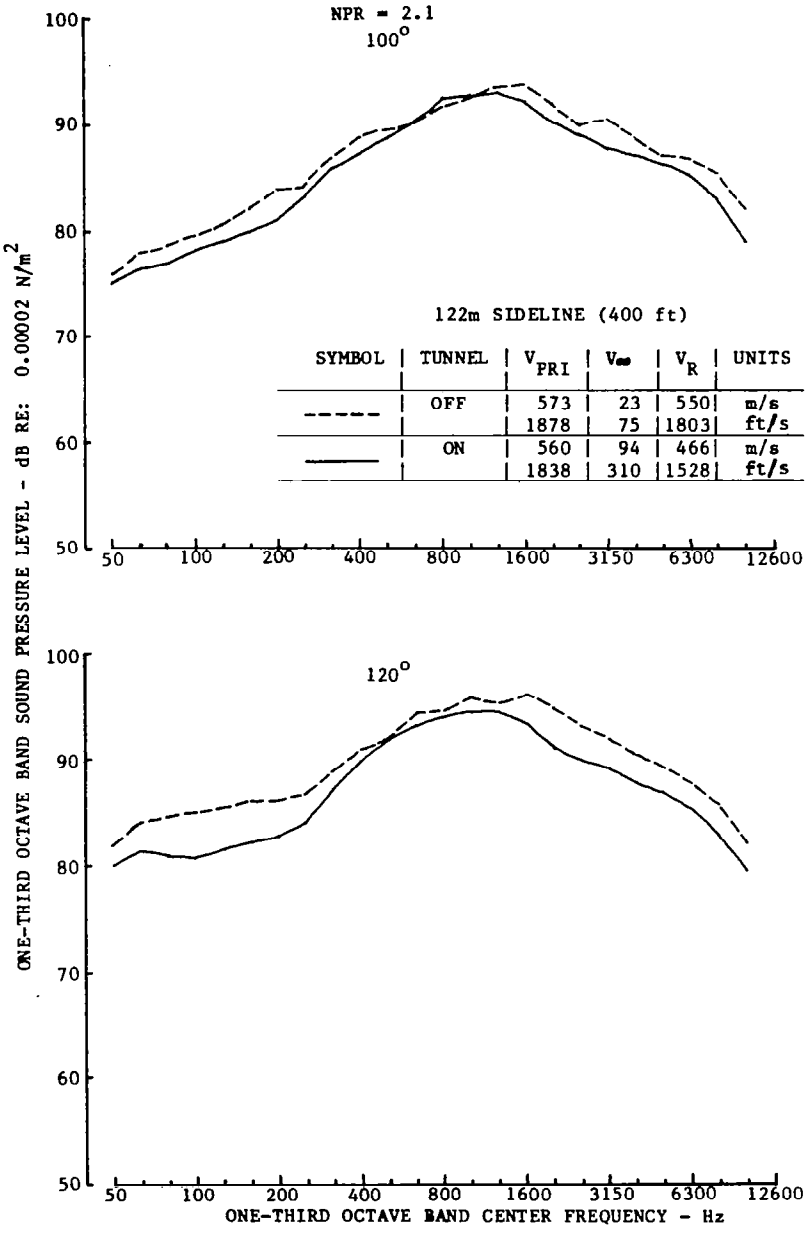

(b) 100° & 120°

Figure 73.—(Continued)

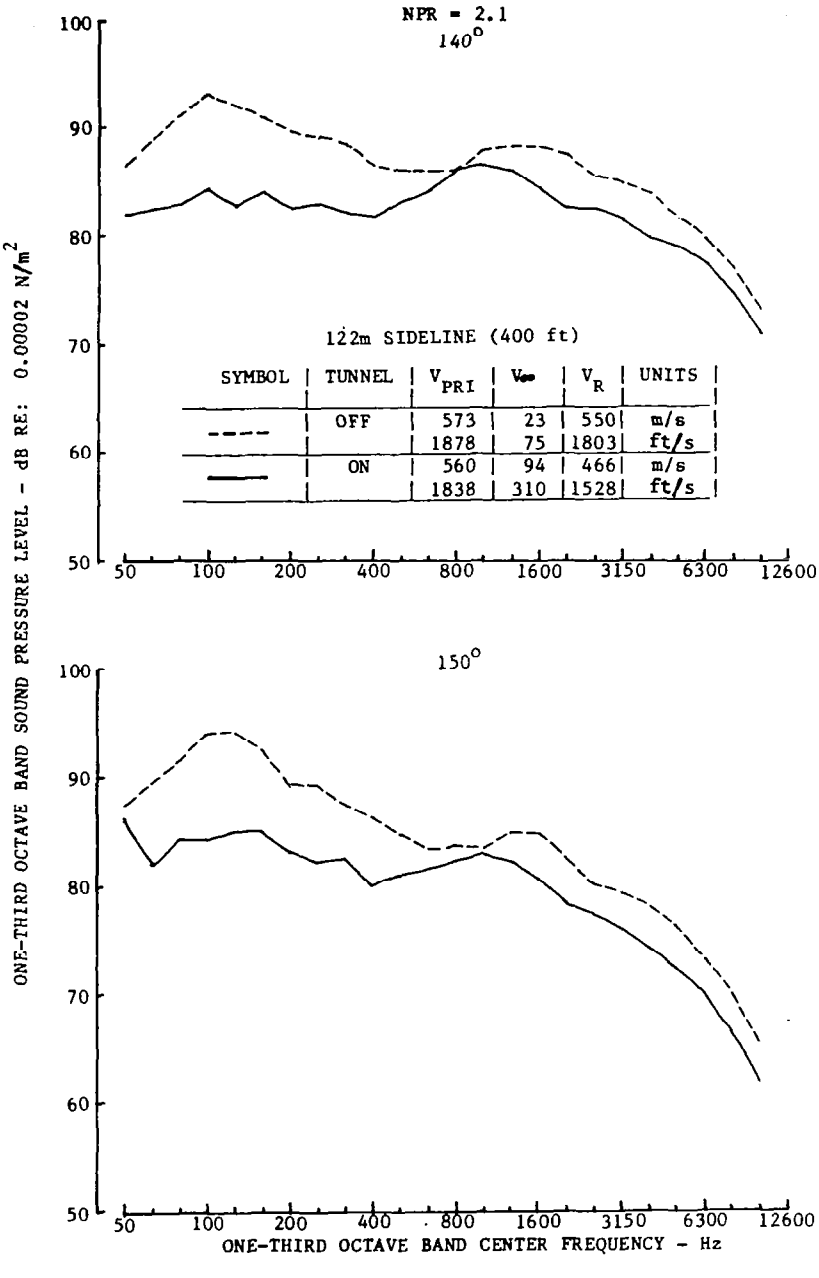

(c) 140° & 150°

Figure 73.–(Concluded)

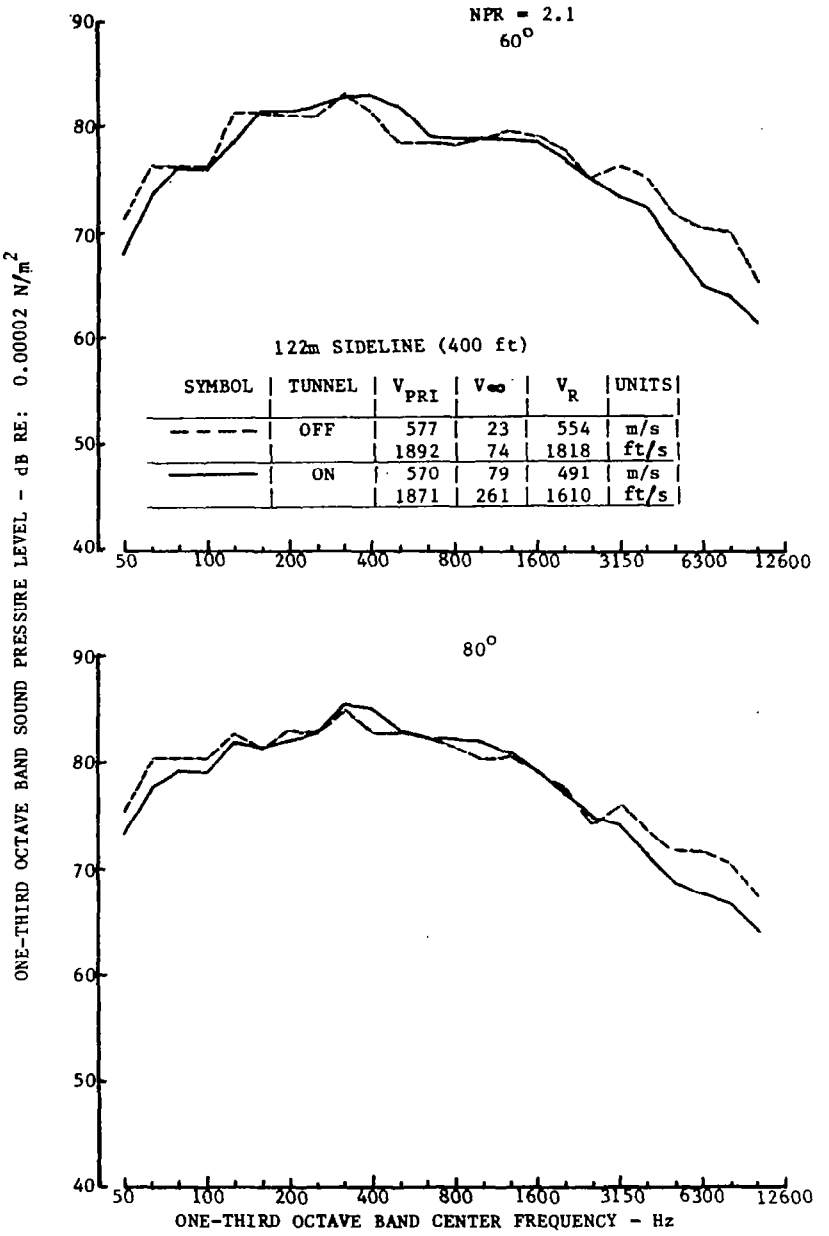

(a) 60° & 80°

Figure 74.—Comparison of Tunnel-Off and -On Spectra, Inverter/Mixer/Shield Configuration

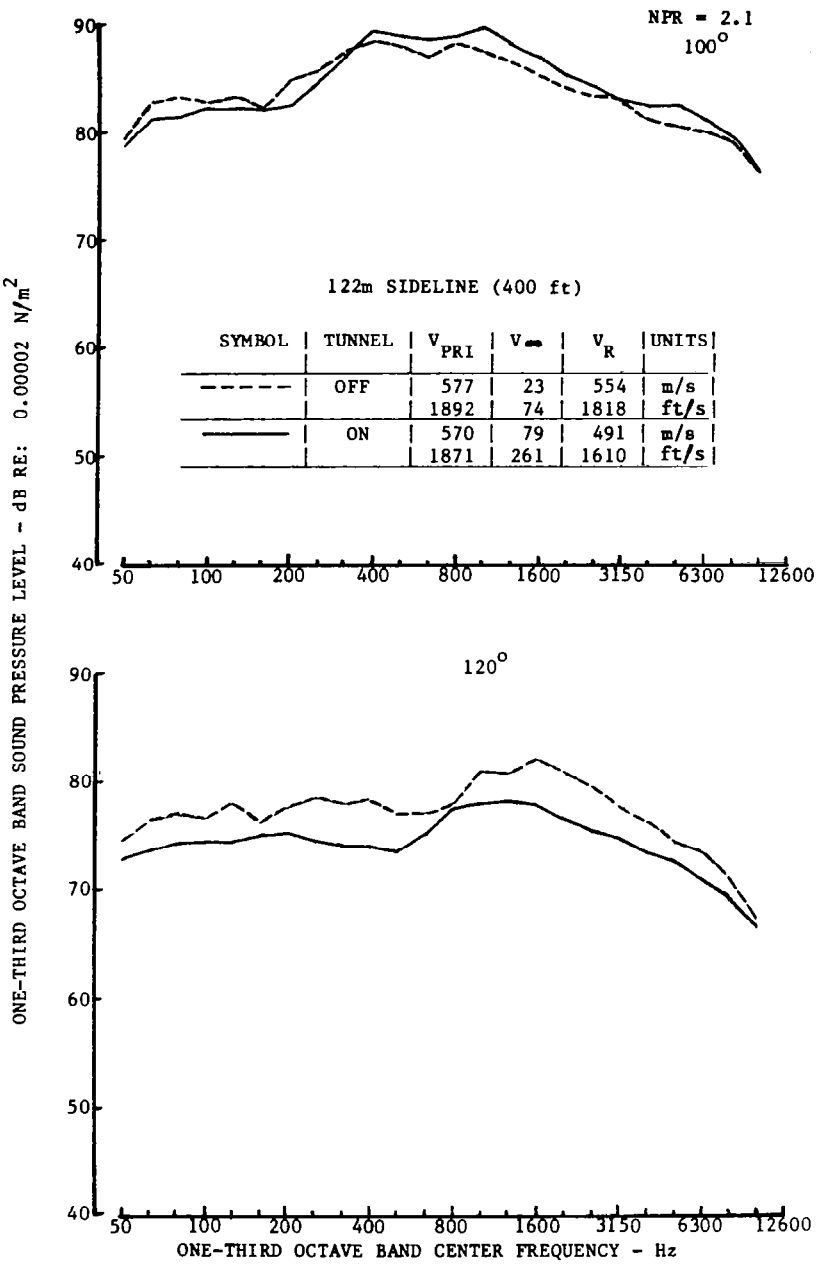

(b) 100° & 120°

Figure 74.—(Continued)

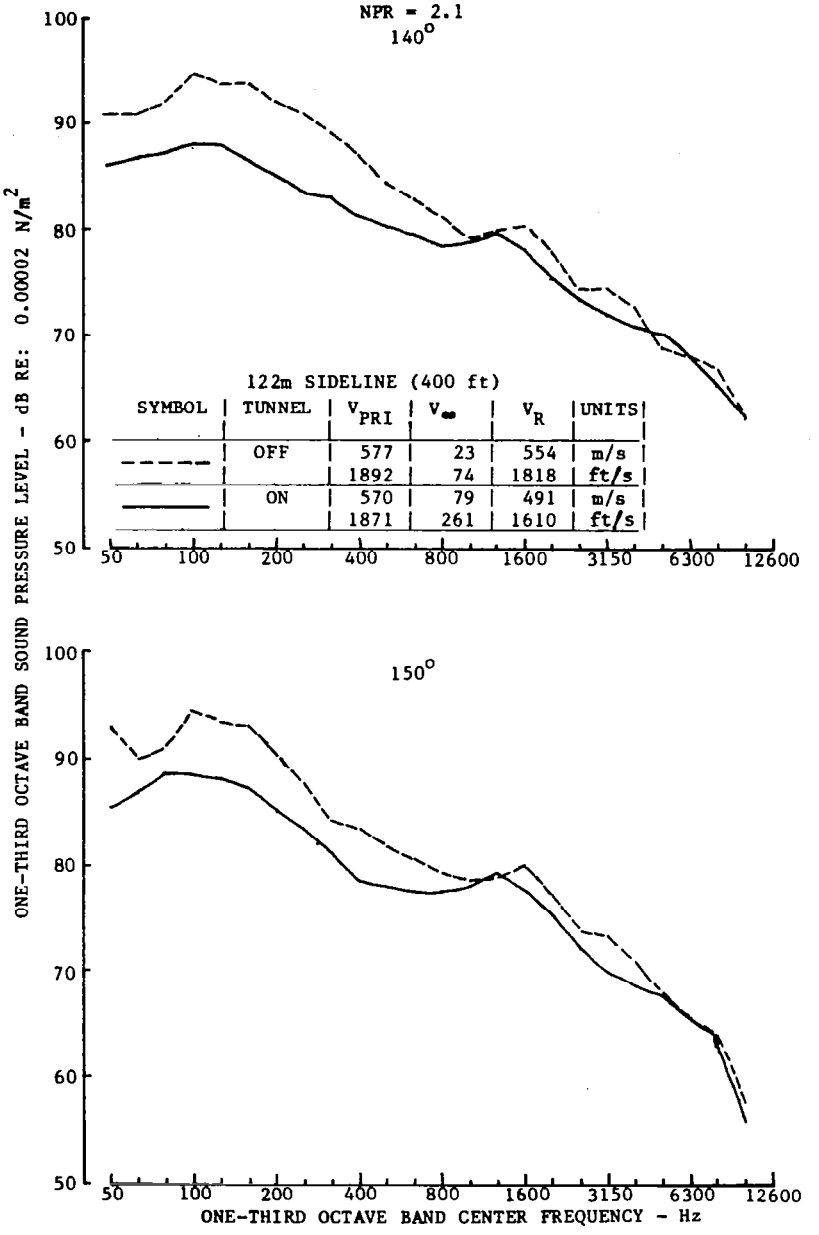

(c) 140° & 150°

Figure 74.—(Concluded)

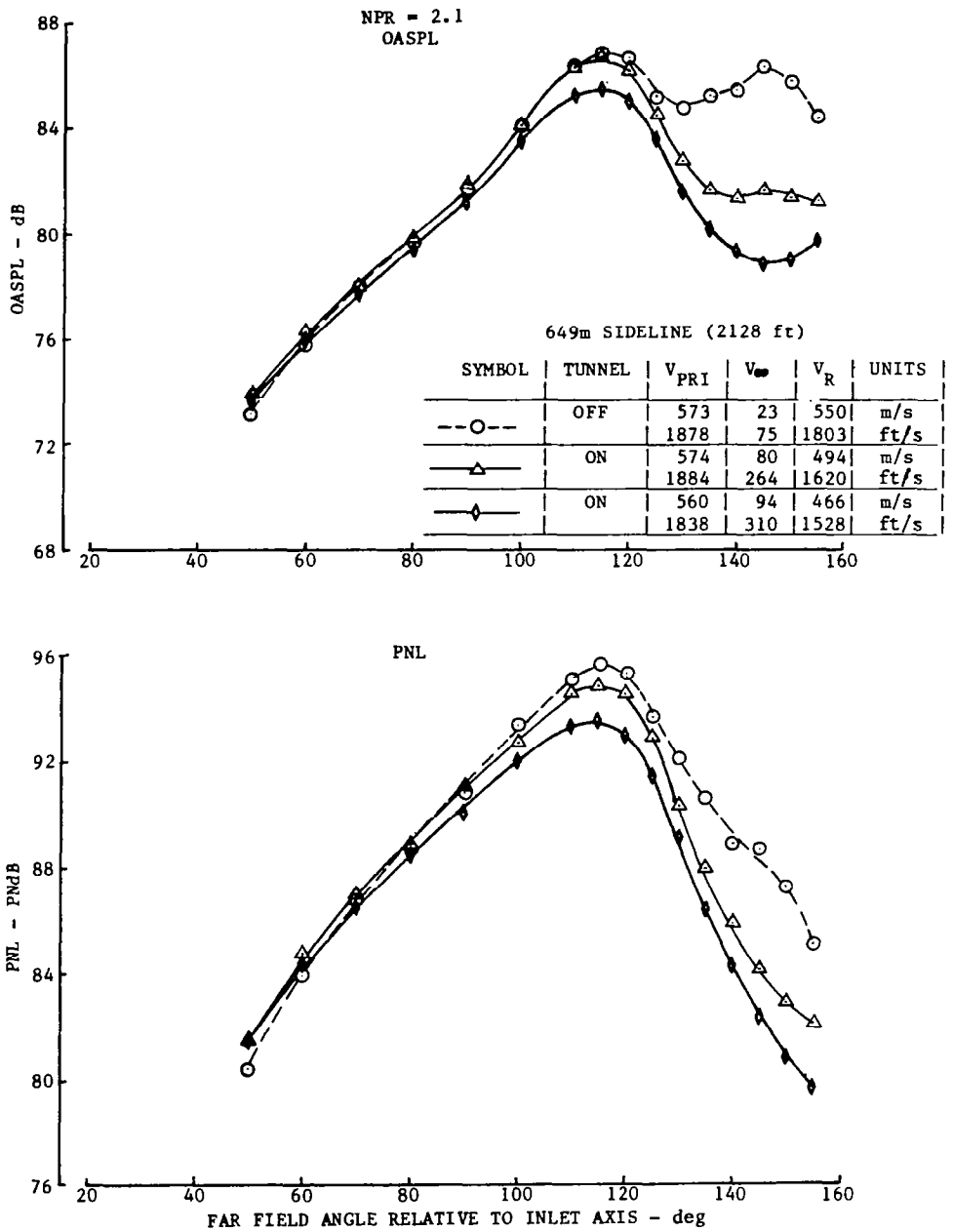

2.1

Figure 75.—Comparison of Tunnel-Off and -On OASPL and PNL Directivities, Inverter/Mixer Configuration

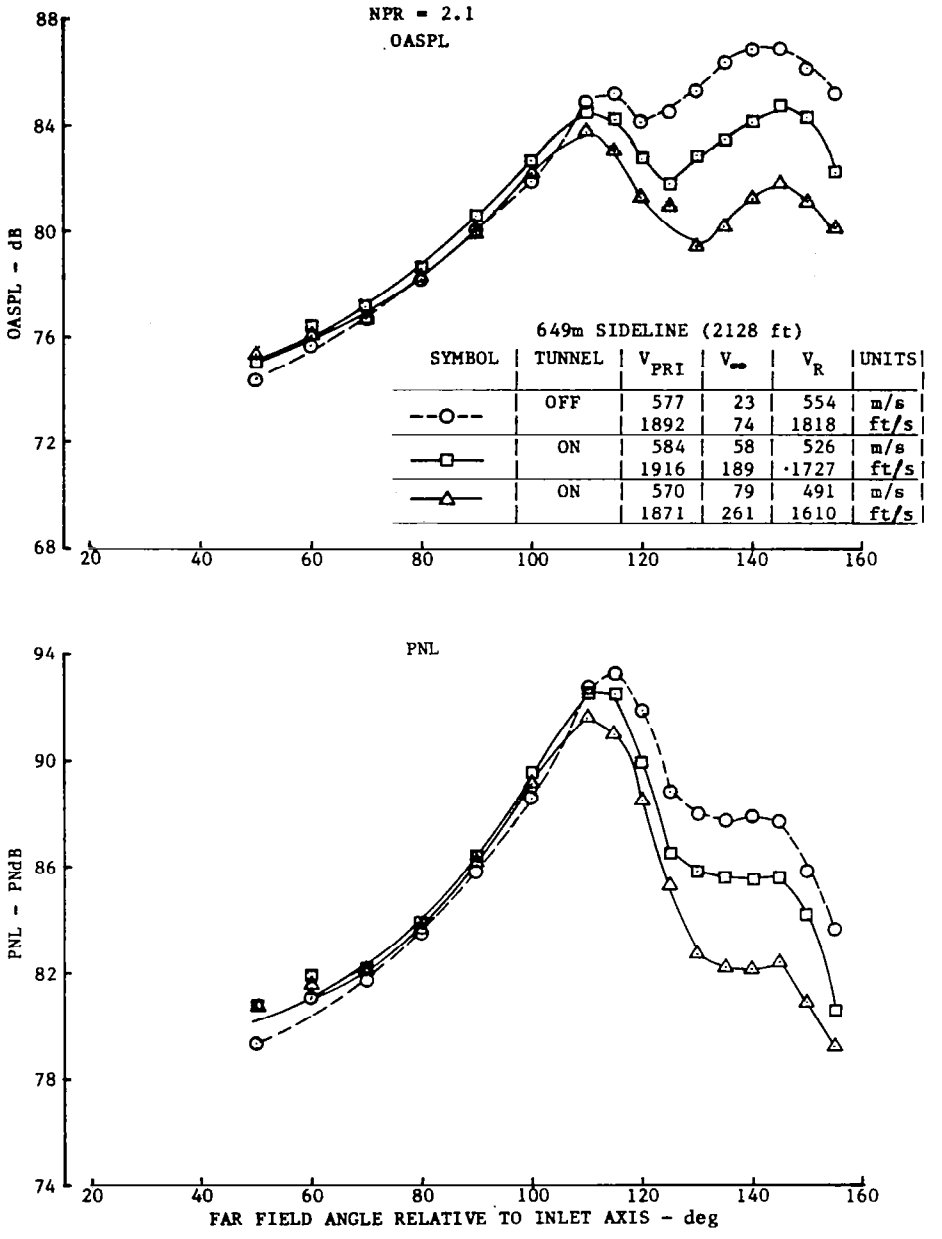

2.1

Figure 76.—Comparison of Tunnel-Off and -On OASPL and PNL Directivities, Inverter/Mixer/Shield Configuration

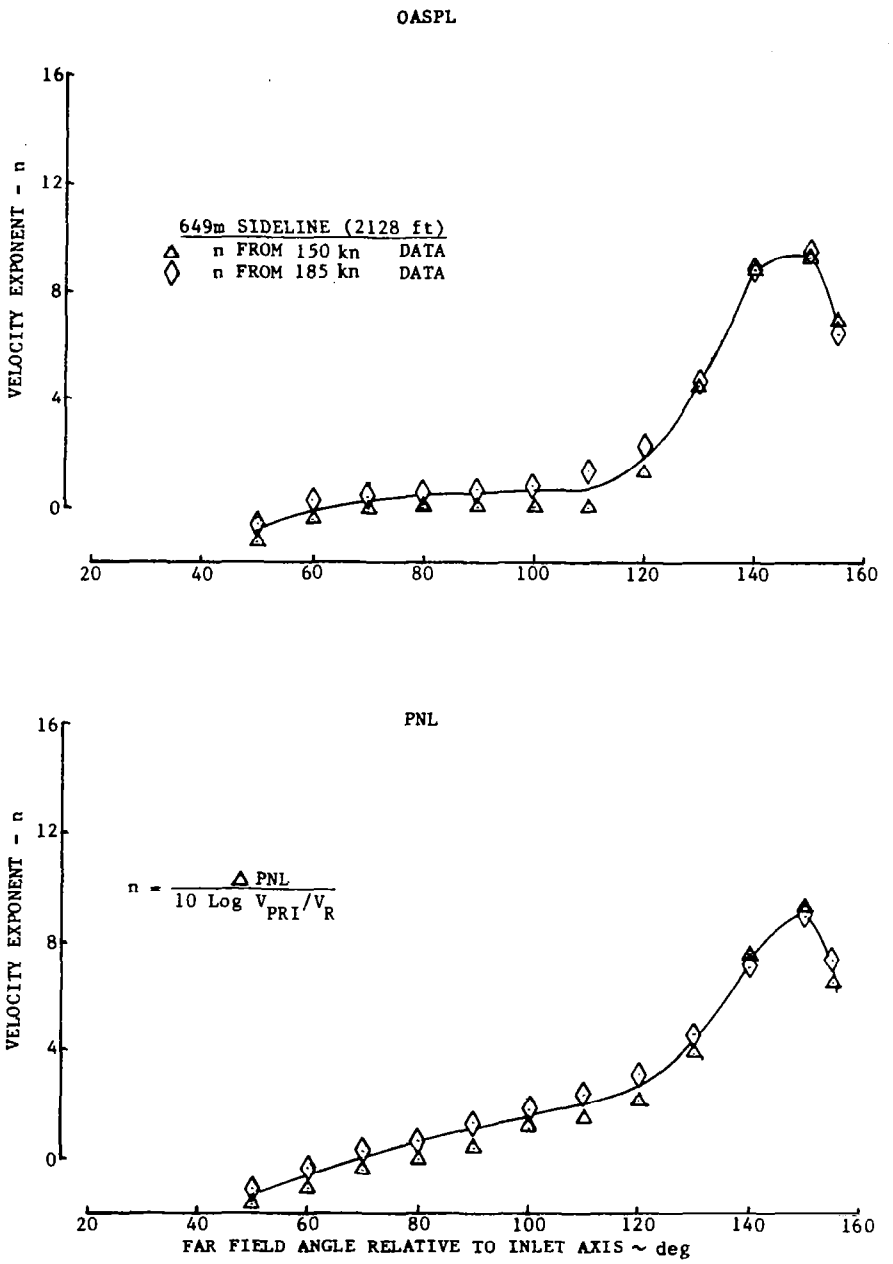

(a) NPR = 2.1

Figure 77.—Velocity Exponents for OASPL and PNL, Inverter/Mixer Configuration

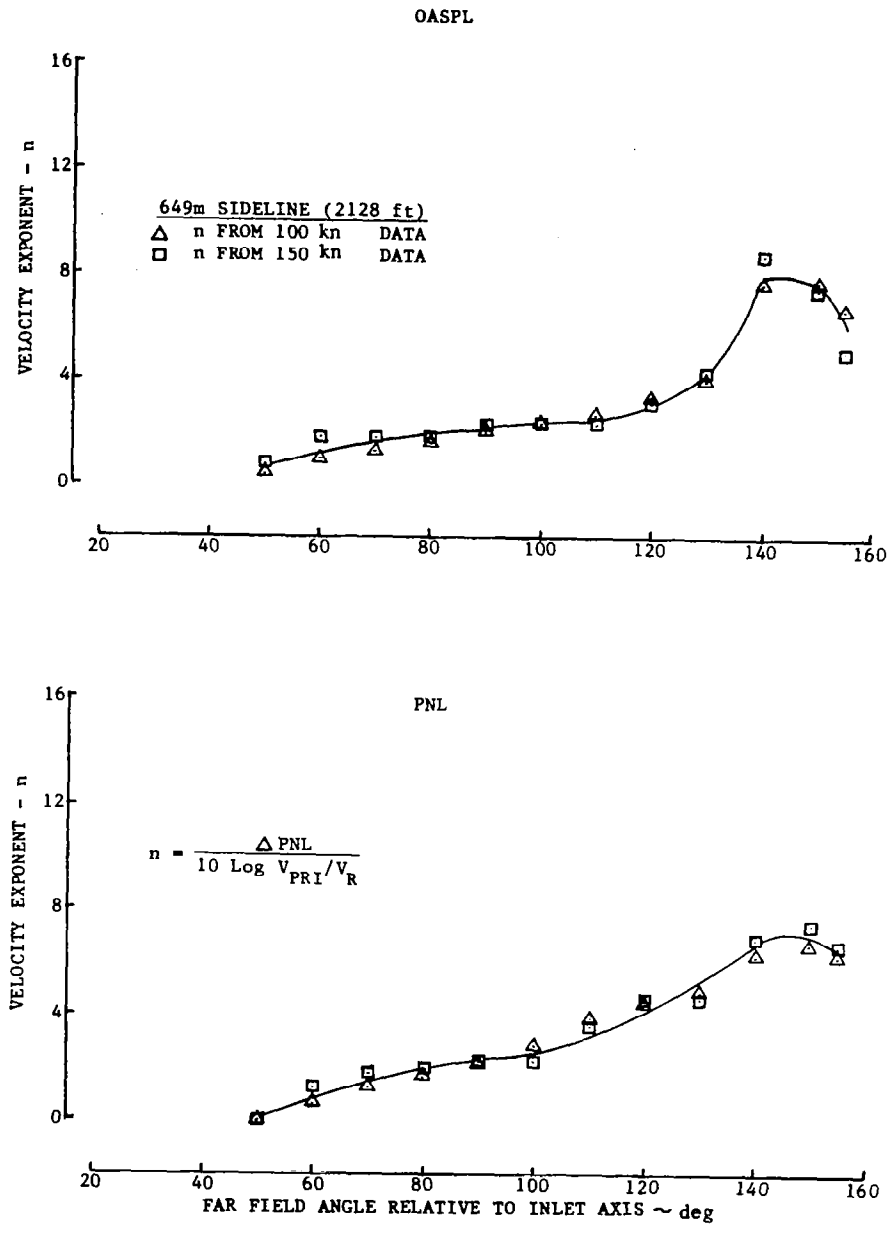

(b) NPR = 1.8

Figure 77.—(Concluded)

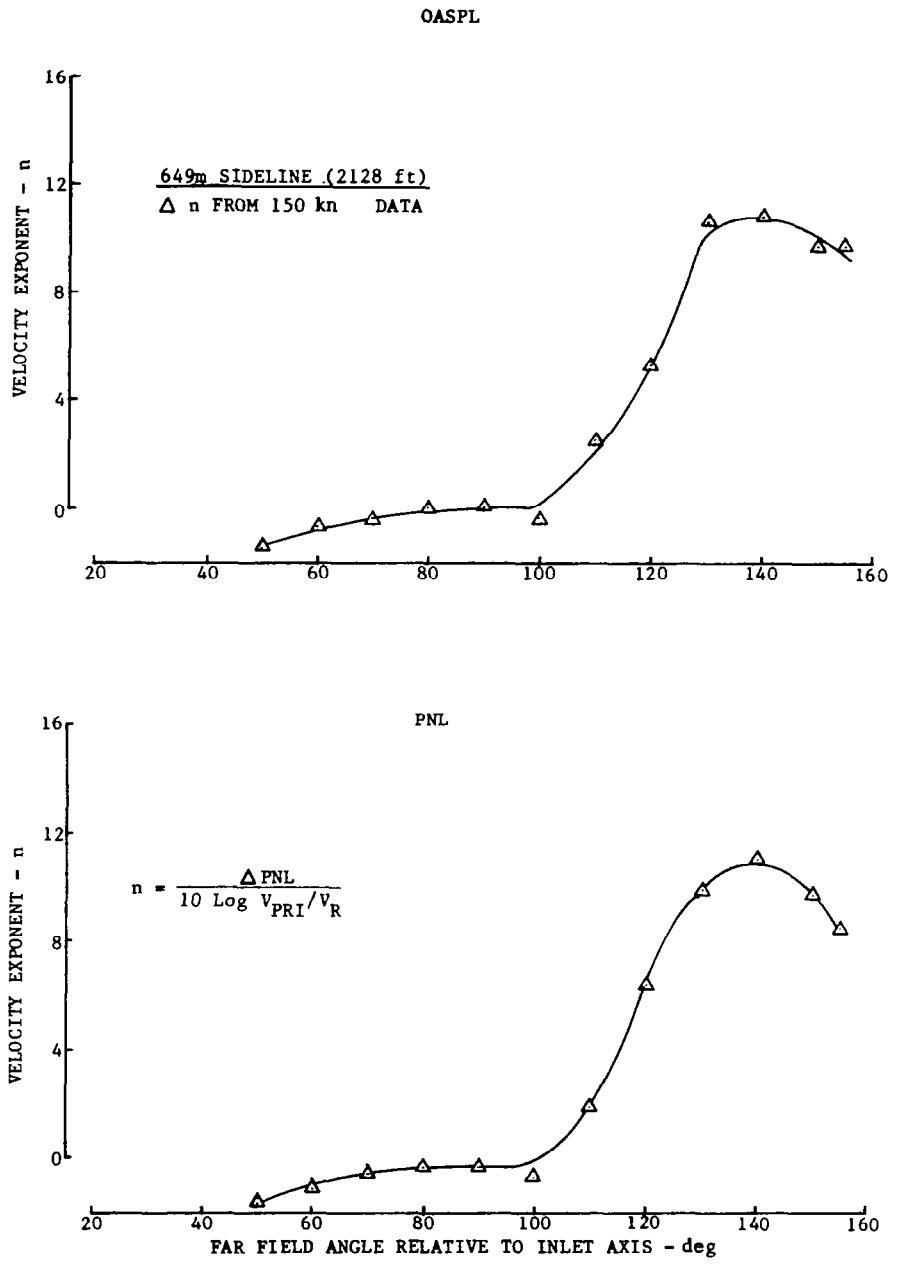

(a) NPR = 2.1

Figure 78.—Velocity Exponents for OASPL and PNL, Inverter/Mixer/Shield Configuration

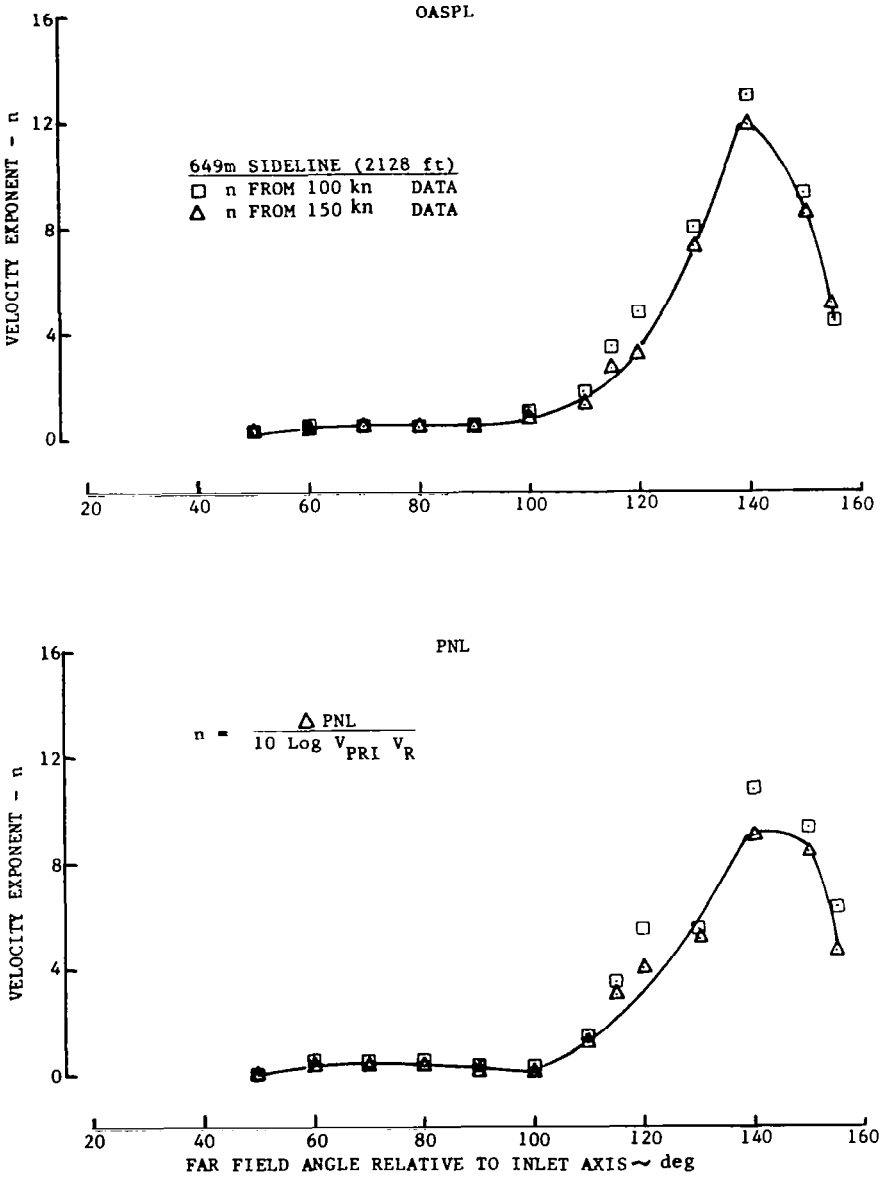

(b) NPR = 1.8

Figure 78.—(Concluded)

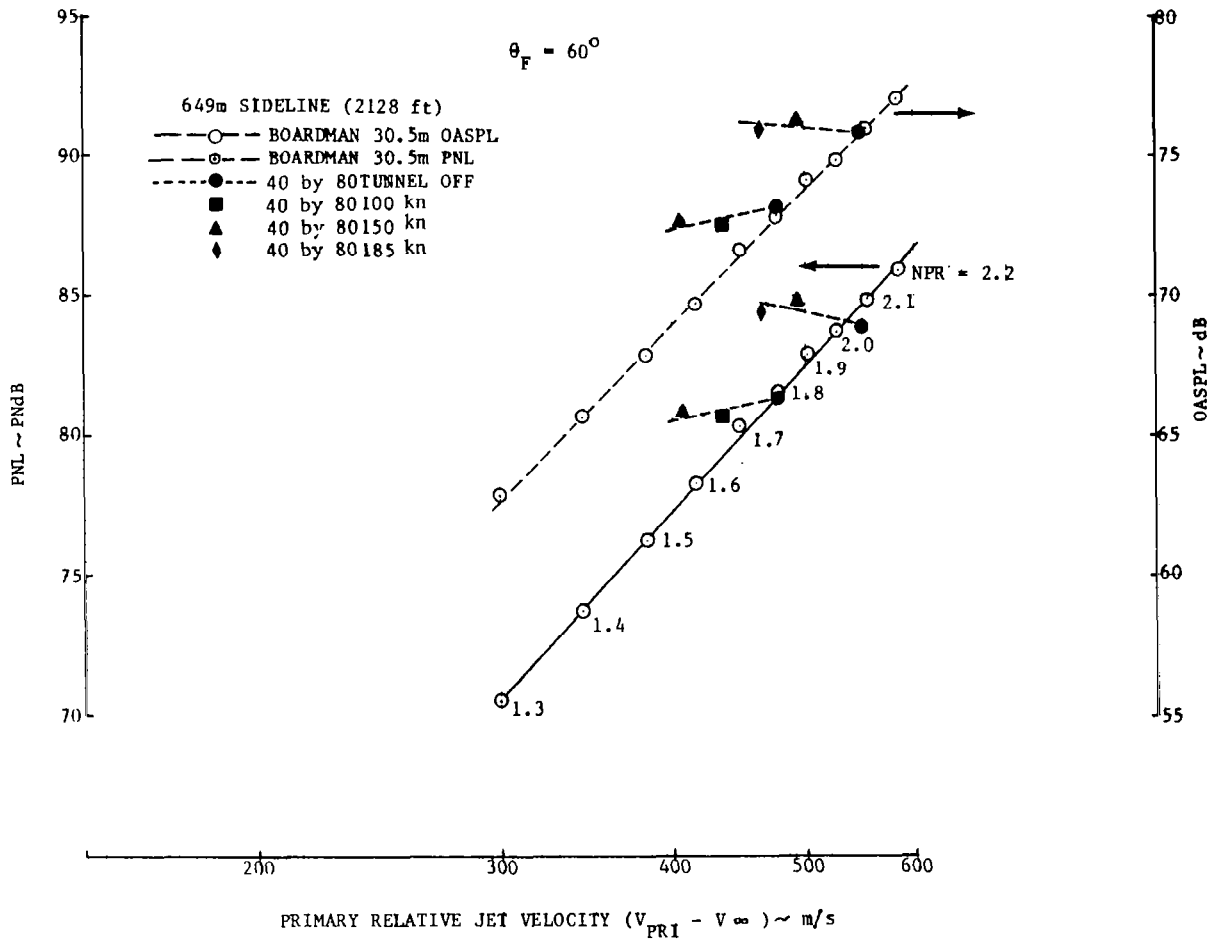

(a) 60°

Figure 79.—Tunnel-Off and -On OASPL and PNL versus Primary Velocity, Inverter/Mixer Configuration

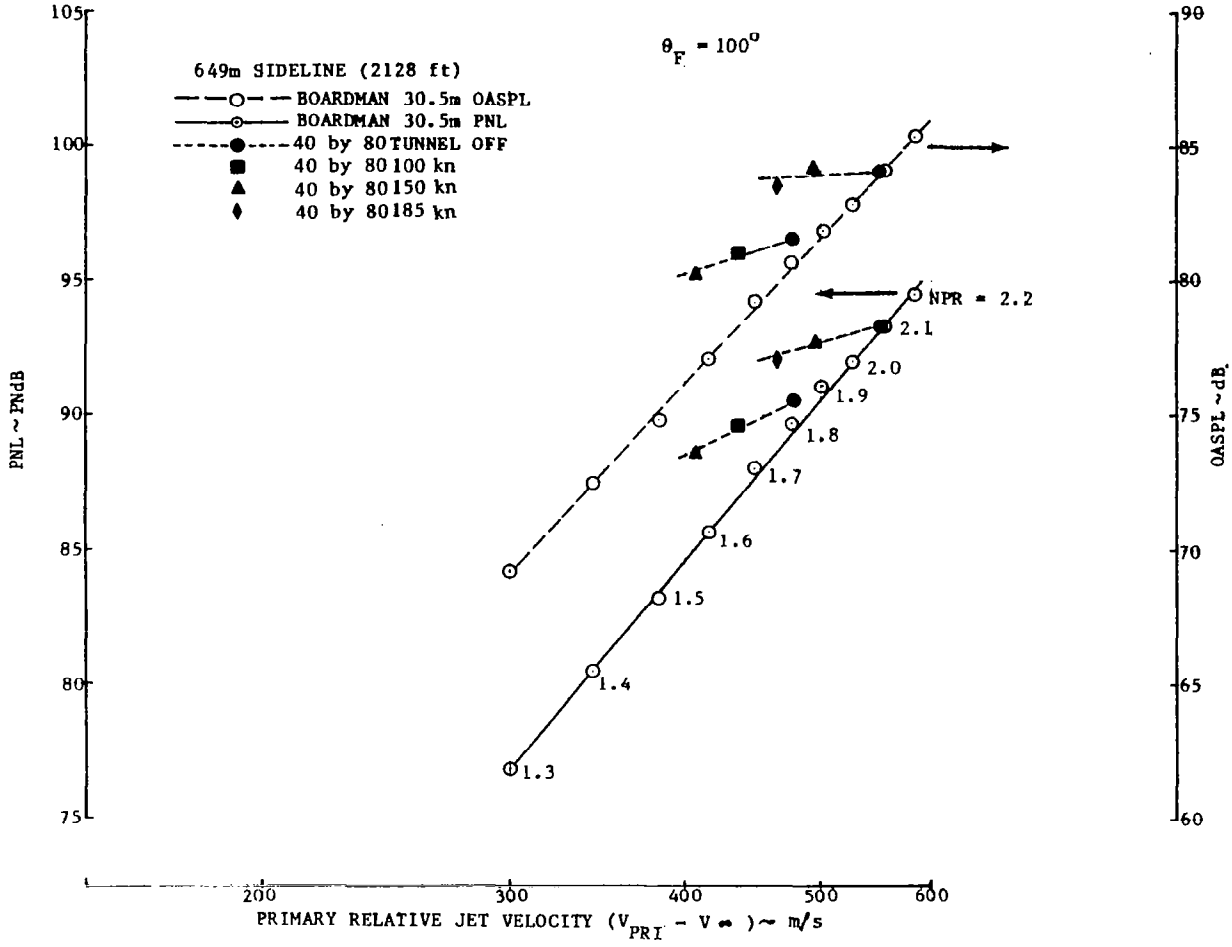

(b) 100°

Figure 79.—(Continued)

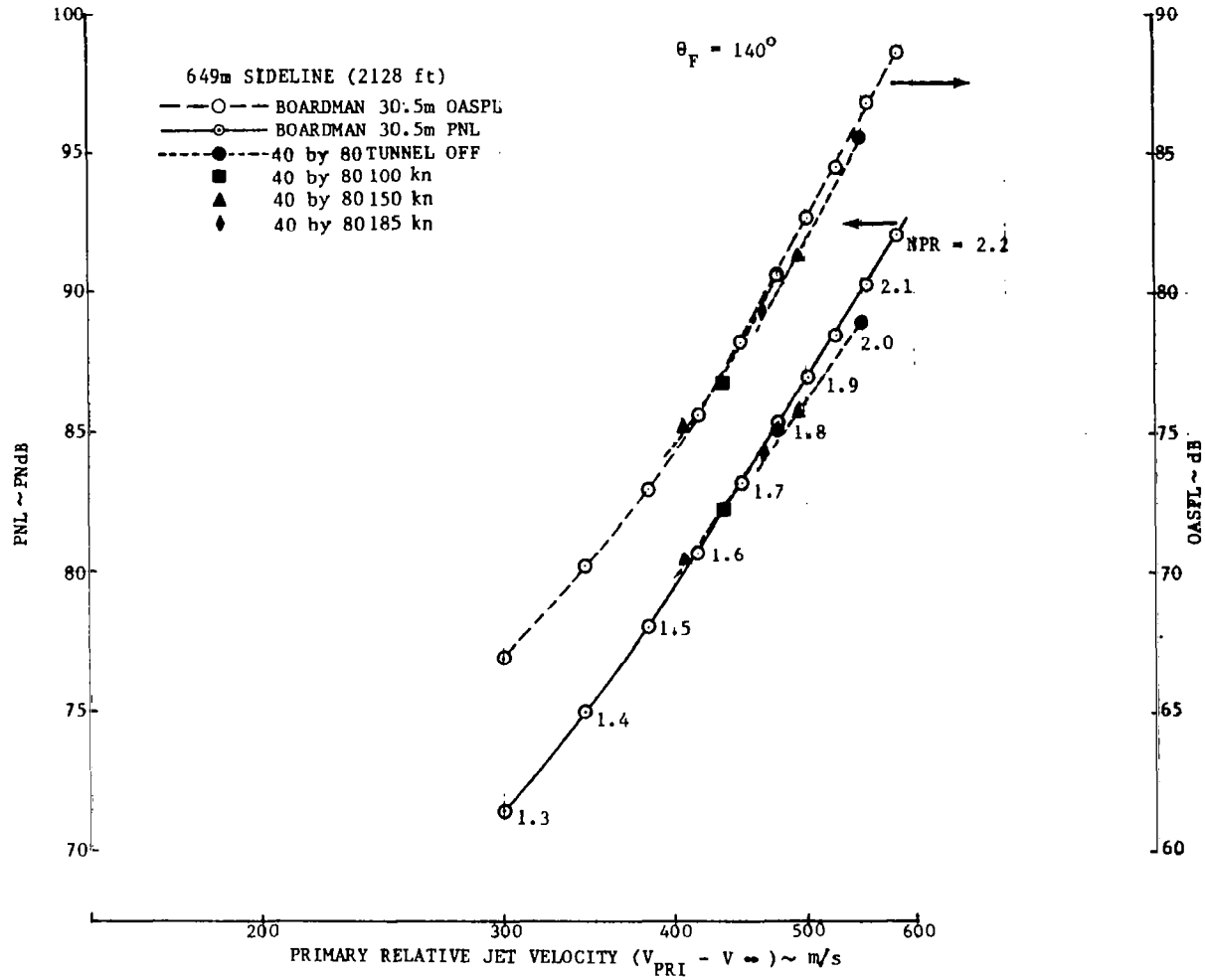

(c) 140°

Figure 79.—(Continued)

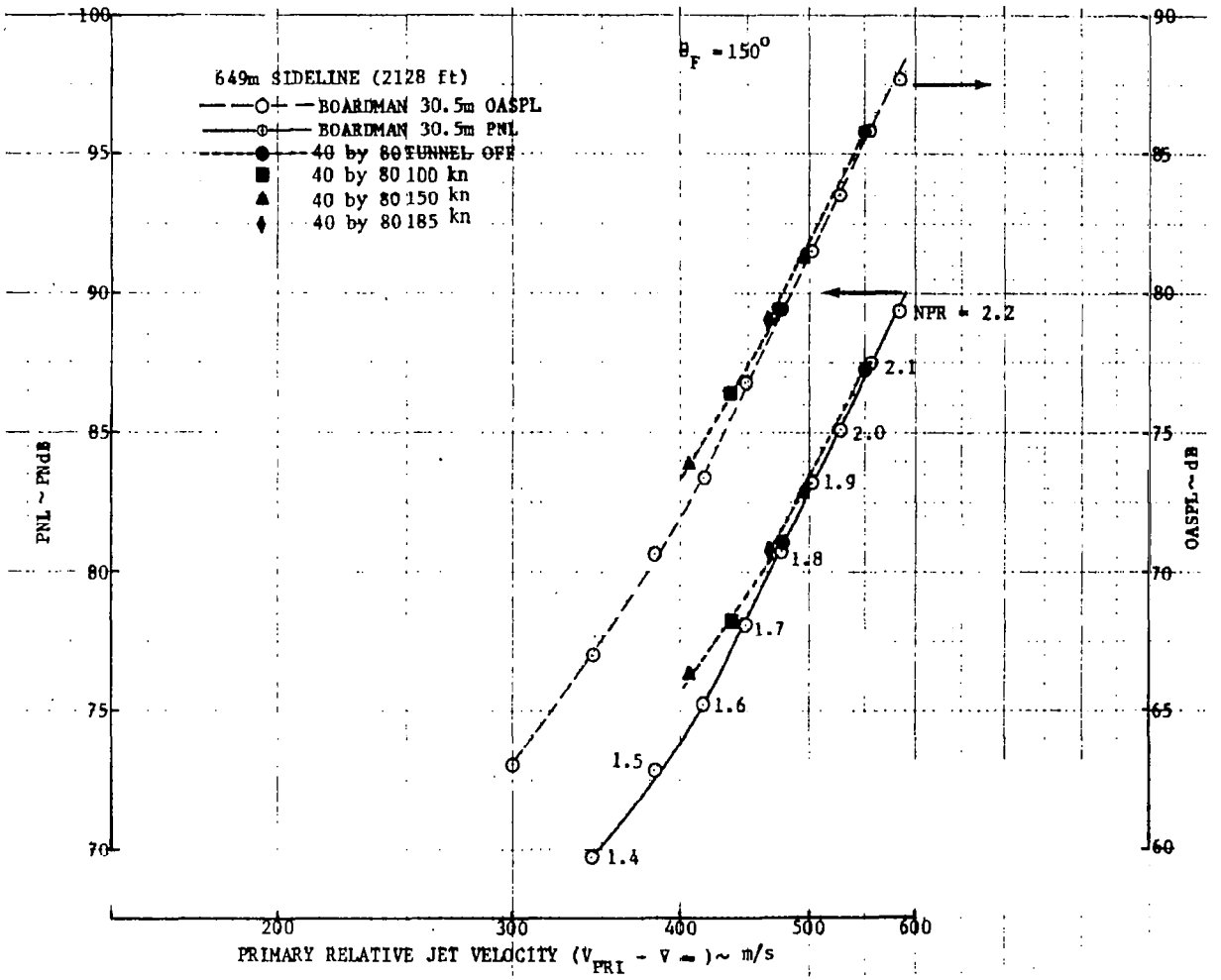

(d) 150°

Figure 79.—(Concluded)

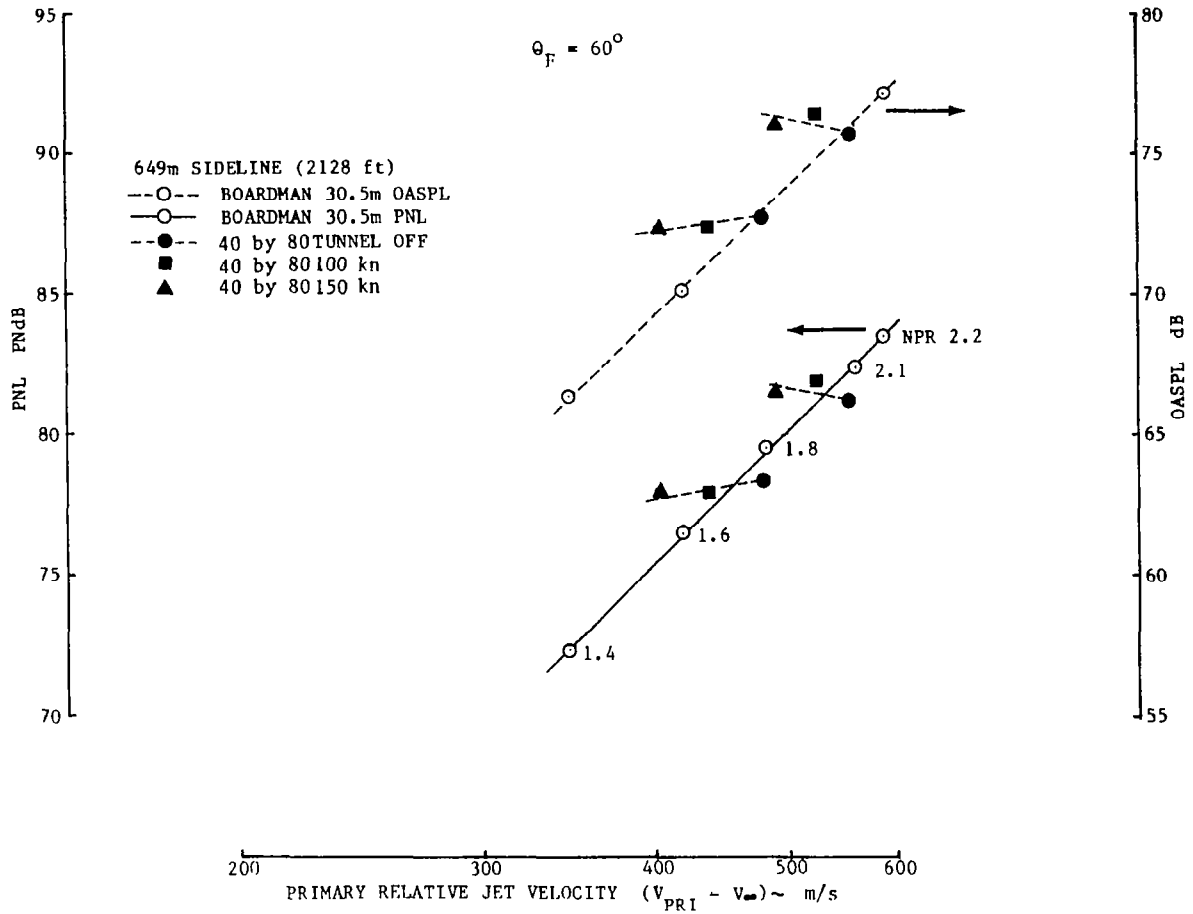

(a) 60°

Figure 80.—Tunnel-Off and -On OASPL and PNL versus Primary Velocity, Inverter/Mixer/Shield Configuration

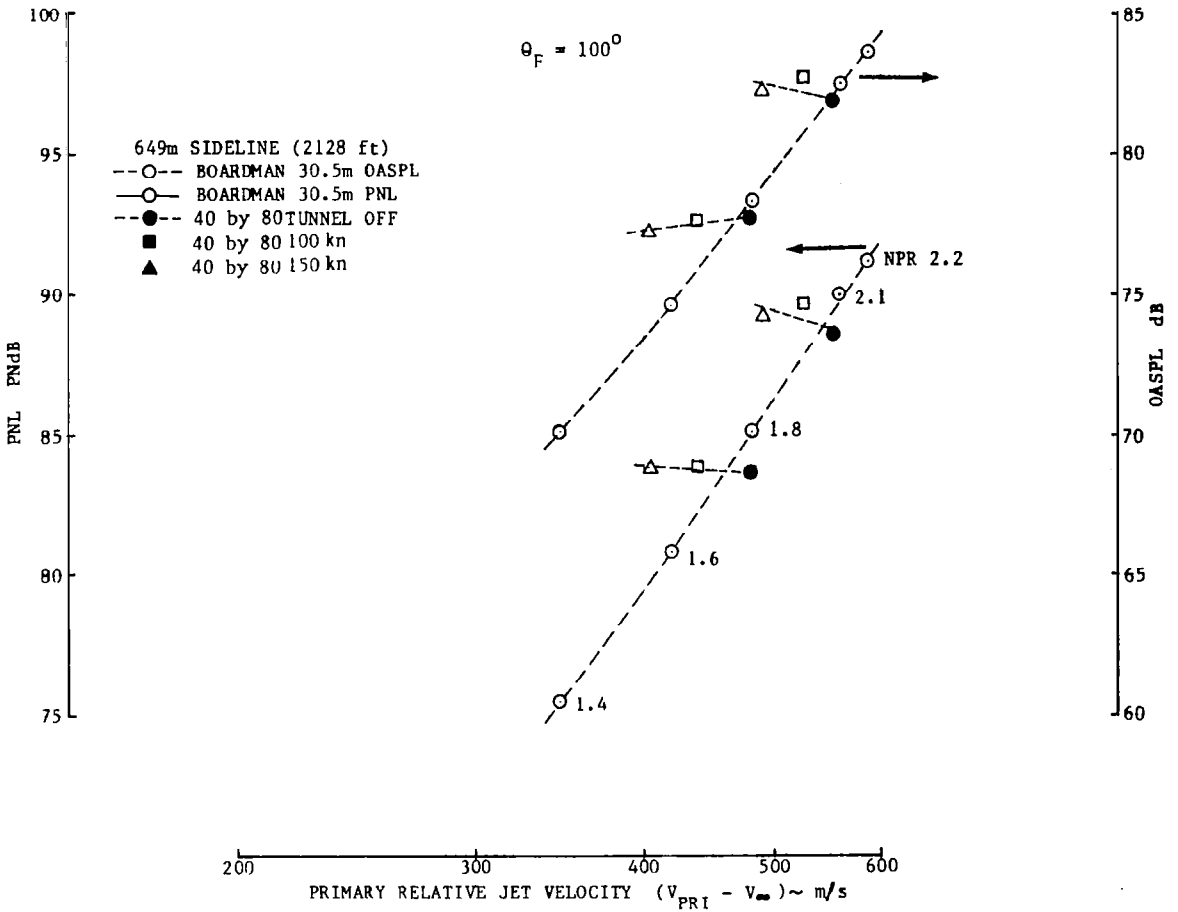

(b) 100°

Figure 80.—(Continued)

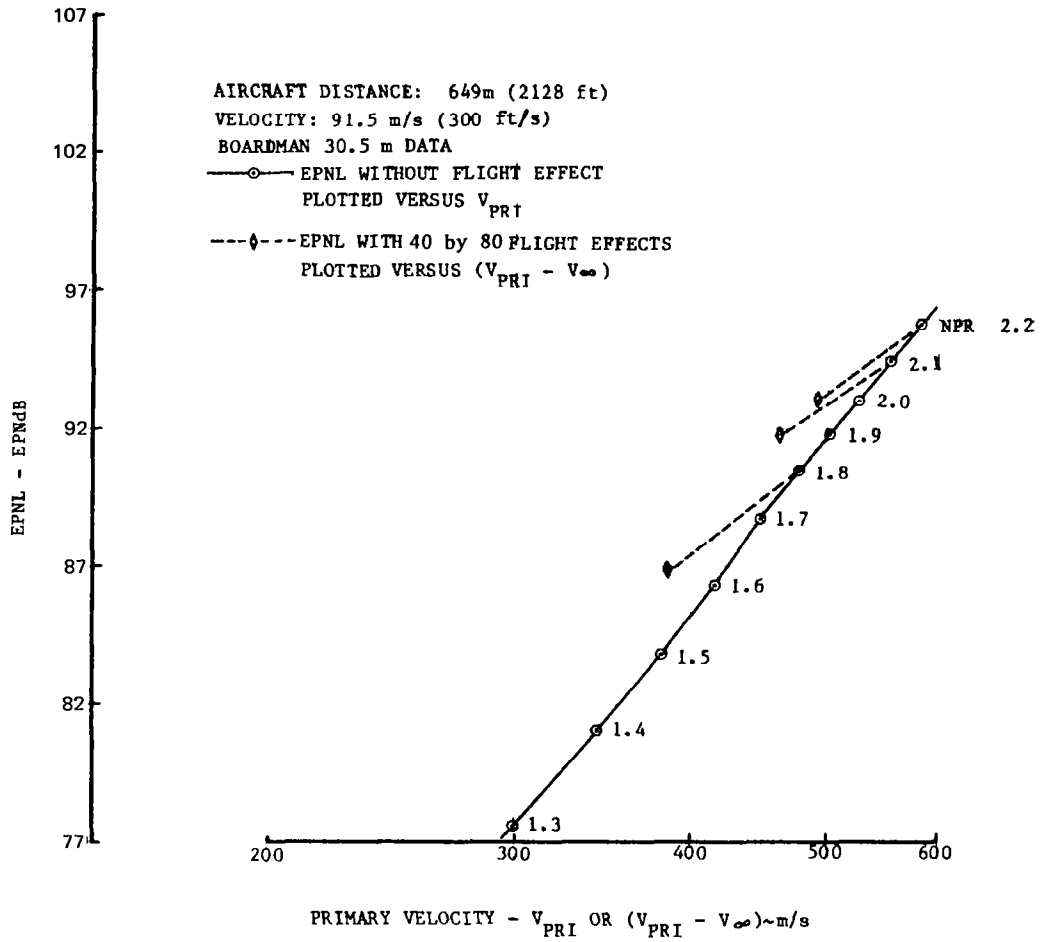

Figure 81.—Static and Estimated Flight EPNL Characteristics, Inverter/Mixer Configuration

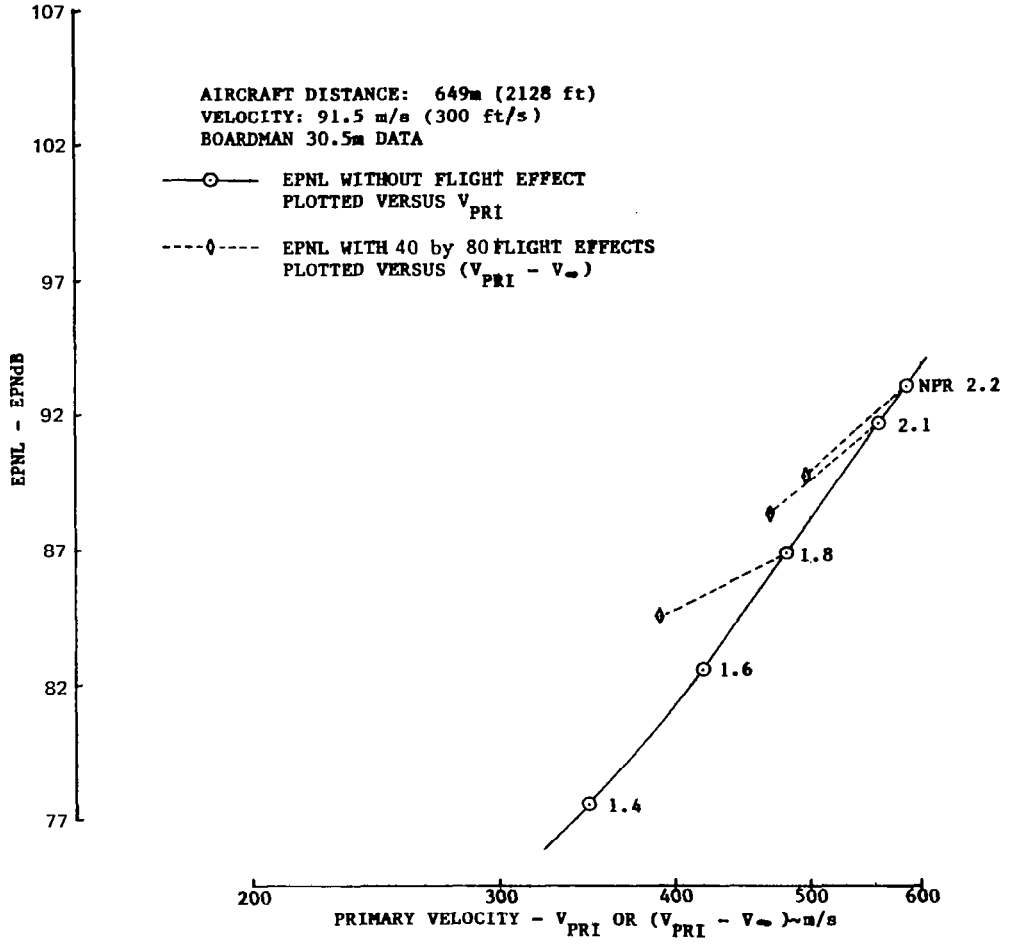

Figure 82.—Static and Estimated Flight EPNL Characteristics, Inverter/Mixer/Shield Configuration

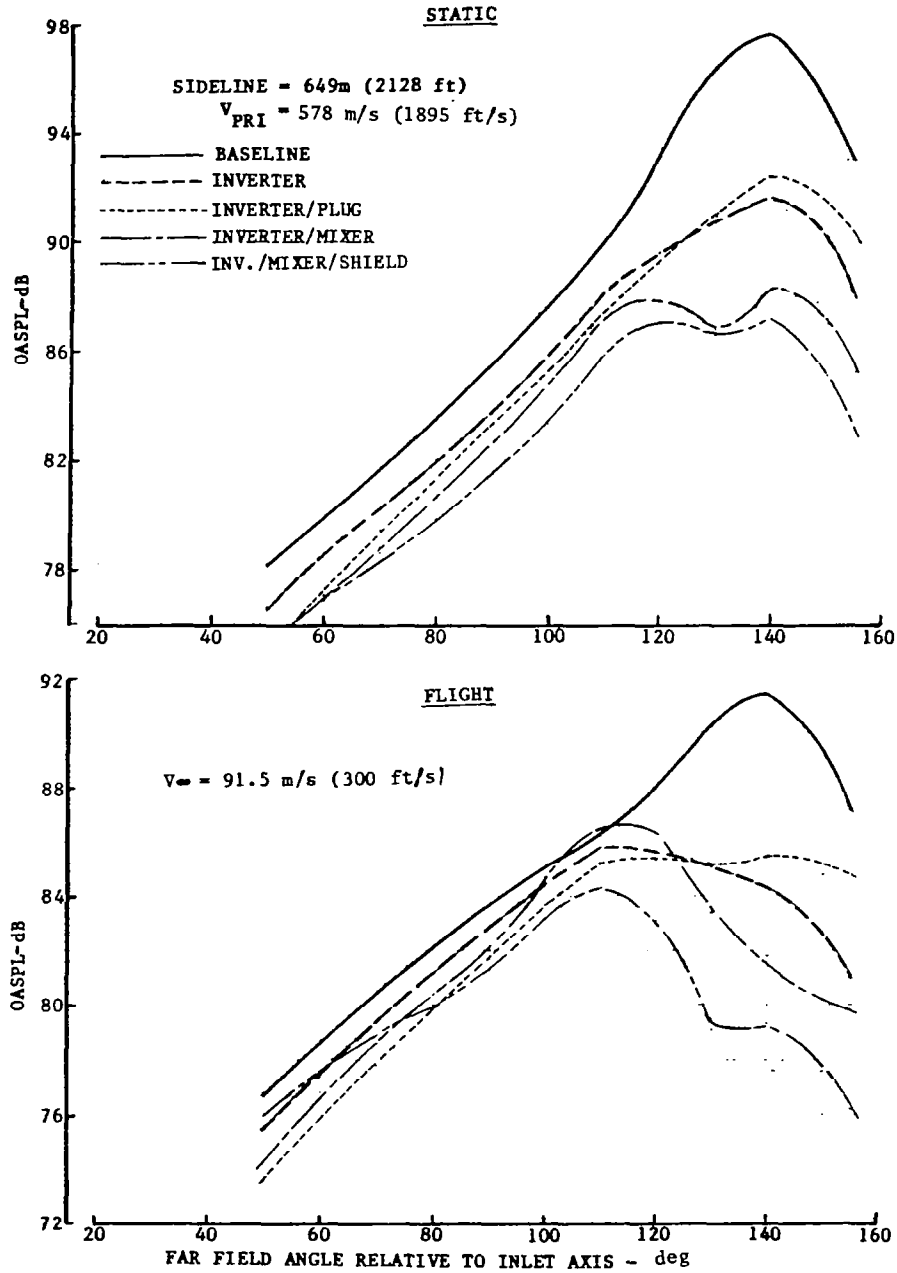

Figure 83.—Comparison of Static and Flight OASPL Directivity for Baseline and Inverted Flow Suppressors

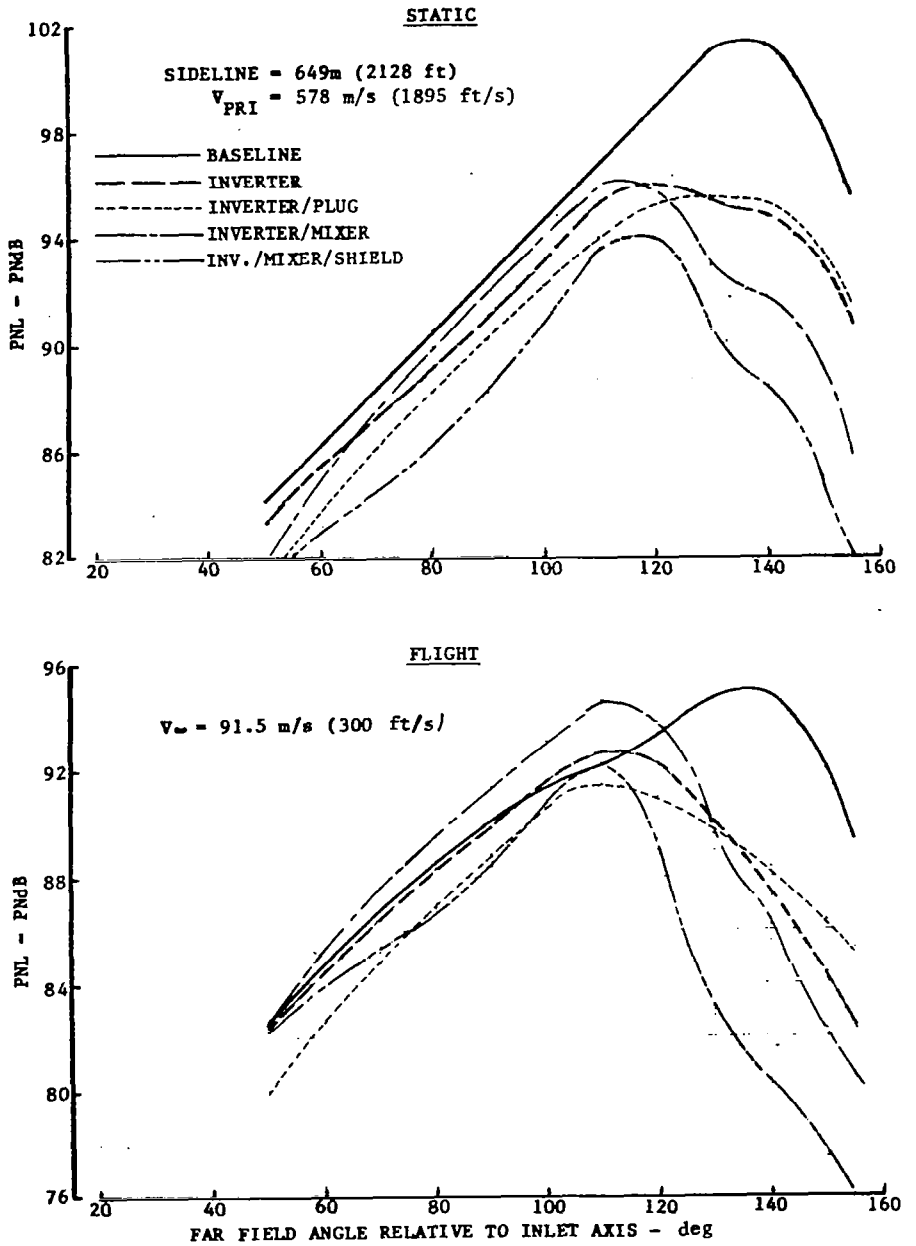

Figure 84.—Comparison of Static and Flight PNL Directivity for Baseline and Inverted Flow Suppressors

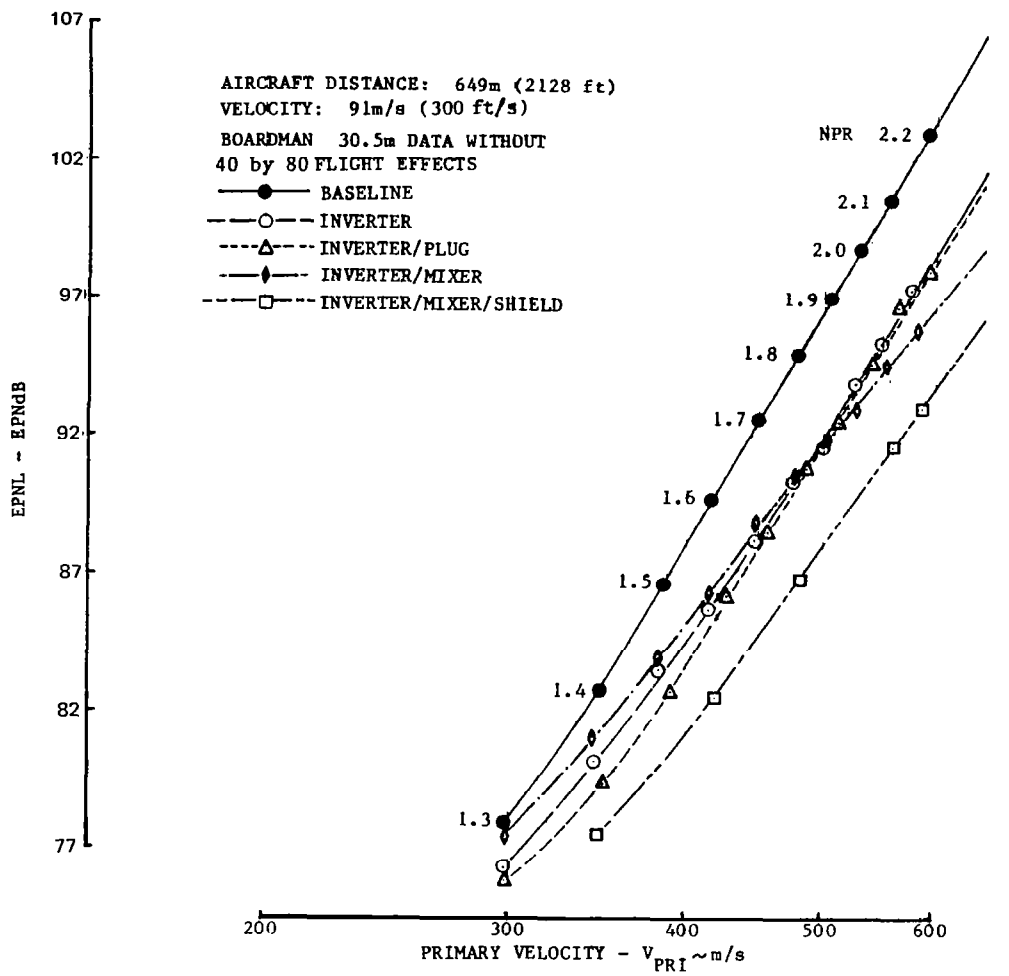

Figure 85.—Comparison of Baseline and Inverted Flow Suppressor EPNL, Static Levels

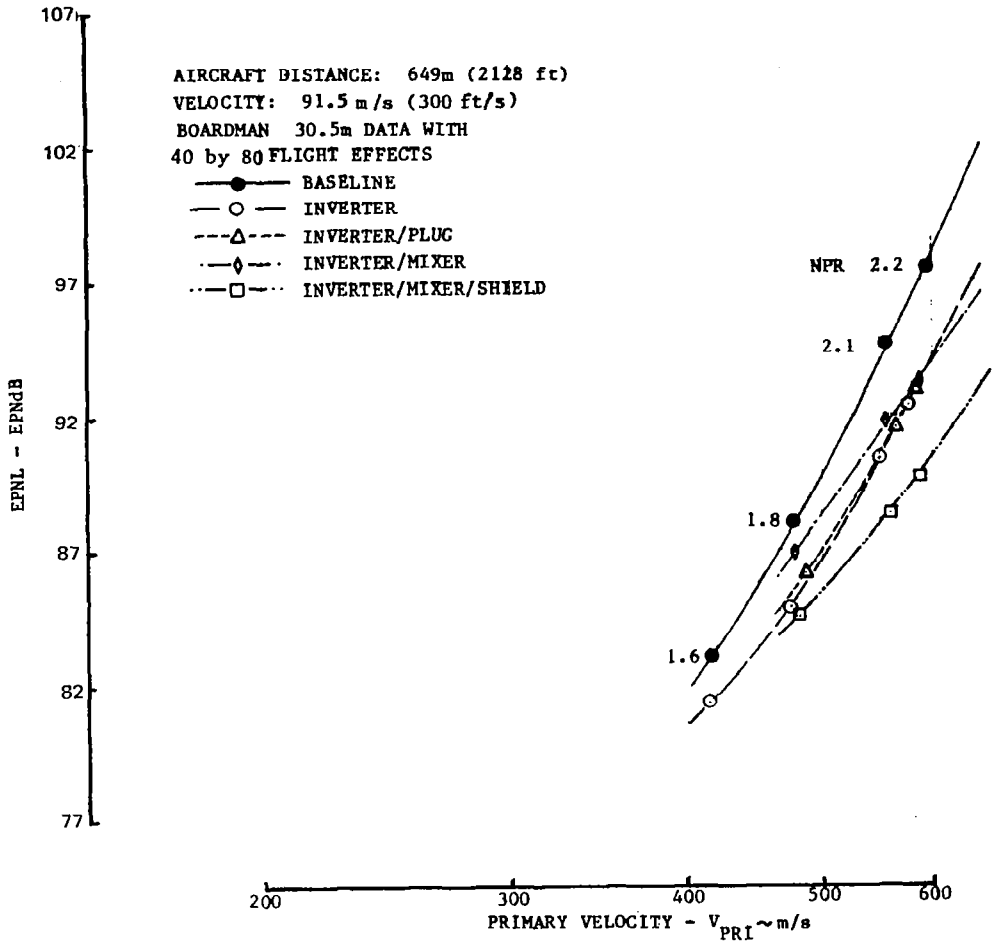

Figure 86.—Comparison of Baseline and Inverted Flow Supressor EPNL, Flight Levels

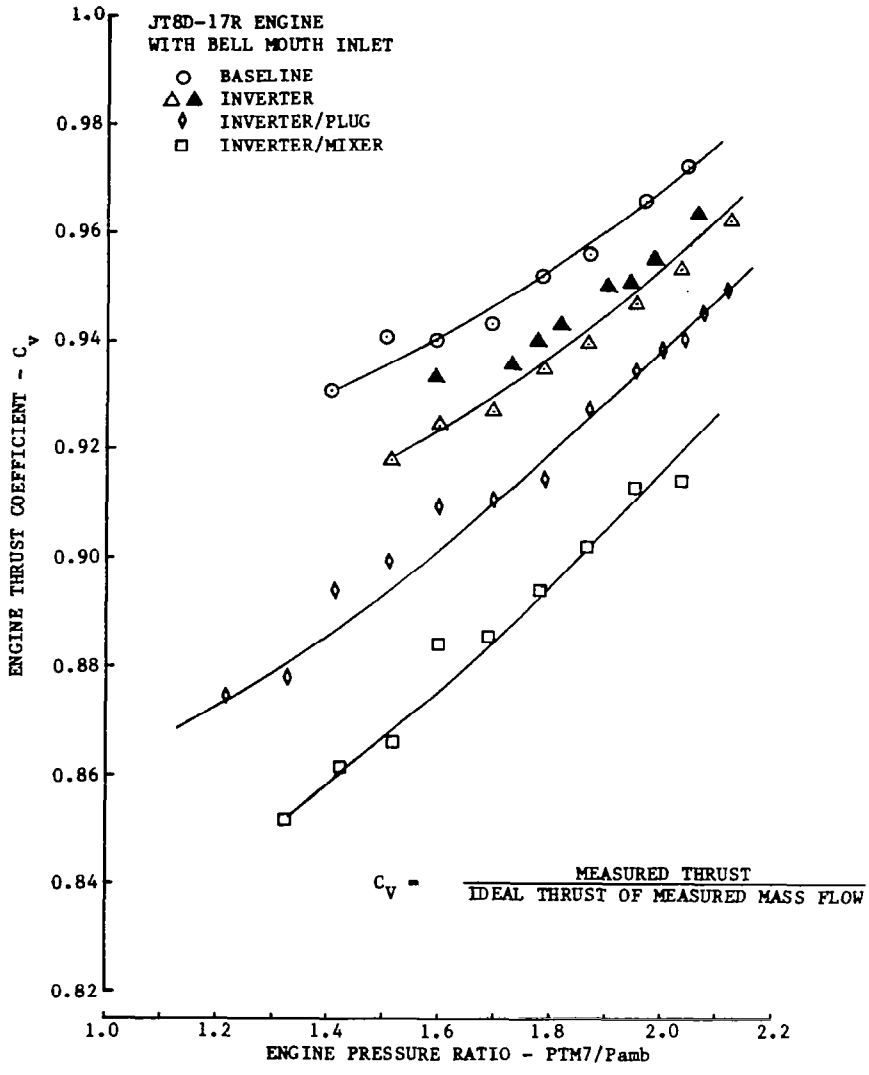

(a) With Bell Mouth Inlet

Figure 87.—Comparison of Engine Thrust Coefficients

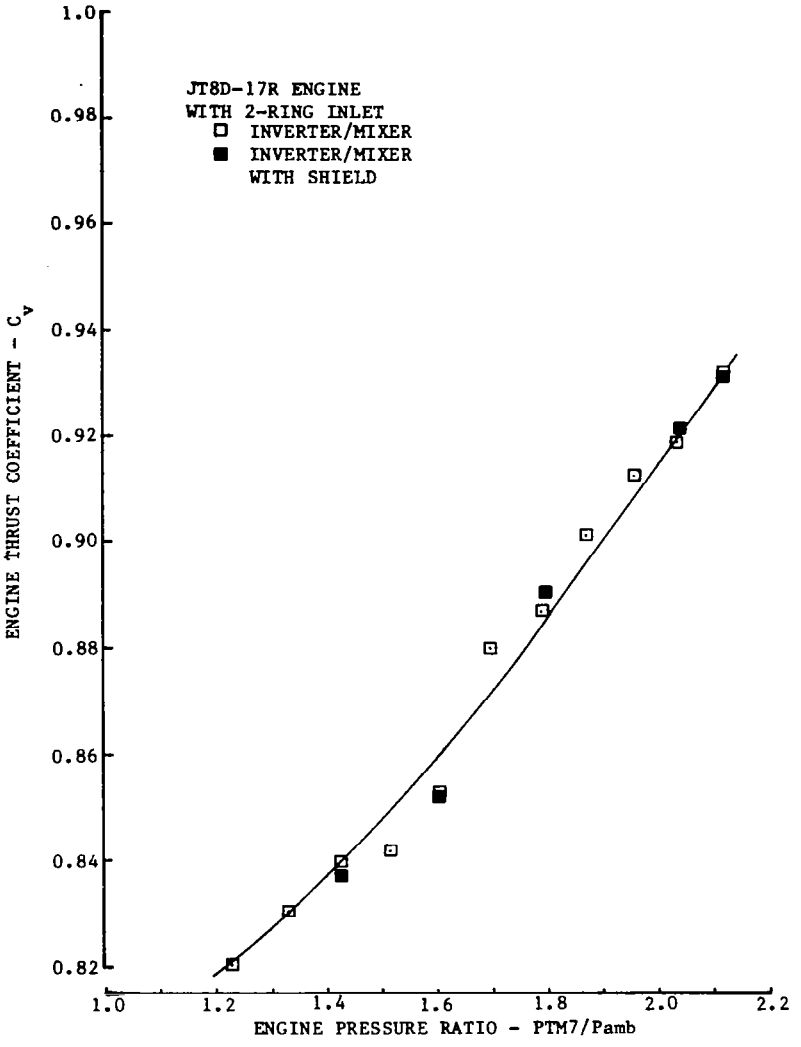

(b) With 2-Ring Inlet

Figure 87.—(Concluded)

TEST 2552TP - JT8D INVERTED FLOW TEST - PHASE I - STATIC TEST
INVERTER EXIT FLOW SURVEY (PRESSURE PLOT)
CONFIG - 2-RING INLET. FLOW INVERTER. RC NOZZLE

1	206.8 N/M^2
2	203.4
3	199.9
4	196.5
5	193.1
6	189.6
7	186.2
8	182.7
9	179.3
0	175.8

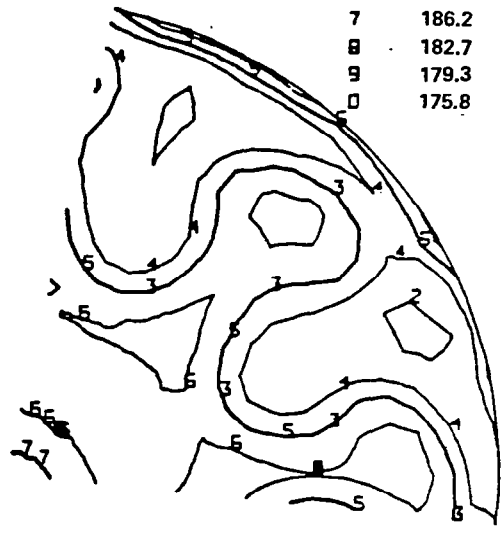

A	172.4
B	168.9
C	165.5
D	162.0
E	158.6

TEST NO.	2552	TEST DATE	20177	CALC. DATE	30977
RUN NO.	19	COND. NO.	1	PAMB N/m^2	100.7
TAMB DEGC	0	PT7 N/m^2	211.7	PTF7 N/m^2	194.0
TT7 DEGC	513	TTF7 DEGC	76	PT7/PAMB	2.102
PTF7/PAMB	1.926	VPRI m/s	551	VFAN m/s	346

Figure 88.—Inverter Exit Flow Survey (Pressure Plot)

TEST 2552TP - JT8D INVERTED FLOW TEST - PHASE I - STATIC TEST
INVERTER EXIT FLOW SURVEY (TEMPERATURE PLOT)
CONFIG - 2-RING INLET. FLOW INVERTER. RC NOZZLE

1	505 °C
2	449
3	393
4	365
5	338

6	310
7	282
8	254
9	227
0	199

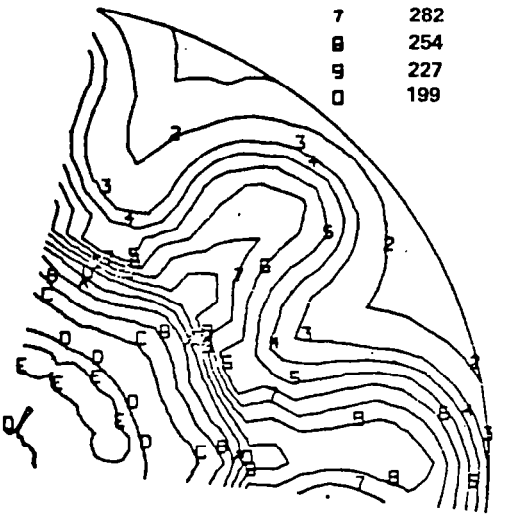

A	171
B	143
C	115
D	88
E	60

TEST NO.	2552	TEST DATE	20177	CALC. DATE	30977
RUN NO.	19	COND. NO.	1	PAMB N/m^2	100.7
TAMB DEGC	0	PT7 N/m^2	211.7	PTF7 N/m^2	194.0
TT7 DEGC	513	TTF7 DEGC	76	PT7/PAMB	2.102
PTF7/PAMB	1.926	VPRI m/s	551	VFAN m/s	346

Figure 89.—Inverter Exit Flow Survey (Temperature Plot)

TEST 2552TP - JT8D INVERTED FLOW TEST - PHASE I - STATIC TEST
INVERTER EXIT FLOW SURVEY (VELOCITY PLOT)
CONFIG - 2-RING INLET, FLOW INVERTER, RC NOZZLE

1	503 m/s
2	488
3	457
4	427
5	412

6	396
7	381
8	366
9	351
10	335

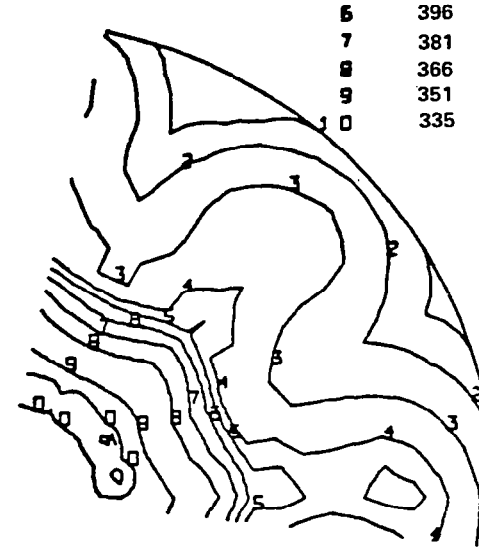

A	320
B	305
C	290
D	274

TEST NO.	2552	TEST DATE	20177	CALC. DATE	30977
RUN NO.	19	COND. NO.	1	PAMB N/m^2	100.7
TAMB DEGC	0	PT7 N/m^2	211.7	PTF7 N/m^2	194.0
TT7 DEGC	513	TTF7 DEGC	76	PT7/PAMB	2.102
PTF7/PAMB	1.926	VPRI m/s	551	VFAN m/s	346

Figure 90.—Inverter Exit Flow Survey (Velocity Plot)

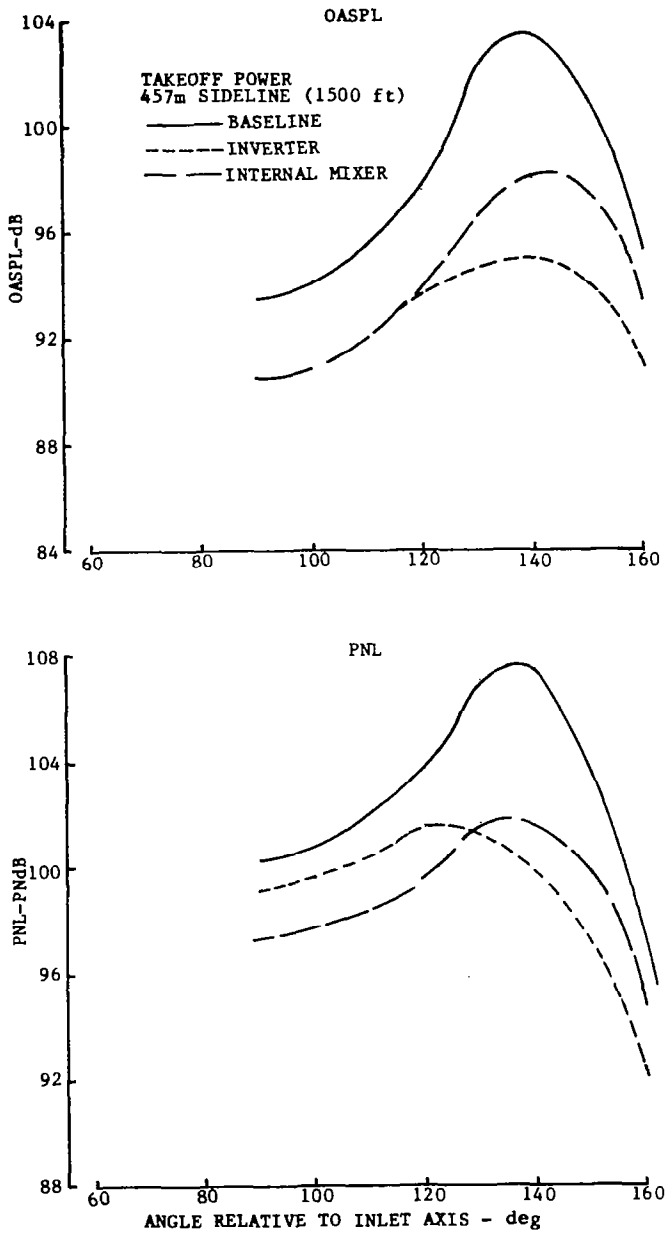

Figure 91.—Comparison of Model Static OASPL and PNL Directivity, Baseline, Inverter, and Internal Mixer

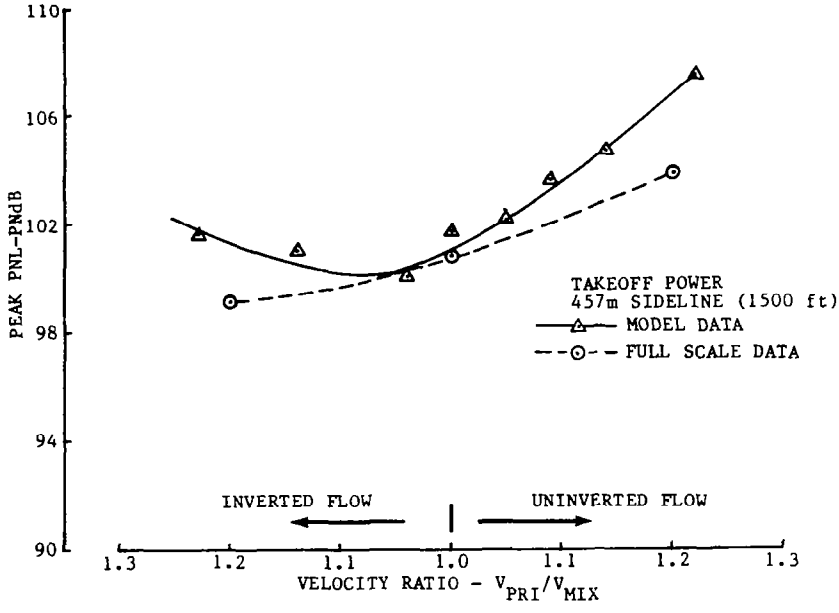

Figure 92.—Model and Full Scale Peak PNL versus Velocity Ratio

1. Report No.	2. Government Accession No.	3. Recipient's Catalog No.
NASA CR -2996		

4. Title and Subtitle	5. Report Date
Flight Effects on Noise Generated by the JT8D Engine with Inverted Primary/Fan Flow as Measured in the NASA-Ames 40- by 80-Foot Wind Tunnel	June 1978
	6. Performing Organization Code
7. Author(s)	8. Performing Organization Report No.
Frank G. Strout	
	10. Work Unit No.
9. Performing Organization Name and Address	11. Contract or Grant No.
Boeing Commercial Airplane Company P. O. Box 3707 Seattle, Washington 98124	NAS 2-9302
	13. Type of Report and Period Covered
12. Sponsoring Agency Name and Address	Contractor Report
National Aeronautics and Space Administration Ames Research Center Moffett Field, California	14. Sponsoring Agency Code

15. Supplementary Notes

16. Abstract

A JT8D-17R engine with inverted primary and fan flows was tested under static conditions and in the NASA Ames 40- by 80-Foot Wind Tunnel to determine static and flight noise characteristics. The major purpose of the program was to evaluate flight effects on noise generated by the inverted flow profile of a large scale engine. The jet noise suppressor concept is of particular interest to Advanced Supersonic large scale engine. The jet noise suppressor concept is of particular interest to Advanced Supersonic Transport engine cycle studies where high jet velocities create a serious noise problem during takeoff operation. Test and analysis techniques developed by a previous model and JT8D enginer test program (NASA CR-2841 and CR-2576) were used to determine the in-flight noise. The engine with inverted flow was tested with a conical nozzle and with Boeing supplied nozzle hardware including a plug nozzle, 20 lobe nozzle, and an acoustic shield. Wind tunnel results show that forward velocity causes significant reduction in peak PNL suppression relative to the uninverted flow. The loss of EPNL suppression is relatively modest. The in-flight peak PNL suppression of the inverter with conical nozzle was 2.5 PNdB relative to a static value of 5.5 PNdB. The corresponding EPNL suppression was 4.0 EPNdB for flight and 5.0 EPNdB for static operation. The highest in-flight EPNL suppression was 7.5 EPNdB obtained by the inverter with 20 lobe nozzle and acoustic shield. When compared with the JT8D engine with internal mixer, the inverted flow configuration provides more EPNL suppression under both static and flight conditions.

17. Key Words (Suggested by Author(s))		18. Distribution Statement
Jet Noise	Suppressor Nozzles	Unclassified, Unlimited
Source Locations	Flight Effects	
Large Scale	Wind Tunnel	
Inverted Flow		Star Category - 07

19. Security Classif. (of this report)	20. Security Classif. (of this page)	21. No. of Pages	22. Price*
Unclassified	Unclassified	238	$9.50

*For sale by the National Technical Information Service, Springfield, Virginia 22161

NASA-Langley, 1978